12-2022

Role of PARP1 and NAD+ Bioavailability in Base Excision and Single-Strand Break Repair

Kate M. Saville

THE UNIVERSITY OF SOUTH ALABAMA
COLLEGE OF MEDICINE

THE ROLE OF PARP1 AND NAD^+ BIOAVAILABILITY IN BASE EXCISION AND SINGLE-STRAND BREAK REPAIR

A Dissertation

Submitted to the Graduate Faculty of the
University of South Alabama
in partial fulfillment of the
requirements for the degree of

Doctor of Philosophy

In

Basic Medical Sciences

By
Kate M. Saville
B.S., The University of Alabama 2014
December 2022

ACKNOWLEDGMENTS

First and foremost, I would like to offer my sincere gratitude to my mentor, Dr. Robert W. Sobol, for the opportunity to work on this very exciting project, for providing guidance and support, and for challenging me to grow as a scientist. I would also like to highlight three exceptional scientists from the Sobol Lab, Dr. Jennifer Clark, Dr. Jianfeng Li, and Dr. Christopher Koczor, and express my deepest appreciation for taking their time to teach me many new skills, for their constant encouragement, and invaluable advice that will benefit me throughout my career. Additionally, I would like to thank my current and former lab mates Dr. Anna Wilk, Dr. Anusha Angajala, Dr. Qingming Fang, Alison Beiser, Md Ibrahim and Rasha Al-Rahahleh for their support inside and outside of the laboratory.

I must offer a special thanks to Dr. Marie Migaud and the Migaud lab for generously gifting the NAD^+ precursors that made this project possible. I would also like to thank Dr. Joel Andrews for developing the MIDAS software and the many hours he spent training me on the confocal microscope. In addition, I would like to thank my dissertation committee, Dr. Mark Gillespie, Dr. Marie Migaud, Dr. Richard Honkanen and Dr. Natalie Bauer for their support, feedback, and guidance through my PhD studies. I would like to extend my thanks to Angela O'Neal, the Associate Director of the BMS program, for always providing support when I needed it, and for reviewing my progress throughout my PhD journey.

I express my deepest gratitude to my parents, Mark and Debbie McConnell for their unwavering love and sacrifices they made on my behalf. I would also like to thank my

sisters Kendall Painter, and Kelsey Wittl, my father-in-law Dr. Augustus Saville and mother-in-law Julie Cook for their love and support.

Finally, and most importantly, I would like to thank my husband, Dr. Grayson Saville, for his unfailing love and support through everything, for supporting our family during my graduate studies, and for encouraging me during the difficulties of this tremendous journey. To my children, Ian, Elijah, Emmett, Tanner, and Emma, I am truly grateful for your love, patience, joy, and laughter that reminded me to smile even through the most difficult days.

TABLE OF CONTENTS

Page

LIST OF TABLES

LIST OF FIGURES

LIST OF ABBREVIATIONS

MNNG: 1-Methyl-3-nitro-1-nitrosoguanidine, 47

2-HG: 2-hydroxyglutarate, 15

5'dRP: 5’ deoxyribophosphate, 31

OGG1: 8-oxoguanine DNA glycosylase, 23

ARH3: ADP-ribosylhydrolase 3, 10

α-KG: alpha-ketoglutarate, 15

ADK: adenosine kinase, 14

APE1: AP Endonuclease 1, 8

APTX: aprataxin, 30

ATM: ataxia-telangiectasia mutated, 24

BER: base excision repair, 4

CHK1: checkpoint kinase 1, 25

Chk2: checkpoint kinase 2, 26

NRH: Dihydronicotinaminde Riboside, 14

DDR: DNA damage response, 3

LIGI: DNA ligase I, 9

LIGIII: DNA ligase III, 9

Polβ: DNA polymerase beta, 9 (when referring to the protein = Polβ; for the human gene = POLB)

DSBR: double-stranded break repair, 25

DSB: double-stranded breaks, 25

EGFP: enhanced green fluorescent protein, 64

FK866: NAMPT inhibitor, 15

GSCs: glioma stem cells, 3

HGG: High grade gliomas (HGGs), 3

HR: homologous recombination, 25

IDH1/2: isocitrate dehydrogenase isoforms 1 or 2, 3

LGG: low grade gliomas, 15

KDM4: lysine demethylase 4, 33

MESH1: metazoan spot1 homolog, 16

MMS: Methyl methanesulfonate, 47

MMR: mismatch repair, 25

MDM2: mouse double-minute 2, 22

MLH1: MutL homolog 1, 26

MSH2: Mut-S-homolog 2, 26

MSH6: Mut-S-homolog 6, 26

NAAD: NA adenine dinucleotide, 13

NAMN: NA mononucleotide, 13

NAPRT: NA phosphoribosyltransferase, 13

NADK: NAD^+ kinase, 16

NADSYN: NAD^+ synthase, 13

NAD: Nicotinamide adenine dinucleotide, 3

NR: nicotinaminde riboside, 13

NMN: nicotinamine mononucleotide, 13

MPG: N-methylpurine glycosylase, 25

NMNAT: NMN adenyltransferase, 13

NOCT: Nocturin, 16

NHEJ: non-homologous end-joining, 25

MGMT: O^6-methylguanine methyltransferase, 25

ORC2: origin replication complex 2, 23

OXPHOS: oxidative phosphorylation, 18

PBD: PAR binding domain, 10

PARGi: PARG inhibitors, 29

PARPi: PARP1 inhibitors, 22

PMS2: PMS1 homlog 2, 26

PARP1: Poly (ADP-Ribose) polymerase 1, 4

PARPs: poly (ADP-ribose) polymerases, 4

PAR: poly-(ADP-ribose), 5

PARG: poly-(ADP-ribose) glycohydrolase, 9

QA: quinoic acid, 13

QRPT: quinolinate phosphoribosyltransferase, 13

RT: radio therapy, 23

ROS: reactive oxygen species, 15

RS: replication stress, 21

SSBR: single-stranded break repair, 4

SIRT: sirtuin, 4

TMZ: temozolomide, 24

TARG: terminal (ADP-ribose) glycohydrolase, 10

XRRC1: X-ray cross-complementing protein 1, 9

ABSTRACT

Kate M. Saville, Ph.D., THE ROLE OF PARP1 AND NAD^+ BIOAVAILABILITY IN BASE EXCISION AND SINGLE-STRAND BREAK REPAIR. December 2022. Mentor: Robert W. Sobol, Ph.D.

High-grade gliomas (HGGs) are malignant, highly metabolically active brain tumors. HGGs are associated with poor patient outcome, attributed to resistance to current therapies, with a survival rate between 12 to 15 months. Gliomas are highly complex tumors, making targeted therapy difficult, highlighting the need for novel approaches and new treatment options. In addition, a large percentage of HGGs are comprised of glioma stem cells (GSCs) that further contribute to therapeutic resistance. Notable characteristics of GSCs are a heightened DNA damage response (DDR) and elevated replication stress that could provide opportunities for therapeutic targeting. A notable feature of many glioma tumors that harbor mutations in isocitrate dehydrogenase isoforms 1 or 2 (IDH 1/2) mutations is reduced levels of the cellular metabolite nicotinamide adenine dinucleotide (NAD^+). NAD^+ is essential for cellular energy homeostasis and is responsible for the regulation of cellular processes such as fatty acid oxidation, glycolysis and the tricarboxylic acid cycle. IDH1/2 mutations are more sensitive to NAD^+ depletion than wild-type cells and, therefore, may be a rational target for chemotherapeutics.

In addition to a role in cellular metabolism, NAD^+ serves as an important cofactor to poly-(ADP-ribose) polymerases (PARPs) and NAD-dependent deacetylases (Sirtuins) in chromatin remodeling. In our lab, we have found that GSCs have increased levels of the DDR protein Poly-(ADP-Ribose) polymerase 1 (PARP1) at both the mRNA and protein expression levels. However, we find that GSCs lack sufficient cellular NAD^+ levels for

robust PARP1 activation. PARP1 is involved in several DNA repair pathways that have evolved to repair specific types of DNA damage. Importantly, the NAD^+ dependent enzymes PARP1 and PARP2, along with the sirtuin isoforms SIRT1 and SIRT6 (NAD^+-dependent deacetylases), comprise a PARP-NAD^+-SIRT axis that plays an essential role in the regulation and coordination of the base excision repair (BER) and single-stranded break repair (SSBR) pathways. The BER/SSBR pathway is responsible for repairing base damage and DNA single-strand breaks that result from both endogenous and exogenous sources, which are essential for genome maintenance. Defects in these pathways have been associated with the onset of cancer and other diseases.

The activation of PARP1 is crucial to the cellular response to both base and SSB damage across the genome (referred to as canonical BER/SSBR) and the response to such lesions that impact replication associated BER/SSBR. The recruitment of and activation of PARP1 is essential for the relaxation of chromatin and recruitment of important BER/SSBR proteins to sites of DNA damage. However, central to that role is the hydrolysis of NAD^+ by PARP1 to form poly-(ADP-ribose) (PAR) polymers. PARP1 covalently modifies itself and other proteins with PAR to facilitate and regulate DNA repair processes. We find that NAD^+ is an important regulator of BER/SSBR as an essential substrate for PARP1. **My hypothesis is that biological variation in cellular NAD^+ levels modulate PARP1 activity, PAR metabolism and the PARP1-interactome to alter both canonical and replication-associated base excision and single-strand break repair. This variation impacts the efficacy of PARG inhibitors as a targeted cancer therapeutic option.**

CHAPTER 1: BACKGROUND

Canonical BER/SSBR

The Base Excision Repair (BER) and Single-Strand Break Repair (SSBR) pathways are converging pathways, responsible for the repair of base damage and single-stranded breaks (SSB), of both exogenous and endogenous sources [1]. The BER/SSBR pathways comprise a synchronized hand-off of the enzymatic products from one protein to the next [1], thereby preventing genome instability by avoiding the accumulation of toxic BER intermediates [1]. This is significant because defects in this pathway result in gene mutations and block glycolysis [2]. BER can be broken down into functional steps, i) lesion recognition and removal of the damaged base by damage specific DNA glycosylases and AP Endonuclease 1 (APE1); ii) PARP1 activation and PAR synthesis to promote chromatin reorganization; iii) DNA-gap tailoring by DNA polymerase beta (Polβ), PNKP, APTX and APLF, followed by; iv) DNA synthesis by Polβ and ligation by DNA ligases I and III (LIGI and LIGIII), and the final step; v) PAR degradation by poly-(ADP-ribose) glycohydrolase (PARG) (along with ARH3 and TARG1) followed by chromatin reorganization (**Figure1.1**).

Given the importance of BER for genome stability, targeting the BER pathway to design novel chemotherapeutics has been an intense area of focus, especially regarding PARP1 and PARP2 [3]. Since many cancer cell types have defects in DNA repair pathways, inhibiting the catalytic activity of PARP1 (and PARP2) has been a treatment strategy to induce synthetic lethality, the concept that two genes are compatible with survival if only one is lost, but if both are lost it leads to cell death [4-6]. However, despite

harboring defects in DNA repair, many cells are insensitive or have developed resistance to such inhibitors [5]. Therefore, it is crucial to understand the mechanisms by which PARP1/PARP2 and other factors regulate canonical BER/SSBR capacity.

While the biochemical analysis of BER and SSBR has been studied extensively *in vitro*, the temporal dynamics of BER/SSBR protein complex assembly and disassembly at the site of DNA damage and how factors such as NAD^+ bioavailability impact recruitment dynamics remains incompletely characterized. Coordination of BER/SSBR complex assembly and disassembly is essential to maintain genome integrity [1]. For example, the key complex formed between Polβ and X-ray-cross-complementing protein 1 (XRCC1) during BER is important to prevent ubiquitylation and subsequent degradation of Polβ by the proteasome, and the recruitment of Polβ to sites of DNA damage is hindered when it is unable to bind to XRCC1 [7, 8].

A major contributing factor to the coordinated assembly of BER complexes, such as XRCC1/Polβ, is the activation of PARP1 at the lesion site [7]. PARP1 activation at the lesion side leads to chromatin relaxation and recruitment of essential DNA repair proteins [9, 10]. XRCC1 is recruited to the lesion site by binding to PAR via its c-terminal PAR binding domain (PBD). Failure of XRCC1 or Polβ to recruit to the lesion site results in the accumulation of PAR, because of unresolved SSBs, leading to genome instability, and the accumulation of double-stranded breaks [11]. Just as critical to PAR synthesis by PARP1 at the DNA lesion site, is the degradation of PAR, by PARG, ADP-ribosylhydrolase 3 (ARH3), and terminal-(ADP-ribose) glycohydrolase (TARG1) for the removal of PAR and ADP-ribose, which allows for the disassembly of PARP1 and BER protein complexes from the DNA following repair [12, 13]. Since PARP1 activity is

essential for coordinated assembly and disassembly of important BER/SSBR protein complexes and is a critical component in the PARP1-NAD^+-SIRT axis, we define NAD^+ as an important regulatory factor for BER/SSBR capacity. I hypothesized that PAR synthesis, and recruitment dynamics of BER/SSBR protein complex assembly and disassembly at the site of DNA damage is dependent on both PARP1 activation and NAD^+ bioavailability.

The focus of this study was to define the extent NAD^+ bioavailability can regulate PAR synthesis by PARP1 and PAR-dependent protein complexes it forms with XRCC1 and Polβ, that facilitate BER/SSBR. Key research questions that prompted these studies are as follows: (1) How and to what extent can NAD^+ bioavailability be modulated in cancer cells; (2) How does NAD^+ bioavailability impact PAR formation in response to DNA damage; and (3) How does NAD^+ bioavailability impact BER/SSBR protein complex assembly and disassembly? Therefore, we hypothesized that cellular levels of NAD^+ can be enhanced to promote PAR accumulation in response to DNA damage to effect canonical BER protein complex assembly and disassembly.

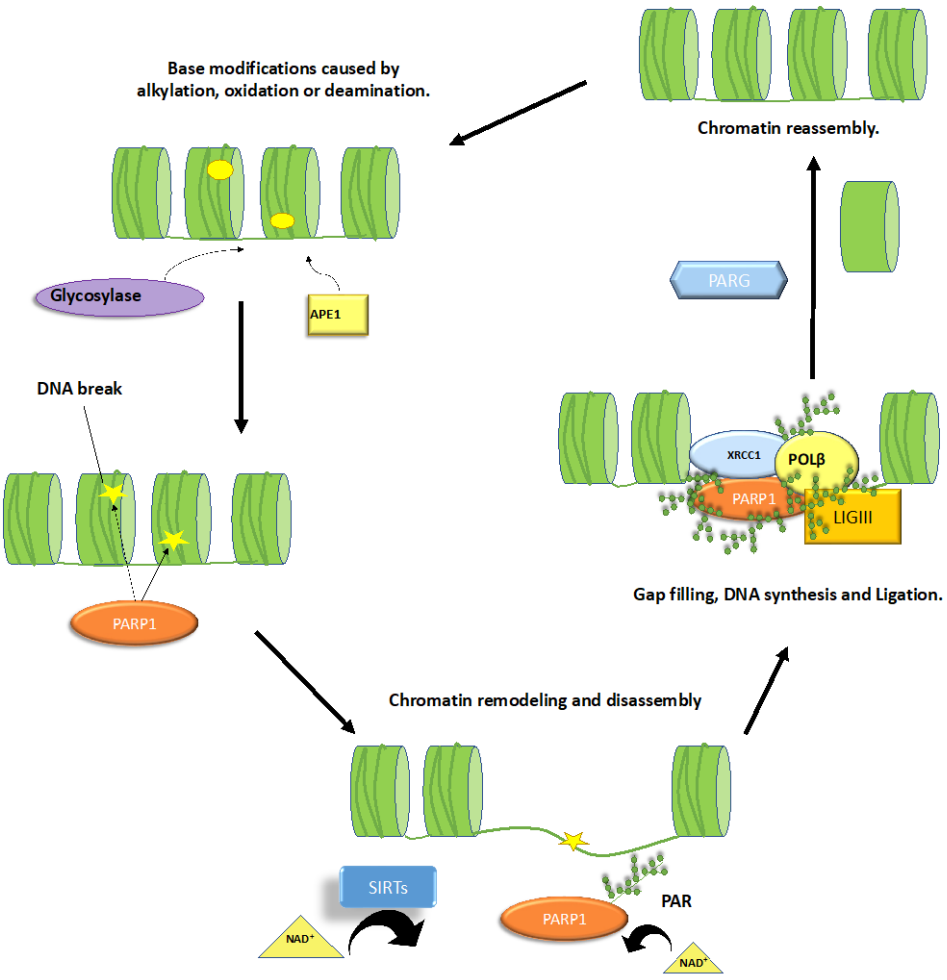

Figure 1.1. Graphic depicting base excision repair/single-stranded break repair.

BER/SSBR occurs in a stepwise manner: 1) The damaged base is recognized and removed by a damage specific glycosylase and APE1 leaving behind a SSB. 2) PARP1 senses the SSB and recruits to the site of DNA damage. SIRT1/6 and PARP1 utilizes NAD^+ to synthesize PAR polymers onto itself and other proteins which facilitates 3) chromatin remodelling and disassembly 4) the recruitment of important DNA repair proteins to the site of DNA damage. 5) PAR polymers are degraded by PARG allowing for the disassembly of PARP1 and other repair proteins. 6) Chromatin reassembly.

NAD^+ Biosynthesis and Metabolism

Metabolism reprogramming is a common feature in Glioma cells and GSCs. Like other cancer cell types, mutations in proteins that regulate redox metabolism and cell cycle progression (CDK2, PTEN, P53, IDH1/2) often lead to adaptations that increase glycolysis and promote proliferation [14, 15]. $NAD(P)^+$ and its reduced forms, NAD(P)H, are essential for redox reactions involved in metabolism, fatty acid oxidation, lipid biosynthesis, cell cycle progression and DNA repair [16]. Because of the importance of NAD^+ to serve in many cellular processes, depletions in cellular NAD^+ have been associated with pathologic outcomes related to diabetes, cardiovascular disease, neurodegeneration, cancer, and aging [17]. There is preclinical and clinical evidence that demonstrates NAD^+ precursors replenish NAD^+ and provide a therapeutic benefit for disease and aging [18-20]. Therefore, there is an emerging interest in targeting NAD^+ biosynthesis for improving patient response to chemotherapeutics [18-20].

There are five pathways cells utilize to synthesize NAD^+: The *de novo* pathway, Preiss-Handler pathway, the Salvage pathway, and the pathways used by NAD precursors NR and NRH [16, 21, 22], and two. (i) NAD^+ can be synthesized *de novo* from tryptophan to quinoic acid (QA) is catalyzed by quinolinate phosphoribosyl transferase (QPRT) to form NAMN [16]. (ii) NA phosphoribosyl transferase (NAPRT) converts nicotinic acid (NA) to NA mononucleotide (NAMN) in the Preiss-Handler pathway [23]. NAMN is converted to NA adenine dinucleotide (NAAD) by NMNA, and NAD^+ synthase (NADSYN) converts NAAD to NAD^+ [16]. (iii) The salvage pathway is the primary pathway cells use to synthesize NAD^+ by recycling NAM. NAM is the product of NAD^+ consumers (PARPs, SIRTs, CD38, CD53, and SARM1) [16, 24, 25]. NAMPT catalyzes the synthesis of NMN

from NAM, and NMN is synthesized to NAD^+ by NMN adenyl transferase (NMNAT) [23]. (iv) Finally, nicotinamide riboside (NR) an NAD^+ precursor, is synthesized into nicotinamide mononucleotide (NMN) by NR kinase (NRK) and converges with the salvage pathway [21]. (v) NRH is synthesized by adenosine kinase (ADK) to form NMNH then is synthesized to NADH by NMNAT which can be oxidized to synthesize NAD^+ [22].

NAM and NA, collectively known as niacin, were previously used supplements for diseases associated with NAD^+ deficiency [22, 26], but NA use has been limited because the high dose required causes painful flushing of the skin [16] . NAM was also successful for treating some conditions of low NAD^+, however, NAM failed to enhance NAD^+ levels similar to NA, possibly because it blocks SIRT activity (discussed later) [16]. NR has been used as a dietary supplement to treat diseases related to NAD^+ deficiency (mitochondrial disease, myocardiopathy, pellagra) for its ability to enhance intracellular NAD^+ levels, without negative side effects [20]. However, NR is not stable in circulation [22]. Recently, NRH, a reduced form of NR, was identified as a potent, orally bioavailable NAD^+ precursor [22, 27, 28] that is reported to increase cellular NAD^+ concentration in the heart, lung, kidneys, liver, brain, muscle, heart, and brown adipose tissue [29].

However, the therapeutic benefit of NRH remains to be elucidated. Alabarse et al, reported that mice supplemented with NRH experienced a decrease in joint inflammation and a decrease in cartilage degradation [29]. Additionally, NRH was reported to relieve early liver injury caused by alcohol consumption, and its reduced form (NMNH) was reported to relieve acute kidney injury (AKI) [30, 31]. Still, other studies demonstrated that such elevated levels of NAD^+ induced by NRH, could promote unfavorable outcomes for some cell types including, inflammation and mitochondrial dysfunction [32]. Chini et al.,

reported that NRH, in contrast to other NAD^+ precursors, could induce a pro-inflammatory response in resting macrophages [32]. Another study reported that NRH inhibited mitochondrial respiration, mitochondrial membrane potential, increased mitochondrial DNA damage, enhanced superoxide production, and induced cell-specific cytotoxicity in Hep2G liver cancer cells, but did not have a similar cytotoxic effect on embryonic HEK293 kidney cells [33]. The enhanced cytotoxicity in HepG2 cells was casually correlated with oxidated products of NRH. Pyridones are the oxidized products of nicotinamide, associated with pathologic outcomes, that exist in methylated or ribosylated forms. Dihydronicotinamide Riboside (NRH) and NR induce 4NADO, an NAD-like species, from 4PY. However, the mechanism by which HepG2 cells confer selective sensitivity to 4PY is not fully defined [34].

However, NAD^+ synthesis is largely dependent on cellular expression of the enzymes involved in each pathway [17, 23, 24, 35]. Unlike other cell types, NAMPT is often overexpressed in glioma cells, which has been associated increased cell proliferation and poor prognosis [36]. Interestingly, in glioma cells, NAPRT gene expression is suppressed, making these cells vulnerable to inhibitors of NAMPT such as FK866 [37-39]. This is especially true for low-grade gliomas (LGG) harboring isocitrate dehydrogenase (IDH)1/2 mutations that have deficiencies in both NAPRT and NAMPT expression [35]. Isocitrate dehydrogenase is an enzyme involved in the TCA cycle that reduces $NADP^+$ to NADPH to form a-ketoglutarate (a-KG) from isocitrate. IDH1 is a major source of NADPH in glioma cells [40]. IDH1 (R132H) mutations occur in 80-90% low grade gliomas (LGGs) and 10% of HGGs [40, 41]. Mutant IDH1 inappropriately oxidizes NADPH to form

$NADP^+$ to synthesize the oncometabolite 2-hydroxyglutarate (2-HG) from alpha-ketoglutarate (a-KG), leading to a significant depletion in cellular NADP(H) pools [35].

NADPH pools are sustained at high levels in normal cells, this is in contrast to many cancer cell types that rely on glycolysis to meet bioenergetic needs [14, 15, 42]. There is increasing evidence that suggests defects in NADP(H) homeostasis is associated with several pathological conditions including tumorigenesis [42-44]. NADH/NADPH are essential electron donors in ROS generation. Reactive oxygen species are produced endogenously by mitochondrial respiration and by the enzyme-catalyzed reactions such as those by the NOX family proteins [16].

The mitochondria produce the majority of cellular ROS during oxidative phosphorylation (OXPHOS) using NADH as an electron donor. Mitochondrial NADH is utilized by complex I of the electron transport system (ETS), along with complex II that utilizes electrons from FADH, to generate an H^+ gradient across the inner mitochondrial membrane (IMM) to generate ATP. Complex I and III produce O_2^- anion as a byproduct of OXPHOS and release it into the cellular matrix [16].

Another source of cellular ROS is produced by NOX proteins, NOX1-5 and DUOX1/2. In contrast to OXPHOS, NOXs produce H_2O_2 or O_2^- for normal cell signaling responses such as, proliferation, migration, and survival. NOXs utilize electrons from NADPH along with an FAD binding region, and transmembrane hemes that allow NOXs to transfer two electrons from cytosolic NADPH to extracellular O_2 to produce O_2^- anion [16, 39]. Other enzymes that utilize NADPH to produce ROS are xanthine oxidase (XO), NOS, lipoxygenase and cytochrome P450 [17]. ROS can also be produced by exogenous

sources such as ionizing radiation, UV, cytokines, growth factors, chemotherapeutics, and environmental toxins [45].

Oxidative stress occurs when there is an imbalance of ROS within the cell. Oxygen radicals spontaneously react with nucleic acids, lipid molecules and proteins causing damage to these molecules leading to pathogenesis, aging, and cancer [45, 46]. NADPH is essential to reduce glutathione (GSH) which is necessary for reducing reactive oxygen species (ROS) [43]. Another pathway responsible for responding to oxidative stress is the Nrf2 regulated NADP(H): quionereductase1 (NQO1) and NRH: quionereductase2 (NQO2). NQO1 and NQO2 are highly important for detoxifying quinones and preventing redox cycling. The primary difference of NQO1 and NQO2 is that NQO1 preferentially uses NADPH as its substrate while NRH is the required substrate for NQO2 [16, 34, 39].

It has been hypothesized that increased ROS in IDH1 mutant cells contribute to replication stress and cell death, however, recent studies have suggested this is likely a result of alterations in replication machinery, rather than depletion of NADPH [45]. $NADP^+$ is synthesized from NAD^+ by NAD^+ kinase (NADK) [42-44]. Interestingly, IDH1 mutant glioma cells demonstrate increased levels of NADK, likely to compensate for reduced NADPH levels [35, 41, 47].

However, it is unknown how IDH1 mutational status impacts the expression of NADP(H) phosphatases, such as metazoan spot1 homolog (MESH1) and Nocturin (NOCT) that are important for restoring NAD(H) pools by removing the phosphate group from NADP(H) [48-50]. MESH1 is an important regulator of cytosolic NAPDH, high levels of MESH1 deplete NADPH levels and lead to ferroptosis, while decreased expression of MESH1 conserves cytosolic NADPH and GSH levels and promotes survival

by reducing lipid peroxidases [48]. NOCT functions as a regulator of metabolism and circadian clock rhythm, that is able to utilize both oxidized and reduced forms of NADP(H) as a substrate, but has a slight preference for NADPH [50]. NOCT temporally regulates NADP(H) pools (mitochondria and cytosol), restores NAD(H)/NADP(H) balance and improves oxidative phosphorylation in the mitochondria (**Figure 1.2**) [49].

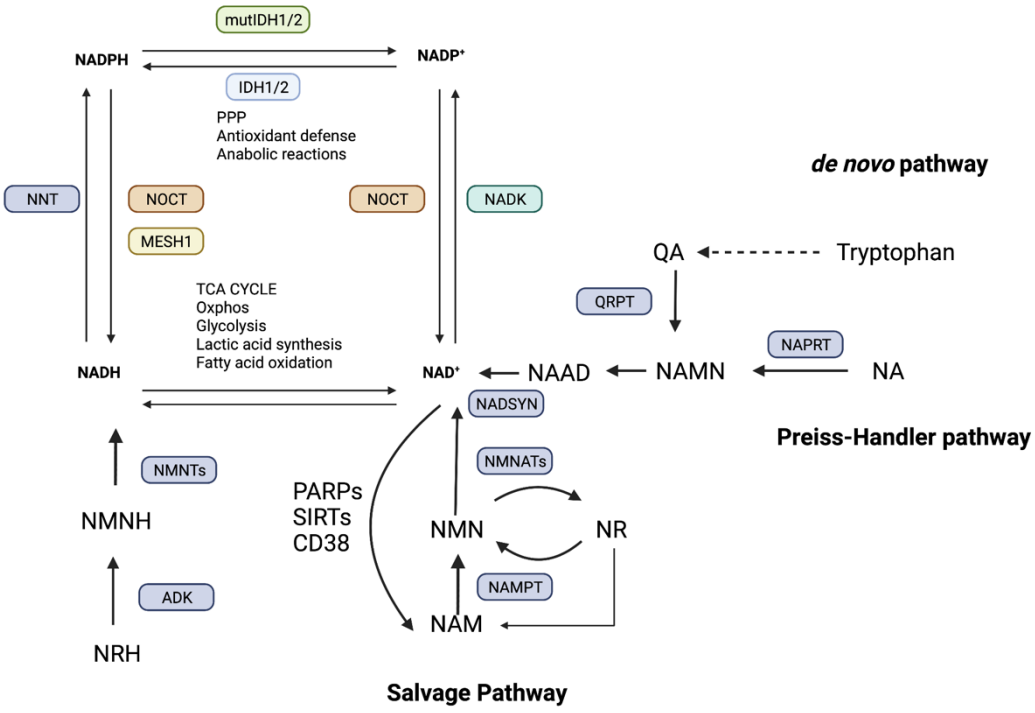

Figure 1.2. Overview of metabolism and its downstream targets.

NAD^+ is synthesized via the *de novo* pathway, Preiss-Handler Pathway and Salvage pathways. The salvage pathway is the primary pathway for cellular NAD^+ synthesis that recycles NAM from NAD^+ consuming enzymes. NR and NRH are NAD^+ precursors that significantly enhance cellular NAD^+ levels. Created in BioRender.

NAD^+ Mediated Regulation of DNA Repair Capacity

In addition to its role in energy metabolism, NAD^+ serves as an essential cofactor for NAD^+ dependent enzyme families, PARPs and SIRTs [22, 51]. PARP1 and SIRT1 are essential for DNA repair [1]. SIRTs are NAD-dependent deacetylases, that function as regulators of transcription factors, and DNA repair proteins including PARP1 [52]. SIRT1 and SIRT6 directly regulate the activity of PARP1 and impact its role in chromatin reorganization and as a regulator of BER/SSBR protein assembly [44]. SIRT1 is able to deacetylate PARP1, specifically in the regions of amino acids 1 to 214 and 477 to 524, whereas HDAC1 only deacetylates in the regions of amino acids 477 to 524 [52]. Under stress conditions, SIRT1 is capable of regulating PARP1 activity at both transcriptional and posttranslational levels by deacetylating PARP1, and repressing PARP1 synthesis at the gene promoter [53].

The role of SIRT6, a member of the sirtuin family, is very intriguing because it participates in both deacetylase and mono (ADP-ribosyl) transferase activities. SIRT6 mono (ADP-ribosyl)-ates PARP1 at Lys521 in response to oxidative stress resulting in PARP1 activation and enhanced DSB DNA repair [54, 55]. SIRT1 and SIRT6 also regulate NAMPT, thereby regulating cellular NADP(H) pools [44]. SIRT1 increases the transcription of NAMPT to produce NAD^+ in response to DNA damage, and SIRT6 deacetylates NAMPT to enhance NAMPT enzyme activity to promote NAD^+ synthesis [44].

PARP1 utilizes NAD^+ as the donor of ADP-ribose units, to catalyze the attachment of PAR polymers onto itself and other acceptor proteins. PARP1 consumes 80% of nuclear and cytosolic NAD^+ in response to DNA damage, therefore it plays a regulatory role by

limiting NAD^+ consumption by SIRTs [2, 12]. However, PARP1 activation and SIRT activity is limited by NAD^+ bioavailability [25, 56]. PARP1 hyperactivation causes NAD^+ depletion that induces a metabolic switch, to promote cell survival in response to DNA damage, inhibiting glycolysis and promoting oxidative phosphorylation (OXPHOS), and adenosine triphosphate (ATP) synthesis [2, 12, 25].

However, NAD^+ levels are not constant across different cell types. This is concerning because fluctuations in cellular levels of NAD^+ impact the activity of NAD^+-consuming enzymes, such as PARP1 and SIRT1, and have been linked to the aging process and cancer [26]. Therefore, low cellular NAD^+ has been correlated with suppressed DNA repair efficiency [57] while elevated NAD^+ provides for robust DNA repair capacity [58, 59]. Our lab has demonstrated that resistance to select genotoxins can be overcome by reducing cellular NAD^+ levels in response to DNA damage [60]. Previous studies by our lab and others have demonstrated that glioma cells with defects in NAD^+ biosynthesis are particularly vulnerable to depletions in NAD^+ [59]. Consistent with this, several studies have demonstrated that IDH1/2 mutant glioma cells demonstrate selective sensitivity to alkylating agents in combination with NAMPT inhibitor FK866 [47].

Additionally, we demonstrated low NAD^+ bioavailability contributes to genome instability by inhibiting cellular PARP1 activation, leading to defects in DNA repair capacity and suppression of BER complex assembly [57]. The structural similarity of $NADP^+$ to NAD^+, which can be recognized by PARPs, but cannot be utilized as a substrate for ADP-ribosylation. Therefore, a high $NADP^+/NAD^+$ ratio can further inhibit PARP1 activity and its response to DNA damage [61]. In contrast, enhanced NAD^+ bioavailability increases PAR accumulation that enhances BER/SSBR protein complex assembly

following DNA damage. Until recently, the extent that cellular NAD^+ can be modulated has been limited by the availability of potent NAD^+ precursors [22]. As previously mentioned, NRH is a potent NAD^+ precursor that can enhance cellular NAD^+ levels up to 10-fold in some cell lines. Further, NRH can enhance PARP1 activation potential to enhance DNA repair capacity (**Figure 1.3**) [22, 62].

However, NRH induced cell-specific cytotoxicity in HepG2 cancer cells but did not impact cell viability in HEK293 embryonic kidney cells [33]. Cell cytotoxicity in HepG2 cells was correlated with enhanced production of oxidized, NAD-like species, 4NADO and 4PYR [34]. This is significant because an increase in oxidized NAD^+ radicals could cause DNA lesions and protein oxidation [45]. Previously, it was hypothesized that oxidized NAD^+ species 2NADO, 4NADO, and 6NADO would function as inhibitors of PARP1. However, we found that 4NADO and 6NADO significantly increased PARP1 enzyme activity *in vitro* although 2NADO had no effect on PARP1 activity (**Appendix Figure 1A-B**). However, further research is required to determine how these oxidized species impact the DDR, PARP1/SIRT activity and the organization of other BER/SSBR proteins *in vivo*.

Overall, fluctuations in cellular NAD(H)/NADP(H) levels can impact DNA repair efficacy, therefore we define NAD^+ as a factor for the regulation of BER/SSBR. While it is well-documented that deficiencies in NAD^+ suppress BER/SSBR complex assembly in response to DNA damage, the extent that NAD^+ synthesis can be modulated to positively effect BER/SSBR complex assembly is not clear. Further, it is not clear how deficiencies in NAD^+ impact chemotherapeutic response in glioma cells, especially those with IDH1/2 mutations [43]. We find that NAD^+ is an important regulator of BER/SSBR as an essential

substrate for PARP1 and PARP2 enzymatic activity and for the assembly of BER protein complexes at the site of DNA damage. Additionally, we find that NAD^+ levels can be modulated to suppress or enhance PARP1/PARP2 activation and BER complex formation, demonstrating the importance of cellular NAD^+ bioavailability for the maintenance of genome stability.

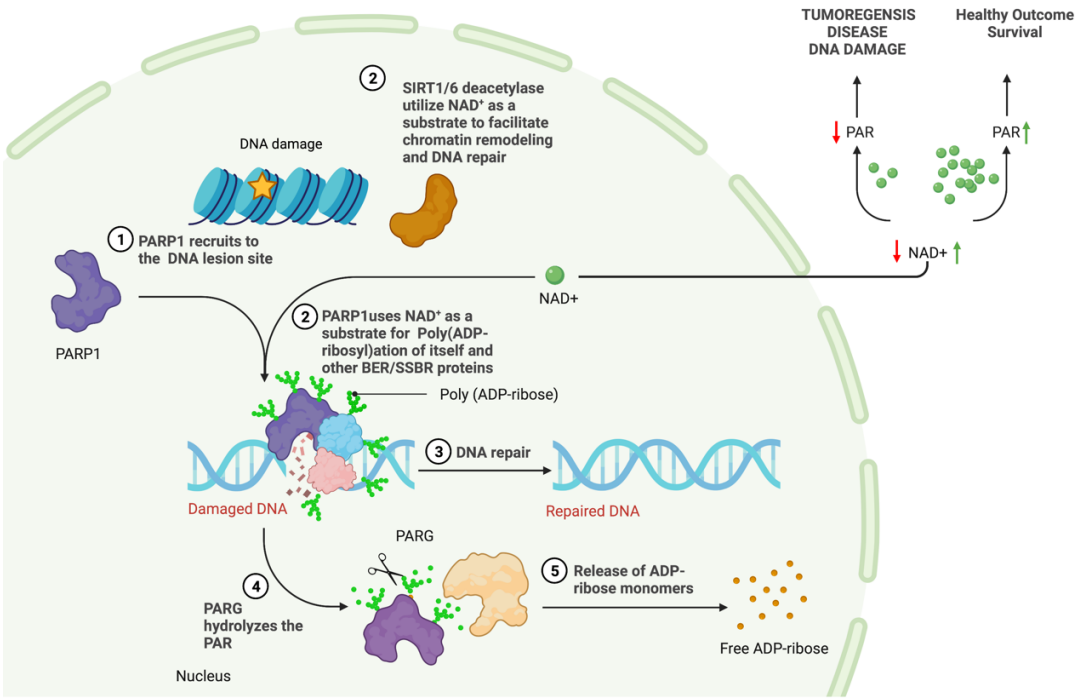

Figure 1.3. Proposed model depicting NAD^+ regulation of DNA repair.

NAD^+ is a substrate of SIRT1/6 deacetylases and PARP1. SIRT1 regulates transcription and PARP1 activity. SIRT6 mono-(ADP-riobosyl)-ates PARP1 leading to enhanced PARP1 activity. SIRT1 and SIRT6 enhance NAD^+ synthesis by increasing NAMPT protein expression and activity. PARP1 consumes 90% of free NAD^+ to synthesize PARP1 polymers and catalyzes covalent attachment of PAR to itself and other DNA repair proteins to facilitate DNA repair. Hyperactivation of PAR induces a metabolic switch, that inhibits glycolysis and increases OXPHOS, thereby preventing the overconsumption of NAD^+ by PARP1. Low NAD^+ levels inhibit PARP1 activation leading to genome instability and tumorigenesis, while high NAD^+ levels increase PARP1 activation and enhance DNA repair capacity leading to a healthy outcome. Created in BioRender.

Replication Dependent BER/SSBR

Despite research efforts to characterize the DDR in glioma, the problem of recurrence and resistance to current chemotherapeutics persists [63]. Recent evidence suggests that the issue of recurrence is related to GSCs with an upregulated DDR, leading to replication stress, ATR and PARP1 activation, and slowed replication fork progression [64-66].

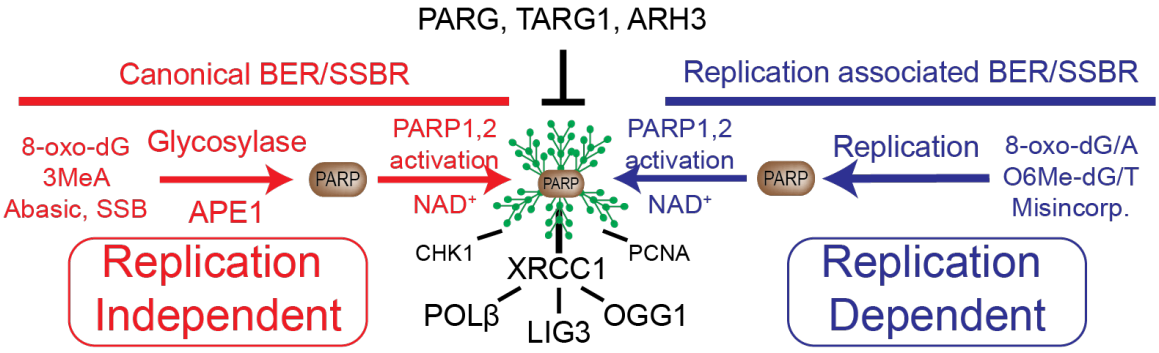

Figure 1.4. Canonical BER/SSBR and replication associated BER/SSBR scheme depicting key steps, proteins, and post-translational modifications (PTM).

The cause of increased replication stress in glioma has often been attributed to increased ROS, but conflicting reports have demonstrated that many glioma cells and GSCs have insufficient ROS required for proper cell maintenance [45, 66-70]. However, more recent reports have demonstrated that replication stress is likely due to a variety of factors including upregulation of transcription, increased origin firing, DNA damage by exogenous and endogenous sources, and the presence of R-loops, a DNA-RNA hybrid that

contributes to the regulation of gene expression and DNA replication [70, 71]. Several reports have demonstrated that ATR inhibition sensitizes BRCA1/2 deficient ovarian and breast cancer cells to PARPi by dysregulating origin firing leading to DSB and replication catastrophe [64, 65]. Similarly, ATR inhibition sensitized IDH1 mutant glioma cells to PARP1 inhibitors (PARP1i) demonstrating that PARP1 plays a significant role in the response to replication stress [72].

The role of PARP1 as a signaling enzyme in the DDR has been well defined [73, 74]. However, more recent efforts have concentrated on the role of PARP1 in response to replication stress. We have further identified a role for PARP1 activation, and its interaction with BER/SSBR proteins during replication, in a mechanism we define as replication dependent BER/SSBR [75]. Every time a cell divides, it must accurately copy billions of nucleotides in synchronization with the cell cycle [76]. Errors in replication can cause genome instability and result in mutations, blocked replication, and DNA breaks [76]. DNA damage is among many conditions that lead to replication stress and fork stalling. S-phase checkpoints ensure genome integrity by coordinating the DDR response to prevent the breakdown of replication forks [67, 76].

PARP1 has been suggested to have several possible roles in DNA replication including replication fork remodeling and processing. PARP1 interacts with RECQ1 to suppress replication restart [77]. Tumor suppressor p53 is a transcription factor that induces transcription of cell cycle proteins involved in replication stress, DNA repair proteins, and apoptosis [78, 79]. The expression of p53 is tightly regulated by the E3 ubiquitin ligase, mouse double-minute 2 (MDM2) homolog. MDM2 and p53 expression are dysregulated in glioma adding to resistance to chemotherapeutics. Recently, MDM2 was reported to

bind to PARP1, inhibiting PARP1 activity leading to destabilization and degradation of PARP1 to promote replication fork progression [80]. In-line with our findings, PARP1 has also been reported to play a role in the recognition of Okazaki fragments and the recruitment of SSBR proteins XRCC1 and LIGIII [81-83], which together with BRCA2, prevents fork degradation by Mre11 [84, 85].

PARP1 also activates CHK1 to facilitate intra-S-Phase checkpoint activation, likely associated with its role in Okazaki fragment processing, and mediating the coordination of DSBR [81, 86]. Recently, another role for BER in intra-S phase arrest was uncovered by targeting BER factor 8-oxoguanine DNA glycosylase (OGG1) [87]. Inhibition of OGG1 induced S-phase arrest, and downregulation of several genes involved in DNA replication. OGG1 overexpression has been reported to confer resistance to radiotherapy (RT) and alkylating agents in glioma [87, 88].

Recently, we demonstrated a possible role for PARP1 in the pre-recognition complex through an NAD^+ dependent interaction with origin replication complex 2 (ORC2), a member of a 6-subunit protein complex essential for initiation of DNA replication [76]. Efforts to target PARP1 and other BER/SSBR factors has been an ongoing area of research interest. More recently, efforts to target vulnerabilities in NAD^+ biosynthesis have demonstrated roles for metabolic regulation of oxidative stress, decreased PARylation, and increased DNA damage leading to replication stress and apoptosis [37, 89, 90]. However, it is unknown how enhanced cellular NAD^+ biosynthesis can impact PARP1 activation potential in NAD^+ deficient glioma cells in response to S-phase induced replication stress.

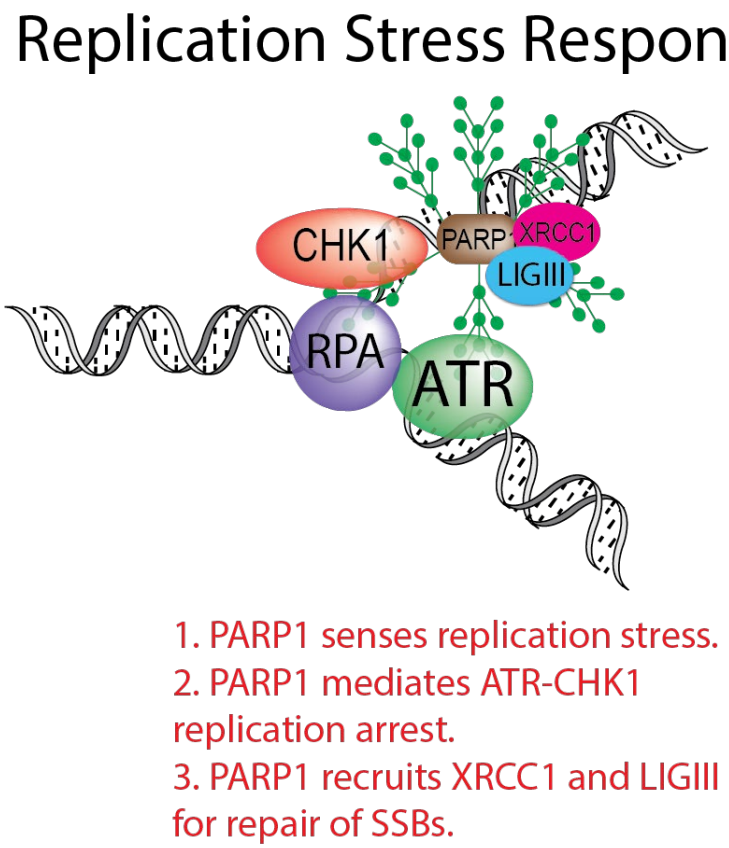

Figure 1.5. PARP1 activation in replication stress.

There are several potential roles for PARP1 in the response to replication stress including repair of endogenous and exogenous DNA damage, as a member of the pre-recognition complex, replication fork remodelling, and processing of Okazaki fragments.

The DNA Damage Response in Glioma

The DNA damage response (DDR) is a collective term for the intricate network of DNA repair pathways that have evolved, to detect and repair specific types of DNA lesions, to maintain genome integrity [91]. Defects in the DDR are a common feature of cancer cells that make them sensitive to DNA damaging agents. The standard treatment for GBM is surgical removal of the tumor and radiotherapy (RT) combined with the DNA alkylating agent temozolomide (TMZ) [15, 90, 92]. However, many GBM tumors and GSCs have an upregulated DNA damage response (ATM, ATR, PARP1, MPG, XRCC1, Polβ, MGMT, DNA-PK) increasing resistance to current therapies [15, 63, 92, 93].

TMZ and radiotherapy induce DNA lesions that produce both single- and double-stranded breaks. Single-strand breaks are repaired by base excision repair (BER), bulky lesions are repaired by nucleotide excision repair (NER) and mismatched bases are repaired by mismatch repair (MMR) pathways [63, 92]. Double-stranded breaks are repaired by error free homologous recombination (HR) or the error prone non-homologous end joining (NHEJ) [60]. The primary lesions introduced by TMZ are N7-methylguanine (N7MeG), N3-methyladenine (N3-mA) and N3-methylguanine (N3-mG). TMZ and radiotherapy also induce oxidative lesions caused by ROS, TMZ produces O6-methylguanine (O^6-mG) lesions and TMZ and radiotherapy produce 8-oxoguanine (8-oxoG) [60, 63, 94].

PARP1 activation plays a central role in the DDR by facilitating the coordination and organization of multiple DNA repair pathways [15, 92, 95]. PARP1 activation of BER/SSBR, is critical to resolve N7-mG and N3-mA lesions, that represent >80% of the damage caused by TMZ [63]. BER factor N-methylpurine glycosylase (MPG), phosphorylated by ataxia -telangiectasia mutated (ATM) kinase, is required for the removal

of N3meA DNA lesions. Aberrant expression of MPG is an independent marker associated with a chemotherapy resistant phenotype, and a poor prognosis in HGGs [93, 96]. Oxidative lesions caused by 8-oxoG are removed by BER protein 8-oxoguanine DNA glycosylase (OGG1) [87, 88].

PARP1 directly interacts with of O^6-methylguanine methyltransferase (MGMT), responsible for the direct removal of cytotoxic O^6-mG lesions [63, 90, 94, 97]. MGMT promotor methylation, is an important biomarker, associated with a better prognosis for patients with GBM, while MGMT overexpression increases resistance to alkylating agents [92]. However, if O^6-mG lesions remain unresolved, an O^6-mG:T lesion activates mismatch repair proteins (MSH2, MSH3, MSH6), leading to activation of ATM and ATR mediated checkpoint pathways that stall cell cycle during DNA repair [92, 94, 98, 99].

ATM and ATR are responsible for activating checkpoint kinases for the regulation of the cell cycle [99-101]. ATR and ATM are both active during intra-S phase, but ATR phosphorylation of checkpoint kinase 1 (CHK1) is the primary kinase active during early and intra-S phase while ATM phosphorylation of checkpoint kinase 2 (CHK2) is the primary kinase active during G_2-phase [102]. However, recent reports have demonstrated that MMR proteins (MSH3 and MSH6) are responsible for ATR-CHK1 mediated DNA repair during S-phase [102]. Deficiencies in MMR are uncommon in primary glioma tumors but are commonly associated with a highly mutable phenotype in recurrent glioma and high grade IDH1 mutant glioma [93, 103]. Complete or partial loss of MMR proteins Mut-S-homolog2 (MSH2), Mut-S-homolog6 (MSH6), MutL homolog1 (MLH1) and PMS1 homolog 2 (PMS2) were found in tumor tissue of patients with HGG [103, 104].

However, decreased expression in MMR proteins has not been reported to impact survival prognosis [103].

Double-stranded breaks are often attributed to unresolved SSBs encountered during replication. More recently, crosstalk between BER/SSBR and MMR pathways have been implicated in replication-independent pathways, in which O^{6}-mG lesions overlap with BER intermediates in the opposite strand leading to DSBs [105]. ATM/ATR checkpoint pathways activate homologous recombination (HR) and non-homologous end-joining (NHEJ) pathways for the repair of double-stranded breaks (DSB) [101]. However, HR is limited to late S-phase and M-phase, whereas NHEJ can function throughout the cell cycle, therefore NHEJ is the predominate pathway for double-strand break repair (DSBR) [100]. DNA dependent protein kinase (DNA-PK) interacts with PARP1, to recruit XRCC1 to stalled replication forks to protect and repair stalled replication forks [106-108]. Alternative NHEJ (Alt-NHEJ), serves as a standby pathway for canonical NHEJ (C-NHEJ) that activates BER/SSBR proteins flap endonuclease 1 (FEN1), XRCC1 and Polβ [106-108].

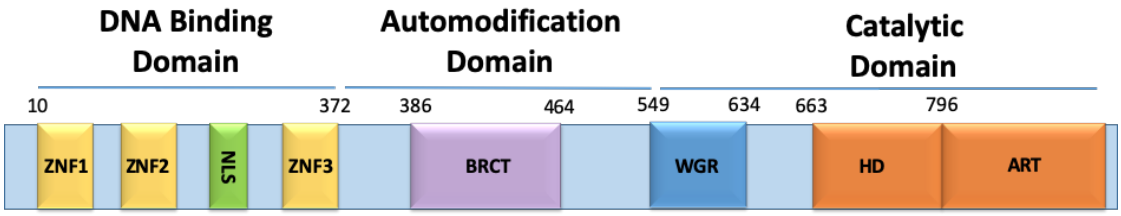

Figure 1. 6. PARP1 protein structure.

PARP1 has a DNA binding domain, containing three zinc finger motifs, an auto modification domain, and a catalytic domain. The DNA binding domain contains a Zinc finger motif that mediates interdomain contacts and PARP1 homodimerization**.** The central automodification domain (AD) contains the BRCT domain that facilitates PARP1 interactions with DNA repair proteins XRCC1 and Topoisomerase I.The catalytic domain contains three subdomains, the WGR domain and the helical domain (HD) and the ADP-ribosyltransferase (ART) domain. The WGR domain, named for its conserved amino acid sequence Trp-Lys-Arg, interacts with ZF1 and ZF3 to form a collapsed PARP1 conformation essential for DNA-damage dependent activation. The HD serves as an auto-inhibitory domain that prevents binding of NAD^+. Following DNA-damage detection, the HD unfolds, releasing its auto-inhibitory function, allowing the ART domain to bind to NAD^+ and perform catalysis.

PARP1, a 116 kDa, modular enzyme, is involved in several DNA repair pathways, and the maintenance of replication fork stability [109]. In the context of BER, PARP1 is critical for the recruitment and complex assembly of the core BER proteins XRCC1 and Polβ [110]. To that end, regulation of PARP1, therefore has the potential to lead to the coordinated regulation of BER/SSBR.

There are 3 major functional domains of PARP1: an N-terminal DNA Binding Domain (DBD), a central Auto-modification Domain (AD), and C-terminal catalytic domain (CAT) (**Figure 1.6**) [55, 111]. The DBD contains three Zinc Finger motifs (ZF1,

ZF2 and ZF3), a Nuclear Localization Signal (NLS) and a caspase 3 cleavage site. The ZF1 and ZF2 motifs recognize DNA damage and bind to double-stranded and single-stranded DNA breaks leading to PARP1 activation [55, 112]. The ZF3 motif mediates interdomain contacts and PARP1 homodimerization [111]. The central AD contains the BRCT domain, which facilitates PARP1 interactions with DNA repair proteins XRCC1 and Topoisomerase I. Additionally, the BRCT domain is flanked by lysine residues that are sites for auto ADP-ribosylation [113, 114].

The catalytic domain contains three subdomains, the WGR domain, the helical domain (HD) and the ADP-ribosyltransferase (ART) domain. The WGR domain, named for its conserved amino acid sequence Trp-Lys-Arg, interacts with ZF1 and ZF3 to form a collapsed PARP1 conformation essential for DNA-damage dependent activation [115]. The HD serves as an auto-inhibitory domain that prevents binding of NAD^+. Following DNA-damage detection, the HD unfolds, releasing its auto-inhibitory function, allowing the ART domain to bind to NAD^+ and perform catalysis [116].

PARP1 utilizes NAD^+ as a substrate to synthesize long, branching PAR chains at the site of DNA damage [1]. The synthesis of PAR by PARP1 at the DNA lesion site is a critical PTM that facilitates chromatin disassembly and BER/SSBR protein recruitment [62, 73]. Auto-ribosylation of PARP1 was the first PTM of PARP1 to be identified along with 3 potential auto-modification sites: Lys498, Lys521 and Lys524 [54, 74]. PARP1 is capable of mediating mono- and poly-(ADP-ribosyl)-ation reactions at these sites. These auto-modification events occur not only in response to DNA damage, but also in response to other PTMs and protein interactions. PARP1 is trans-modified by heterodimerization with other PARP family members including PARP2, which is important for efficient DNA

damage repair by BER [74, 117]. PARP1 modifies other repair factors by covalently attaching PAR to acceptor proteins [73]. Failure of PAR to form at the lesion site leads to replication fork stalling as a result of unrepaired SSBs leading to replication fork collapse and DSBs that are repaired by homologous recombination (HR) [118]. Therefore, cells defective in HR and BER/SSBR are hypersensitive to alkylating agents, because of unresolved DNA damage, leading to genomic instability [118].

Frequently, in cells that acquire chemotherapy resistance, there is an upregulation of DNA repair proteins [100]. PARP1 has been found to be overexpressed in breast, ovarian, lung, colon and glioma tumors [95, 119-122]. PARP1 inhibitors were developed to selectively target ovarian cancers with defects in HR referred to as synthetic lethality, have been approved for use in ovarian and breast cancers, but have more recently been approved for clinical trials in glioblastoma in combination with alkylating agents and RT [4, 64, 100, 122, 123].

Inhibiting PARP1 interferes with BER/SSBR pathways by blocking PARylation and recruitment of essential repair factors to the site of DNA damage. The mechanism of action common among all PARP1 inhibitors is unrepaired SSBs that interfere with replication, lead to fork collapse, and the accumulation of DSBs [124]. IDH1/2 mutant gliomas that harbor defects in HR proteins (ATM and RAD51) are selectively sensitive to PARPi, especially in combination with ATR inhibitors and TMZ [72]. More recently, the PARP1 inhibitor Olaparib was approved for clinical trials for patients with recurrent HGG harboring IDH1 mutations. However, there was only a partial response in 2 of 35 patients, consistent with clinical reports describing PARP1 resistance in patients with BRCA

deficient ovarian and breast cancer, demonstrating the need to explore other biomarkers in recurrent IDH1 mutant cancers for understanding tumor resistance [125].

PARG Inhibitors

The process of PARylation by PARP1 and dePARylation by PARG is tightly regulated and critical to the DNA damage response in both SSB and DSB repair [126, 127]. PAR has several ADP-ribose units connected by glycosidic bonds. PARG is responsible for hydrolyzing ~90% of the glycosidic bonds between ADP-ribose units [128]. The degradation of PAR chains is critical for several cellular processes including DNA repair, and NAD^+ recycling [129, 130]. Particularly BER/SSBR, which is dependent on PARP and PAR degradation, is stalled because essential repair proteins are not able to access the site of DNA damage and remain bound to PAR [56, 131]. PARP1 remains stalled in its active state, and is unable to continue repair at other sites of damage [129].

Several PARP inhibitors have had success in clinical trials. However, clinical reports of PARPi resistance have elevated the interest in alternative approaches to induce synthetic lethality with PARG inhibitors (PARGi) [5]. Surprisingly, PARGi have had low success until recently because of low cell permeability [127, 132]. Until recently, PDD00017273 was the only potent, cell permeable PARGi that is commercially available, but has not been successful because of its poor stability *in vivo* [132]. However, more recent studies have reported the success of newly developed PARG inhibitors *in vitro* and *in vivo*, including potent inhibition of PARPi resistant BRCA 1/2 mutant cell lines [127, 132, 133]. Additionally, these studies reported that DNA damage caused by gamma radiation, oxidizing agents and alkylating agents improves the sensitivity of ovarian and IDH1 mutant glioma cells to PARG inhibition [130, 132, 133]. The enhanced sensitivity of HR deficient

cells to PARGi is likely associated with replication fork lesions leading to an accumulation of DSBs [56, 127, 129, 130]. Several reports have demonstrated that PARGi sensitivity is correlated with decreased expression of replication-associated proteins, leading to toxic hyperPARylation and replication catastrophe [56, 127, 133].

Despite elevated PARP1 and PARG protein expression and increased replication stress, many glioma cells and GSCs are insensitive to PARGi unless combined with RT or alkylating agents [56, 129, 130]. However, many glioma cells and GSCs are defective in NAD^+ biosynthesis [15, 35, 122], this is significant because PARP1 activation potential is limited by NAD^+ bioavailability, and therefore could impact the efficacy of PARGi. However, the extent that NAD^+ can be modulated in glioma cells to impact PARG inhibitor efficacy is unknown. Given the importance of NAD^+ for regulating PARP1 mediated DDR, it is extremely important to define how defects in NAD^+ biosynthesis impacts the efficacy of chemotherapeutics, especially those that target proteins involved in DNA repair and replication.

Targeting BER/SSBR

As mentioned previously, BER/SSBR repairs most DNA damage caused by alkylating agents [1, 13, 90]. Therefore, there has been increased interest in targeting BER/SSBR proteins in combination with alkylating agents to overcome chemotherapeutic resistance in glioma [134]. Just as critical to activation of PARP1 to the DNA lesion site is the complex it forms with XRCC1 and Polβ for the resolution of toxic BER intermediates [135]. XRCC1 serves as a scaffolding protein for recruitment and stabilization of DNA repair proteins such as aprataxin (APTX), OGG1, Polβ and LIGIII [117, 136, 137]. Cells deficient in XRCC1 are selectively sensitive to alkylating agents leading to toxic

hyperPARylation [138]. Deficiencies in XRCC1 are synthetically lethal in combination with ATM inhibitors [93].

Consistent with our studies, Hirota et al, reported XRCC1 deficient cells were more sensitive to alkylating agents than cells deficient in PARP1 or Polβ [8, 93]. Overexpression of XRCC1 in several patient-derived glioma tumors has been associated with a poor prognosis [138]. Further, overexpression of XRCC1 counteracted sensitivity of cancer cells to alkylating agents and PARP1 inhibitors, by facilitating the recruitment of BER/SSBR factors and the release of trapped PARP1 from the DNA lesion site [139-143]. Tebbs et al. reported Xrcc1 knock-out was lethal in mouse embryos but found that even reduced levels of XRCC1 supported healthy development, DNA repair, and normal sensitivity to alkylating agents [144].

Currently, there are no known inhibitors of XRCC1. Proteins that are not enzymes have been historically difficult to target, because their activities are dependent on protein-protein interactions, and are often labeled as "undruggable" [145]. However, the development of high-throughput drug-screening technology has advanced drug discovery for targeting protein-protein interactions [145]. Therefore, further research will be required to determine if targeting the protein-protein interactions of XRCC1 would be an effective treatment strategy for targeting chemotherapy resistant tumors.

Polβ overexpression has also been associated with resistance to alkylating agents in many tumor cell types including HGGs [131]. The removal of the damaged base leaves behind a SSB with a 3'-OH group and a toxic 5' deoxyribophosphate (dRP), formed as a product of APE1 [96, 135, 146]. The dRP lyase activity of Polβ serves an important role for preventing the buildup of toxic BER intermediates [147]. Failure of Polβ to form a

complex with XRCC1 at the lesion site leads to Polβ degradation and an accumulation of DSBs, because of the buildup of toxic intermediates, that is further enhanced by deficiencies in HR [135].

Several reports have demonstrated that Polβ deficiency is synthetically lethal in glioma cells deficient in HR in combination with alkylating agents or PARGi [8, 131]. Additionally, Polβ deficiency and defects in HR are reported to overcome resistance to alkylating agents caused by overexpression of MPG in glioma [60, 93, 96]. Polβ deficiency was also synthetically lethal in glioma cells deficient in MMR protein MSH2 associated with unresolved 8-oxoG lesions [87, 148, 149]. However, the development of a selective Polβ inhibitor has been challenging because of its structural similarity with other DNA polymerases. Recently, the development of a selective, covalent inhibitor of Polβ was reported to act synergistically with alkylating agents *in vitro*, but was not cytotoxic alone [150]. However, the effects of Polβ inhibition *in vivo* remain to be elucidated.

IDH1 Mutant Glioma

Mutations in the IDH1 gene occur primarily in cases of secondary glioblastoma (GBM) (85%) and low-grade glioma (65%) but are rare in primary GBM (5%), with the most common mutation occurring at IDH1 (R132H) (80%) [43]. The current treatment for GBM is surgery followed by radiation therapy combined with DNA alkylating agents [151, 152]. The prognosis for GBM patients with IDH1 mutant glioma is more favorable than IDH1 wildtype GBM because these tumors are sensitive to alkylating agents [152, 153]. However, over time, up to 75% of IDH1 mutant glioma cases progress to WHO grade IV glioblastoma and develop resistance to alkylating agents [97, 154]. Additionally, IDH1 mutations are often sustained during remission, leading to an increased risk of recurrence [97, 154]. Therefore, it is important to define the mechanism by which IDH1 mutant gliomas confer sensitivity to alkylating agents to develop a more targeted chemotherapeutic approach.

IDH1(R132H) is a gain of function mutation that couples with NADPH to reduce alpha-ketoglutarate (α-KG), leading to an overproduction of the oncometabolite 2-hydroxyglutarate (2-HG) [155]. Under normal conditions, IDH1 couples with $NADP^+$ to oxidize isocitrate to produce α-KG. Several cellular processes are altered because of 2-HG overproduction, including metabolism and epigenetic regulation of gene expression [40, 154].

IDH1 mutant gliomas are dependent on the metabolite NAD^+ to drive the production of 2-HG, leading to depleted cellular NAD^+ levels [47]. NAD^+ supply is further compromised by significantly reduced expression of NAPRT, an enzyme involved in NAD^+ synthesis [35]. NAD^+ is essential for cellular energy homeostasis and is responsible

for the regulation of cellular processes such as fatty acid oxidation, glycolysis, and the tricarboxylic acid cycle [35]. Given the significant role of NAD^+ for many cellular processes, exploiting the vulnerability of IDH1 mutant gliomas to depletion of NAD^+ has been an intense research interest for the development of new treatment strategies [35, 90].

In addition to the role in cellular metabolism, NAD^+ is an essential cofactor for poly (ADP-ribose) polymerases (PARPs) and NAD-dependent deacetylases (Sirtuins) in chromatin remodeling [1, 59, 62, 153]. PARP1 consumes NAD^+ in response to DNA damage [24]. Tateishi et al. reported that PARP1 drastically depleted NAD^+ levels in IDH1 mutant cells when treated with the DNA alkylating agent temozolomide (TMZ), and the hypersensitivity to TMZ was further enhanced in combination with inhibitors of nicotinamide phosphotransferase (NAMPT), an important enzyme involved in the NAD^+ biosynthesis pathway [90, 92].

Conversely, PARP1 inhibitors are similarly effective for enhancing the chemosensitivity of IDH1 mutant gliomas to alkylating agents [4, 72, 123, 134, 156]. Predictably, the inhibition of PARP1 reverses the effect of NAD^+ depletion by alkylating agents and inhibitors of NAMPT [130, 156]. Hypersensitivity of IDH1 mutant glioma to PARP inhibition is conferred by defects in HR DNA repair resulting in hypersensitivity to PARP inhibition [123, 156]. The mechanism by which HR is impaired in IDH1 mutant cancer is mediated by 2-HG inhibition of methyltransferases lysine demethylase 4A and 4B (KDM4A and KDM4B), resulting in hypermethylation of histone 3 lysine 9 (H3K9) and the suppression of repair factors involved in HR [72]. Defects in HR are reported to contribute to IDH1 mutant sensitivity to select DNA agents and synthetic lethality with PARP inhibitors, referred to as a state of BRCAness [156, 157]. Despite harboring defects

in HR repair, many cells are insensitive or have developed resistance to PARP inhibitors [158-161]. However, the therapeutic benefit of this approach remains ill-defined, considering the variable response observed in patients with IDH1 mutant glioma to PARP inhibitors [5, 130]. Therefore, it is crucial to uncover the mechanisms by which PARP1 and other factors regulate BER/SSBR in IDH1 mutant glioma.

BER is responsible for repairing base damage caused by oxidation, deamination, and alkylation [1, 92, 162]. Therefore, defects in BER increase the chemosensitivity of cancer cells to DNA damage caused by alkylating agents [91]. The process of repairing base damage occurs in a series of steps; beginning with the removal of the damaged base by one of the 11 damage-specific DNA glycosylases, incision by AP Endonuclease (APE1), DNA end processing facilitated by XRCC1 and Polβ, gap-filling by Polβ and ligation by Ligase III (LIGIII) [1].

The synchronized assembly and disassembly of BER repair factors relies heavily on DNA damage-induced synthesis of PAR, and NAD^+ bioavailability [62]. PARP1 hydrolyzes NAD^+ to facilitate and regulate the recruitment of DNA repair protein complex assembly such as XRCC1, Polβ and LIGIII [1, 59]. Previously, we demonstrated that NAD^+ is a regulating factor for PARP1 activity and can be modulated to suppress PARP1 activation or enhance PARP1 activation in response to DNA damage [56, 59, 62]. Further, we reported that XRCC1 and Polβ recruitment and complex formation is dependent on PAR accumulation at the lesion site. Therefore, fluctuations in NAD^+ impact the recruitment of XRCC1 and Polβ for complex assembly at the DNA lesion site [62].

However, just as critical as the role of PAR, is the complex it forms with XRCC1, which serves as a scaffolding protein for other BER proteins such as Polβ and LIGIII [62,

135]. Our lab and others have reported that XRCC1 deficient cells are hypersensitive to DNA damaging agents, leading to hyperaccumulation of PAR, and buildup of toxic BER intermediates [56, 62, 135]. Furthermore, overexpression of XRCC1, a phenotype found in many cancer cell types, provides resistance to alkylating agents [91, 134, 137].

XRCC1 recruitment of Polβ is necessary to prevent the buildup of 5'dRP lesions. Polβ is a bifunctional DNA polymerase responsible for DNA synthesis and 5'dRP lyase activity [146, 163]. The regulation of Polβ expression is important since overexpression of Polβ has been associated with resistance to alkylating agents, and deficiency in Polβ results in hypersensitivity to DNA alkylating agents leading to apoptosis and chromosomal degradation [150, 164-166].

Equally important to BER/SSBR protein complex assembly at the DNA lesion site, is complex disassembly facilitated by PARG. After DNA synthesis and ligation is complete, PAR is degraded by PARG followed by the disassembly of DNA repair complexes and chromatin reassembly [129]. Failure of PARG to hydrolyze PAR leads to toxic hyperPARylation, replication stress, ATR-CHK1 activation or apoptosis [127, 132, 133]. In an effort to overcome the emerging problem of PARP inhibitor resistance, small-molecule inhibitors of PARG have been developed to prevent dePARylation, which stalls replication in cell cycle phases G1/S and G2 [127]. Despite the importance of PARG for hydrolyzing PAR polymers, PARG inhibitors have been unsuccessful for inducing cytotoxicity unless combined with radiotherapy or alkylating agents [130].

Consistent with other reports, we found that GSCs and LN428 glioblastoma cells were insensitive to PARG inhibition unless co-treated with alkylating agents or radiation [56, 127, 130, 133]. Further, we demonstrated that GSCs and glioma cells have insufficient

NAD^+ to induce a robust PAR response following PARG inhibition. However, supplementation with NAD^+ precursor NRH significantly increased NAD^+ bioavailability and enhanced PARG inhibitor induced hyperPARylation and intra-S phase arrest leading to apoptosis [56]. Further, we demonstrated that BER/SSBR is required to process DNA damage encountered during replication since GSCs and glioma cells deficient in XRCC1 demonstrated synthetic lethality to PARG inhibition alone [56]. The importance of the BER/SSBR pathway for resolving DNA damage during replication is further supported since it was recently reported that PARG inhibition was synthetically lethal for cells deficient in Polβ [131].

Nageshima et al, recently reported that PARG inhibition combined with alkylating agents promoted selective sensitivity in IDH1 mutant glioma by inducing hyperPARylation and cellular NAD^+ depletion [130]. Further, co-treatment with a PARG inhibitor moderately enhanced sensitivity of recurrent, malignant IDH1 mutant tumors to alkylating agents. Currently, it is unknown how low NAD^+ and IDH1 mutational status impacts BER/SSBR response to alkylating agents or PARG inhibition [130]. Considering the importance of BER/SSBR pathway for the repair of replication independent and replication dependent DNA damage, it is important to define how BER/SSBR is modulated in IDH1 mutant glioma for predicting patient response to current chemotherapeutics.

Here, we report that overproduction of the oncometabolite 2-hydroxyglutarate in IDH1 mutant glioma cells suppresses BER/SSBR by significantly reducing Polβ protein expression, thereby increasing chemosensitivity of IDH1 mutant glioma to alkylating agents independent of NAD^+ bioavailability. Further, we find that PARG inhibition is synthetically lethal for IDH1 mutant glioma deficient in Polβ, and NRH can enhance

cellular NAD^+ to enhance ATR-Chk1 mediated cell death in IDH1 mutant glioma. These studies highlight the importance of BER for maintaining genome stability and supports ongoing efforts to target BER enzyme activity as a strategy to sensitize or re-sensitize drug resistant GBM to chemotherapeutics.

CHAPTER II: MATERIALS AND METHODS

Cells and Cell Culture Conditions

Glioma stem cells (GSCs) were derived from high-grade glioma tumors and were either a mesenchymal subtype (GSC-83, GSC-326) or a proneural subtype (GSC-19, GSC-84), and maintained as previously described [75, 167]. LN428 is an established glioblastoma cell line with mutations in PTEN and p16 [57]. A549 and U2OS cells were purchased from ATCC. LN428 cells were maintained in MEM media supplemented with FBS (10% heat inactivated), 1% anti-anti (antibiotic and antimycotic) (Gibco, cat#15240-062) and 1% glutamax (Gibco, cat#35050061). U2OS and A549 cells were cultured in DMEM media, 10% FBS, 1% Pen-strep, 1% glutamine. U-87 MG (ATCC, Cat# HTB-14) and U-87 IDH1 (R132H) (ATCC, Cat# HTB-14IG) glioma cell lines were purchased from ATCC. U-87 MG and U-87 IDH1-R132H cells were cultured in Eagle's Minimum Essential Media (EMEM) (ATCC, cat#30-2003) with 10% heat-inactivated fetal bovine serum (Biotechne, Cat#S11150) and 1% Pen-strep (Gibco, cat#15070-063). All cells were maintained at 37°C with 5% CO_2. U-87MG IDH1 (R132H) mutant cells were maintained only until passage #7 to control for high mutability in these cell lines.

Quantitative Real-Time PCR (qRT-PCR)

The expression of PARP1, PARP2, XRCC1, PolB, LIGIII and APTX mRNA was determined using Taqman Gene Expression Assay probes from Life Technologies. PARP1: probe ID: Hs00242302_m1; XRCC1: Hs00959834_m1, PARP2:

Hs00193931_m1PolB:Hs01099715_m,LIGIII:Hs00242692_m1,PCNA:Hs0069686 3_g1, APTX: Hs00544364_m1. β-Actin (probe ID: Hs99999903_m1) was used as an internal control. ABI StepOnePlus RT-PCR system was used to perform qRT-PCR reactions according to the manufacturer's protocol. mRNA expression was analyzed per the instruction of the manufacturer (ΔΔCT method). Samples were repeated in triplicate and the results shown are the mean ±SEM of three analyses.

PARP1 and XRCC1 Knockout by CRISPR/Cas9

Guide RNAs (gRNAs) targeting PARP1 or XRCC1 were provided by Wim Vermeulen, (Erasmus MC, Netherlands), and created using the CRISPR Design Tool [168], as previously described. Each separate gRNA was cloned into pLentiCRISPRv2 lentivirus, produced to then transduce LN428 cells, as previously described [62]. PARP1 or XRCC1 knockout was confirmed by immunoblot analysis of whole cell lysates.

ORC2 Knockout by CRISPR/Cas9 in LN428 Cells

LN428/ORC2-KO cells were created by transfection of ribonucleoprotein complexes including Cas9 and a mixture of three single-guide RNAs (sgRNAs) [169] targeting an early exon of the ORC2 gene (Synthego). LN428 cells were seeded at a density of $2x10^5$ cells per well (6-well plate). After 24 hours incubation, the cells were transfected with a mixture of sgRNAs, Cas9 and the CRISPRMAX-Cas9 transfection reagent (Cat# CMAX00008, Thermo Fisher Scientific) in serum-free OptiMEM (Cat# 31985070, Thermo Fisher Scientific). After 48 hours, media containing the transfection reagent was

replaced with fresh media and allowed to grow for another two days. Validation of gene knockout was then confirmed by immunoblot using whole cell lysates, as compared to control. The primary and secondary antibodies used are listed in **Appendix B**.

Cell Extract for Immunoblot Analysis

Cells were seeded at a density of 3×10^5 cells in 2 mL of normal growth media in a single well of a 6-well dish. Cells were lysed in 100µl of 2x clear laemmli buffer (65.8 mM Tris-HCl, pH 6.8, 2.1% SDS, 26.3% (w/v) glycerol). Whole cell lysates were heated at 95°C for 10 minutes followed by centrifugation at 1200 RPM for 5 minutes. The supernatant was collected, and samples were prepped by adding sample buffer (4x clear Laemmli buffer, 0.005% bromophenol blue, 5% β-mercaptoethanol) (v/v) to lysate. Samples were vortexed, then heated at 95°C for 5 minutes. Samples were cooled to room temperature, then centrifuged at 1200 RPM for 5 minutes.

Immunoblot

Whole cell protein lysates (30µg protein) were loaded onto precast NuPAGE® Novex® 4%–12% Bis-Tris gels and electrophoresed for 1hr at 120V. Following gel electrophoresis, proteins were transferred onto a nitrocellulose membrane using a Turboblotter (Bio-Rad). The membrane was rocked in blocking buffer (TBS buffer with 0.05% Tween-20 and supplemented with 5% blotting grade non-fat dry milk; Bio-Rad) for 1 hr at room temperature and subsequently incubated with primary antibodies diluted in blocking buffer overnight at 4°C. The primary antibodies and their dilutions are listed in the key resources table in **Appendix B**. After washing, membranes were incubated with secondary antibodies

diluted in blocking buffer for 1 hr at room temperature. The following HRP conjugated secondary antibodies were used: Bio-Rad Goat anti-mouse-HRP conjugate and Bio-Rad anti-rabbit-HRP conjugate (see key resources table in **Appendix B**). After washing, the membrane was illuminated with a chemiluminescent HRP substrate (Cat# PI34035, Fisherscientific), and imaged using a Bio-Rad Chemi-Doc MP imaging system. ImageLite software was used to quantify protein bands and normalized to B-actin or PCNA control.

PAR Immunoblot Lysate Prep and Analysis

Cells were seeded at a density of $3x10^5$ cells per well in a 6-well tissue culture treated plate, in 2 mL of normal growth media and allowed to grow overnight. Cells were treated with MNNG (10μM, 20μM, or 30μM), NRH (100μM) or PARGi (10μM) as described in the figure legends. Cells were treated with the following inhibitors, as described below and in the legends: PARP1/2 inhibitor (ABT-888, Veliparib; Tocris, Cat#7026); PARG inhibitor (PDD00017273; Tocris, Cat#5952/1). U2OS, A549 and LN428 cells were seeded in 100mm plates at a density of $5x10^5$ cells/well and cultured overnight for 18 hrs. Cells were then treated with FK866, NRH, ABT-888 or H_2O_2 as indicated in the figure legends and as follows: For FK866 treatments, cells were treated with FK866 (50nM) and cultured for another 24 hr before lysis; for NRH treatments, cells were treated with NRH (100μM) for 4 hr before lysis; for ABT-888 treatments, cells were treated with ABT-888 (10μM) for 1 hr before lysis and for H_2O_2 treatments, cells were treated with H_2O_2 (100μM or 300μM) for 15 mins before lysis. To prepare PAR-stable whole cell lysates, cells were washed 3x with cold 1 X PBS and lysed in 500μL (100mm dish) and 100μL (6-well dish) of 2x clear

laemmli buffer (2% SDS, 20% glycerol, 62.5mmol/l Tris-HCl pH6.8). Cells were washed twice with 1X PBS, PBS was aspirated and cells were lysed in 100µL of 2x clear laemmli buffer (2% SDS, 20% glycerol, 62.5mmol/l Tris-HCl pH6.8). Cell lysates were then heated at 95°C for 15 mins followed by centrifugation for 5 mins at 1200 rpm. Immunoblot samples were prepared v/v with 4x blue Laemmli buffer (4x clear Laemmli buffer, 0.005% bromophenol blue, 5% β-mercaptoethanol) and heated for an additional 5 minutes at 95°C then centrifuged for 5 minutes at 1200 rpm. Lysates (30µg protein) were loaded on a 10-well or 15-well NuPAGE, Novex 4%–12% Bis-Tris gel, and allowed to run for 1 hr at 120V. Gel electrophoresis separated proteins were transferred onto a nitrocellulose membrane using a Turboblotter (Bio-Rad). The nitrocellulose membrane was placed on a rocker in blocking buffer (1X TBST + 5% milk) at room temperature for 30 mins. The membrane was then incubated in PAR antibody (1:1000) diluted in blocking buffer overnight at 4°C. The following day, the membrane was washed 3x in TBST (5 min) and the secondary antibody was allowed to incubate on the membrane at room temperature for 1 hr. The following HRP conjugated secondary antibody was used: Bio-Rad Goat anti-mouse-HRP conjugate (see key resources table found in **Appendix B**). After washing, the membrane was illuminated with a chemiluminescent substrate. Protein bands were imaged using a Bio-Rad Chemi-Doc MP imaging system.

Cell Viability Analysis

U-87 MG and U-87 IDH1-R132H cells were seeded at a density of 800 cells per well in a Black, culture treated, 96-well dish and treated with MNNG with a top dose of 1µM and a 1:2 serial dilution for 5days (120 hours); MMS with a top dose of 4mM and a 1:2 serial

dilution for 5 days (120 hours); PDD00017273 with a top dose of 10μM and a 1:2 serial dilution or NRH (100μM) or PDD00017273 with a top dose of 10μM and a 1:2 serial dilution. After 5 days, each well was washed with 200μL of 1X PBS. 40μL of PBS was added to each well and cell viability was determined using the CellTier-Fluor Cell viability kit (Promega, cat#G6080) according to the manufacturer's instructions. Fluorescence values were determined using the Cytation 7 plate reader with Gen5 software (Biotek). Cell viability was determined as a percent of fluorescence compared to DMSO control. For LN428, LN428/XRCC1-KO and LN428/PARP1-KO, cells were treated with PDD00017273 with a top dose of 10μM and a 1:2 serial dilution or NRH (100μM) and PDD00017273 with a top dose of 10μM and a 1:2 serial dilution. After 5 days, each well was washed with 200 μL of 1X PBS. Hoechst 33342 nucleic acid stain was added to 1X PBS (1:2000) 200μL/well and cells were incubated at 37°C with 5% CO_2 for 15 minutes. The cells were washed with 1X PBS and fluorescent images of each well were acquired using Celigo Image Cytometer (Nexcelom), and nuclei positive for Hoechst stain were counted and automatically.

NAD^+ Measurements

The cellular level of NAD^+ and NADH was measured using the Enzychrome NAD^+/NADH colorimetric assay kit (BioAssay Systems, Cat#E2ND-100), following the supplier-provided protocols with minimal changes, as we have described previously [57]. Cells were seeded in a 6-well plate at a density of $2x10^5$ cells per well for NAD^+ measurements and $3x10^5$ cells per well for NAD^+ pool measurements (NAD^+ plus NADH). After 24 hours,

cells were treated with NRH (100μM) for 0, 0.5, 1, 2, 4, 8 or with FK866 (50nM) for 24 hours. Following treatment, cells were harvested and a suspension of $2x10^5$ cells were divided in half for measuring NAD^+ and NADH, respectively, or a suspension of $1x10^5$ cells was used for the NAD^+ measurement only. Cell pellets were immediately homogenized using plastic pestles and the extraction of NAD^+ and NADH was performed in the provided lysis buffers. Extracts were heated at 60°C for 5 min and neutralized with the provided buffers. Samples were centrifuged at 14,000 RPM and the supernatant was immediately assayed for measurements of NAD^+/NADH content using a Microplate Reader (BioTek) at 565 nm. U-87 MG and U-87 IDH1 (R132H) cells were seeded at a density of $2.5x10^4$ cells in full culture media in each well of a white, 96-well, culture-treated plate and allowed to incubate overnight at 37°C. The following day, cells were treated with a DMSO control and PDD00017273 (10μM) or NRH (100μM) for 1, 2, 4, 6, and 8 hours. Cells were lysed in 25μL of 200 μM NaOH + 1% DTAB. Protein concentrations were measured by Nanodrop A280 analysis. Each sample was diluted in 80μL of NaOH+1% DTAB and 25μL of each sample was moved to 4 new wells for individual measurements of NAD^+, NADH, $NADP^+$ and NADPH using the Promega NAD/NADH-Glo Assay (Cat# G9071) and Promega NADP/NADPH-Glo Assay (Cat# G9081). NAD^+ metabolite measurements were carried out according to manufacturer's instructions.

Poly-ADP-ribose (PAR) Immunoprecipitation (IP)

GSC-83 cells were treated with thymidine (2mM) for 48 hours. Half of the cells remained in growth medium with thymidine (2mM) for 1 hour and then supplemented with NRH

(100μM)/PARGi (10μM) for 1 hour. The cells were then collected for PAR analysis by immunoblot or for PAR-IP (PAR-IP, control). For replication release, cells were washed once with 1X PBS (10ml) and cultured in normal growth medium for 1 hour followed by a treatment with NRH (100μM) and PARGi (10μM) for 1 hour (PAR-IP, 1hr thymidine release). For each, PAR-modified or PAR-bound proteins were then either evaluated by immunoblot or isolated by incubating cell lysate with PAR-agarose resin (Tulip Biolabs, Cat# 4306) as per the manufacturer's instructions.

BioID Proximity Protein Labeling

LN428 and GSC-83 cells were transduced with a lentiviral vector expressing a PARP1-BirA fusion protein. Viral transduction was carried out as described above. LN428/PARP1-BirA and GSC-83/PARP1-BirA cells were seeded in a 150 mm, culture treated dish at a density of 3-5x10^7 cells per dish and allowed to incubate overnight. The following day, cells were supplemented with thymidine (2mM) for 48 hours. On the 5^{th} day, media was aspirated, and cells were washed with 1X PBS. Cells were replenished with full culture media +/- thymidine and co-treated with NRH and PARGi, as indicated in the figure legends. Cells were supplemented with 100 mM biotin for 1 hour prior to lysis. Cells were washed 2 times in ice cold 1X PBS, scraped in 10 mL of ice-cold 1X PBS, transferred to a 15mL conical tube, and centrifuged for 5 min at 1200 rpm. PBS was removed and were lysed with 500mL of IP lysis buffer (1.2 mM EDTA, 16.7 mM Tris HCl pH 8, 150mM NaCl, 1 mM PMSF, protease inhibitors) and transferred to a 1mL microfuge tube, 50mL of cell lysate was reserved for input analysis, and the remaining cell lysate was rolled with 50 mL streptavidin magnetic beads for 18 hours. The following day, cells were washed 3x

in wash buffer #1 (0.2% SDS in milliQ water), wash buffer #2 (0.1% deoxycholate, 1% Triton X-100, 500mM NaCl, 1mM EDTA, 50 mM HEPES pH 7.5), wash buffer #3 (250 mM LiCl, 0.5% NP-40, 0.5% deoxycholate, 1mM EDTA, 10mM Tris pH 8.1) and wash buffer #4 (50 mM Tris pH 7.4, 50mM NaCl) for 5 minutes each. Proteins were eluted in 50 mL of elution buffer (2% SDS, 25mM biotin in wash buffer #4) and boiled for 15 minutes, then analyzed by immunoblot.

DNA Fiber Assay

DNA replication fork progression was determined by the Replication Combing Assay (Genomic Vision, Cat# EXT-001). LN428 cells were grown to 30% confluency in 100 mm dishes and treated with DMSO, NRH (100μM), PARGi (10μM) or co-treatment with NRH and PARGi for 4 hours. Following the treatment, cells were labeled with IdU (25μM) for 30 minutes. Cells were washed 2 times with 1X PBS, trypsinized and centrifuged at 800 x g for 5 minutes. Cells were washed with 1X PBS twice and the pellet was resuspended in an agarose plug followed by cell lysis and agarose gel digestion in disposable DNA reservoirs (Genomic Vision, Cat# RES-001). Stretching the naked DNA on coverslips (Genomic Vision, Cat# RES-001) was performed as described by the manufacturer. Cover slips were dehydrated at 65°C for 2 hours followed by immunostaining. Cover slips were blocked for 30 minutes with Block Aid, followed by staining with mouse anti-BrdU (40μl) and rat anti-BrdU (8μl) in 1632μl of Block Aid for each cover slip (1 hour). Coverslips were washed with 1xPBS-Tween 0.05%, 3 times for 5 min each, on an orbital agitator plate (100 RPM) followed by addition of 2μL of goat anti-mouse Cy3 in 1998μL of Block Aid. Coverslips were then washed with 1xPBS-Tween 0.05%, 3 times for 5min each, on an

orbital agitator plate (100 RPM). Coverslips were mounted on a microscope slide using Prolong Gold antifade mounting media (Invitrogen, P36934) and the slides were imaged by confocal microscopy. NIS elements software length measurement tool was used to measure fiber length, graphed using Prism 8 (Graphpad Prism) and statistical significance determined by one-way Anova analysis.

Chemicals and Reagents

All chemicals and reagents used for these experiments are listed in the key resources table found in **Appendix B**. Dihydronicotinamide Riboside (NRH; 1-[(2R,3R,4S,5R)-3,4-Dihydroxy-5-(hydroxymethyl)tetrahydrofuran-2-yl]-4H-pyridine-3-carboxamide) was prepared as described [22], provided by Dr. Marie Migaud. NRH was dissolved in distilled H_2O to prepare a stock solution (100mM) and stored at -80˚C. FK866 (NIMH #F-901; IUPAC name: (E)- [4-(1-Benzyoylpiperidin-4-yl)butly]-3-(pyridin-3-yl)acrylamide; CAS number: 201034-75-5) was obtained from the National Institute of Mental Health Chemical Synthesis and Drug Supply Program (Bethesda, MD). FK866 was dissolved in DMSO to prepare a stock solution at a concentration of 1 mM and stored at -80˚C. 1-Methyl-3-nitro-1-nitrosoguanidine (MNNG) (Sigma-Aldrich, Cat# 129941), was dissolved in DMSO for a stock solution of 100mM. Methyl methane sulfonate (MMS) (Thermo Fisher Scientific, Cat# 156891000) was dissolved in DMSO for an 8M stock solution. D-2-Hydroxyglutaric Acid (Cayman Chemical, Cat# 25895) was prepared in DMSO under inert gas in a 100mM stock solution. PDD00017273 (Torcis, Cat# 5952) was dissolved in DMSO for a 10mM stock solution.

Lentivirus Production

Lentiviral transduction was performed as follows: cells ($1x10^5$) were seeded into 6-well plates. The following day, lentiviral particles (1ml) were added to 1 mL of normal cell culture media with polybrene (2mg/ml). Cells were incubated at 32˚C overnight, lentiviral particles were aspirated from cells and replaced with 2mL of normal culture media. For stable cell lines: cells were cultured for 48 hr at 37˚C, then placed in selection media (normal growth media + 100 μg/mL puromycin or hygromycin) for 1-2 weeks.

Lentiviral Transduction

Lentiviral particles were generated by co-transfection of 4 plasmids into 293-FT cells using the TransIT-X2 Transfection reagent, including the packaging vectors (pMD2.g(VSVG), pVSV-REV and pMDLg/pRRE) and the Cas9 and gRNA expressing shuttle vectors designed to target PARP1 or XRCC1 (kindly provided by Wim Vermeulen, Erasmus MC, Netherlands). Lentivirus-containing supernatant was collected 48 hrs after transfection and then passed through 0.45mM filters to isolate the viral particles free from cell debris, as described previously [7, 12]. The lentivirus particles were then further concentrated using Lenti-X Concentrator (Takara Bio, Cat# 631231), as per the manufacturer's instructions.

Laser Micro-irradiation

For laser micro-irradiation, 4×10^4 cells were seeded into each well of an 8-chamber glass bottom vessel (Cat# 155409, Thermo Fisher Scientific). After 24 hours, laser micro-irradiation was performed using a Nikon A1r confocal microscope equipped with equipped with 6 visible wavelength lasers 405, 441, 514, 561 and 647nm, coherent and a customized

355-nm UVA laser. Cells were treated with FK866 (50nM) were cultured for another 24 hr before laser microirradiation. Cells were treated with NRH (100 mM) for 4 hours before laser microirradiation. Cells were maintained with humidity at 37°C and 5%. Live cells were imaged using a 40x (NA = 1.4) oil-immersion objective. A 355nm laser was used for micro-irradiation, cells were stimulated for 2.5s per site with the 355-nm laser in parallel, and time lapse images were collected every 15 s during a 10-20 min interval. For U-87MG/EGFP-Polβ and U-87MG/IDH1 (R132H)/EGFP-Polβ a 355nm laser was used for micro-irradiation, cells were stimulated for 5s per site with the 355-nm laser in parallel, and time lapse images were collected every 2s during a 2 min interval. Images of focal recruitment were quantified using MIDAS (Microirradiation detection analysis system) for quantitation of and statistical analysis of focal recruitment, described previously [58]. Forty individual cells (2 sets of 10 cells were performed on 2 separate days) were analyzed and used to generate recruitment profiles and kinetic parameters.

Immunofluorescence Confocal Microscopy

For immunofluorescence analysis of LN428/LivePAR cells, $5x10^4$ cells were seeded into each well of an 8-chamber cover-glass bottom vessel (Thermo Fisher Scientific, Cat# 155409). Cells were fixed with 100% ice cold methanol for 5 minutes, followed by 4% paraformaldehyde for 10 min and permeabilized with a 0.3% Triton X-100 solution in 1X PBS for 10 min. Cells were washed with 1X PBS and blocked in blocking buffer (10% normal goat serum, 0.1% TBS, in 1X PBS) for 30 min and incubated with the PAR (1:400), PCNA (1:400) or RPA (1:250) primary antibodies in antibody dilution buffer (1% normal bovine serum, 0.1%TBS in TBS) for 1 hr at room temperature, cells were washed 3 times

with 1X PBS and incubated with goat anti-mouse antibody conjugated to Alexa 568 (1:500) and a goat anti-rabbit antibody conjugated to Alexa 647 (1:500). Nuclei were stained with NucBlue Fixed (Thermo Fisher Scientific, Cat# R37606). Fixed cells were imaged with a Nikon A1r laser scanning confocal microscope, using a 20x objective.

ATP and Cell Membrane Integrity Measurements

U-87 MG and U-87 IDH1 (R132H) mutant cells were seeded in a white, culture treated 96-well plate, at a density of $1.0x10^5$ cells/well in serum free media, supplemented with 5% glucose or 1% galactose, and allowed to incubate for 24 hours. The following day, the media was aspirated from each well, and cells were treated with NRH (6 hours) at the doses indicated in the figure legends. Cell membrane integrity and ATP measurements were determined using multiplex Mitochondrial ToxGlo Assay (Promega, Cat# G8000) according to manufacturer's instructions.

Statistical Analysis

Data is represented as the mean +/- standard deviation from 2-4 independent experiments. Student's t-test was used for comparisons between two groups. For multiple comparisons, one-way ANOVA or two-way ANOVA was used. Averages and standard error of the mean (SEM) were calculated from the means (on technical replicates) of multiple independent experiments (n = number of independent experiments) unless stated otherwise. P values are listed in the figure legends as follows: *$p < 0.05$, **$p < 0.01$, ***$p < 0.001$, ****$p < 0.0001$. Statistical analyses were performed using GraphPad PRISM apart from values determined in MIDAS.

CHAPTER III: RESULTS

NAD^+ Bioavailability Regulates PARP1 Activation Potential in Response to DNA Damage

For these studies, we chose three tumor derived cell lines: U2OS, an osteosarcoma cell line; A549 CCL-185, a lung carcinoma epithelial cell line; and LN428, a glioblastoma cell line, as models for evaluating the impact of NAD^+ bioavailability on PARP1 activation and BER/SSBR protein recruitment in response to DNA damage. To determine the extent we can modulate cellular NAD^+ levels in each cell line, we performed an NAD^+ analysis following treatment with the NAMPT inhibitor FK866, and a time course analysis following supplementation with the NAD^+ precursor NRH. Consistent with previous reports, our preliminary NAD^+ analysis revealed that NRH was significantly more potent in LN428 cells as compared to other NAD^+ precursors (NR, NMN, NAR, NARH) (**Appendix figure A.4**) [29, 32]. Hence, we utilized NRH for the purpose of enhancing cellular NAD^+ bioavailability in LN428, U2OS and A549 cells.

Each cell line was treated with 50nM FK866 for 24 hours, or treated with NRH for 0.5, 1, 2, 4, or 8 hours, and whole cell lysates were analyzed for NAD^+/NADH concentration. Following FK866 treatment, we observed an ~80% decrease in cellular NAD^+ levels across all cell lines (**Figure 3.1A-C**). This is consistent with previous studies by our lab and others, that observed a significant decrease in cellular NAD^+ levels in all cell lines treated with FK866 [37, 57].

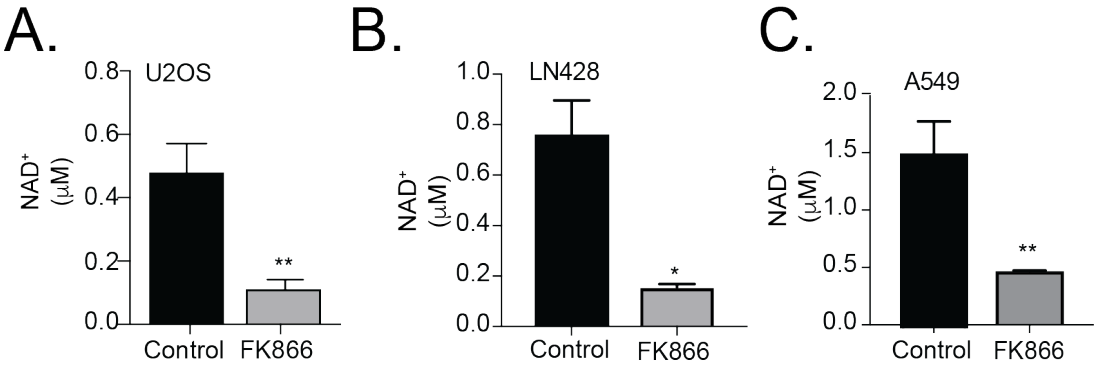

Figure 3.2. FK866 decreases cellular NAD$^+$ levels.

A. U2OS NAD$^+$ levels after 24-hour treatment with FK866 (50nM) treatment, n=6 (**p<0.01; Student's T test); B. LN428 NAD$^+$ levels after 24-hour treatment with FK866 (50nM) treatment, n=6 (*p<0.05; Student's T test); C. A549 NAD$^+$ levels after 24-hour treatment with FK866 (50nM) treatment, n=6 (**p<0.01; Student's T test).

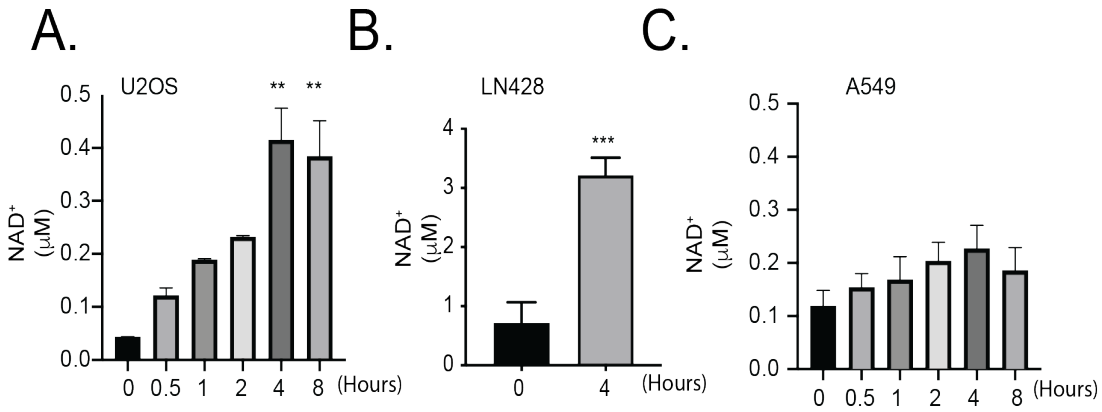

Figure 3.1. NRH enhances cellular NAD$^+$ levels in U2OS and LN428 cells but not A549 cells.

A. Measurement of NAD$^+$ levels in U2OS cells following time course treatment with NRH (100μM) n=3 (**p<0.01; One-way ANOVA); B. Measurement of NAD$^+$ levels in LN428 cells following 4-hour treatment with NRH (100μM) n=3 (***p<0.001; Student's T test); C. Measurement of NAD$^+$ levels in A549 cells following time course treatment with NRH (100 μM) n=3 (One-way ANOVA).

Following supplementation with NRH, U2OS cells reached maximal peak NAD$^+$ levels between 4-8 hours of treatment with an ~8-fold increase **(3.2A)** in cellular NAD$^+$,

and LN428 cells reached maximal peak NAD^+ levels after 4 hours with a 3-4-fold increase in cellular NAD^+ (**Figure 3.2B**). However, there was no significant change in cellular NAD^+ levels in A549 cells, following supplementation with NRH (**Figure 3.2C**), [170] possibly because A549 cells have lower protein levels of ADK, NMNAT1 or because of NADH to NRH conversion by NUDT family proteins [62].

Further, there were no observed changes in NADH in A549 or U2OS cells (**Figure 3.3A-B**). Therefore, the A549 cell line provided an opportunity to observe the effects of NRH on PAR formation and BER complex assembly and disassembly independent of an increase in NAD^+ levels. To determine the effects of NAD^+ bioavailability on PAR formation following DNA damage, we treated cells with 200μM and 300μM H_2O_2 for 15 minutes alone or co-treated with FK866 or NRH and determined PAR formation by immunoblot analysis. Reactive oxygen species (ROS), such as H_2O_2, produced as a byproduct of cellular metabolism, are responsible for endogenous oxidative DNA damage resulting in base lesions that are primarily repaired by BER/SSBR [171, 172].

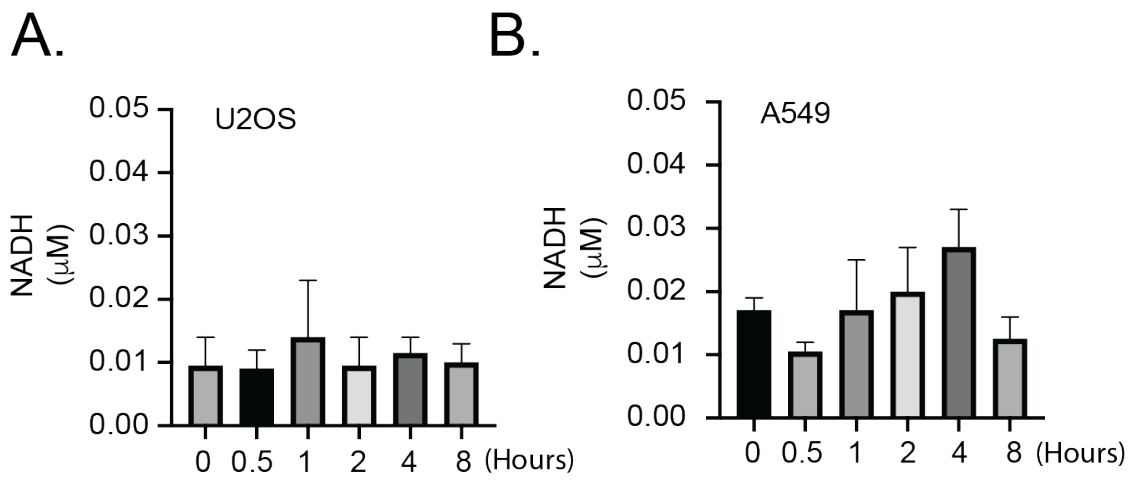

Figure 3.3. NADH analysis following treatment with NRH.

A. Measurement of NADH levels in U2OS cells following time course treatment with NRH (100μM), n=3 (One-way ANOVA). B. Measurement of NADH levels in A549 cells following time course treatment with NRH (100μM), n=3 (One-way ANOVA).

Following treatment with H_2O_2 alone, we observed a dose response increase in PAR formation in H_2O_2 treated U2OS (**Figure 3.4**), LN428 (**Figure 3.5**) and A549 (**Figure 3.6**) cells as compared to the control, which is consistent with reports from our lab and others demonstrating that H_2O_2 induces DNA damage and PARP1 activation within the 50μM-300μM dose ranges [171, 173, 174]. Since NAD^+ is required for PAR synthesis, we reasoned that low NAD^+ bioavailability would greatly reduce PAR formation. We treated cells with FK866 for 24 hours, 15 minutes prior to lysis, cells were treated with 200μM H_2O_2, 300μM H_2O_2 or media only. In-line previous reports from our lab, FK866 treatment completely abrogated PAR accumulation even in the presence of H_2O_2 in all three cell lines [57].

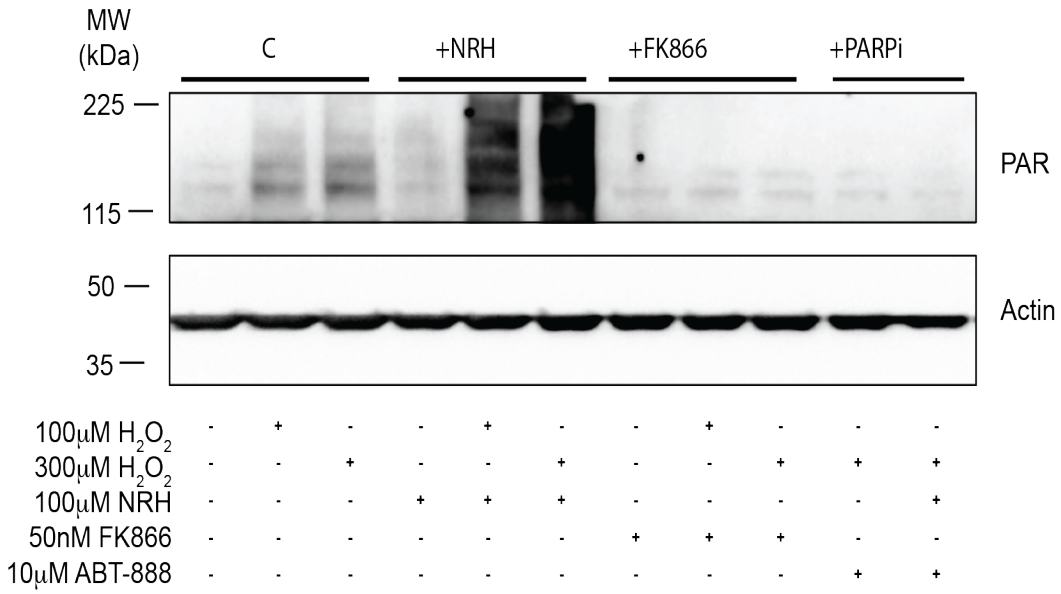

Figure 3.4. NAD$^+$ bioavailability regulates PAR accumulation in response to DNA damage in U2OS cells.

Immunoblot analysis of PAR in U2OS cells, following treatment with H_2O_2 (200μM or 300μM, 15 min.) compared to H_2O_2 and pre-treatment with NRH (100μM, 4 hours), H_2O_2 and pre-treatment with FK866 (50nM, 24 hours), H_2O_2 and ABT-888(10 μM, 1 hour) or H_2O_2 and pre-treatment with NRH (4 hours) and ABT-888 (1 hour).

Based on our model, reasoned that enhanced NAD$^+$ should induce a robust PAR response following DNA damage (**Figure 1.3**). U2OS, A549 and LN428 cells were treated with NRH for 4 hours. Prior to lysis, cells were treated with either 200μM H_2O_2, 300μM H_2O_2 or media only. Following treatment with NRH alone, we did not observe a change in PAR accumulation as compared with the control in U2OS, A549 or LN428 cells. However, when U2OS and LN428 cells were co-treated with NRH and H_2O_2 we observed a robust increase in PAR formation compared with either NRH or H_2O_2 treatment alone. We did not observe an increase in PAR accumulation in A549 cells co-treated with NRH and H_2O_2 as compared to H_2O_2 treatment alone. This data is consistent with the NAD$^+$/NADH assays in which NRH treatment significantly increased cellular NAD$^+$ in both U2OS cells (**Figure**

3.4) and LN428 cells (**Figure 3.5**) but did not significantly increase cellular NAD^+ levels in A549 cells (**Figure 3.6**). To support our hypothesis that the observed PAR formation was a result of PARP1 activation, we co-treated each cell line with NRH, H_2O_2, and 10μM ABT-888, a small molecule inhibitor that blocks the catalytic activity of PARP1 and PARP2 [109]. Co-treatment with ABT-888 in the presence of NRH and H_2O_2, completely suppressed the PAR signal in U2OS (**Figure 3.4**) and A549 (**Figure 3. 6**).

Together, these data support our hypothesis that NAD^+ is a regulating factor for PARP1 activity and can be modulated to suppress PARP1 activation (FK866) or enhance PARP1 activation (NRH) in response to DNA damage in U2OS and LN428 cell lines. Our hypothesis is further supported since inhibition of PARP1 and PARP2 activity by ABT-888 completely extinguishes the PAR signal in the presence of H_2O_2 alone and when combined with NRH. Further, since there was no observable change in the PAR signal when A549 cells were co-treated with NRH and H_2O_2, as compared to H_2O_2 alone, our data supports the conclusion that the increased PAR accumulation observed following treatment with NRH and H_2O_2 is due to increased NAD^+ biosynthesis from NRH and not as an off-target effect.

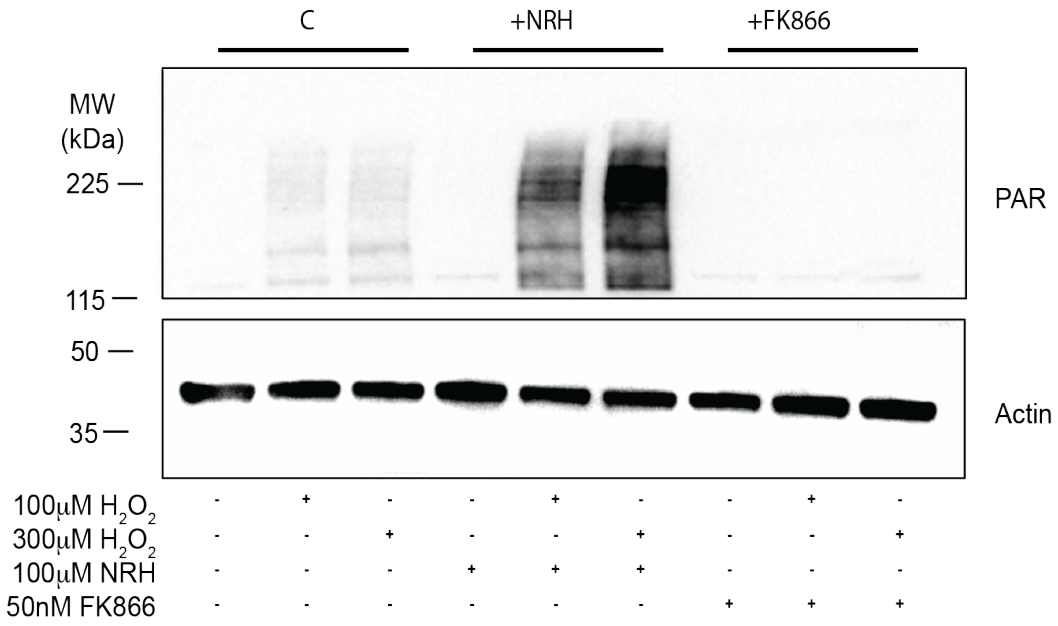

Figure 3.5. NAD^+ bioavailability regulates PAR accumulation in response to DNA damage in LN428 cells.

Immunoblot analysis of PAR in LN428 cells following treatment with H_2O_2 (200μM or 300μM) for 15 min. compared to H_2O_2 and pre-treatment with NRH (100μM) for 4 hours or H_2O_2 and pre-treatment with FK866 (50nM) for 24 hours.

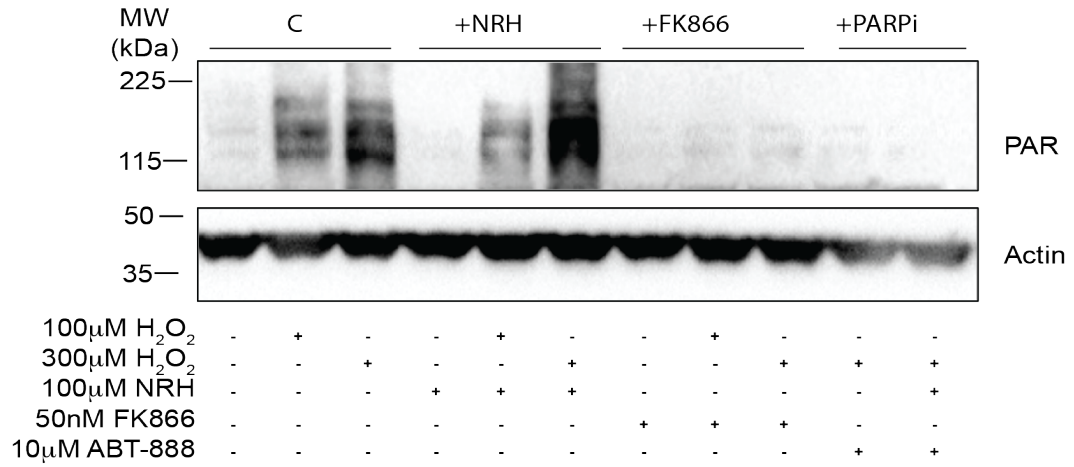

Figure 3.6. NAD$^+$ bioavailability regulates PAR accumulation in response to DNA damage in A549 cells.

Immunoblot analysis of PAR in A549 cells following treatment with H_2O_2 (200μM or 300μM, 15 min.) compared to H_2O_2 and pre-treatment with NRH (100μM, 4 hours), H_2O_2 and pre-treatment with FK866 (50nM) 24 hours, H_2O_2 and ABT-888 (10μM,1 hour) or H_2O_2 and pre-treatment with NRH (4 hours) and ABT-888 (1 hour).

The Effect of NAD$^+$ Modulation on PARP1 Activation and the Dynamics of BER/SSBR Protein Complex Assembly and Disassembly

As we demonstrated, depletion of cellular NAD$^+$ by FK866 causes suppression of PARP1 activation in response to DNA damage in U2OS, A549, and LN428 cells. Whereas supplementation with NRH increased cellular NAD$^+$ in U2OS and LN428 cells, resulting in robust PAR activation, it had no effect on cellular NAD$^+$ or PAR formation in A549 cells. Therefore, to next determine how NAD$^+$ bioavailability impacts PARP1 activation and the subsequent recruitment of essential BER/SSBR proteins (XRCC1 and Polβ) at the DNA lesion site, we applied confocal laser microirradiation, using a 355-nm laser, to induce site-specific DNA damage.

Laser microirradiation with a UVA 355-nm laser has been reported to cause mostly base damage and single-stranded DNA breaks, with very few double-stranded DNA breaks, and microirradiation with a 405-nm laser is reported to induce both DSBs and SSBs [175]. To validate that most of the damage caused by the 355-nm laser was not DNA double-stranded breaks, we quantified the recruitment of fluorescently labeled 53BP1, a protein involved in DSBR, to the site of laser induced DNA damage after stimulation with either a 405-nm laser or by stimulation with the 355-nm laser [176, 177]. We found that 53BP1 responded to stimulation with the 405-nm laser, however, did not respond to stimulation with the 355-nm laser, suggesting that the 355-nm laser does not produce measurable DNA double-stranded breaks (Koczor et al, supplemental figure S1A and S1B) [58].

To quantify the assembly/disassembly of fluorescently labeled BER proteins to sites of laser-induced DNA damage we used MIDAS (Modular Irradiation Detection Analysis System), a software package created for the acquisition, stimulation (irradiation) and analysis of data from microirradiation experiments. Following laser micro-irradiation, time-lapse images of a single laser-induced DNA damage focus are recorded and analyzed for intensity. The data from multiple cells (>35) is then combined to determine the recruitment kinetic profiles for each of the fluorescently labeled proteins. Although cells in each image field are irradiated sequentially, cell-specific timing offsets are measured for each irradiation event, allowing for precise calculation of timing on a per-cell basis. Key endpoints obtained include (1) Peak Intensity, (2) Time to peak and (3) Half-life of recruitment. Peak intensity measures the average, normalized peak recruitment intensity of each microirradiation event against time. Time to peak measures the average time required,

from the beginning of each microirradiation event, to reach maximal peak intensity. Half-life of recruitment measures the time it takes to for each miroirradiation event to reach 50% of the peak recruitment intensity.

We began these experiments by creating lentiviral vectors to express the BER/SSBR proteins XRCC1 and Polβ fused with EGFP. EGFP is used as a reporter protein for direct and sensitive visualization of protein kinetics and recruitment to DNA lesions. Cells transduced with EGFP fused proteins can be visualized by confocal microscopy for real-time observation of the DNA repair process after exposure to laser microirradiation induced DNA damage [178]. U2OS and A549 cells were transduced with XRCC1-EGFP (**Figure 3.7B**) and EGFP-Polβ (**Figure 3.8A-B)** and protein expression was confirmed by immunoblot [58, 62].

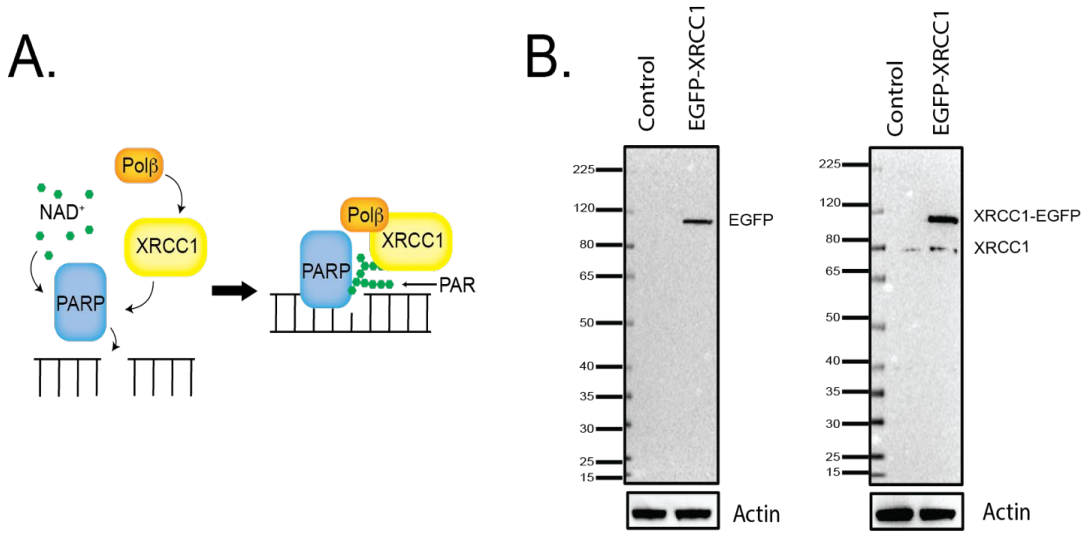

Figure 3.7. PAR accumulation at the DNA lesion site is regulated by NAD^+ bioavailability.

A. Graphic demonstrating PARP1 activation at the DNA lesion site and subsequent recruitment of XRCC1 followed by Polβ; B. Immunoblot of EGFP (left) and XRCC1 (right) protein expression in U2OS cells as compared to U2OS/XRCC1-EGFP cells.

First, we established the recruitment kinetics of untreated XRCC1-EGFP and Polβ-EGFP as a control in U2OS cells and A549 cells. Both XRCC1-EGFP and Polβ-EGFP formed foci upon stimulation with 355 nm laser in U2OS cells. Surprisingly, the recruitment profiles of XRCC1 and Polβ were varied. Previous reports from our lab and others suggest that Polβ and XRCC1 form a complex upon DNA damage, and therefore, should have similar recruitment profiles [12, 13]. However, we found that Polβ time to recruitment peaked much earlier (30s) than XRCC1 (90s). We saw similar recruitment profiles for Polβ and XRCC1 in A549 cells, however; the recruitment peaks were delayed, demonstrating cell-specific recruitment dynamics [58] .

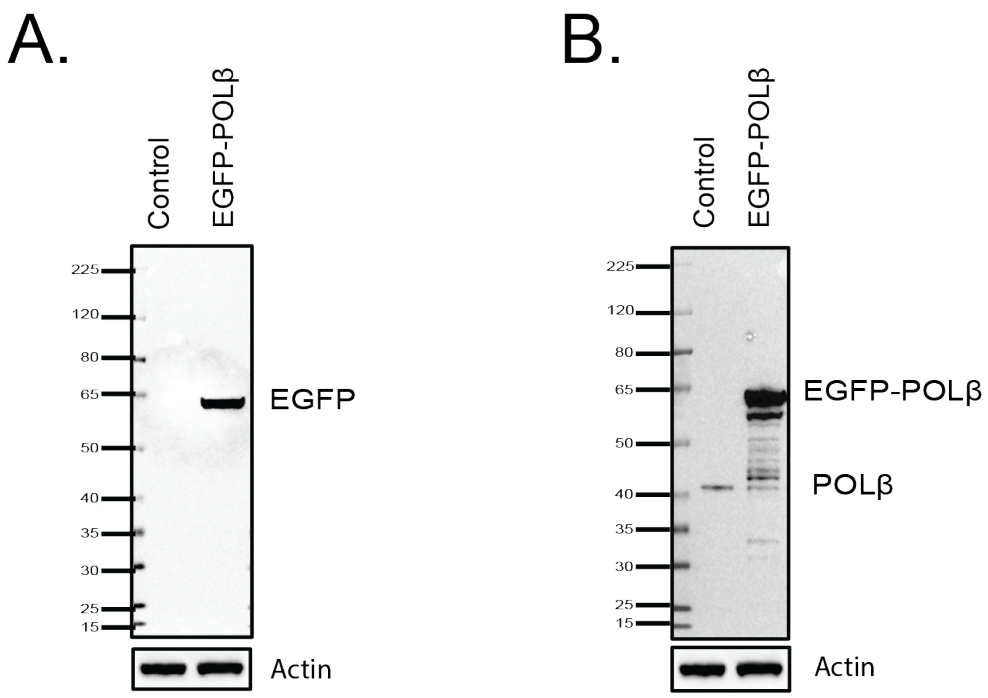

Figure 3.8. Immunoblot of EGFP-Polβ protein expression compared to WT.

A. Immunoblot of EGFP protein expression in U2OS/EGFP- Polβ cells compared to U2OS (WT); B. Immunoblot of endogenous Polβ protein expression in U2OS/EGFP-Polβ cells compared to U2OS (WT) cells.

However, to establish how PAR kinetics impacts the recruitment dynamics of XRCC1 and Polβ, there arose a need for the development of a real-time visualization tool to observe PAR accumulation *in vivo*. For this purpose, we created LivePAR, developed by Dr. Christopher Koczor, a genetically encoded PAR-binding domain with an EGFP tag, allowing for the real-time visualization of PAR kinetics. EGFP was fused to each of the 10 known PBDs of known PAR binding proteins (**Figure 3.9A**). We evaluated the recruitment of each PBD under similar conditions as XRCC1 and Polβ. Following 355-nm laser micro-irradiation, we found that only the WWE domain of RNF146 was able to recruit to the DNA lesion site. We confirmed EGFP expression and that PARP1 and PARP2 expression

were not altered in LivePAR cells expressing the WWE domain of RNF146 fused to EGFP (**Figure 3.9B**).

As evaluated in U2OS and A549 cells, inhibition of PARG results in a sustained PAR signal following stimulation with a 355nm laser, and inhibition of PARP1 suppresses the PAR signal [58]. Similarly, loss of PARP1 suppressed PAR signaling following treatment with H_2O_2 in LN428 cells and reduced immunofluorescence of phosphorylated DDR proteins γH2AX and CHK1, two proteins reported to interact with PARP1 in response to DNA damage and replication stress (**Appendix Figure A.2**) [86, 179, 180].

To determine how depletion of NAD^+ would affect PAR formation, we treated U2OS and A549 cells with 50nM FK866 for 24 hours. Based on the PAR immunoblot results, we reasoned that depleting NAD^+ would largely abrogate the PAR signal in both U2OS and A549 cells, resulting in slower recruitment kinetics of XRCC1 and Polβ. We observed a reduced recruitment intensity in Polβ (37%), XRCC1 (35%), and LivePAR (24%) expressing cells, but there was no change in time to peak or half-life of recruitment in either U2OS cells (**Figure3.10A-C**) or A549 cells (**Figure 3.11A-C**).

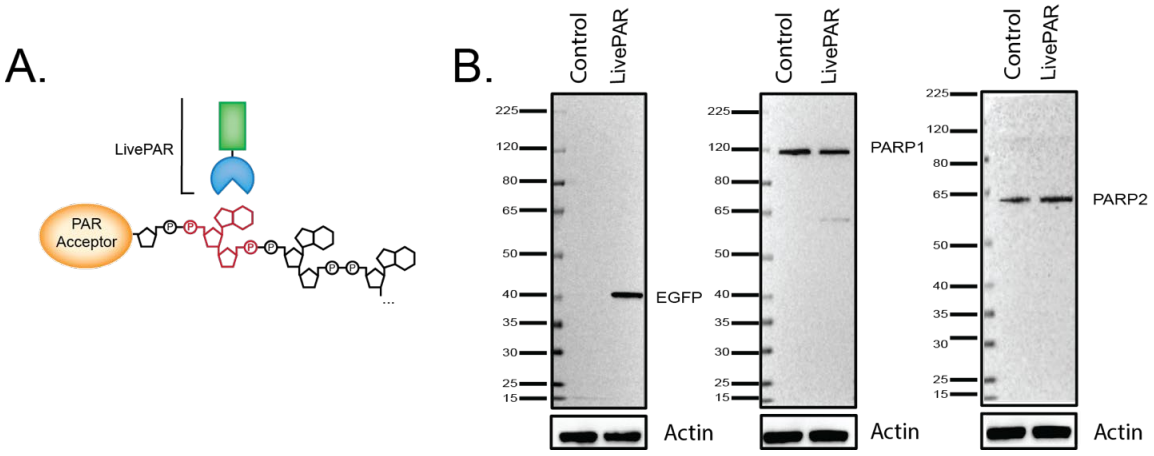

Figure 3.9. PAR accumulation at the DNA lesion site is regulated by NAD^+ bioavailability.

A. Graphic demonstrating LivePAR binding to the iso-ADP-ribose sub-domain of poly (ADP-ribose). B. Immunoblot of EGFP (left), PARP1 (middle) and PARP2 (right) expression inU2OS cells as compared to U2OS/LivePAR cells.

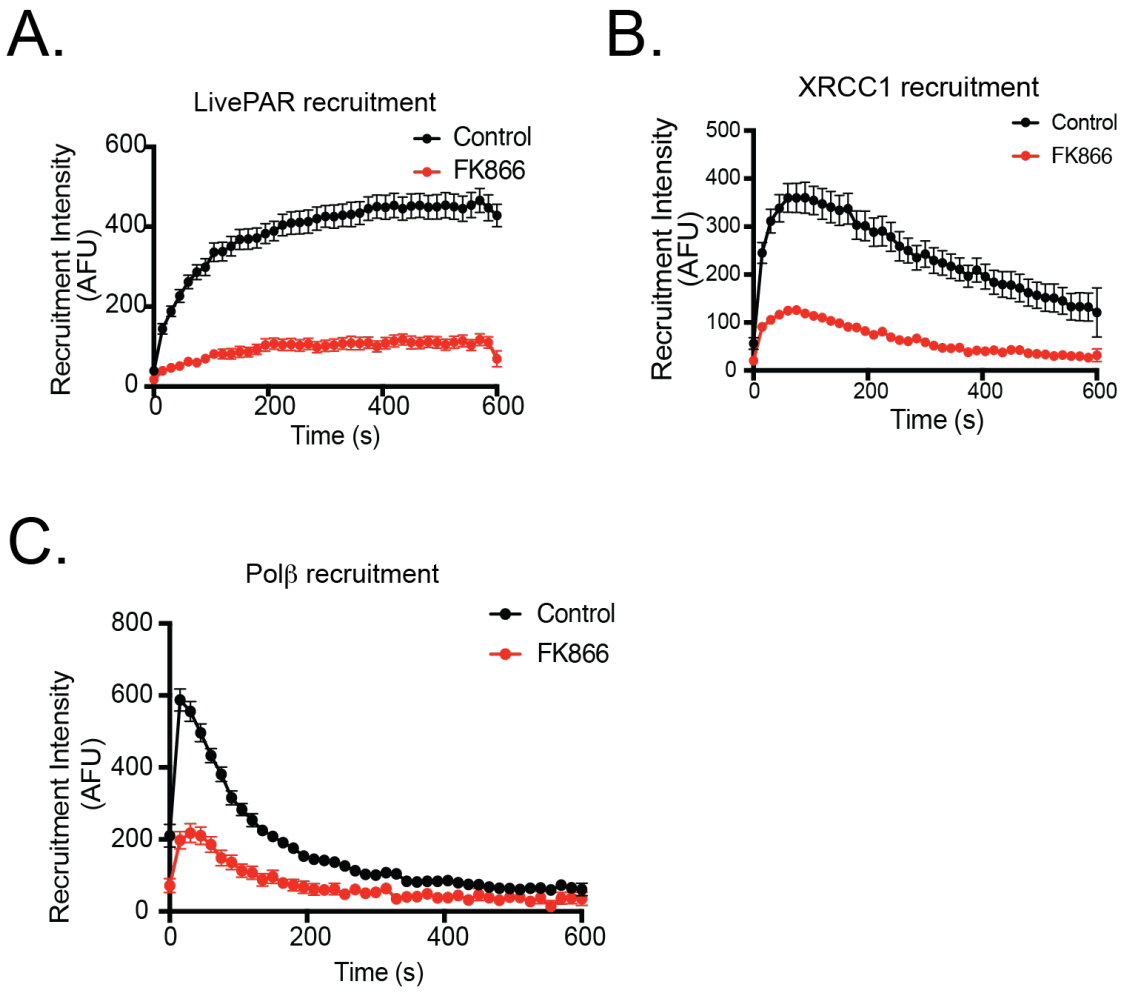

Figure 3.10. FK866 suppresses the recruitment intensity of LivePAR, Polβ, and XRCC1 at the DNA lesion site in U2OS cells.

A. Recruitment of LivePAR following treatment with FK866 (50nM) 24 hours; B. Recruitment of XRCC1-EGFP following treatment with FK866 (50nM) 24 hours; C. Recruitment of EGFP-Polβ following treatment with FK866 (50nM) 24 hours.

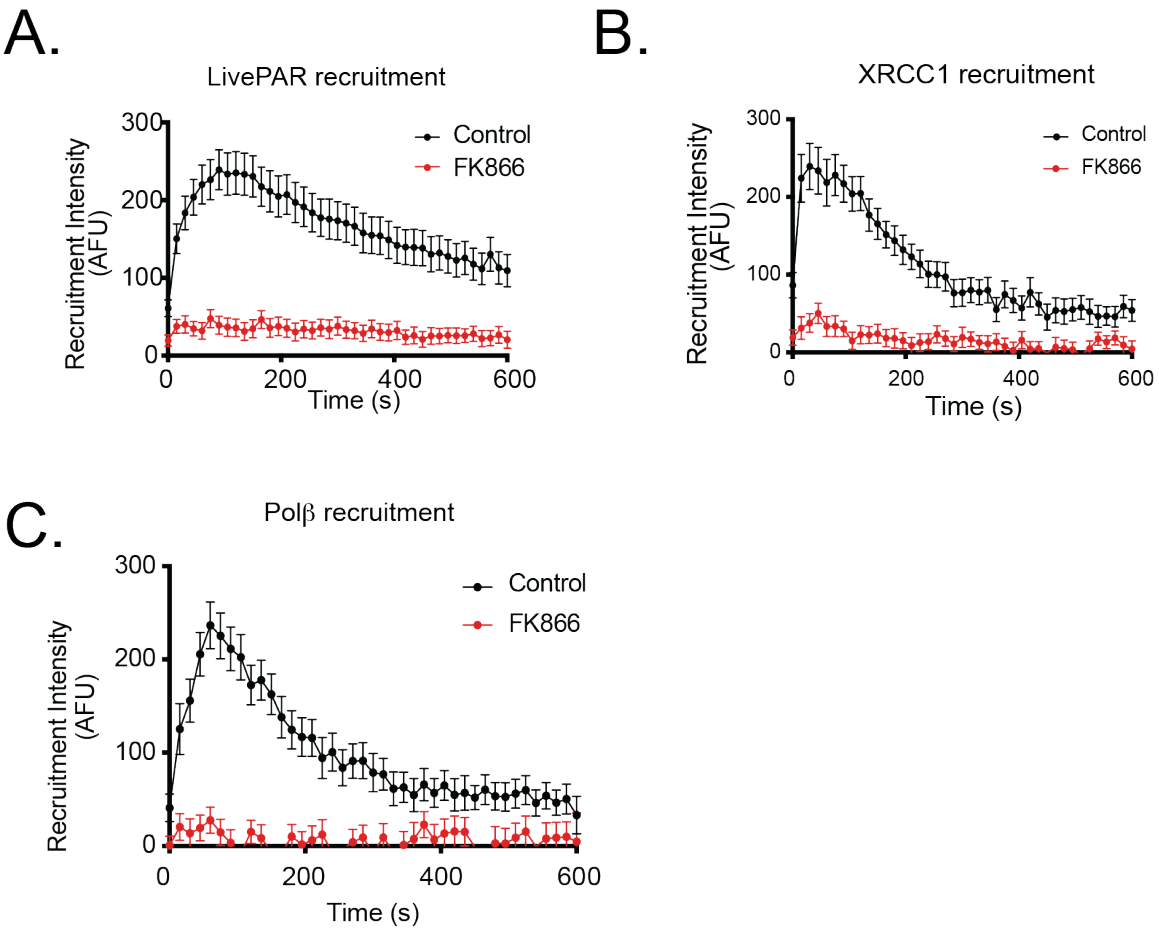

Figure 3.11. FK866 suppresses the recruitment intensity of LivePAR, Polβ, and XRCC1 at the DNA lesion site in A549 cells.

A. Recruitment of LivePAR following treatment with FK866 (50nM) 24 hours; B. Recruitment of XRCC1-EGFP following treatment with FK866 (50nM) 24 hours; C. Recruitment of EGFP-Polβ following treatment with FK866 (50nM) 24 hours

To determine how enhanced NAD^+ impacts recruitment kinetics, we treated each cell line with 100μM NRH for 4 hours (based on the time to peak NAD^+ levels). We found that NAD^+ does not affect the kinetics of BER/SSBR assembly and disassembly but alters the magnitude of protein recruitment. NRH enhanced peak recruitment intensities of Polβ

(45%), XRCC1 (94%), and LivePAR (88%) in U2OS cells (**Figure 3.12**); however, I observed no change in recruitment intensity or kinetics of XRCC1, Polβ, or LivePAR in A549 cells compared to the control, consistent with the results of the NAD^+/NADH and PAR immunoblot analysis (**Figure 3.13**). There was no change in the time to peak recruitment intensity or half-life of recruitment observed for either FK866 or NRH treatment, suggesting that increased NAD^+ bioavailability does not impact BER complex assembly or disassembly other than to increase the magnitude of recruitment.

Based on previous reports for our lab and others, that suggest FBS contains enzymes that degrade NAD^+ intermediates, we cultured all cell lines in media supplemented with 10% heat inactivated FBS [59, 181]. However, following supplementation with NRH, we did not observe any changes in NAD^+ bioavailability or protein recruitment intensity or kinetics, within our treatment time (4 hours) in U2OS cells cultured in regular FBS compared to cells cultured in media with heat inactivated FBS (**Appendix Figure A.3A-D**). This is consistent with previous reports that found NRH, and NR are stable in cell culture media supplemented with regular FBS up to 4 hours and are removed from the media by cellular consumption [33].

We find that our hypothesis is partially supported in that XRCC1 and Polβ recruitment intensity is dependent on PARP1 activity, which can be altered by NAD^+ bioavailability. However, NAD^+ bioavailability and PARP1 activity does not alter recruitment kinetics of XRCC1 or Polβ assembly and disassembly but does not alter the level of complex formation.

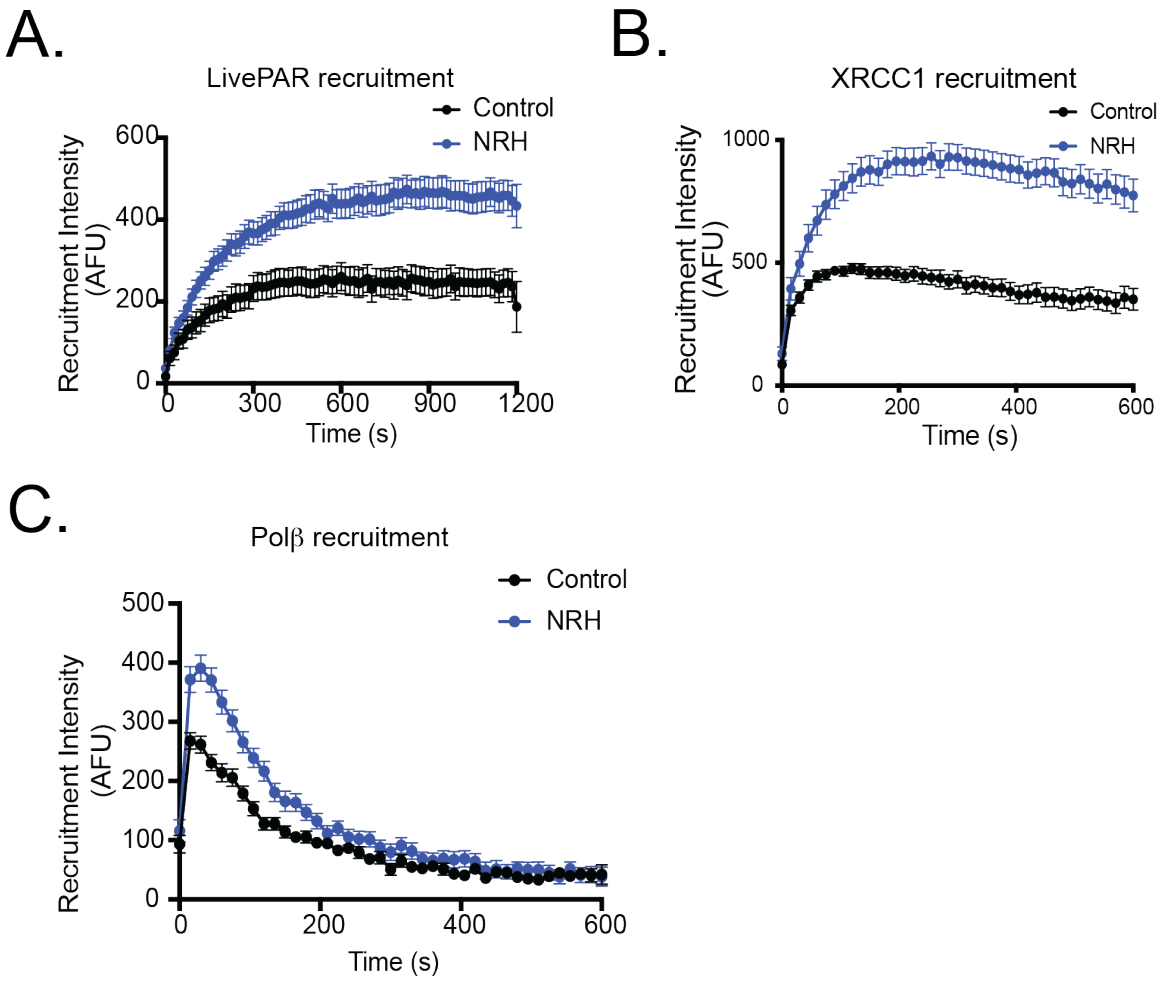

Figure 3.12. NRH enhances recruitment intensity of LivePAR, XRCC1 and Polβ at the DNA lesion site in U2OS cells.

A. Recruitment of LivePAR following treatment with NRH (100μM), 4 hours; B. Recruitment of XRCC1-EGFPfollowing treatment with NRH (100μM), 4 hours; C. Recruitment of EGFP-Polβ following treatment with NRH (100μM), 4 hours.

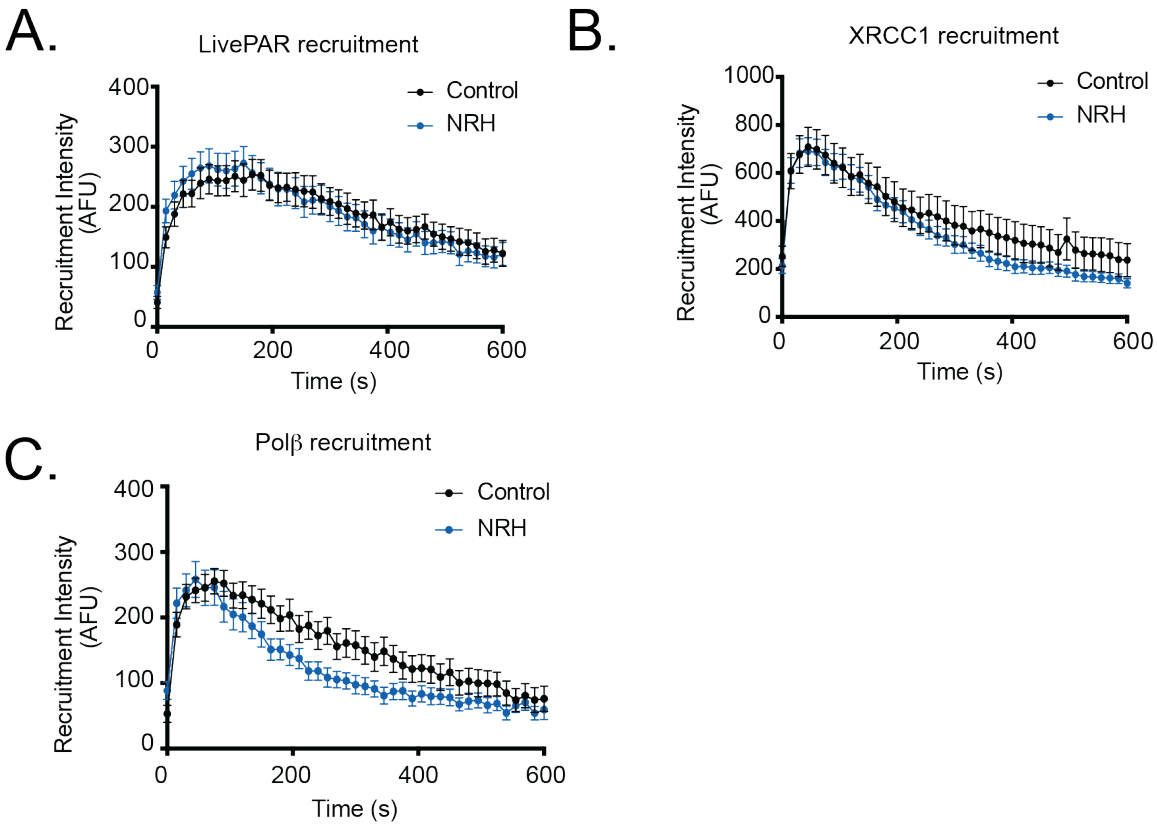

Figure 3.13. NRH does not alter recruitment intensity of LivePAR, XRCC1 and Polβ at the DNA lesion site in A549 cells.

A. Recruitment of LivePAR following treatment with NRH (100 μM), 4 hours; B. Recruitment of XRCC1-EGFPfollowing treatment with NRH (100 μM), 4 hours; C. Recruitment of EGFP-Polβ following treatment with NRH (100 μM), 4 hours.

Increased Cellular NAD^+ Bioavailability Induces PARP1 Activation and Replication Fork Suppression

Previously, we demonstrated that PARP1 and PARG are highly elevated at the protein and mRNA level in glioma stem cells (GSCs) as compared to normal astrocytes [56]. Therefore, we reasoned that PARG inhibition (PARGi) could induce cytotoxic, hyperaccumulation of PAR leading to apoptosis, as previously reported [75]. Although PARGi reduced cell growth by 70%, only 5% cell death was observed with the highest PARGi (10μM) dose in GSC-83 cells, unless PARGi treatment was combined with irradiation, which induced cell death up to 80% in GSC-83 cells [56]. However, inhibition of PARP1 completely rescued the cytotoxic effect of combined PARGi and irradiation, demonstrating that robust PARP1 activation is necessary for the success of PARG inhibitors (PARGi) [56].

As we demonstrated, low NAD^+ bioavailability is a limiting factor for PAR synthesis in LN428 cells. Therefore, we hypothesized that despite having elevated PARP1 protein levels, GSCs lack sufficient NAD^+ for a robust PAR response. To determine the extent that NAD^+ can be modulated in GSC-83 cells, we completed a time course treatment with NRH, and measured NAD^+ content. We found that NAD^+ synthesis peaked at 6 hours and increased cellular NAD^+ as much as 6-10-fold in GSC cells (**Appendix Figure A.4B),** as compared to LN428 cells, NAD^+ where synthesis peaked at 4 hours and increased cellular NAD^+ levels 3-4-fold **(Figure 3.14A-B)**.

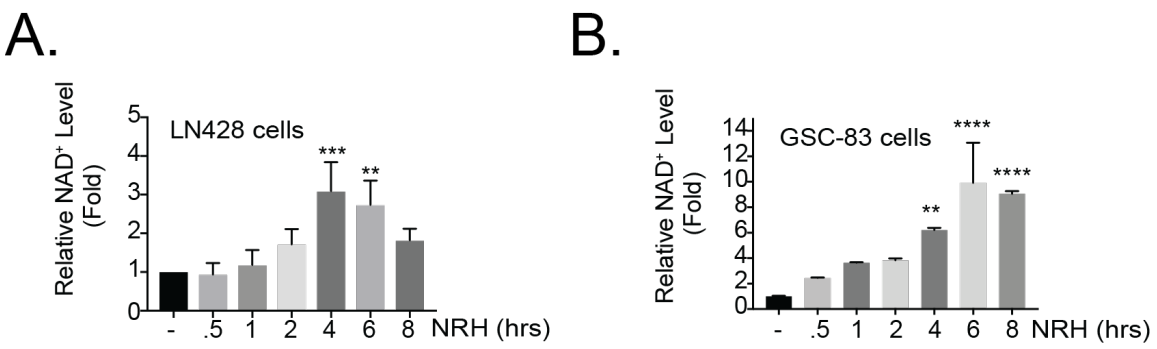

Figure 3.14. NRH enhances cellular NAD^+ levels and induces spontaneous PAR accumulation.

A. NAD^+ levels following time course treatment of LN428 cells with NRH (100μM), n=3 (***p<0.001; **p<.01; One-way ANOVA); B. NAD^+ levels following time course treatment of GSC-83 cells with NRH (100 μM), n=6 (****p<0.0001; ***p<0.001; **p<.01; One-way ANOVA).

Previously, we demonstrated in LN428 cells that NRH enhanced NAD^+ bioavailability and increased PAR synthesis following DNA damage (**Figure 3.10A-C and 3.12A-C**). Similarly, we demonstrated a robust PAR response in GSC-83 cells following co-treatment of NRH and DNA damaging agents [56]. Consistent with reports that NRH is converted to NAD^+ by adenosine kinase (ADK) activity, we found that inhibition of ADK blocks NRH induced NAD^+ synthesis in GSC-83 and LN428 cells (**Figure 3.15A-B).** Therefore, we reasoned that a major factor related to the regulation of PARP1 in GSCs and glioma is related to defects in NAD^+ biosynthesis.

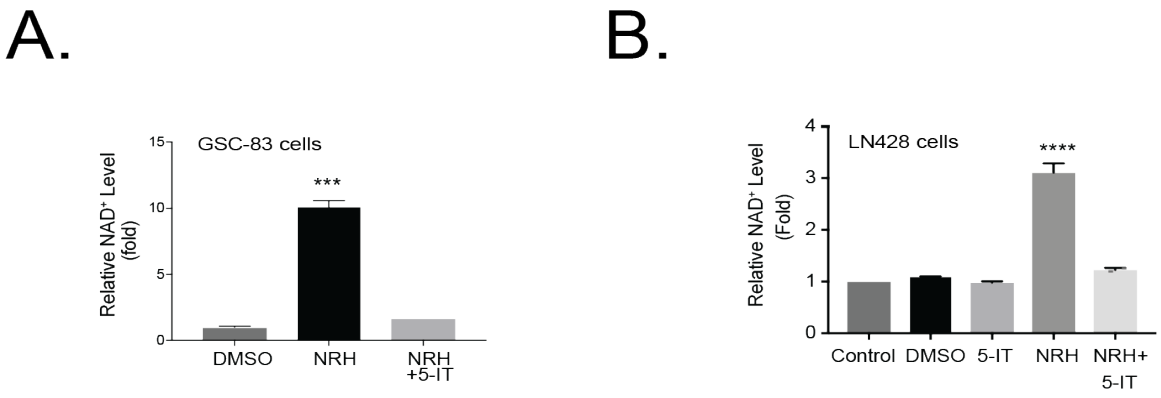

Figure 3.15. ADK inhibitor 5-IT suppresses NRH induced NAD^+ synthesis.

A. GSC-83 NAD^+ analysis following treatment with DMSO, NRH (100 μM) 6 hours or co-treatment with NRH and ADK inhibitor 5-idotubericidin (5-IT) for 6 hours. n=6 (***p<0.001; One-way ANOVA); B. LN428 NAD^+ analysis following treatment with DMSO, NRH (100μM) 4 hours or co-treatment with NRH and ADK inhibitor 5-idotubericidin (5-IT) for 6 hours n=3 (****p<0.0001; One-way ANOVA).

Selective PARGi-induced Cytotoxicity in Glioma Cells is Dependent on NRH-Enhanced Cellular NAD^+ Bioavailability and PARP1 Activation

Elevated levels of PARP1 and PAR accumulation in response to replication stress leads to a slowing of replication fork progression [180]. Several reports have demonstrated that PARGi induced apoptosis is caused by hyperactivation of PARP1 in response to replication stress [81, 182]. Since NAD^+ is a substrate of PARP1 [1], we reasoned that insufficient NAD^+ levels could suppress PARP1 activation potential in GSC-83 and LN428 cells in response to PARGi. This could explain why cells are not sensitive to PARGi unless combined with DNA damaging agents to enhance PAR accumulation.

Surprisingly, treatment with NRH also resulted in low levels of PAR accumulation between 6-8 hours in GSC-83 cells, and between 4-8 hours in LN428 cells, and increased

expression of the replication stress marker γH2AX. This is consistent with our finding that GSCs and glioma cells lack sufficient NAD^+ to produce a robust PAR response (**3.16A**).

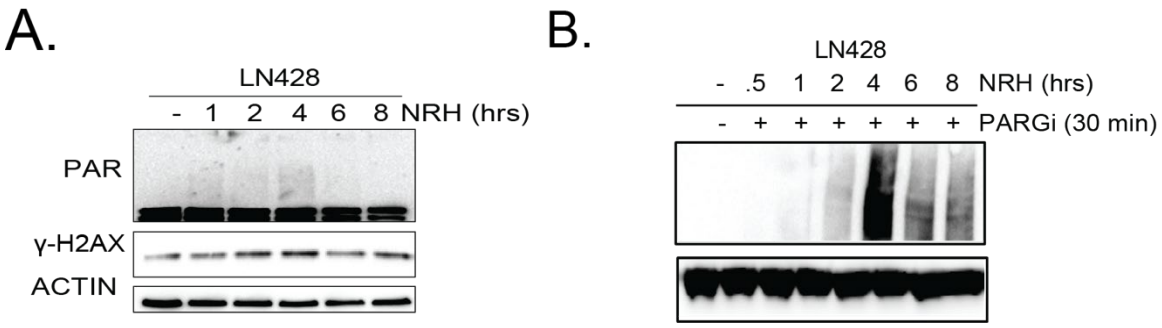

Figure 3.16. NRH induces PAR accumulation and enhances PARGi induced PARylation.

A. Immunoblot of PAR accumulation and replication marker yH2AX in LN428 cells following time course treatment with NRH (100μM) at the times indicated; B. Immunoblot of PAR accumulation following co-treatment of NRH (100μM) and PARGi (10 μM) in LN428 cells at the times indicated.

Because the NRH enhanced cellular NAD^+ levels were able to enhance PAR accumulation alone, in contrast to other NAD^+ precursors (**Appendix Figure A.4**), we reasoned that co-treatment of NRH and PARGi would act synergistically to induce robust hyperPARylation compared to NRH or PARGi alone. We found that co-treatment of NRH with PARGi induced robust hyperPARylation in GSCs and LN428 (**Figure 3.16B**) that was sustained up to 72 hours (**Figure 3.17**).

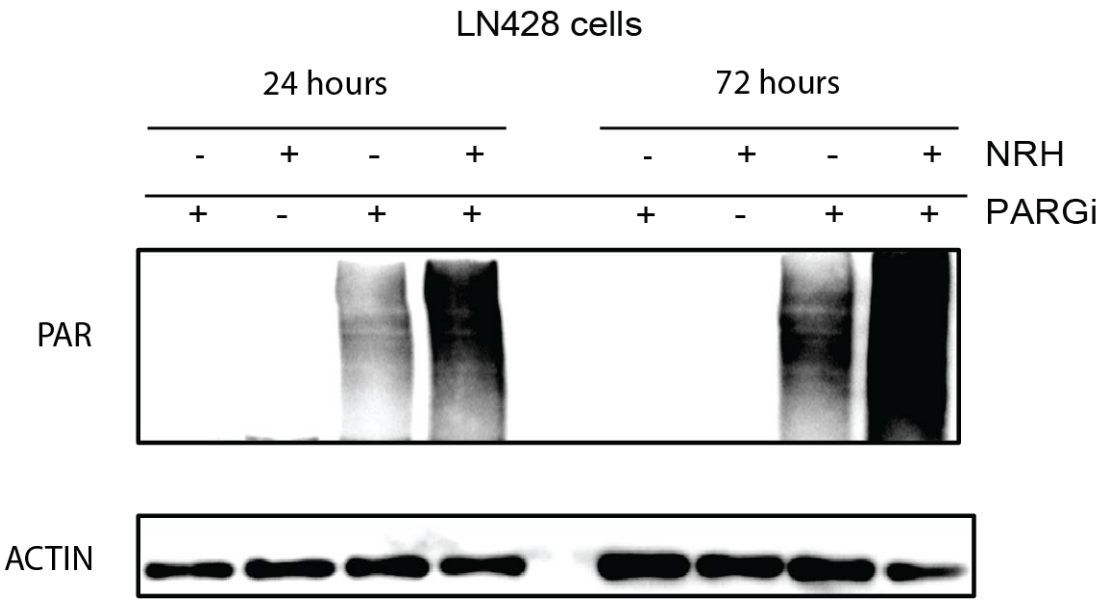

Figure 3.17. NRH enhances PARGi induced PAR accumulation up to 72 hours.

Immunoblot of PAR accumulation following co-treatment of in LN428 cells with PARGi (10μM) alone or supplemented with NRH (100μM) for 24 or 72 hours.

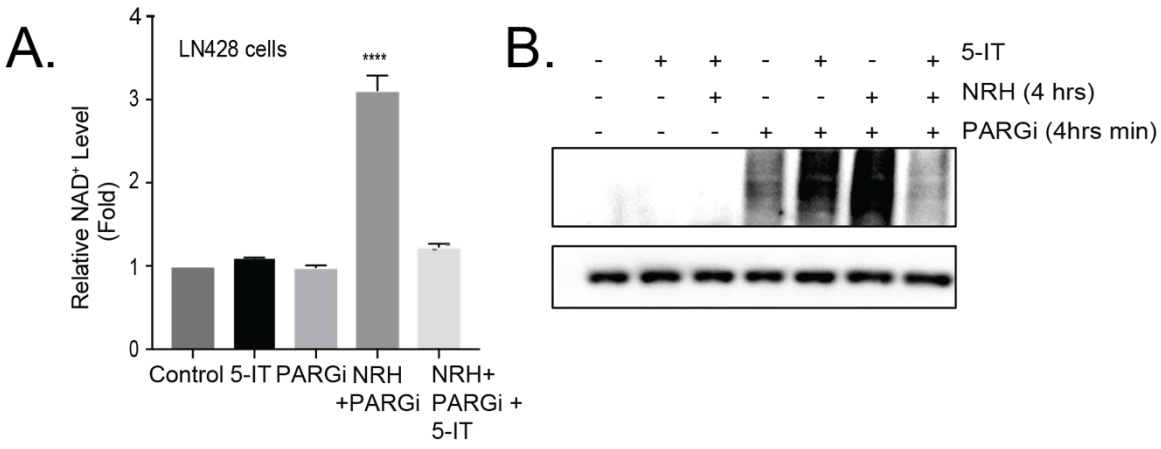

Figure 3.18. NRH enhanced NAD^+ biosynthesis and NRH enhanced PARylation induced by PARGi is abrogated by ADK inhibition.

A. LN428. NAD^+ analysis following treatment with PARGi or 5-IT or co-treatment NRH+PARG or co-treatment NRH+PARGi+5-IT n=3 (****$p<0.0001$; One-way ANOVA). B. Immunoblot of PAR accumulation following treatment with NRH, 5-IT, PARGi, co-treatment of NRH (100 μM) and PARGi (10 μM) or co-treatment with NRH+PARGi+5-IT in LN428 cells, 4 hours.

Consistent with previous reports, the ADK inhibitor 5-IT suppressed NRH induced NAD^+ synthesis and suppressed PAR accumulation in LN428 cells (**Figure 3.18A-B**) and GSC-83 cells (**Figure 3.19A-B)**. During S-phase, PARP1 activation at the replication fork acts as a replication stress sensor, for the organization of the S-phase checkpoint pathways to induce replication arrest [183]. However, loss or inhibition of PARP1 enhances replication fork velocity, since DNA lesions that normally induce replication stress, remain undetected by the replication machinery [183]. If NRH enhanced PARylation and increased γH2A.X phosphorylation is because of PARP1 activation at the replication fork, we reasoned that treatment with NRH should decrease replication fork velocity. We utilized the DNA fiber assay to observe the genotoxic effects of NRH or PARGi induced hyperPARylation on replication fork speed. The DNA fiber assay is a robust tool, used to

analyze interrupted DNA replication, caused by genotoxic agents. The assay depends on the ability of the cell to incorporate thymidine analogs during DNA replication. Following treatment, individual DNA fibers are isolated and stretched on a microscope slide, fixed with 100% ethanol followed by immunostaining and confocal imaging. The length of each DNA fiber can then be measured and replication fork velocity is calculated by dividing the length of each DNA fiber over time using the standard conversion 1μM = 2 kb (**Appendix Figure A.5**) [184].

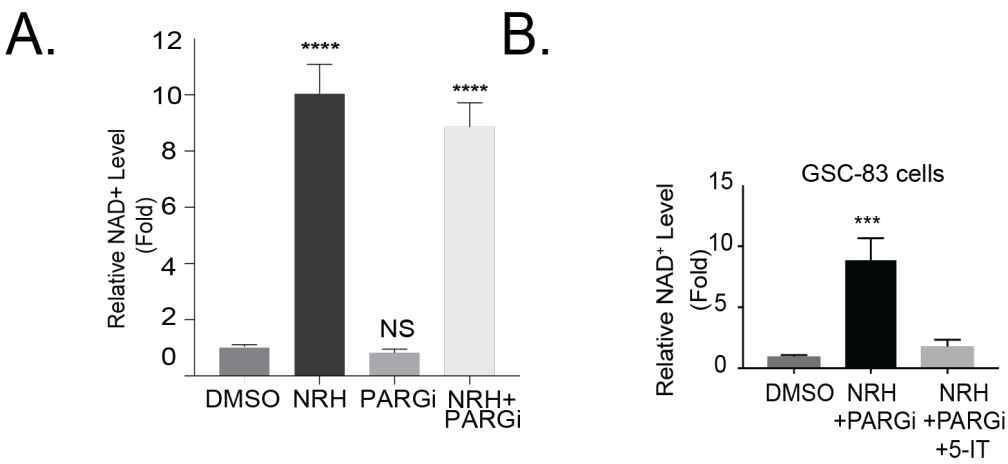

Figure 3.19. NRH induced NAD^+ synthesis is abrogated by 5-IT.

A. NAD^+ analysis in GSC-83 cells following treatment with NRH (100 μM), PARGi or NRH + PARGi 6 hours. n=3 (****p<0.0001; One-way ANOVA); B. NAD^+ analysis in GSC-83 cells following treatment with following co-treatment NRH+PARG and co-treatment NRH+PARGi+5-IT n=3 (****p<0.001; One-way ANOVA).

We found that NRH significantly suppressed replication fork velocity in LN428 cells between 4-6 hours of treatment, consistent with our NAD^+ and PAR immunoblot analyses demonstrating NAD^+ biosynthesis and PAR accumulation peaked 4 hours after NRH supplementation (**Figure 3.19A-B**). Additionally, we found that NRH suppressed

replication fork progression similarly to PARGi, but we observed the greatest effect of replication fork speed suppression when we co-treated the cells with NRH and PARGi (**Figure 3.20B**). This suggests that NRH enhances NAD^+ biosynthesis and PARP1 activation potential in response to replication stress.

PARP activation at the fork leads to the activation of the S-phase checkpoint arrest and stalled fork progression. PARG inhibition prevents dePARylation and replication restart leading to an accumulation of PAR on PARP1 and other acceptor proteins [133]. There are several possible consequences of PARG inhibition including trapping PAR binding proteins and preventing downstream processing leading to G1/S and G2 phase arrest, an accumulation of DNA lesions, and an increase in unligated Okazaki fragments [182]. If instability persists, it leads to replication catastrophe, accumulation of double-stranded breaks and apoptosis [81, 182].

Therefore, we anticipated that co-treatment of PARGi with NRH would create a synergistic effect to promote cell death, because of toxic hyperPARylation leading to activation of the S-phase checkpoint, and apoptosis because of unresolved DNA damage. Like GSC-83 cells, LN428 cells were insensitive to PARGi alone, following treatment with PARGi alone (120 hours) we only observed ~10% decrease in cell viability. However, we found that co-treatment of PARGi and NRH resulted in 99% cell death by 5 days (120 hours) in GSC-83 cells [75] and ~85% cell death after 120 hours (5 days) in LN428 cells (**Figure 3.21**).

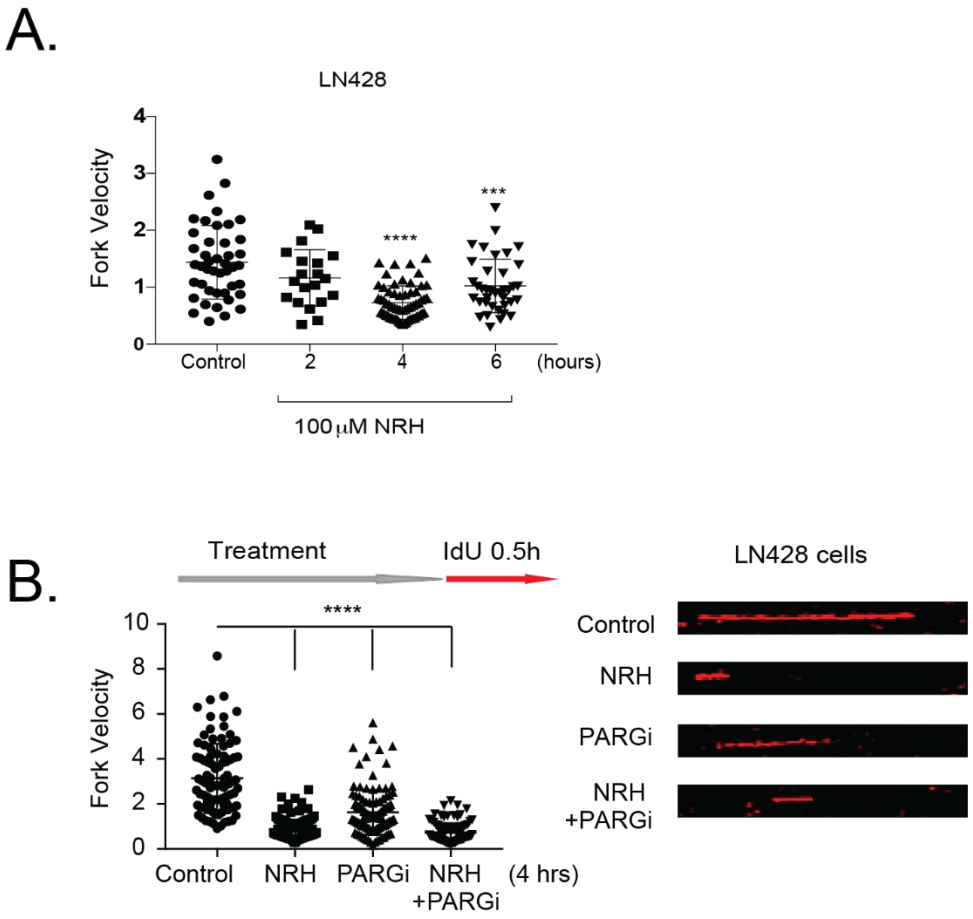

Figure 3.20. NRH enhances PARGi induced hyperPARylation and slows replication fork velocity.

A. DNA Fiber analysis of LN428 cells following treatment with NRH (100 μM) for the times indicated (****p<0.0001; ***p<.001; One-way ANOVA); B. DNA Fiber analysis of LN428 cells following treatment with NRH (100 μM), PARGi (10 μM) or co-treatment with NRH and PARGi for 4 hours (****p<0.0001; ***p<0.001; One-way ANOVA) (Completed with Dr. Jennifer Clark).

We found that NRH enhanced the cytotoxic effect of PARGi, consistent with our immunoblot analysis where we observed a sharp increase in cleaved caspase 3/7 activity [56]. To demonstrate that robust PAR accumulation in response to NRH/PARGi treatment was a result of PARP1 activation, we treated LN428 cells with the PARP1/2 inhibitor ABT-

888 for 1 hour, followed by co-treatment with NRH and PARGi (4 hours) and found that ABT-888 suppressed the PAR signal. As a follow up approach, we repeated the PAR immunoblot analysis in the LN428/PARP1-KO cell line to determine if PAR synthesis, following co-treatment with NRH and PARGi, was dependent on PARP1. We knocked out PARP1 using the CRISPR-Cas9 system, with guide RNA sequences designed to target PARP1, as described previously [58]. We observed that PAR formation following treatment with PARGi (24 hours) was largely suppressed compared to the parental LN428 cells. Although co-treatment with NRH and PARGi induced a greater PAR response compared to PARGi treatment alone, the signal was still very low.

We reasoned that the PAR signal in the absence of PARP1 was due to the redundant activity of PARP2. We found that when we co-treated LN428/PARP1-KO cells with the PARP1/2 inhibitor ABT-888, the PAR signal was fully suppressed (**Figure 3.22**). Consistent with our PAR analysis, LN428/PARP1-KO cells were not sensitive to treatment with PARGi or co-treatment with NRH and PARGi after 5 days (**3.23A-B**).

We find that PARP2 activity is possibly involved in the replication stress response, but to a lesser degree than PARP1, as others have reported [180]. Together, these studies support our hypothesis that NAD^+ modulates PARP1 activation potential in GSC-83 and LN428 cells, and co-treatment with PARGi and NRH enhances PAR synthesis and induces apoptosis and cell death.

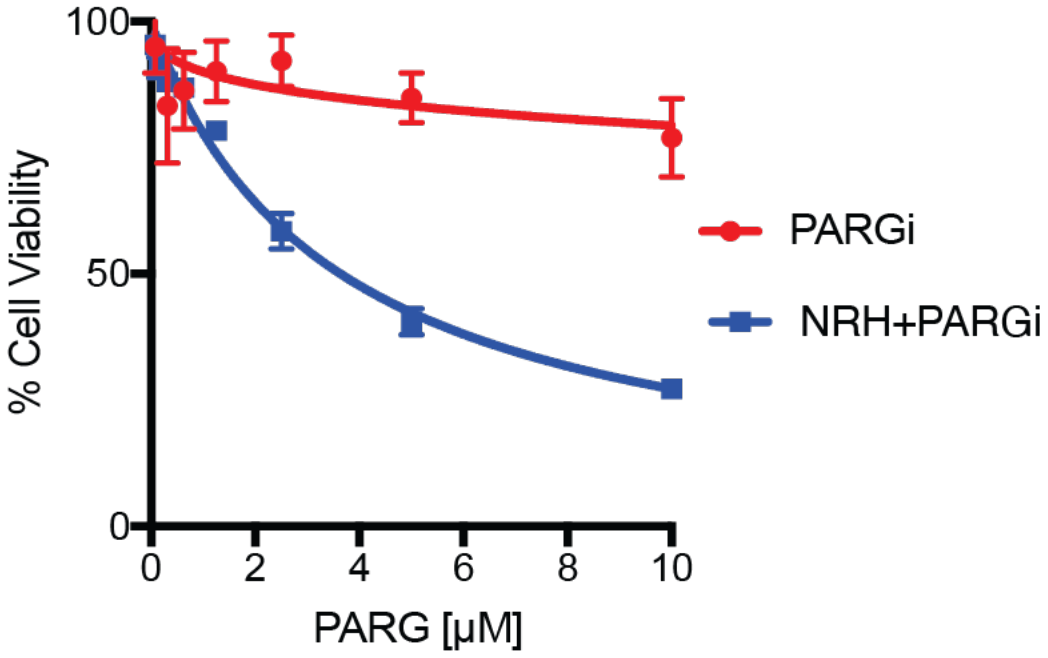

Figure 3.21. NRH enhances the cytotoxic effect of PARGi in LN428 cells.

Cell viability in LN428 cells treated with PARGi for 120 hours at the doses indicated or NRH (100μM) + PARGi for 120 hours.

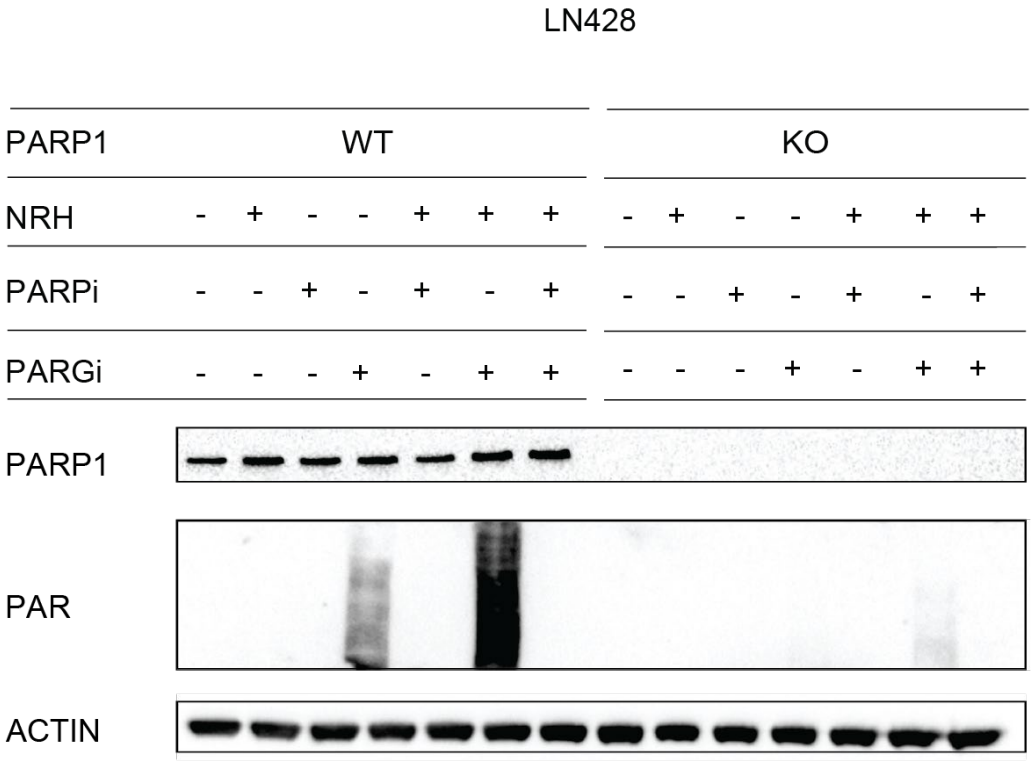

Figure 3.22. NRH + PARGi hyperPARylation is dependent on PARP1 activation.

Immunoblot of PAR following treatment with NRH, PARGi, NRH + PARGi or NRH+PARGi+ABT-888 in LN428 WT and LN428/PARP1-KO cells.

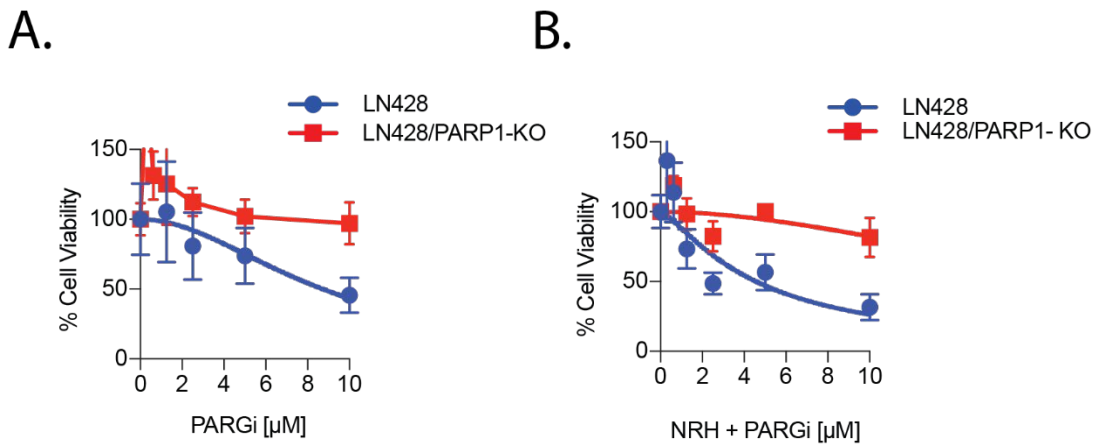

Figure 3.23. NRH + PARGi hyperPARylation and cell death is dependent on PARP1 expression.

A. Cell viability in LN428 WT and LN428/PARP1-KO treated with PARGi for 120 hours at the doses indicated; B. Cell Viability following treatment of LN428 WT and LN428/PARP1-KO cells with NRH (100µM) + PARGi for the doses indicated (120 hours).

PARGi-induced S-phase arrest and checkpoint activation require enhanced cellular NAD^+ from NRH exposure

A second condition of our model is that PAR accumulation, in response to NRH and PARGi treatment, is a replication-associated response [56]. We demonstrated that NRH/PARGi treatment enhanced PARylation and slows replication fork velocity. Therefore, we would expect to see an increase in PARP1 interaction with replication-associated proteins in response to NRH/PARGi induced hyperPARylation. To demonstrate that NRH and PARG induced hyperPARylation is a replication-associated response, we supplemented GSC-83 and LN428 cells for 48 hours with thymidine to block replication. Thymidine is a DNA synthesis inhibitor that can arrest cells at the G1/S border [185].

We treated cells for 18 hours with thymidine, replenished media for 9 hours, followed by the addition of thymidine for another 18 hours. At the end of the second 18-hour time point, cells either remained in thymidine arrest or were washed and treated with full media. Both populations were then treated with NRH/PARGi for 6 hours. We found that the PAR signal was completely abrogated in cells arrested with thymidine. However, when we removed the thymidine and replenished cells with growth media followed by NRH/PARGi treatment, we found that the PAR signal was restored in the GSC-83 cells [56] and the LN428 cells (**Figure 3.2.24**). Together, this data suggests that co-treatment of NRH and PARGi enhances PARP1 activation potential, in response to replication, activates the S-phase checkpoint and blocks DNA replication.

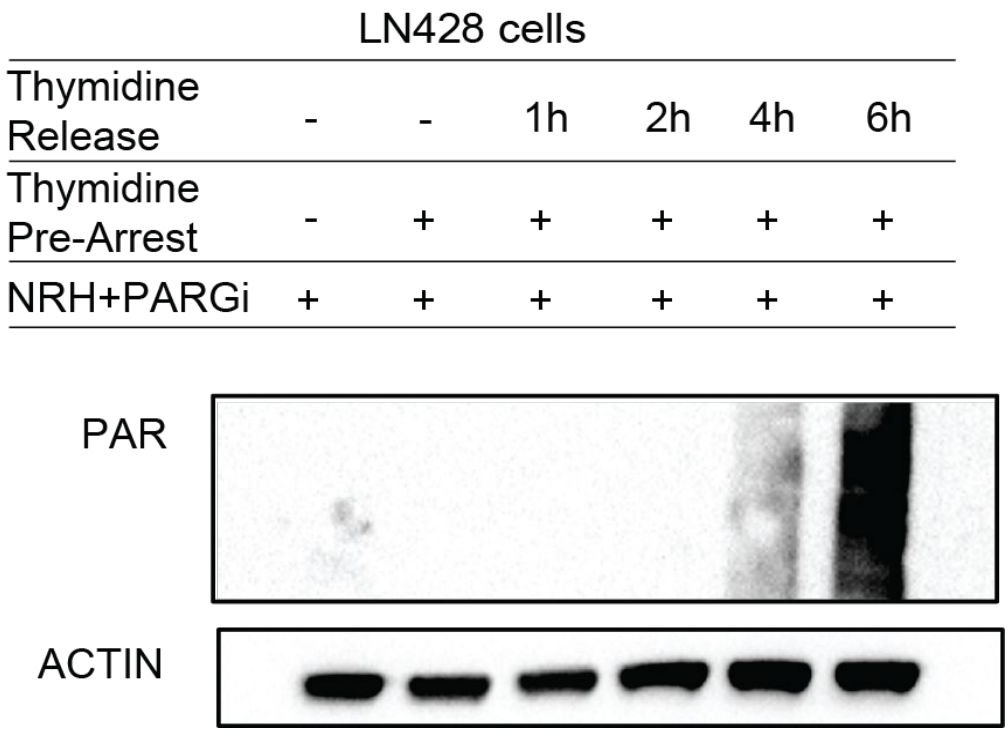

Figure 3.24. NRH + PARGi hyperPARylation is dependent on replication.

LN428 cells were treated with 2mM thymidine for 48 hours. Cells co-treated with NRH (100 μM) and PARGi (10 μM) for 6 hours w/o thymidine block (lane #1). Cells that remained in thymidine block were co-treated with NRH (100 μM) and PARGi (10 μM) for 6 hours (lane #2). Cells that were released from thymidine were co-treated with NRH (100 μM) and PARGi (10μM) 1h (lane #3), 2h (lane #4), 4h (lane#5), 6h(lane #6)

To further to validate our findings that NRH/PARGi induced hyperPARylation is associated with S-phase, we applied an *in vivo* approach by expressing our live-cell PAR probe (LivePAR) in LN428 cells, to observe co-localization of PAR with replication-associated proteins. Replication foci are thought to form in the nucleus because of multiple replicons forming simultaneously in each focus. Several reports have demonstrated that PAR foci form in the nucleus in response to PARG inhibition alone [127], therefore, we hypothesized that we should visualize PAR co-localized with replication foci in the nucleus

over a 24-hour period, following treatment with NRH/PARGi if PAR is formed as a replication-associated response.We treated cells with DMSO, NRH, PARGi and a combined treatment of PARGi/NRH, and followed PAR formation over 24 hours. Images were captured by confocal microscopy every 15 minutes over a 24-hour period. We observed that PAR aggregates began to form in the nucleus of some cells as early as 15 minutes following NRH/PARGi treatment, with intensity peaking around 4 hours (**Figure 3.25**).

However, to confirm our hypothesis, that PAR aggregates were only formed in cells undergoing replication in S-Phase, we co-treated LN428/LivePAR cells with NRH and PARGi for 4 hours and observed that LivePAR aggregates were co-localized with PAR and the replication-associated proteins PCNA (**Figure 3.26**) and RPA (**3.27**), suggesting that PAR foci are formed at sites of replication.

Together, these results demonstrate that PAR accumulation in response to co-treatment with NRH and PARGi enhances PARP1 activation potential in response to replication stress at the replication fork, blocks replication and induces an S-phase checkpoint arrest.

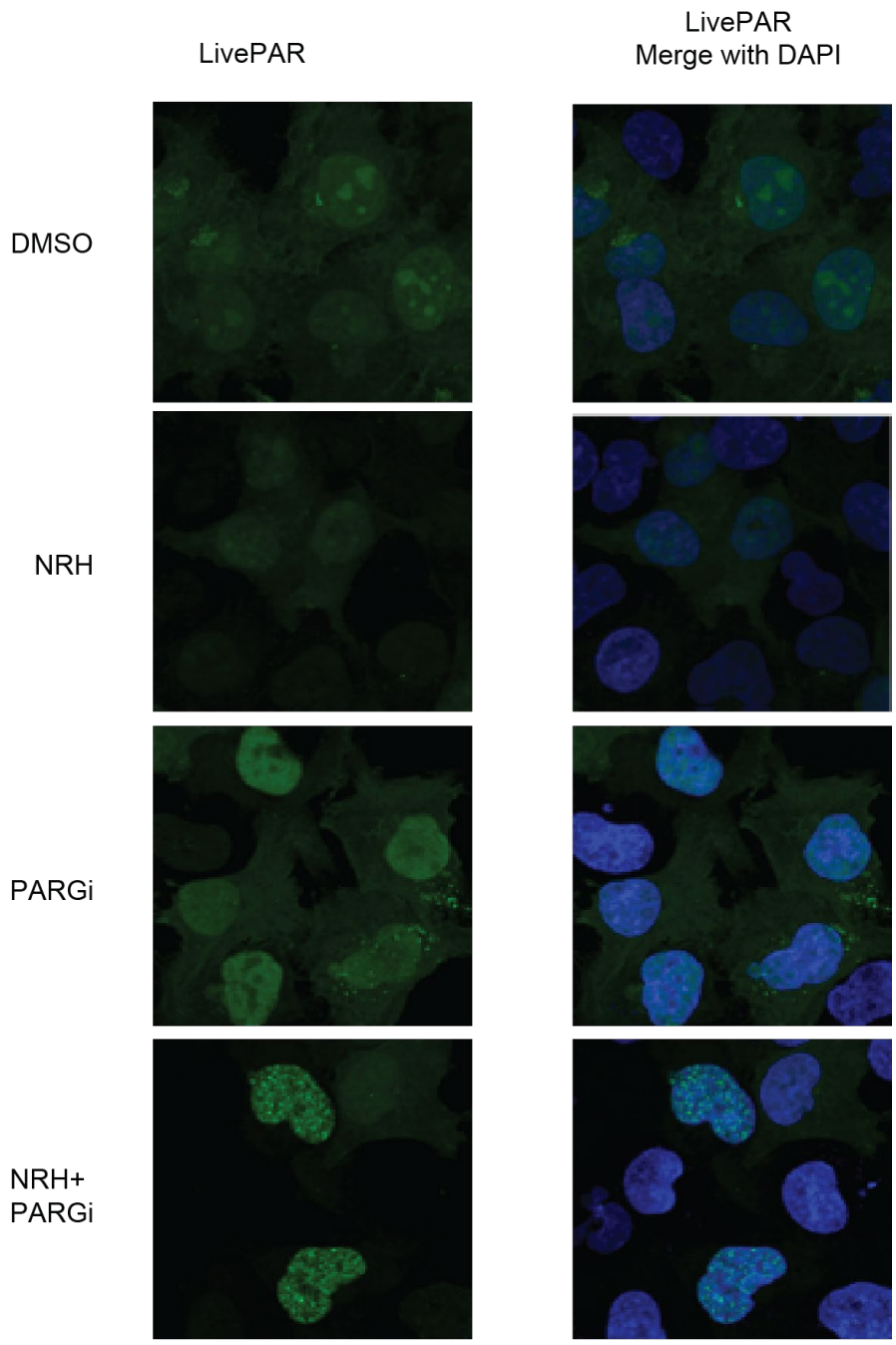

Figure 3.25. LivePAR foci induced by NRH/PARGi.

Fluorescent confocal images of nuclear foci of PAR, as detected with the EGFP- WWE domain of the LivePAR probe in LN428/LivePAR following treatment with DMSO, NRH (100μM), PARGi (10μM) or co-treatment of NRH and PARGi (4 hrs).

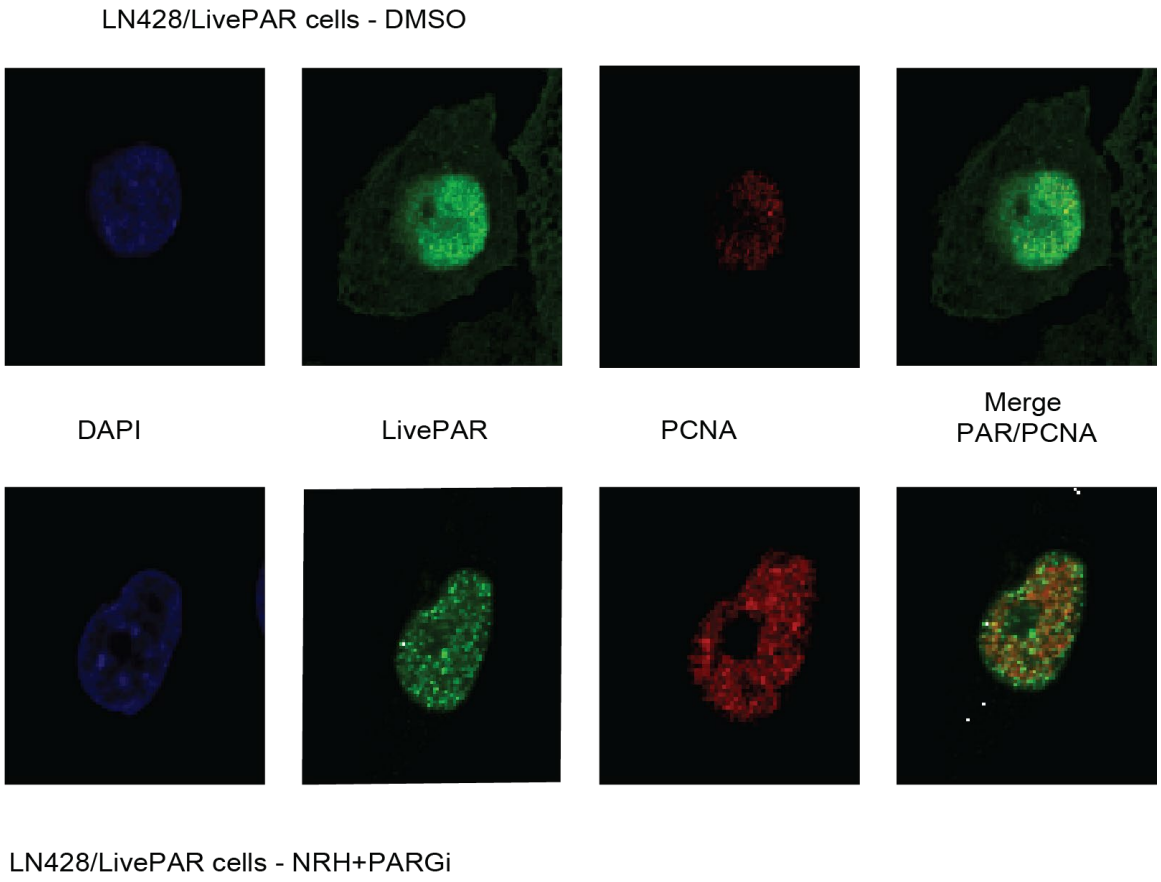

Figure 3.26. Co-treatment of NRH and PARGi induced replication foci in LN428/LivePAR cells co-localized with PCNA.

Cells treated with DMSO (TOP) or NRH/PARGi, 4 hrs (BOTTOM). Fluorescent, confocal images of LN428/LivePAR cells demonstrating colocalization of LivePAR foci with PCNA, following treatment with NRH/PARGi (BOTTOM).

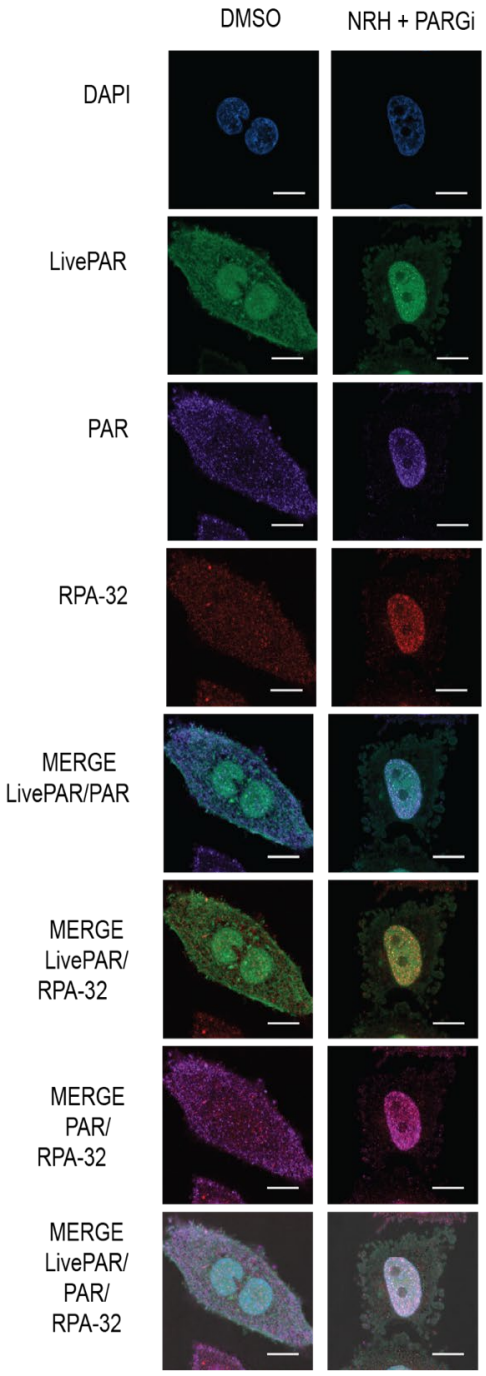

Figure 3.27. Co-treatment of NRH and PARGi induced replication foci in LN428/LivePAR cells co-localized with RPA-32 and PAR.

Cells treated with DMSO (LEFT) or NRH/PARGi, 4 hrs (RIGHT). Fluorescent confocal images of LN428 cells, revealing colocalization of NRH/PARGi- induced nuclear foci of LivePAR with PAR and RPA-32, as detected by immunofluorescence (RIGHT).

Replication Associated PARP1 Activation Coordinates BER/SSBR Pathway Engagement and PAR-induced Assembly of the Replication Initiation Complex

We have demonstrated that NRH enhances PARGi induced hyperPARylation, in response to replication stress, and slows replication fork progression. Previous reports have demonstrated that BER/SSBR proteins XRCC1 and LIGIII, together with PARP1, are involved in the recognition of Okazaki fragments [81, 83]. As we have demonstrated, NAD^+ biosynthesis can be modulated to enhance PAR synthesis and the recruitment of BER/SSBR proteins XRCC1 and Polβ to the site of DNA damage. Therefore, we anticipated that we would find BER/SSBR proteins and novel replication associated PARP1 interacting proteins following co-treatment with NRH and PARGi in the absence of DNA damage.

The traditional co-immunoprecipitation (co-IP) assays, that identify protein-protein interactions within the cell lysate, are limited because they are unable to detect weak or transient protein interactions that occur *in vivo*. Additionally, co-IP not only detects protein interactions that form in the cell, but also detects protein aggregates that form in the cell lysate [186]. However, the BioID system allows for the temporal and spatial identification of protein interactions *in vivo,* including direct, transient, or weak interactions, within a specific time frame [186, 187].

The BioID approach utilizes a mutant bacterial biotin protein ligase (BirA-R118G), fused to a specific protein of interest, that is then expressed in mammalian cells [186]. The enzymatic activity of wild type BirA normally functions by creating activated biotin, utilizing ATP and biotin to form biotinyl-5'-AMP, then biotinylates the surface of biotin carboxyl carrier protein subunits by transferring the activated biotin to a specific lysine

residue. However, the mutant BirA (R118G) behaves promiscuously by enhancing the early release of activated biotin from the catalytic site and allowing the biotinylation of primary amines of proteins within a ~10nm radius of the BirA fusion protein (**Figure 3.28A**) [186, 187]. The biotinylated proteins can then be purified by using magnetic streptavidin beads and detected by immunoblot or mass spectrometry [186]. The limitations of the BioID approach include the detection of proximal proteins that do not directly interact with the BirA fusion protein, and the need to express a fusion protein [186].

We applied the BioID approach, by expressing PARP1 fused to biotin ligase (BirA-R118G) in LN428 and GSC-83 (LN428/PARP1-BirA and GSC-83/PARP1-BirA) cells, to identify NAD^+ dependent changes in PARP1 protein-protein interactions. Our initial proteomics screen and differential analysis identified PARP1 interaction with XRCC1 and several replication-associated proteins (ORC2, PCNA and RFC1), in conditions of high NAD^+ (NRH), which were suppressed in conditions of low NAD^+ (FK866). We confirmed PARP1 protein interactions with biotinylated proteins (ORC2 and PCNA, and XRCC1) by immunoblot analysis, and found that the interactions were further enhanced by NRH/PARGi (**Figure 3.28B-C**).

To determine if ORC2, XRCC1, and PCNA could be binding to PAR, and not just interacting with PARP1, we utilized the PAR Af1521 macrodomain, bound to agarose beads to capture PAR-modified and PAR-bound proteins in cell lysates. The Af15212 macrodomain contains a 190 amino acid domain from *Archaeoglobus fulgidus* that is capable of binding to a subset of PAR with high affinity allowing for the capture of PAR and PAR-binding proteins [75]. To determine if the increased interaction with replication proteins (PCNA and ORC2) and the BER protein XRCC1 is a replication associated

interaction, GSCs were treated with thymidine for 48 hours prior to treatment with NRH/PARG (1 hour). We found that PAR accumulation and PAR binding with PARP1, XRCC1, ORC2, PCNA along with RPA was significantly enhanced in replicating cells following treatment with NRH/PARGi, but PAR binding was suppressed in cells that were replication arrested (**Figure 3.29A-B**).

As a follow up approach, we treated LN428 and GSC-83 cells (LN428/PARP1-BirA and GSC-83/PARP1-BirA) with a double thymidine block in the presence of NRH/PARGi and compared to thymidine release 1 hour (GSC-83) and 6 hours (LN428) after release. We found, after thymidine release, there was a significant increase of PARP1 interaction with BER proteins XRCC1 and Polβ and replication-associated proteins PCNA or ORC2 (**Figure 3.29B**). This suggests that NRH/PARGi enhanced PARP1 activation and interaction with replication-associated proteins (ORC2, PCNA and RPA-32) and BER/SSBR proteins (XRCC1 and Polβ) is occurring at sites of replication in response to replication stress.

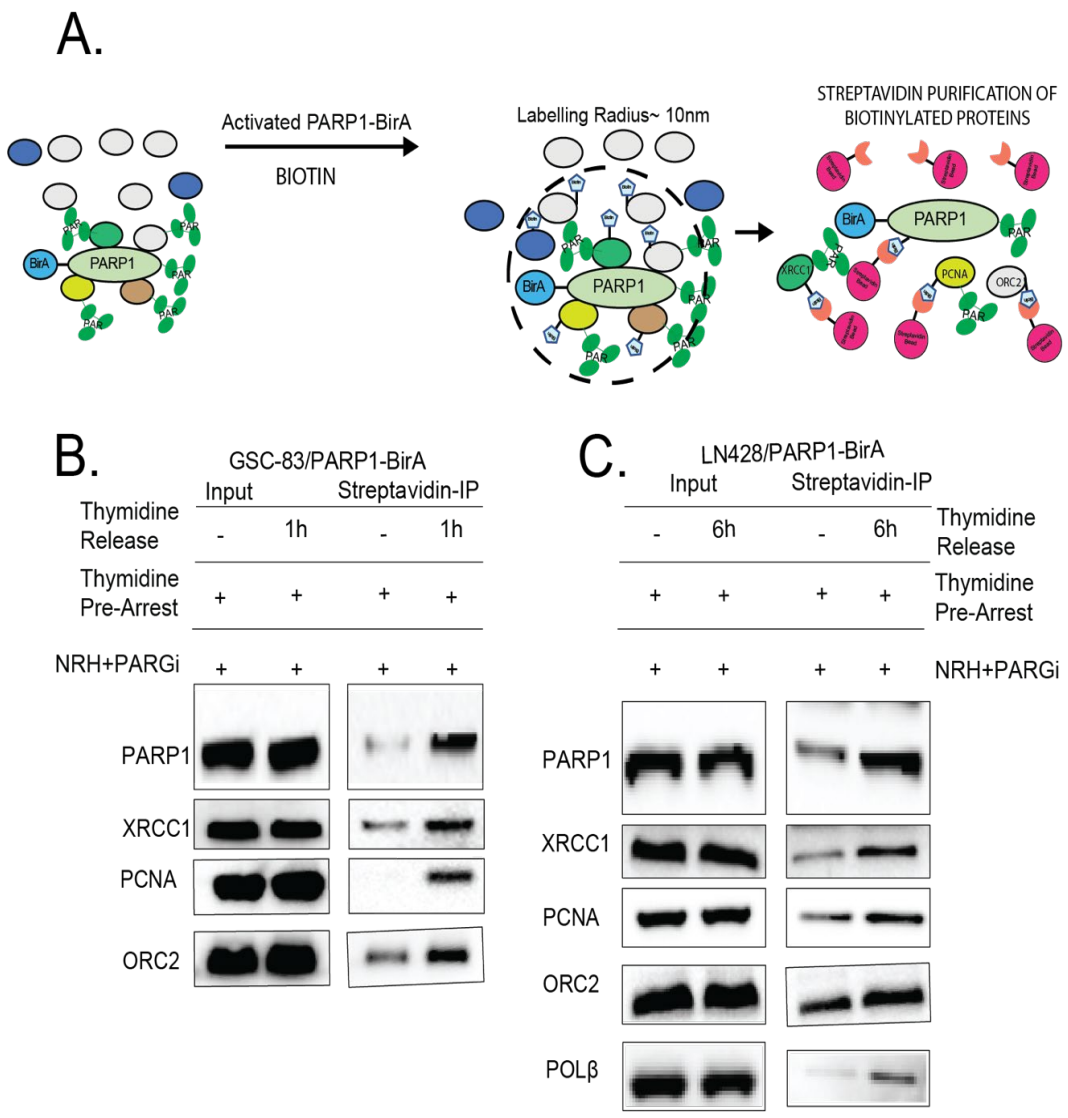

Figure 3.28. Replication-associated PARP1 activation coordinates BER/SSBR pathway engagement and PAR-induced assembly of replication complex proteins.

A. Graphic demonstrating BioID capture of biotinylated proteins following incubation with magnetic, streptavidin beads; B. Immunoblot analysis of PARP1, XRCC1, PCNA and ORC2 of whole cell lysates (input) and of biotinylated proteins captured by BioID, streptavidin-IP after GSC-83/PARP1-BirA cells were thymidine arrested or released and treated with NRH (100μM) + PARGi (10 μM) for 1 h; C. Immunoblot analysis of PARP1, XRCC1, PCNA, Polβ and ORC2 of whole cell lysates (input) and of biotinylated proteins captured by streptavidin-IP after LN428/PARP1-BirA cells were arrested or released and then treated with NRH (100 μM) + PARGi (10 μM) for 6 h.

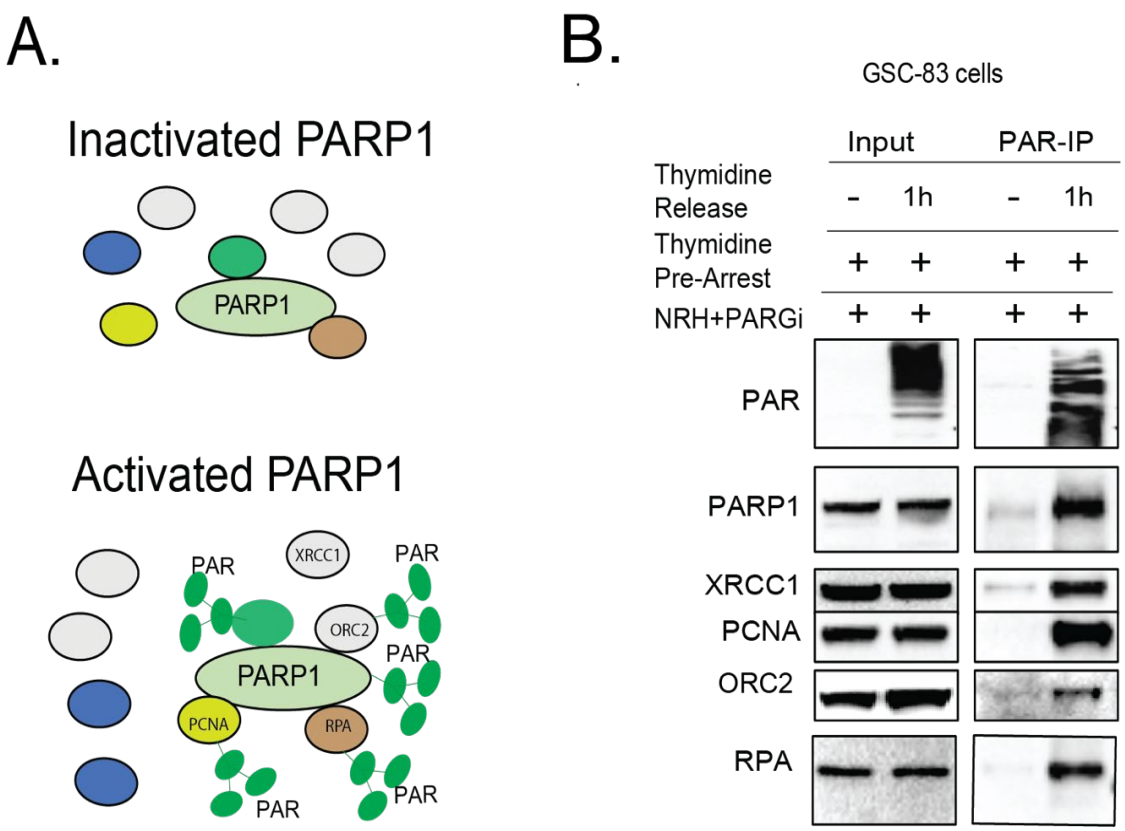

Figure 3.29. Replication-associated PARP1 activation coordinates BER/SSBR pathway engagement and PAR-induced assembly of replication complex proteins.

A. Graphic demonstrating PAR-IP with anti-PAR following incubation with anti-PAR resin beads; B. Immunoblot analysis of PAR, PARP1, XRCC1, PCNA, ORC2 and RPA from whole cell lysates (input) and after PAR-IP isolated from thymidine arrested or released GSC-83 cells, co-treated with NRH (100μM) + PARGi (10μM) for 1h (Completed with Dr. Jianfeng Li).

Together, these results suggested to us that PARP1 and BER/SSBR could play an important role at the replication fork for either repair of base damage, SSB repair or processing of Okazaki fragments as a form of long-patch BER. Therefore, we hypothesized that the activation of PARP1 and PARP2 and subsequent interaction with BER/SSBR proteins, is required for DNA repair encountered during replication. Consistent with our

hypothesis, we found that treatment with NRH/PARGi resulted in a significant increase in PAR accumulation LN428/XRCC1-KO cells as compared to LN428 WT cells. Additionally, we found that the XRCC1-KO cells were selectively sensitive to both PARGi and co-treatment with PARGi and NRH as compared to parental LN428 cells (**Figure 3.30A-B**). This demonstrates that XRCC1 is required in the response to replication stress.

Additionally, we found that inhibiting flap endonuclease 1 (FEN1) significantly enhanced PAR accumulation following combined NRH and PARGi treatment. FEN1 is a BER/SSBR enzyme involved in long-patch repair, reported to play a role in processing the 5' ends of Okazaki fragments by cleaving short- and long-flaps [56]. Further, we found that PARP1 interaction with ORC2, a member of the 6-member subunit initiation complex, is essential during replication stress. Like XRCC1 and FEN1, loss of ORC2 enhances NRH induced PARylation, supporting other studies that suggest ORC2 is involved in the response to replication stress (**Figure 3.31**) [188, 189]. Together, this data suggests a role for PARP1 and BER/SSBR in replication stress and a possible role for processing of Okazaki fragments.

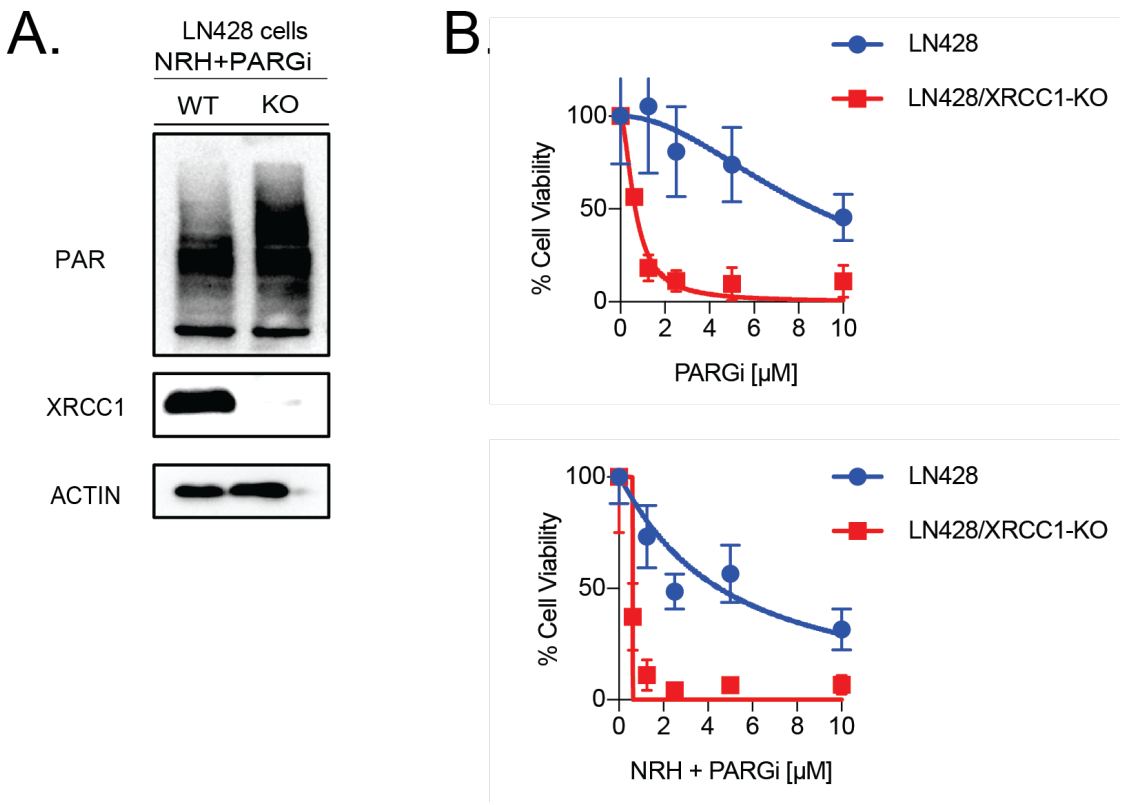

Figure 3.30. Expression of XRCC1 is required in the response to replication stress.

A. Immunoblot analysis of XRCC1 and of PAR from lysates of LN428/WT or LN428/XRCC1-KO cells treated with NRH (100μM) + PARGi (10 μM) for 4h. B. Cell viability analysis of LN428/WT or LN428/XRCC1-KO treated with PARGi for 120 hours at the doses indicated (top) or Cell viability analysis of LN428/WT or LN428/XRCC1-KO treated with NRH (100 μM) + PARGi for 120 hours at the doses indicated (bottom).

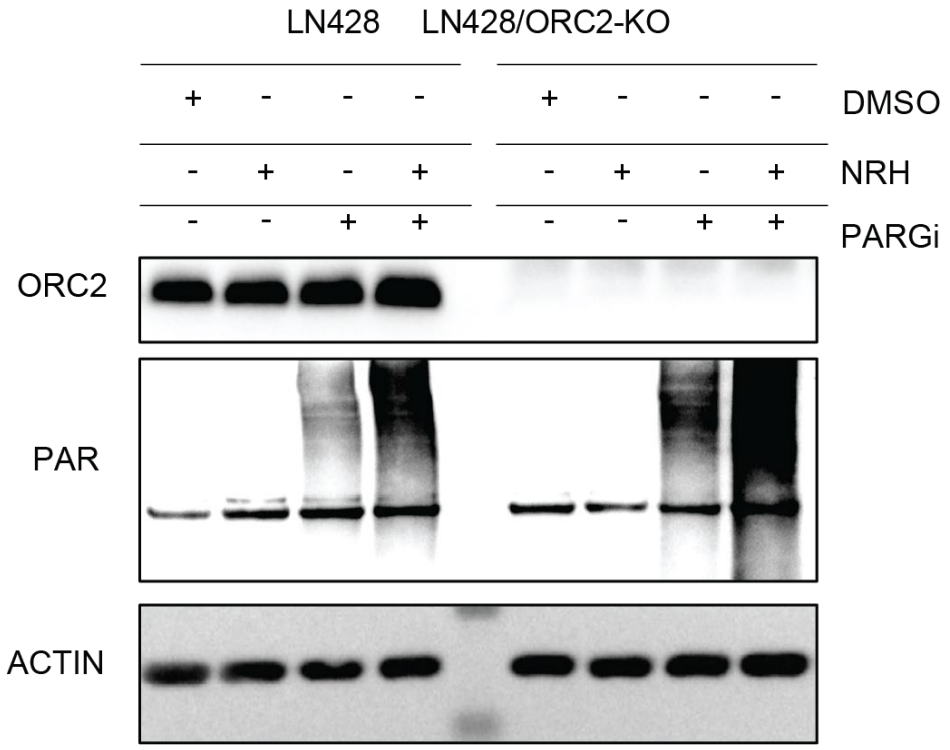

Figure 3.31. Loss of ORC2 expression enhanced PARylation in response to co-treatment with NRH and PARGi.

Immunoblot analysis of ORC2 and of PAR from lysates of LN428/WT or LN428/ORC2-KO treated with NRH (100μM), PARGi (10μM) or co-treated with NRH + PARGi for 4 h, β-Actin was used as the loading control.

IDH1 Mutant Cells Regulate NADP(H) Pools by Suppression of NADP(H) Phosphatases MESH1 and NOCT

NAD^+ homeostasis is disrupted in IDH1 mutant glioma cells because of the overconsumption of NADPH to produce the oncometabolite 2-HG. Additionally, U-87MG/IDH1(R132H) cells have been reported to have downregulated NAPRT and NAMPT protein levels, two enzymes involved in NAD^+ synthesis [47]. The NADP/NADPH pools are maintained in IDH1 mutant glioma by overexpression of NADK, which synthesizes NAD^+ to $NADP^+$ [35]. However, other reports have hypothesized that IDH1 mutant cells have adapted other mechanisms for cytosolic NADPH synthesis from NADH [190, 191], but it is unknown if expression levels of NADP(H) phosphatases are altered in IDH1 mutant glioma cells. First, we measured cellular NAD^+ metabolite levels in U-87MG, a cell line that expresses wildtype IDH1 and U-87MG/IDH1(R132H), an isogenic cell line derived from the parental U-87MG cell line (**Figure 3.32**) [192].

Consistent with previous reports, cellular NAD^+/NADH and NADPH levels were significantly decreased in the IDH1 mutant compared to the parental cell line (**Figure 3.33 A-D**) [35, 191]. However, $NADP^+$ was not significantly altered in the U-87MG/IDH1(R132H) cell line, compared with the parental U-87MG cell line. Next, we analyzed protein expression of NADP(H) phosphatases MESH1 and NOCT by immunoblot. We observed a significant decrease in MESH1 and NOCT protein expression in U-87MG/IDH1(R132H) cells compared to the U-87MG cell line (**Figure 3.34A-C).** This is significant because the depletion of NADP(H) phosphatases prevents restoration of NAD(H) pools in the mitochondria and the cytosol [48, 50], and for use by NAD^+ consuming enzymes such as PARP1 and SIRT1/6.

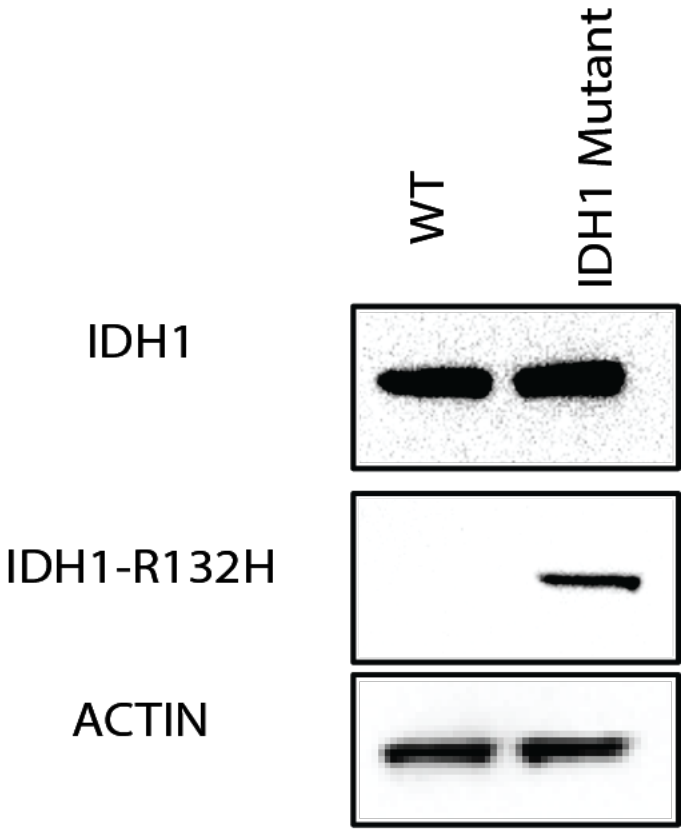

Figure 3.32. Characterization of IDH1 WT and IDH1 mutant cell models.

Immunoblot analysis of wildtype IDH1 and mutant IDH1-R132H protein expression from whole cell lysate of U-87MG (WT) cells compared to U-87MG/IDH1(R132H) cells.

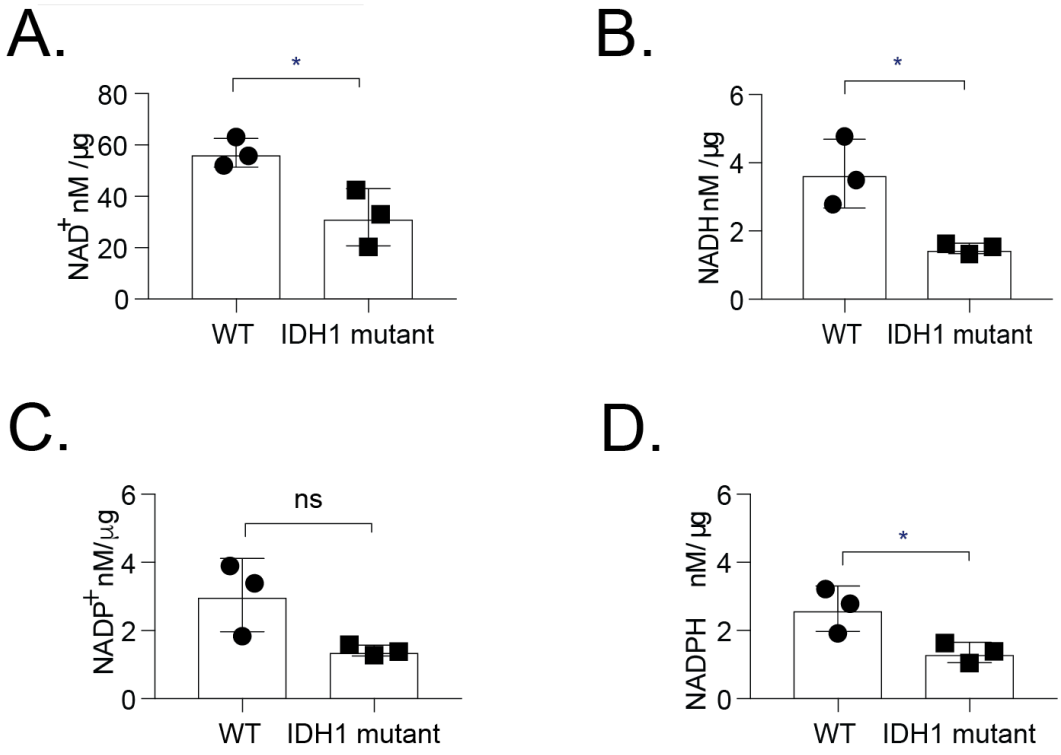

Figure 3.33. Cellular NAD^+ metabolite levels are suppressed in IDH1 mutant cells.

A. NAD^+ analysis in U-87 MG cells compared to U-87MG/IDH1(R132H) n=3 ($p^*<0.05$; Student's t-test); B. NADH analysis in U-87 MG cells compared to U-87MG/IDH1(R132H) n=3 ($p^*<0.05$; Student's t-test); C. $NADP^+$ analysis in U-87 MG cells compared to U-87MG/IDH1(R132H); D. NADPH analysis in U-87 MG cells compared to U-87MG/IDH1(R132H) n=3 ($p^*<0.05$; Student's t-test)

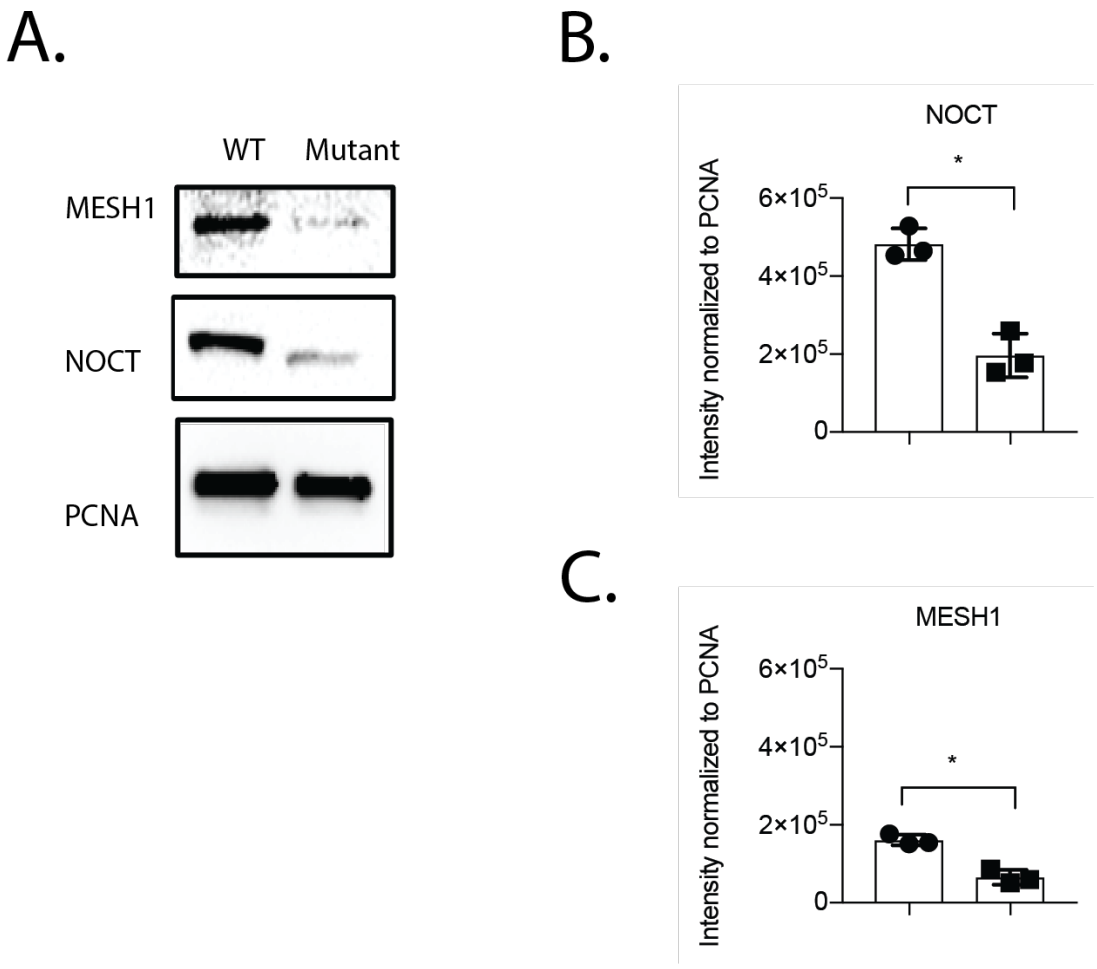

Figure 3.34. MESH1 and NOCT phosphotransferase protein expression is suppressed in IDH1 mutant cells.

A. Immunoblot analysis of MESH1 and NOCT protein expression in U-87MG compared to U-87MG/IDH1(R132H) cells; B. Analysis of immunoblot NOCT protein expression normalized to PCNA, n=9 ($p^*<0.05$; Student's t-test); C. Analysis of immunoblot MESH1 protein expression normalized to PCNA, n=9 ($p^*<0.05$; Student's t-test).

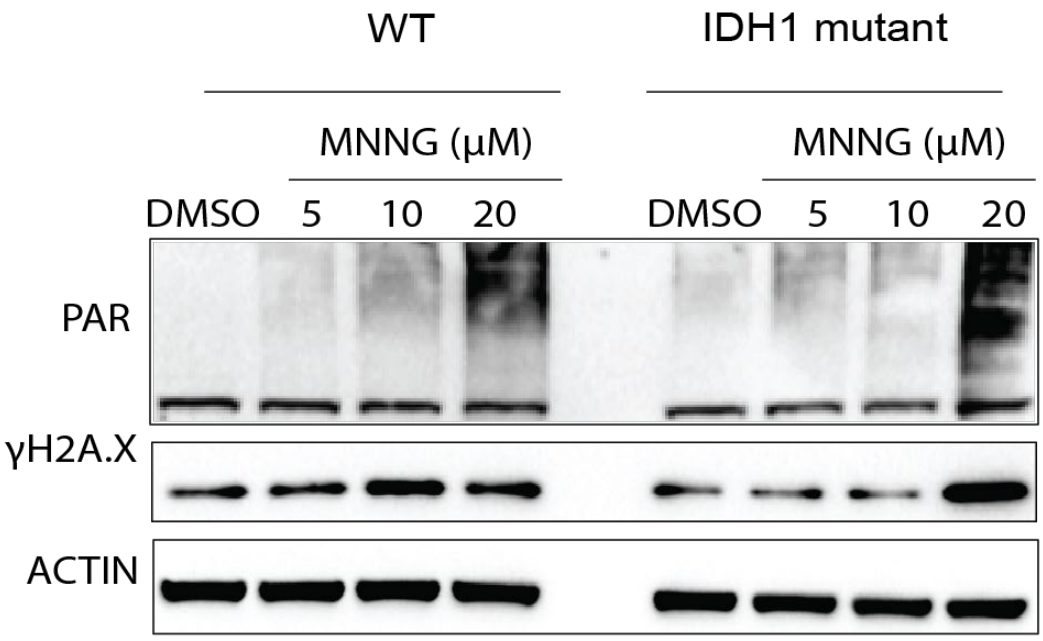

Figure 3.35. Low NAD^+ bioavailability does not alter PARP1 activation in response to DNA damage in IDH1 mutant cells.

PAR Immunoblot of U-87MG cells compared to U-87MG/IDH1(R132H) analysis of and yH2AX following treatment with MNNG (5 μM, 10 μM, 20 μM) 30 minutes. treatment with MNNG (5 μM, 10 μM, 20 μM) 30 minutes.

Selective Sensitivity to Alkylating Agents is not Dependent on NAD^+ Mediated Regulation of PARP1 in U-87MG/IDH1(R132H) Cells.

As we demonstrated, NAD^+ is an essential regulator of PARP1 and BER complex assembly[62], and therefore we reasoned that the low basal NAD^+ levels in U-87MG/IDH1(R132H) cells could impair PARP1 activation potential in response to damage caused by the DNA alkylating agents MMS and MNNG.

Surprisingly, there was no observable difference in PAR accumulation following a dose-response treatment with the DNA alkylating agent MNNG after 15 minutes. However, we did observe a slight increase in phosphorylation of γH2A.X, a sensitive

marker of DNA damage and replication stress, in the IDH1 mutant cell line compared to the WT cell line (**Figure 3.35**). This is consistent with previous reports demonstrating increased γH2A.X levels in U-87MG/IDH1(R132H) cells, following DNA damage with alkylating agents [193, 194].

However, to determine if low NAD bioavailability impacted PAR accumulation at the DNA lesion site, we applied the use of confocal laser microirradiation. First, we transiently expressed LivePAR in U-87MG and U-87MG/IDH1(R132H) cells using a lentiviral vector (described previously) [62]. We developed the LivePAR probe as an imaging tool for real-time visualization of PAR levels that reflects accumulation and degradation of PAR in live cells. Consistent with our immunoblot analysis, we observed rapid recruitment of LivePAR in both the U-87MG and IDH1 mutant cell lines. However, there was no measurable difference in the recruitment kinetics of LivePAR to the lesion site (**Figure 3.36 A-C**). Together, this data suggests that the low basal NAD^+ levels in U-87MG/IDH1(R132H) cells do not significantly impact PAR accumulation in response to DNA damage caused by alkylating agents or microirradiation.

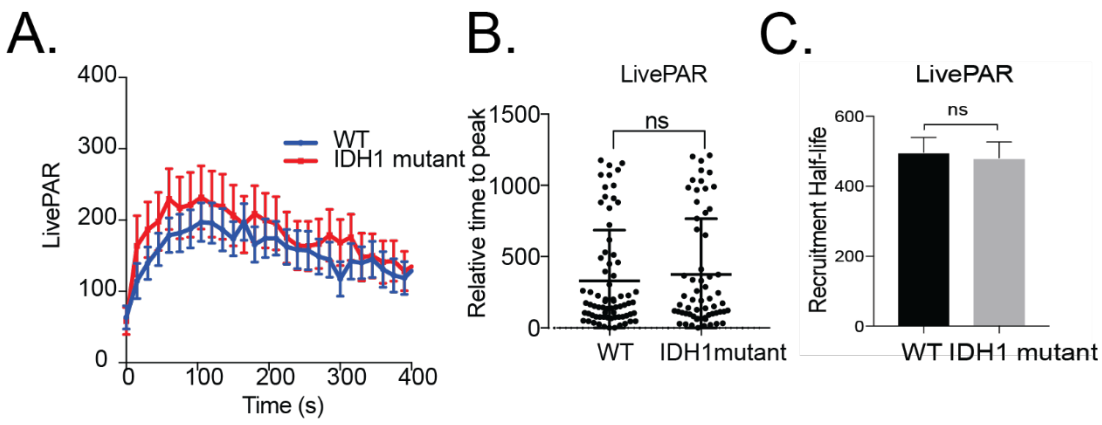

Figure 3.36. Low NAD^+ bioavailability status does not alter PARP1 activation in response to DNA damage in IDH1 mutant cells.

A. Recruitment of LivePAR in U-87 MG/LivePAR and U-87MG/ IDH1(R132H)/LivePAR cells; B. Relative to peak recruitment of U-87 MG/LivePAR and U-87MG/ IDH1(R132H)/LivePAR cells as determined by MIDAS; C. LivePAR half-life of recruitment.

Polβ Protein Expression and BER Complex Assembly is Suppressed in IDH1 Mutant Cells.

Gene and protein expression of several DNA repair proteins, including those involved in HR and MMR, are dysregulated in U-87MG/IDH1(R132H) cells [195]. Lin et al., reported that IDH1 mutant sensitivity to temozolomide (TMZ) was enhanced by suppressed ATM expression, thereby inhibiting the ATM/CHK2 pathway [193]. Interestingly, ATM activation of MPG is required for the recognition of and BER mediated removal of bases damaged by alkylating agents [91, 93]. Therefore, inhibiting BER/SSBR proteins XRCC1, Polβ and LIGIII in ATM deficient cells, can sensitize cells to alkylating agents [93]. We reasoned that IDH1 mutant sensitivity to alkylating agents could be caused by defects in ATM and BER protein expression and activity.

Therefore, we investigated the protein expression of the BER proteins PARP1, PARP2, XRCC1, and Polβ compared to PCNA (loading control). Protein analysis by immunoblot revealed that Polβ expression was significantly decreased in IDH1 mutant cells, but there was no significant change in PARP1, PARP2, XRCC1 or PCNA expression (**Figure 3.37 and 3.38A-D**). Interestingly, we did not find any significant changes in mRNA expression of PARP2, XRCC1, Polβ, LIGIII, or APTX; however, gene expression of PARP1 was significantly enhanced in IDH1 mutant cells compared to U-87MG (**Figure 3.39**), demonstrating that gene expression and mRNA expression do not always concur [196].

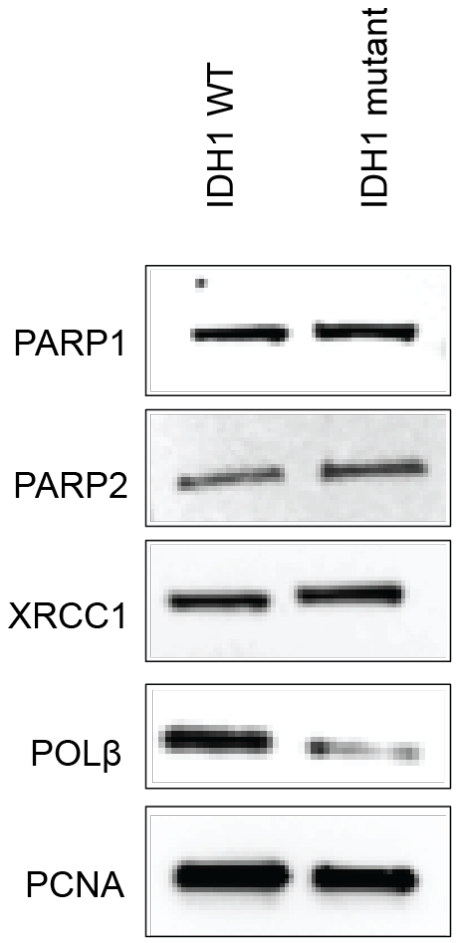

Figure 3.37. Polβ protein expression is suppressed in IDH1 mutant cells.

Immunoblot analysis of PARP1, PARP2, XRCC1, and Polβ compared to PCNA as a loading control in U-87MG cells compared to U-87MG/IDH1(R132H) cells.

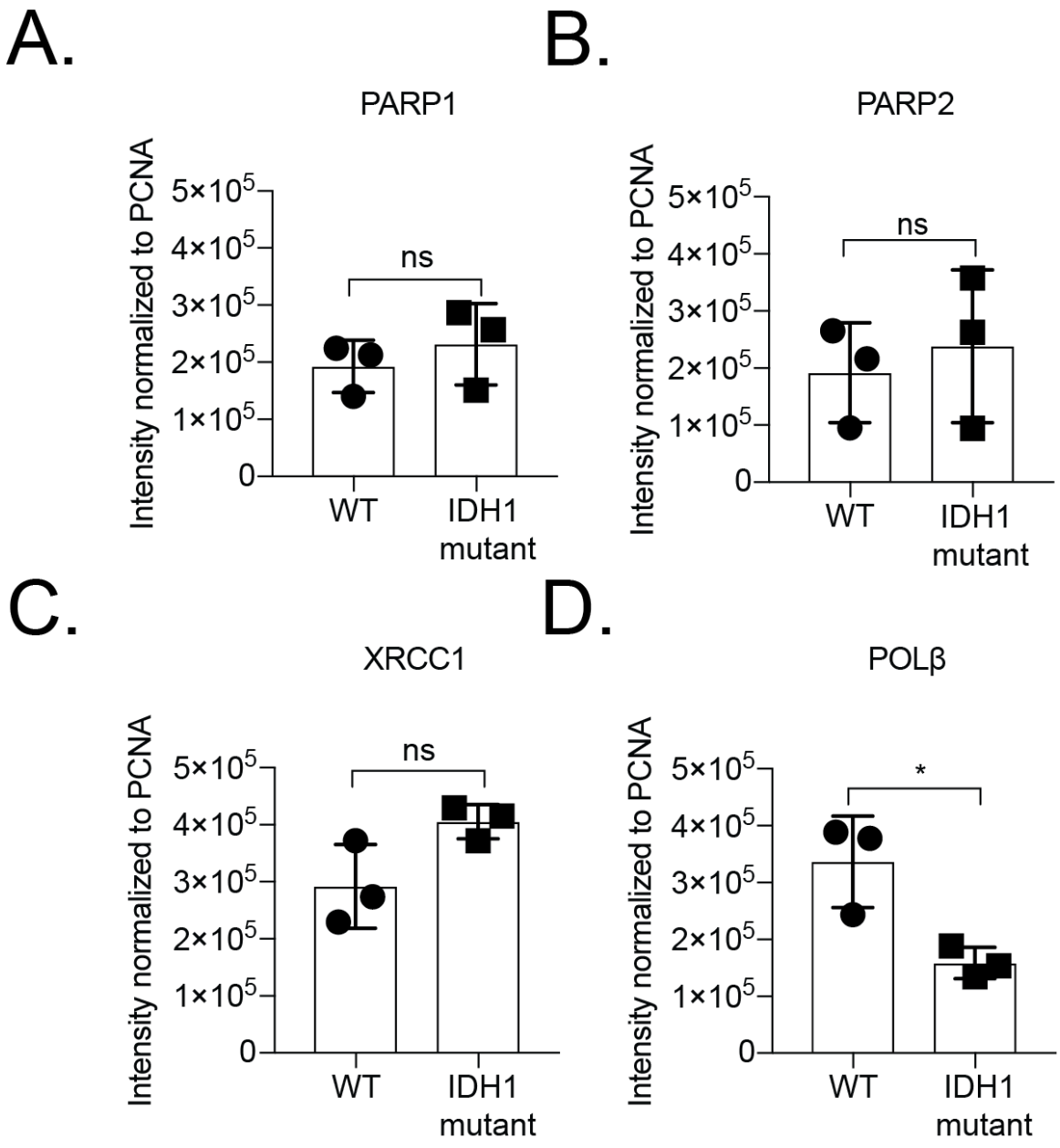

Figure 3.38. BER protein expression normalized to PCNA.

A-D. Analysis of immunoblot expression of PARP1, PARP2, XRCC1, Polβ normalized to PCNA, n=9 ($p<*0.05$; Student's t test).

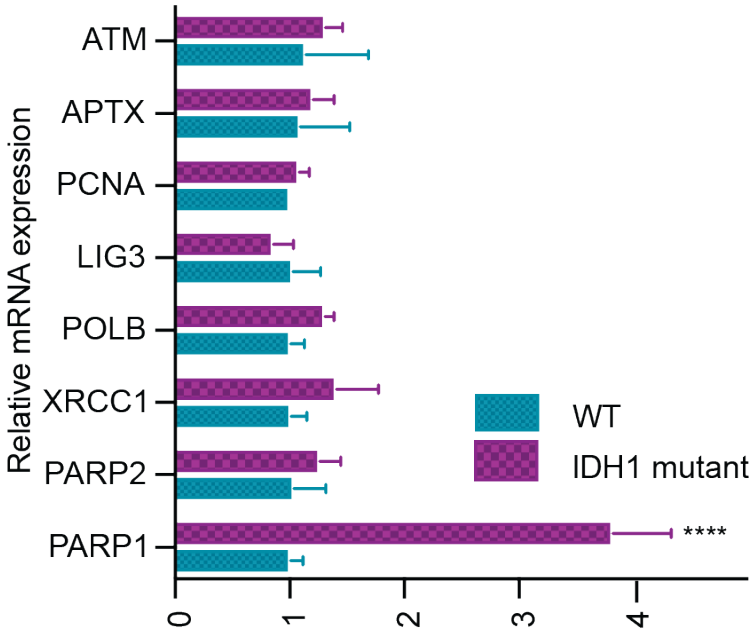

Figure 3.39. Characterization of BER/SSBR gene expression.

Relative mRNA expression levels of ATM, APTX, PARP1, PARP2, PolB, XRCC1, LIGIII, XRCC1 and PCNA normalized to actin in U-87MG compared to U-87 MG/ IDH1(R132H) cells, n=3 (****p<0.0001, multiple t-test analysis).

XRCC1 and Polβ are mutated in a high percentage of cancers, leading to suppressed enzyme activity of Polβ at the DNA lesion site [58, 137]. Failure of Polβ to form a complex with XRCC1 at the DNA lesion site leads to Polβ degradation and genome instability [1, 8, 58, 197]. Therefore, we reasoned that protein recruitment dynamics, of XRCC1 or Polβ to the DNA lesion site, could be impaired in IDH1 mutant cells. Lentiviral vectors expressing EGFP fused XRCC1 and EGFP fused Polβ were transduced into U-87 MG and U-87 MG/IDH1(R132H) cells, and protein expression was confirmed by immunoblot (**Appendix Figure A.5**).

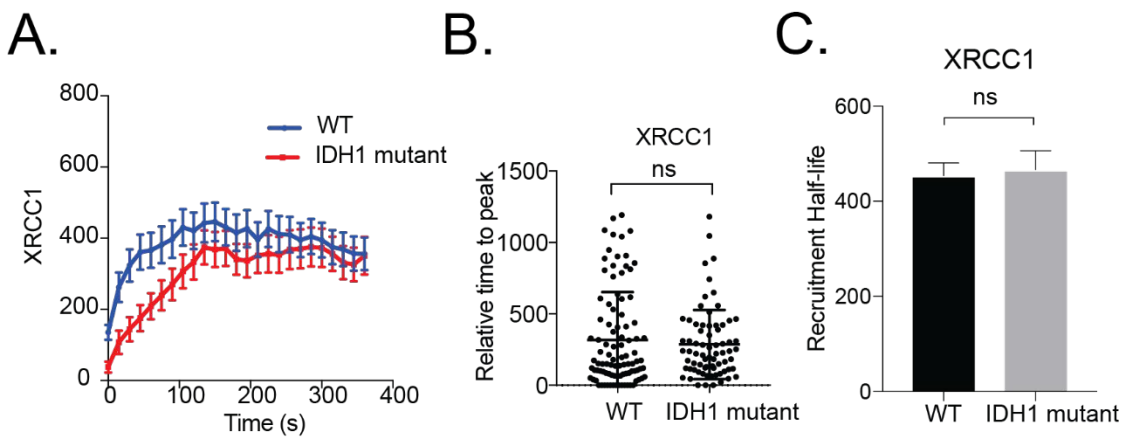

Figure 3.40. XRCC1 protein recruitment kinetics are not altered in IDH1 mutant cells compared to IDH1 WT.

A. Recruitment of XRCC1 in U-87 MG compared to U-87 MG/ IDH1(R132H) cells; B. XRCC1 relative time to peak as determined in MIDAS; C. XRCC1 half-life of recruitment.

Following laser microirradiation, XRCC1-EGFP and Polβ-EGFP rapidly recruited to the site of 355-nm laser-induced DNA damage in both U-87MG and U-87MG/ IDH1(R132H) cells. Consistent with the recruitment profile of LivePAR, there was no significant change in recruitment dynamics of XRCC1 or Polβ in the U-87 MG/ IDH1(R132H) cell line as compared to the U-87MG cell line (**Figure 3.40-C and 3.41A-C**).

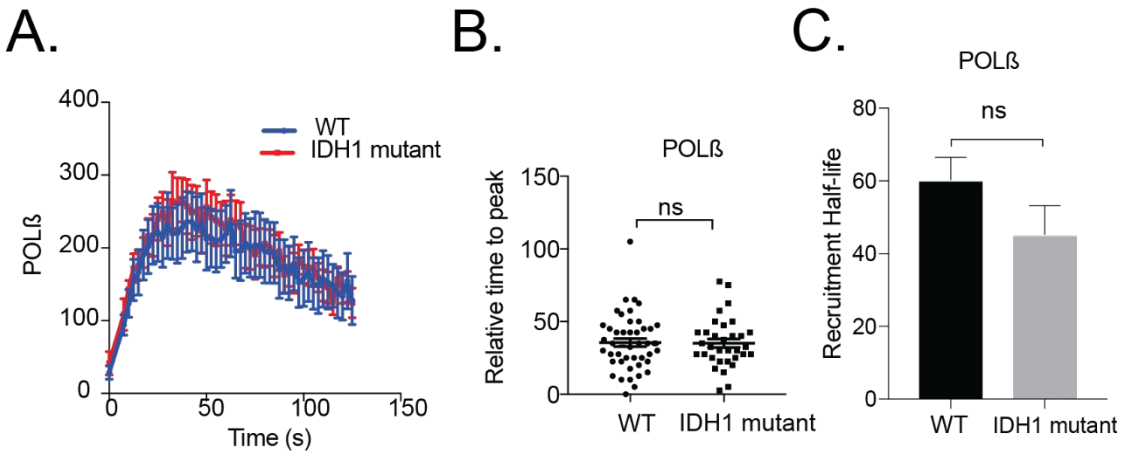

Figure 3.41. Polβ protein recruitment kinetics are not altered in IDH1 mutant cells compared to IDH1 WT.

A. Recruitment of Polβ in U-87MG compared to U-87MG/IDH(R132H) cells; B. Polβ relative time to peak as determined in MIDAS; C. Polβ half-life of recruitment.

Oncometabolite 2-HG Suppresses Polβ Protein Expression

2-Hydroxyglutarate (2-HG) inhibits methyltransferase activity, causing widespread epigenetic changes, resulting in DNA repair gene suppression and genome instability [40, 41, 198]. The regulation of the levels of the homologous recombination (HR) proteins ATM and RAD51 by 2-HG has been reported to confer IDH1 mutant hypersensitivity to DNA damaging agents and PARP inhibitors [4, 123, 198]. Although the regulation of α-KG dependent methyltransferases such as TET and KDM are well documented for the suppression of homology directed repair (HDR) [156, 157], recent reports have emerged that suggest 2-HG could play a role in regulating enzyme activity beyond epigenetic control, including those involved in metabolism and DNA repair such as NF-KB and DMNT1 [199]. Since Polβ mRNA levels were not significantly different in the U-

8MG/IDH1 (R132H) compared to the U-87MG cell line, it is unlikely that Polβ protein regulation is a result of epigenetic regulation of Polβ gene expression in the IDH1 mutant.

Therefore, to determine if 2-HG alone could suppress Polβ protein expression, we supplemented cells with 500μM and 1 mM of D-2-HG for 2 hours and analyzed Polβ protein expression by immunoblot. Interestingly, we found a dose-response decrease in Polβ expression in the U-87 MG cell line with the 1mM dose suppressing Polβ protein expression levels similarly to the U-87 MG/ IDH1(R132H) cell line (**Figure 3.42**). This suggests that the regulation of Polβ expression in the IDH1 mutant may be 2-HG dependent.

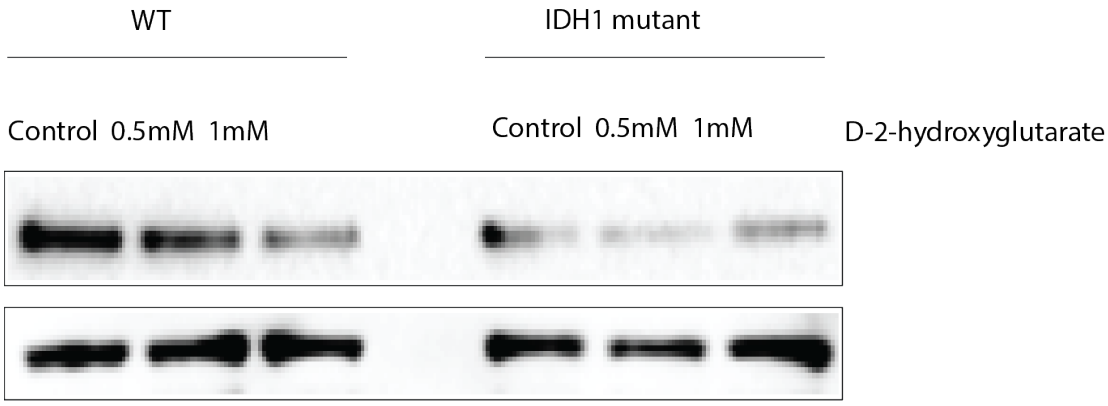

Figure 3.42. Oncometabolite 2-HG suppresses Polβ protein expression.

Immunoblot analysis of U-87 MG and U-87 MG/ IDH1(R132H) cells treated with D-2-HG (0.5 mM and 1 mM) for 2 hours, n=3.

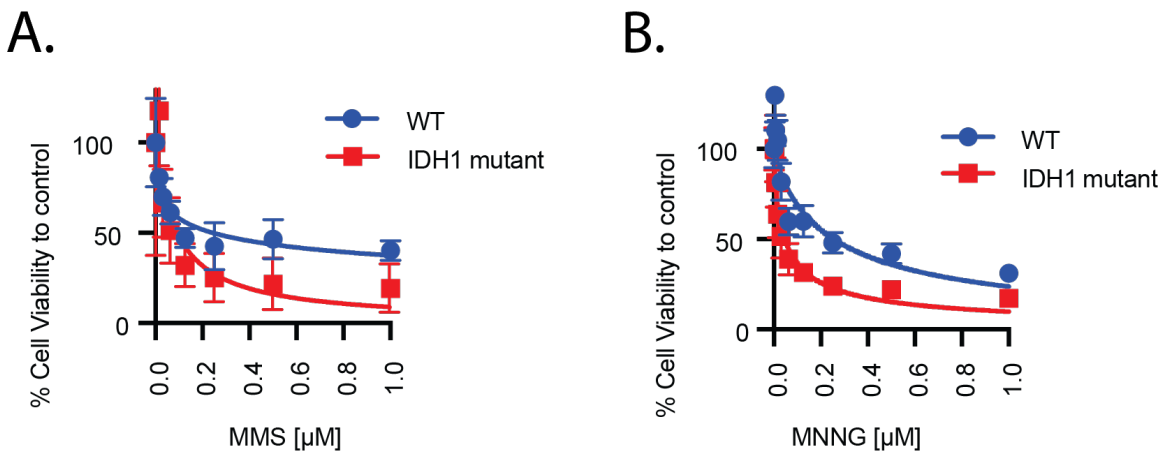

Figure 3.43. IDH1 mutant cells deficient in Polβ show enhanced sensitivity to alkylating agents.

A. Cell viability assay of U-87MG and U-87 MG/IDH1(R132H) cells treated with MMS for 120 hours as indicated; n=3; B. Cell viability assay of U-87MG and U-87MG/ IDH1(R132H) cells treated with MNNG for 120 hours as indicated, n=3.

Polβ Deficiency Enhances Sensitivity of IDH1 Mutant Cells to Alkylating Agents

Although cells deficient in Polβ demonstrate normal growth and viability, they are extremely sensitive to alkylating agents, especially in combination with defects in HR [98, 163, 197]. Cabelof et al. reported even a 50% suppression of Polβ protein expression leads to an increase in SSBs, mutagenicity and chemosensitivity to DNA alkylating agents [8] and overexpression of Polβ contributed to resistance to alkylating agents and poor cancer prognosis [131]. We treated U-87MG and U-87MG/IDH1(R132H) cells with DNA alkylating agents, MNNG or MMS at the doses indicated, and measured cell viability after 5 days (120 hours). Cell viability was measured using an assay that measures constitutive protease activity in live cells. The permeable, live-cell, fluorescent, peptide substrate enters the cell, where it is cleaved by protease activity, to generate a fluorescent signal that

positively correlates with the number of living cells. Consistent with previous reports, U-87MG/IDH1(R132H) cells were significantly more sensitive to MNNG, and MMS compared to the U-87 MG (**Figure 3.43 A-B**) [152, 200].

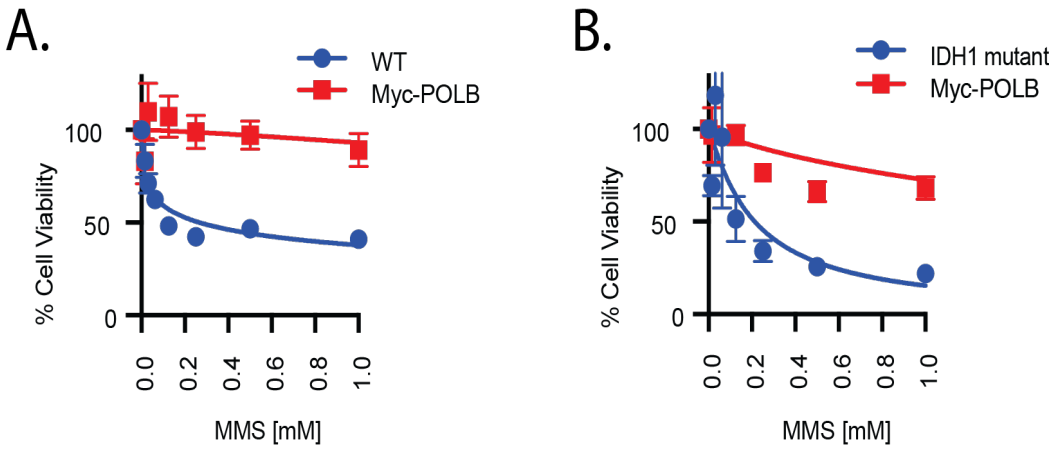

Figure 3.44. Overexpression of Polβ in IDH1 mutant glioma cells induces an MMS resistant phenotype.

A. Cell viability assay of U-87 MG and U-87 MG /Myc-PolB cells treated with MMS for 120 hours as indicated. B. Cell viability assay of U-87MG and U-87MG/IDH(R132H)/Myc-PolB cells treated with MMS for 120 hours as indicated n=3.

Next, we overexpressed Polβ in U-87MG and U-87MG/ IDH1(R132H) cells to determine if Polβ overexpression could rescue the hypersensitive phenotype of IDH1 mutant cells to treatment with MMS or MNNG. Polβ fused with a Myc tag on the N-terminus, was expressed in cells by lentiviral transduction, and protein expression was confirmed by immunoblot (**Appendix figure A.7)**. Each cell line was treated with MNNG or MMS, as indicated in the figure legend, and cell viability was determined after 5 days (120 hours). We found that Polβ overexpression fully rescued the hypersensitive phenotype of the U-87 MG/IDH1(R132H) cell line to MMS or MNNG (**Figure 3.44 A-B and 3.45**

A-B). This is consistent with previous reports that found expression of wildtype Polβ in Polβ deficient cells fully rescued from sensitivity to MMS [131, 147, 165]. These data suggest that IDH1 mutant glioma cancers confer sensitivity to alkylating agents because of suppressed BER/SSBR functional capacity. Since cells with defects in BER/SSBR are selectively sensitive to PARG inhibitors, we expanded our model to investigate how Polβ deficiency impacts IDH1 mutant sensitivity to PARG inhibition.

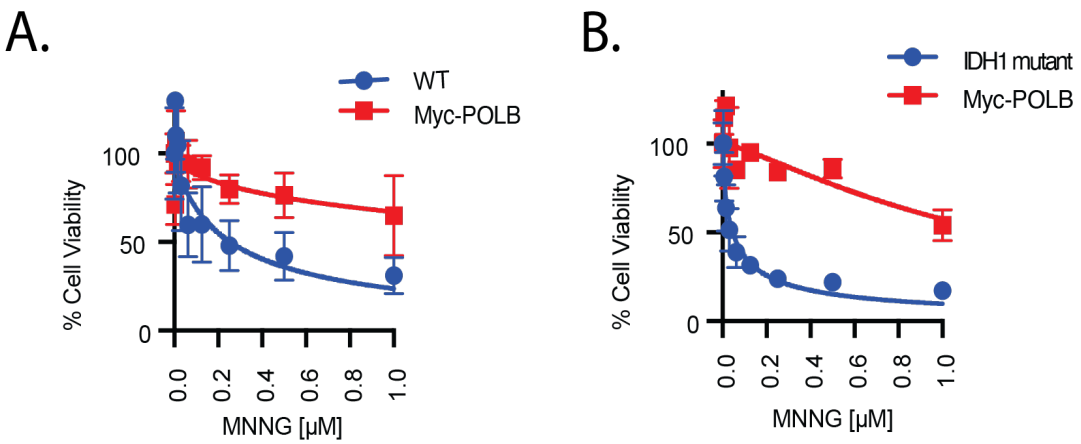

Figure 3.45. Overexpression of Polβ rescues IDH1 mutant cells from sensitivity to MNNG.

A. Cell viability assay of U-87 MG and U-87 MG /Myc- Polβ cells treated with MMS for 120 hours as indicated; B. Cell viability assay of U-87MG and U-87MG/IDH(R132H)/Myc- Polβ cells treated with MMS for 120 hours as indicated, n=3.

PARG Inhibition Enhanced Cytotoxicity in IDH1 Mutant Glioma Cells Deficient in Polβ

PARP1 and PARG are central to BER/SSBR for the assembly and disassembly of DNA protein complexes, respectively. The development of several promising PARG inhibitors has renewed research interests for targeting dePARylation as a strategy to overcome PARP inhibitor resistance. As our lab and others have demonstrated that deficits in BER/SSBR protein expression induce hyperPARylation, replication stress, and enhanced sensitivity to treatment with the PARG inhibitor PDD00017273 [56, 68, 93]. Ali et al, found that ovarian cancers deficient in Polβ show enhanced replication stress, demonstrated by the accumulation of ATR and $pCHK^{ser345}$, and PARG inhibition was able to induce hyperPARylation and synthetic lethality in these cell lines [131]. Similarly, IDH1 mutant cells have elevated levels of replication stress and increased protein levels of ATR and $pCHK^{ser345}$ [72, 193]. Therefore, we reasoned that PDD00017273 would induce synthetic lethality in Polβ deficient U-87MG/IDH1(R132H) cells because of toxic hyperPARylation in response to elevated levels of replication stress.

We treated U-87MG and U-87MG/IDH1(R132H) cells with PARGi (10μM) for the times indicated in the figure legend and found that PAR accumulated in both the U-87MG and U-87MG/IDH1(R132H) cell line and peaked between 6- 8 hours. Additionally, PARGi induced elevated protein expression of replication stress and DNA damage marker γH2A.X (**Figure 3.3.15**), indicating PARGi alone was sufficient to induce replication arrest in U-87MG/IDH1(R132H) cells. PAR accumulation was significantly higher in the mutant compared to the WT, which is consistent with previous reports that Polβ deficient

cells have higher accumulation of PAR in response to PARGi and enhanced replication stress [131] and my previous data that demonstrated Polβ interacts with PARP1 in response to replication stress.

We treated cells with PARGi at the doses indicated for 5 days (120 hours) and determined cell viability. We observed that the U-87MG/IDH1(R132H) cell line was selectively sensitive to PARGi compared to the U-87MG cells (**Figure 3.46**). To determine if suppressed Polβ enhanced the sensitivity of IDH1 mutant cells to PARGi we treated U-87MG/myc-PolB and U-87MG/IDH1(R132H)/ myc-PolB cells with PARGi for 5 days (120 hours) (**Figure 3.47A-B**). Next, we measured cellular NAD^+ levels after time-course treatment with PARGi, and found after 8 hours, there was not a significant decrease in cellular NAD^+ levels, suggesting that the depletion of NAD^+ was not a significant factor for U-87MG/IDH1(R132H) chemosensitivity to PARGi (**Figure 3.48 A-D**). Together, this data suggests that Polβ deficiency induces enhanced lethality in IDH1 mutant cells in response to PARGi, inducing hyperPARylation and replication arrest, without depleting cellular NAD^+ levels.

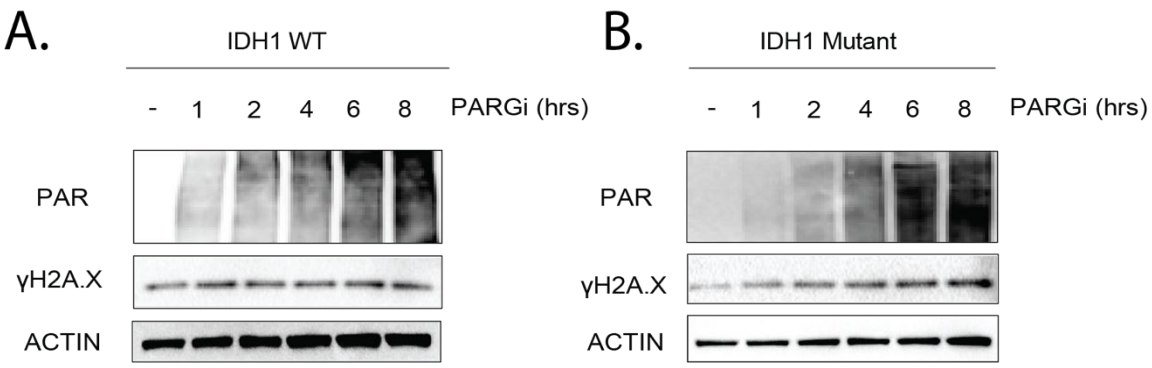

Figure 3.47. PARGi induced hyperPARylation.

A. Immunoblot analysis of PAR in U-87MG treated with PARGi (10 μM) for the times indicated; B. Immunoblot analysis of PAR in U-87MG/IDH(R132H) treated with PARGi (10 μM) for the times indicated, n=2.

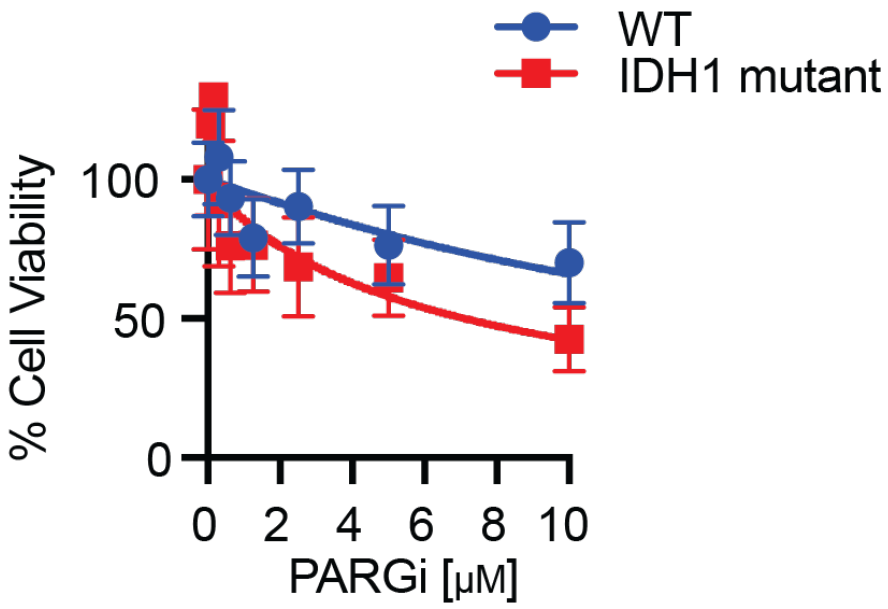

Figure 3.46. IDH1 mutant cells deficient in Polβ show increased sensitivity to PARGi.

Cell viability assay of U-87MG and U-87MG/IDH1(R132H) cells treated with PARGi as indicated, n=4.

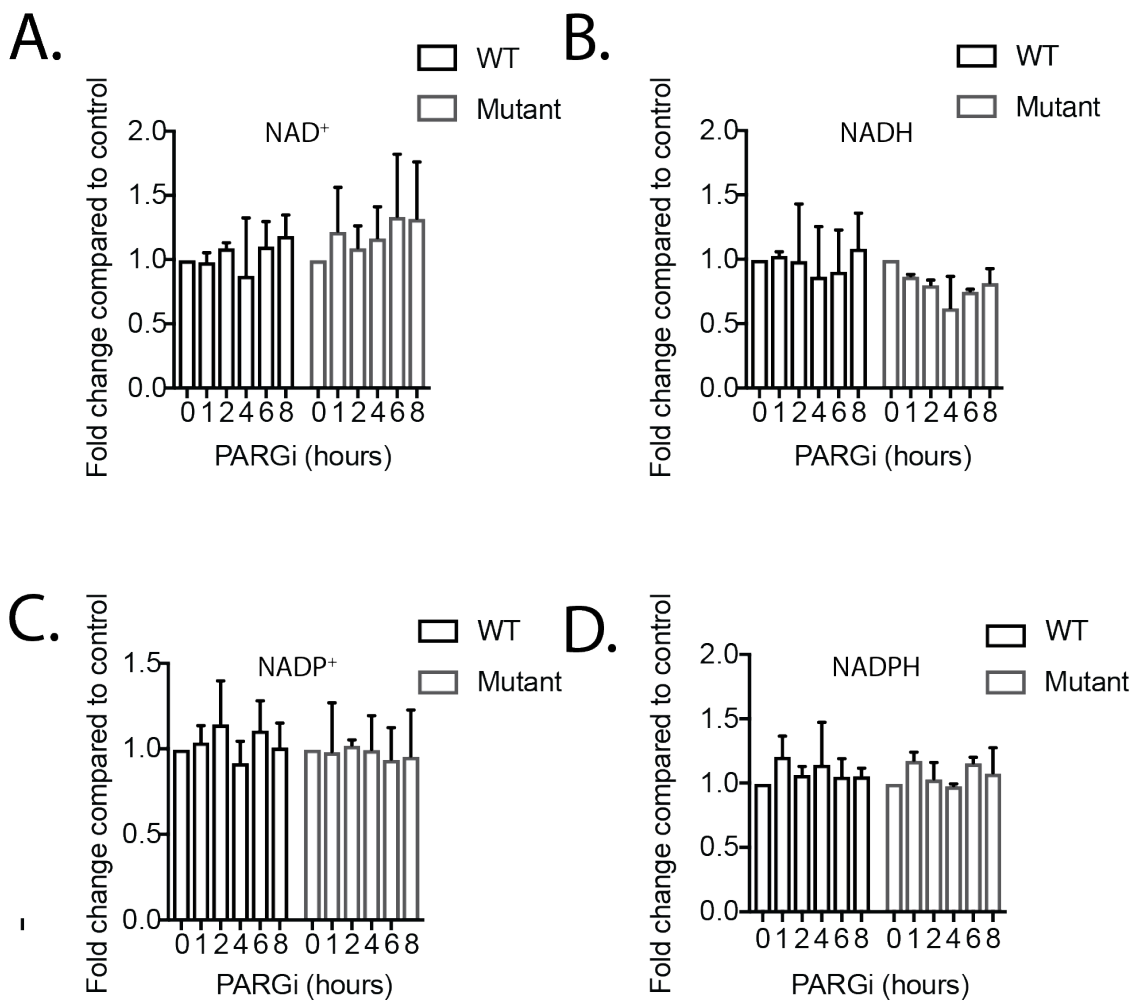

Figure 3.48. PARGi does not deplete cellular NAD^+/NADH and $NADP^+$/NADPH levels in IDH1 mutant glioma cells.

A. NAD^+ analysis of U-87MG compared to U-87MG/IDH1(R132H) following treatment with PARGi (10 μM) for the times indicated; B. NADH analysis of U-87MG compared to U-87MG/IDH1(R132H) following treatment with PARGi (10 μM) for the times indicated; C. $NADP^+$ analysis of U-87MG compared to U-87MG/IDH1(R132H) following treatment with PARGi (10 μM) for the times indicated; D. NADPH analysis of U-87MG compared to U-87MG/IDH1(R132H) following treatment with PARGi (10 μM) for the times indicated n=3 (Two-way ANOVA).

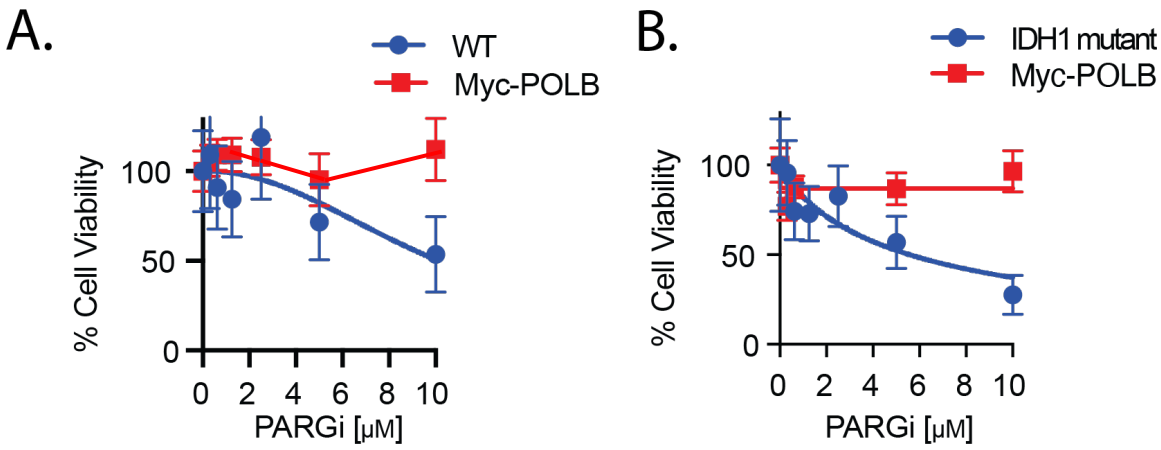

Figure 3.49. Overexpression of Polβ in IDH1 mutant cells enhances resistance to PARGi.

A. Cell viability assay of U-87MG and U-87MG/myc-Polβ cells treated with PARGi as indicated. B. Cell viability assay of U-87MG/IDH1(R132H) cells and U-87/IDH1(R132H)/myc-Polβ cells treated with PARGi as indicated, n=3.

IDH1 Mutant Glioma Regulates NRH Catabolism to Enhance and Stabilize NADPH Pools

Recently, it was reported that IDH1 mutant sensitivity to co-treatment with PARG and TMZ was due to hyperPARylation and NAD^+ depletion [130]. Further, it was reported that supplementation with the NAD^+ precursor NAM moderately decreased sensitivity PARGi and co-treatment with TMZ and PARGi [130]. However, previously, we found that NAM is insufficient to induce a robust PAR accumulation in response to DNA damage [56, 59]. This is possibly because NAM inhibits SIRT1/6 activity, which is necessary to enhance PARP1 activity [1, 44, 52]. However, co-treatment with NRH induced hyperPARylation, consistent with increased cellular NAD^+ levels up to 72 hours after treatment, and enhanced sensitivity to PARGi in GSCs and glioma cells by inducing CHK1 activation and intra-S phase arrest leading to apoptosis [56].

We reasoned that NRH would be sufficient to increase NAD^+ in U-87MG/IDH1(R132H) cells and induce spontaneous replication stress mediated PAR accumulation. We supplemented cells with NRH (100μM) and measured cellular NAD^+ levels at the times indicated. We found NRH increased cellular NAD^+ levels up to 4-fold in U-87MG cells, and up to 3-fold in IDH1 mutant cells with peak NAD^+ levels between 4-6 hours (**Figure 3.50A**). We observed a 40-50-fold increase in NADH levels in the U-87MG/IDH1(R132H) cells between 1-6 hours, however there was no significant change in cellular NADH levels in the U-87MG cells after supplementation with NRH (**Figure 3.50B**). We did not observe a significant change in $NADP^+$ levels in the U-87MG cells or U-87MG/IDH1(R132H) cells following treatment with NRH (**Figure 3.50C**); however, there was a small significant peak in NADPH at 4 hours in the U-87MG cells, while

NADPH levels were increased ~40-fold (4 hours) in the U-87MG/IDH1(R132H) cell line (**Figure 3.50D**). This suggests that U-87MG/IDH1(R132H) cells modify metabolism in reverse to synthesize NADPH from NADH to produce 2-HG (**Figure 3.51**).

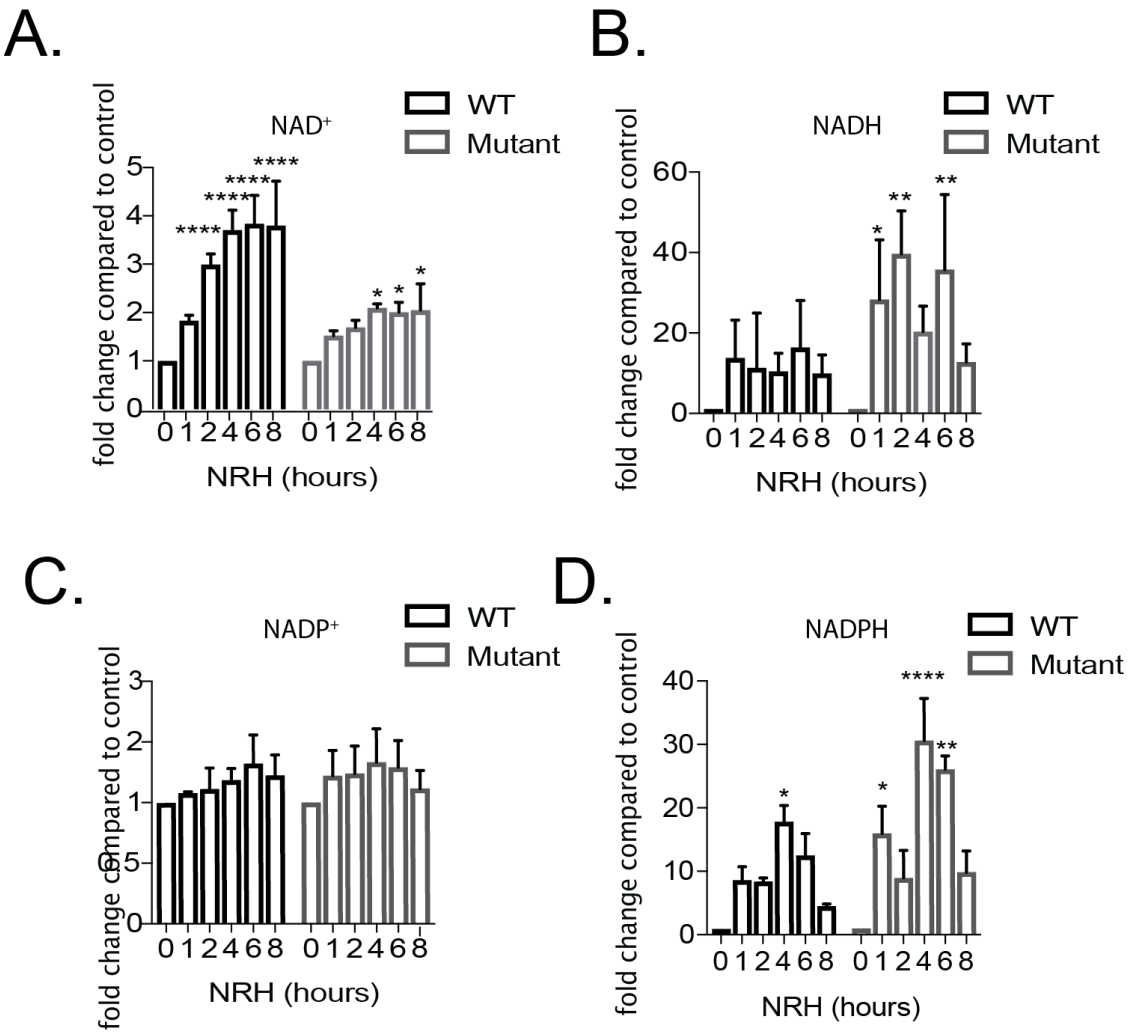

Figure 3.50. NRH enhances cellular NAD^+ metabolite bioavailability in U-87MG cells and U-87MG/IDH1(R132H) cells.

A. NAD^+ analysis of U-87MG cells and U-87MG/IDH1(R132H) cells following treatment with NRH (100 μM) for the times indicated; B. NADH analysis of U-87MG cells and U-87MG/IDH1(R132H) cells following treatment with NRH (100 μM); C. $NADP^+$ analysis of U-87MG cells and U-87MG/IDH1(R132H) cells following treatment with NRH (100 μM for the times indicated; D. NADPH analysis of U-87MG cells and U-87MG/IDH1(R132H) cells following treatment with NRH (100 μM) for the times indicated ($p<*0.05$; $p<**0.01$, $p<***0.001$; $p<****0.001$; Two-way ANOVA).

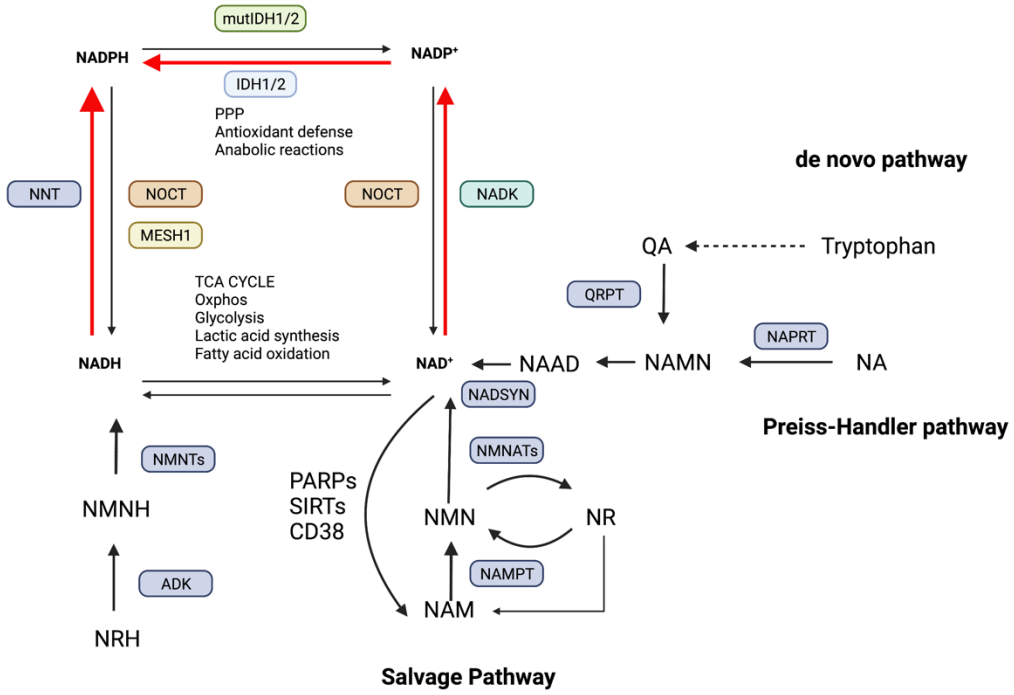

Figure 3.51. Graphic demonstrating altered NAD$^+$/NADH metabolism in IDH1 mutant cells.

IDH1 cells have reduced NAPRT and NAMPT expression levels leading to suppressed NAD(P)/NAD(P)H levels that are further suppressed by mutIDH1overconsupmtion of NADPH for the overproduction of 2-HG. NADK levels are over expressed driving the conversion of NAD to NADPH. IDH1 mutant cells suppress expression of NOCT and MESH1 phosphatases preventing them from restoring NAD/NADH pools.

NAD$^+$ Enhances Chemosensitivity of Polβ Deficient IDH1 Mutant Cells to PARG Inhibition

Next, we treated cells with NRH (100μM) and analyzed whole cell lysates by immunoblot to determine if enhanced NAD$^+$ could induce spontaneous PARylation. Consistent with our previous studies, NRH was able to promote elevated levels of PAR in both the U-87MG/IDH1(R132H) and U-87MG cell lines, consistent with NRH enhanced NAD$^+$ biosynthesis that peaked at 8 hours for both cell lines (**Figure 3.52A-B**).

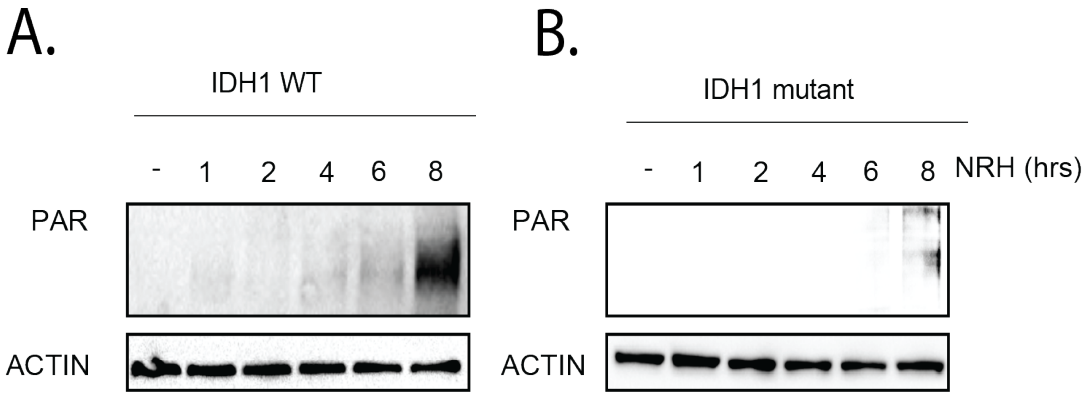

Figure 3.52. NRH enhances PARP1 activation in U-87MG cells, and U-87MG/IDH1 (R132H) cells.

A. PAR immunoblot analysis of U-87MG cells treated with NRH (100μM) for the times indicated; B. PAR immunoblot analysis U-87MG/IDH1(R132H) cells treated with NRH (100μM) for the times indicated, n=3.

As mentioned previously, ROS produces several DNA lesions that can lead to abasic sites, single- and double-stranded breaks, mismatched bases, DNA cross-links or base modifications, leading to gene and protein mutations, aging, and tumorigenesis. Most oxidative lesions such as 8-hydroxyguanine, formamidopyrimidines, and 5-hydroxyuracil

are repaired by BER/SSBR, which requires the activation of PARP1 at the lesion site to initiate DNA repair [201, 202]. There are several ROS that are generated in cells including hydrogen peroxide, hydroxyl radical, singlet oxygen, and superoxide. The half-life of H_2O_2 is the longer than other ROS, and many ROS are converted to H_2O_2 within the cell, such as the conversion of O_2^- to H_2O_2 by superoxide dismutase [202-204]. Therefore, we measured H_2O_2 as a method to reflect a general change in cellular ROS levels to determine if the spontaneous increase in PAR could possibly be due to pyridones synthesized from NRH, as previously reported in HEPG3 cells [33, 34].

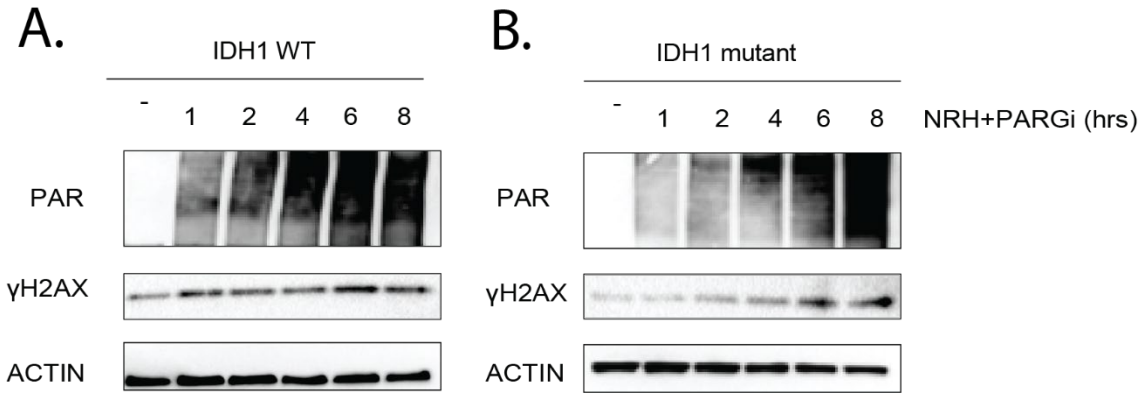

Figure 3.53. PAR Immunoblot following time course treatment with NRH + PARGi in U-87MG and U-87/IDH1 (R132H) cells.

A. U-87MG treated with NRH (100µM) + PARGi (10µM) for the times indicated; B. IDH1-R132H treated with NRH (100 µM) + PARGi (10µM) for the times indicated, n=2.

However, we did not observe a significant difference in ROS levels of U-87MG cells as compared to the U-87MG/IDH1(R132H) cells, although, there was a significant increase in ROS in the culture media as compared to U-87MG cells (6 hours) and U-

87MG/IDH1(R132H) cells (8 hours), suggesting that ROS were produced in the cell culture media abiotically following supplementation with NRH (**Appendix Figure A7)**. An explanation for the reduced ROS in U-87MG cells and U-87MG/IDH1 (R132H) cells, compared to the cell culture media alone, could be the elevated levels of NADPH available for redox metabolism [16]. However, recent reports have demonstrated that IDH1 mutants are dependent on Nrf2 mediated pathways for ROS scavenging [205, 206]. Therefore, an increase in NADPH and NRH could further enhance the Nrf2 mediated activation of NADPH:NQO1 and NRH:NQO2 in the response to oxidative stress to reduce the cycling of ROS [34, 205].

To determine if NRH caused mitochondrial dysfunction, we utilized a multiplexed kit assay that measures ATP and cell membrane integrity following treatment with xenobiotic compounds. These two subsets of data can be combined to represent either mitochondrial dysfunction or unrelated cell cytotoxicity. Cells produce ATP by glycolysis (cytoplasm) and OXPHOS (mitochondria). Therefore, cells that depend more on OXPHOS for ATP production are more sensitive to mitochondrial toxicants. To determine if NRH was a mitochondrial toxicant, we seeded each cell line in either serum free media, supplemented with 1% glutamate or serum free media supplemented with glucose. Cells that are more dependent on glycolysis for ATP are more sensitive to mitochondrial toxicants in media supplemented with glutamate than in media supplemented with glucose [207].

Consistent with previous reports, we did find that NRH caused mitochondrial dysfunction [33] in the U-87MG and U-87MG/IDH1(R132H) cell lines, but only at concentrations higher that 100μM (**Appendix Figure A.8 and Appendix Figure A.9**).

Since U-87MG and U-87MG/IDH1 (R132H) mutant cells rely on glycolysis for their bioenergetic needs, we found they were more sensitive to the mitotoxic effects of NRH in media supplemented with glutamate. Consistent with this, we found that NRH (100μM) did not significantly decrease cell viability after 5 days of treatment (**Appendix Figure A.10**). Another explanation for the lack of NRH induced cytotoxicity could be, like HEK293 cells, U-87MG/IDH1(R132H) cells are more glycolytic, and therefore produce fewer ROS compared to cells that primarily undergo OXPHOS to meet bioenergetic needs [33].

We reasoned that the NRH-induced increase in cellular NAD^+ would be sufficient to enhance PARGi induced hyperPARylation. Consistent with the NAD^+ analysis, PAR and γH2AX accumulation peaked between 6-8 hours after co-treatment with NRH (100 μM) and PARGi (10 μM) in both the U-87MG/IDH1(R132H) cells and U-87MG cells (**Figure 3.53A-B**). However, we found that the PAR accumulation was significantly enhanced in U-87MG/IDH1(R132H) cells as compared to the U-87MG cells (**Figure 3.54**).

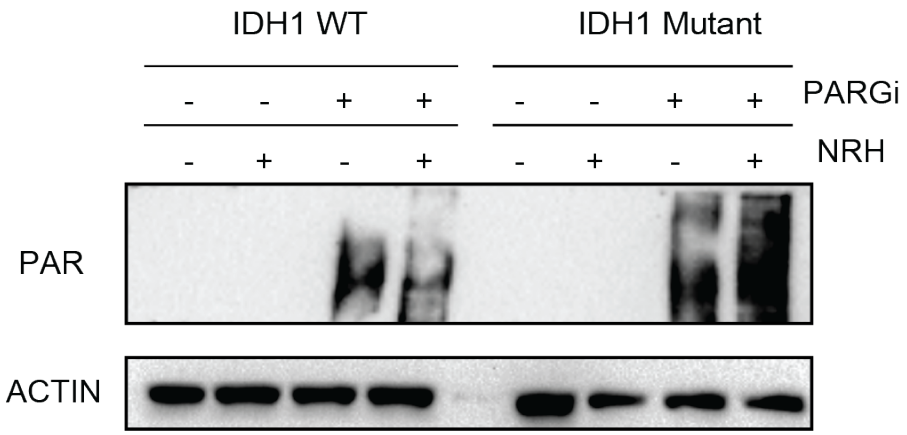

Figure 3.54. PARGi induced hyperPARylation is enhanced by NRH in IDH1 mutant cells.

Immunoblot analysis of PAR in U-87MG cells as compared to U-87MG/IDH1(R232H) celss treated with DMSO (control), NRH (100μM), PARGi (10μM) or co-treatment with NRH and PARGi for 8 hours, n=2.

To confirm that NRH + PARGi induced hyperPARylation was a result of PARP1 activation during replication, we treated cells with thymidine for 48 hours to arrest the cells in G1/S phase. We observed an increase in PAR accumulation and p21protein levels in cells that were released from thymidine induced arrest and co-treated with NRH and PARGi. This is significant because elevated p21 protein expression triggers replication arrest in intra S-phase because of DNA lesions encountered during replication [208] (**Figure 3.55**). In contrast, cells that remained in thymidine induced arrest demonstrated suppressed PAR accumulation and p21 protein level, even after treatment with NRH and PARGi (**Figure 3.55**). Additionally, PARylation was significantly enhanced in the U-87MG/IDH1(R132H) cell line compared to the U-87MG cells (**Figure 3.55**). We co-treated cells with NRH and PARGi at the doses indicated in the figure legends and determined cell viability after 5 days (120 hours) (**Figure 3.56A-B**). NRH enhanced the

cytotoxic effect of PARGi in both the U-87MG cells and U-87MG/IDH1(R132H) cells compared to PARGi alone. This suggests that NAD^+ bioavailability is a limiting factor for PARGi response in these cell lines. However, cell viability was only decreased to ~50% in the U-87MG cells and cell viability was decreased ~85% in the U-87MG/IDH1(R132H) cells at the highest dose of PARGi (10μM), suggesting that either the treatment time was too short to allow for adequate sensitivity, or there are subpopulations of cells in the U-87MG/IDH1(R132H) cell line that are resistant to treatment with NRH + PARGi.

We reasoned that the enhanced sensitivity of the IDH1 mutant cell line to NRH and PARGi was a result of suppressed Polβ and defective BER leading to toxic hyperPARylation and S-phase arrest. Therefore, we co-treated U-87MG cells and U-87MG/IDH1(R132H) cells, both overexpressing myc-Polβ, with NRH (100μM) and PARGi to determine of overexpression of Polβ could rescue the sensitive phenotype of the IDH1 mutant cell line. After 5 days, we found that overexpression of Polβ completely rescued the U-87MG/IDH1(R132H) cell line from sensitivity to co-treatment with NRH + PARGi. These studies suggest that Polβ deficiency and NAD^+ bioavailability drive the sensitivity of U-87MG/IDH1(R132H) cells to PARG inhibition (**Figure 3.57A-B**).

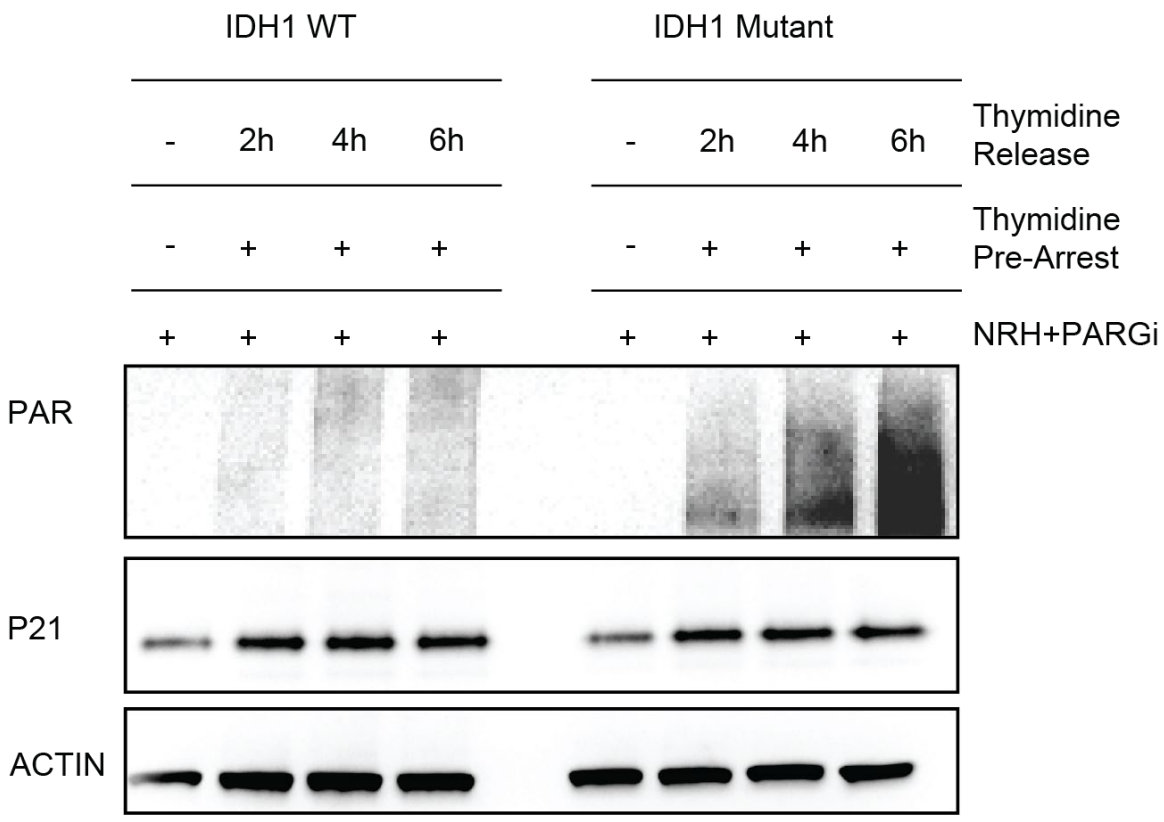

Figure 3.55. NRH + PARGi induced hyperPARylation in IDH1 mutant cells is dependent on replication.

Immunoblot analysis of PAR and P21. U-87MG cells and U-87/IDH1(R132H) cells were treated with 2mM thymidine for 48 hours. Cells that remained in thymidine block were co-treated with NRH (100 μM) and PARGi (10 μM) for 6 hours. Cells that were released from thymidine were co-treated with NRH and PARGi for the times indicated, n=2.

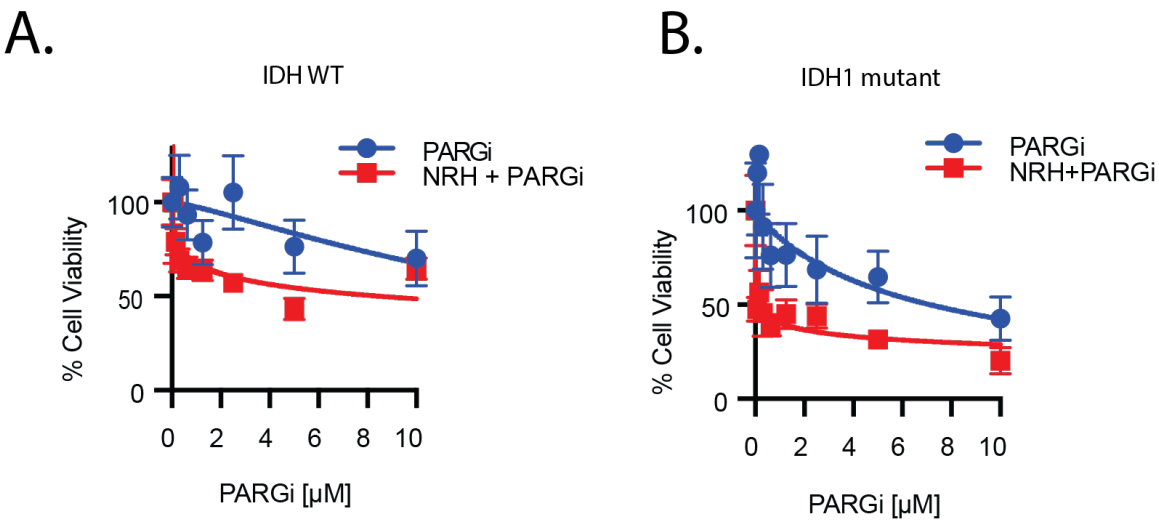

Figure 3.56. Polβ deficient IDH1 mutant cells are selectively sensitive to co-treatment with PARGi + NRH.

A. Cell viability assay following treatment with PARGi for the doses indicated or co-treatment with NRH (100μM) and PARGi for 120 hours in U-87MG cells. B. Cell viability assay following treatment with PARGi at the doses indicated for 120 hours or with NRH (100μM) and PARGi for 120 hours in U-87MG/ IDH1(R132H) cells, n=3.

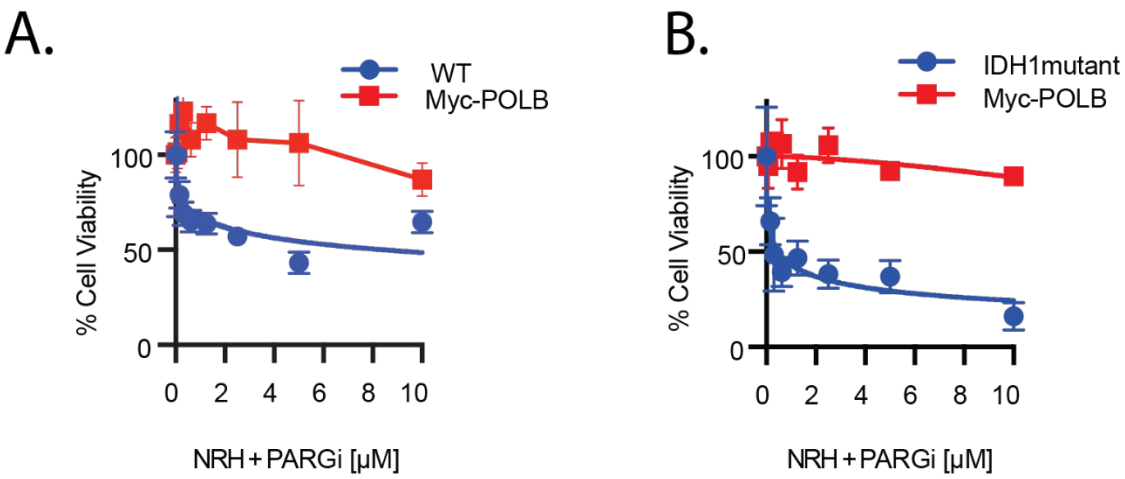

Figure 3.57. Overexpression of Polβ rescues hypersensitive IDH1 mutant phenotype to NRH + PARGi.

A. Cell viability following treatment with PARGi for the doses indicated in U-87MG and U-87MG/myc-Polβ cells. B. Cell viability following co-treatment with NRH (100 μM) and PARGi for the doses indicated 120 hours in U-87MG/IDH1(R132H) and U-87MG/IDH1(R132H)/myc-Polβ cells, n=3.

CHAPTER IV: DISCUSSION

NAD^+ Regulates PARP1 Activation Potential and Recruitment of BER/SSBR Proteins Polβ and XRCC1 to Sites of DNA Damage

Despite many years of research devoted to understanding the complexities of the DDR, the dynamics of DNA repair protein complex assembly and disassembly remain incompletely characterized [63]. However, understanding the temporal and spatial dynamics of DNA repair protein-protein interactions and factors that regulate complex formation is still an intense research interest to understand disease, aging, and cancer, especially for the development of chemotherapeutics [1, 98]. Molecular analysis of DNA repair proteins has allowed for the characterization of enzyme activity, protein kinetics, and protein-protein interactions. Until recently, characterizing the coordination of BER/SSBR repair proteins during the repair process has been limited by the lack of robust *in vivo* tools [122, 176]. Confocal laser micro-irradiation of cells expressing fluorescently labeled DNA repair proteins is a powerful instrument for examining the repair of SSBs (355-nm laser) and DSBs (405-nm laser) in live cells [177]. We utilized MIDAS, a high throughput data acquisition and analysis software package to characterize the assembly/disassembly of BER/SSBR proteins, in response to laser induced DNA damage, and in conditions of high NAD^+ bioavailability (NRH) or low NAD^+ bioavailability (FK866) [62].

We found that treatment with the NAMPT inhibitor FK866 suppresses cellular NAD^+ levels in LN428, U2OS and A549 cells by nearly 80%. Supplementation with NRH was able to enhance cellular NAD^+ levels up to 8-fold in U2OS cells and up to 4-fold in

LN428 cells, but not in A549 cells, demonstrating that NAD^+ synthesis is dependent on the metabolic profile of each cell line. Specifically, reports that suggest A549 cells are deficient in ADK and NMNAT1 [62, 170, 209], two key enzymes responsible for NRH catabolism. Deficiency in ADK and NMNAT1 could explain the insensitive phenotype of A549 cells to NAD^+ precursor NRH. Other possible explanations could include the NUDT family of enzymes that synthesize NADH to NRH [62]. However, this is unlikely since we did not observe any changes in cellular NADH levels in A549 cells or U2OS cells following treatment with NRH. However, further research measuring all NAD^+/NADH and $NADP^+$/NADPH metabolites will be required to determine if A549 cells are able to catabolize NRH to produce other NAD^+ metabolites.

We found that NRH significantly enhanced PARylation in response to DNA damage induced by H_2O_2, in U2OS and LN428 cells, which was abrogated by FK866 or treatment with the PARP1/2 inhibitor ABT-888. For laser microirradiation experiments, NRH enhanced the peak recruitment intensity of LivePAR (88%), XRCC1 (94%) and Polβ (44%) in U2OS cells, but did not impact the recruitment profiles of LivePAR, XRCC1 or Polβ in A549 cells consistent with the results from the NAD^+ analysis. In contrast, FK866 reduced peak recruitment intensities in LivePAR (24%), XRCC1 (35%), Polβ (37%) in both U2OS and A549 cells. Together, our data suggests that NAD^+ regulates the activation potential of PARP1 in response to DNA damage, and the subsequent protein recruitment intensity of DNA repair proteins XRCC1 and Polβ, but does not alter protein recruitment kinetics (**Figure 4.1.1**).

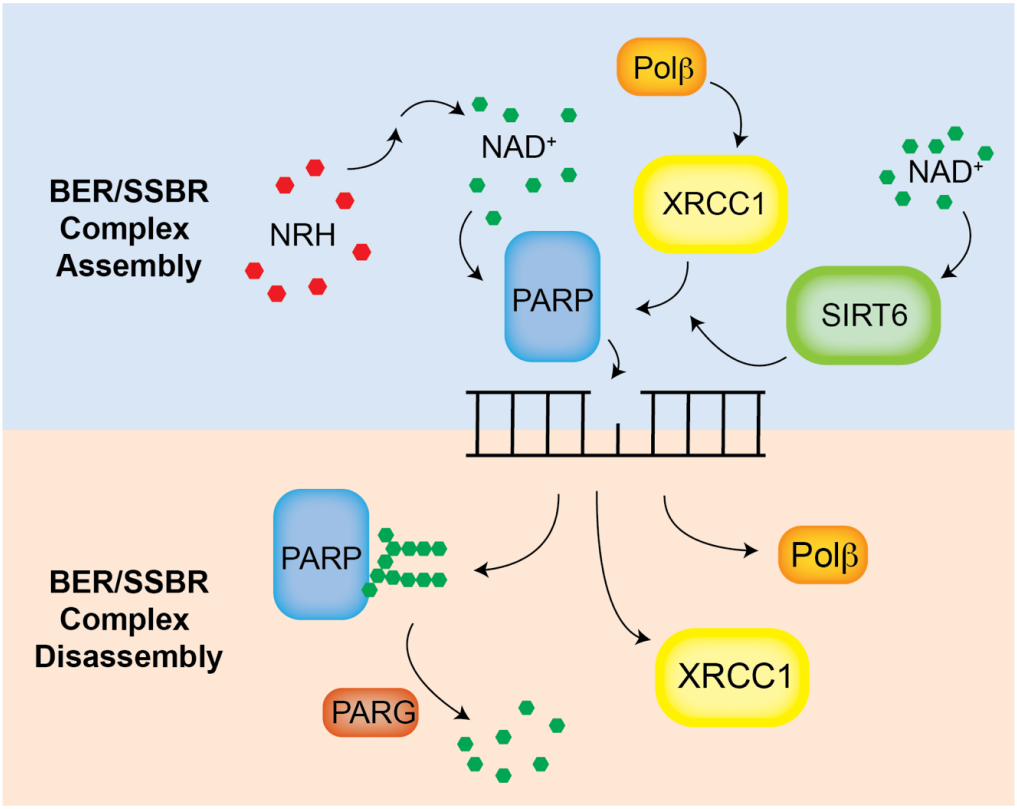

Figure 4.1. Model of PARP1 activation and BER/SSBR protein assembly/disassembly in response to DNA damage.

PARP1 utilizes NAD^+ as a substrate to form PAR leading to the assembly of XRCC1 followed by Polβ. NRH enhances cellular NAD^+ levels and enhances PAR accumulation at the lesion site, thereby, increasing the recruitment of XRCC1 and Polβ, at the lesion site. Following DNA repair, PARG hydrolyzes PAR polymers allowing for the dissociation of Polβ, followed by XRCC1 and PARP1 from the DNA.

NAD^+ Bioavailability Regulates PARG Inhibitor Induced PARP1 Activation and Replication-associated BER/SSBR, S-phase Checkpoint Arrest, and Apoptosis in Glioma Cells

Previous data from our lab and others demonstrated that GSCs and glioma cells have elevated PARP1 and PARG protein expression levels, indicating that PARG inhibitors may be a successful treatment strategy [210]. However, we demonstrated that GSCs and LN428 glioma cells were insensitive to PARGi unless combined with IR or alkylating agents. PARP1 activity is tightly regulated by NAD^+ bioavailability. As we demonstrated previously, PARP1 and therefore BER/SSBR activity, and DNA repair capacity is suppressed in conditions of low NAD^+ [59]. However, enhanced NAD^+ bioavailability increases PARP1 activation, complex formation with other BER/SSBR proteins, and enhances DNA repair capacity [209, 210]. Therefore, we reasoned that a major factor related to the activation of PARP1 in GSCs and glioma is caused by defects in NAD^+ biosynthesis.

We demonstrated that supplementation with the NAD^+ precursor NRH significantly enhanced NAD^+ levels in all 4 GSC cell lines (6-10 fold) and LN428 cells (3-4 fold), promoted PAR accumulation, and blocked replication fork progression [210]. Together, this suggests that GSCs and LN428 cells may have insufficient NAD^+ to elicit robust PARP1 and PARP2 activation, consistent with reports that many GSCs and gliomas, especially those with IDH1/2 mutations that are deficient in NAD^+ [67, 210, 211]. Further, we found PARP2 activity is involved in the replication stress response, but to a lesser degree than PARP1 [210], as others have reported [180] We demonstrated that loss of PARP1 significantly suppressed PARylation and enhanced resistance to PARGi or co-

treatment with NRH and PARGi.

Previously, we reported that NAD^+ biosynthesis could be modulated to increase PARP1 interaction with BER/SSBR proteins [209]. Therefore, we investigated the NAD^+ induced PARP1 interactome, by using the BioID approach, we expressed PARP1-BirA in LN428 cells and performed a differential analysis of biotinylated proteins. We found that many of the proteins identified in our analysis were replication-associated proteins (PCNA, ORC2, RFC1), further analysis identified BER/SSBR proteins XRCC1 and Polβ. Our PAR capture immunoprecipitation identified interaction with XRCC1, ORC2, PCNA and RPA, which suggested to us that these proteins form a complex with PARP1 in response to replication stress in the absence of exogenous DNA damage. Further, this highlights a role for PARP1 recruitment of BER/SSBR proteins at the replication fork.

Although the interaction of PARP1 with XRCC1 and PCNA during replication has been reported in other studies [142, 208], to our knowledge, we are the first to report PARP1 complex formation with Polβ and ORC2 as a replication-associated response. Previous reports have speculated that Polβ is active during the cell cycle and has been suggested to play a role in mitosis. However, we observed increased PARP1 interaction with Polβ in replicating cells, as compared to cells that were under replication arrest by thymidine block, suggesting that Polβ interaction with PARP1 may be important complex involved in the response to replication stress.

The origin replication complex (ORC) forms a 6-subunit complex, in which ORC2 is the second protein in the complex [76]. ORC is reported to be involved in the initiation of replication by recruiting pre-replication complex (Pre-RC) proteins, such as, cdc6 and MCMs to the origin site. The pre-RC is dissociated prior to replication [76]. However,

there are no studies that report PARP1 directly interacts with ORC2, and none that report the interaction of ORC2 and PARP1 as a replication stress response. One study reported that PARP1 negatively regulates Epstein-Barr virus replication by PARylation activity with OriP preventing the recruitment of ORC2 to the OriP [71]. Another study suggested ORC2 regulates the replication of Kaposi's sarcoma-associated herpesvirus (KSHV) by ADP-ribosylation of KSHV-associated replication protein latency-associated nuclear antigen (LANA) thereby preventing recruitment of ORC2, cdc6 and MCMs to the origin site [212]. However, recently it was reported that ORC2 may have a role in replication stress since it was reported that Plk1 phosphorylates ORC2 at serine 188, to facilitate replication under stress conditions, to maintain genome integrity by preventing telomere DNA damage [188, 189].

In addition to NAD^+ regulation of PARP1 activation, we find that BER/SSBR protein XRCC1 and replication-associated protein ORC2 regulate PAR accumulation. Further, we find that loss of XRCC1 sensitizes LN428 cells to PARGi, demonstrating that PARP1 interaction with XRCC1 is required to maintain genome integrity during replication. Therefore, we find that the interaction of PARP1 with BER/SSBR proteins (XRCC1 and Polβ) and replication associated proteins (ORC2, RPA and RFC1) suggests a role for BER/SSBR in Pre-RC assembly and response to replication stress that is regulated by PAR accumulation, NAD^+ bioavailability and PARG.

Our findings are consistent with reports describing the role of PARP1 in replication [118, 182, 213], Okazaki fragment processing [81] and replication fork remodeling [96, 214-217]. Together, these data sets support our hypothesis that PARP1 activation, following PARGi + NRH treatment, organizes BER/SSBR as a replication-associated

response. Additionally, these studies highlight XRCC1 protein expression as a possible biomarker for predicting chemotherapeutic response to PARGi. Further, we demonstrate the therapeutic potential for NAD^+ supplement NRH combined with PARGi for patients with high grade glioblastoma (**Figure 4.2.1**).

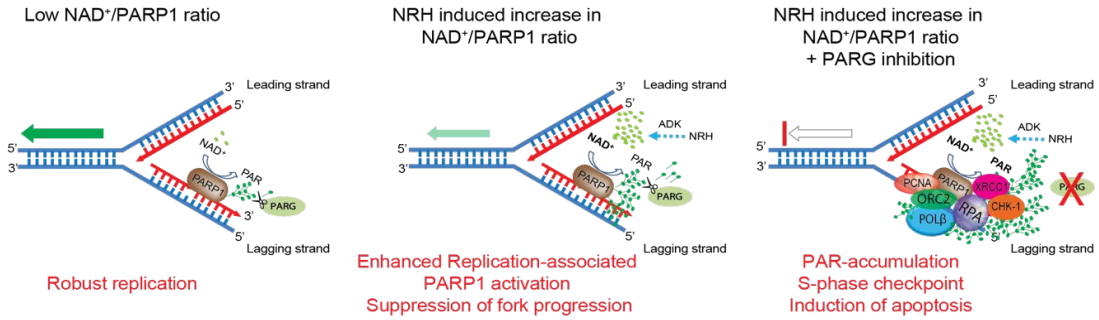

Figure 4.2. Model of replication associated BER/SSBR in response to PARGi and NRH treatment.

Left panel: Low NAD^+/PARP1 ratio can suppress PARP1 activation at the fork, allowing for increased replication speed; Middle panel: Enhancing the NAD^+/PARP1 ratio with NRH increases replication-associated PARP1 activation potential and causes slowed replication fork progression; Right panel: Co-treatment of NRH to enhance cellular NAD^+ levels with PARG inhibition, prevents dePARylation resulting in a robust accumulation of PAR at the replication fork and the accumulation of BER/SSBR proteins (XRCC1 and Polβ) and replication associated proteins (RPA, ORC2 and PCNA) triggering CHK1 activation leading to replication catastrophe and apoptosis.

The Oncometabolite 2-HG Enhances Cellular Cytotoxicity to Alkylating Agents and PARG Inhibition in Glioma Cells by Suppressing DNA Polymerase Beta

The prognosis for patients with IDH1 mutant GBM is generally more favorable because these tumor types are more sensitive to DNA damage caused by alkylating agents [40]. However, IDH1 mutations often progress to GBM grade IV, causing resistance to DNA alkylating agents [43]. IDH1 mutations drive the overproduction of 2-HG, leading to depletion of NAD^+ metabolites and inhibition of TET and KDM methyltransferases [43, 90]. Inhibition of TET and KDM methyltransferase activity causes hypermethylation of DNA histones and epigenetic alterations in metabolism and DNA repair gene expression [156, 157]. However, the mechanism by which IDH1 mutant cells confer sensitivity to alkylating agents remains unclear. Here, we report a unique mechanism by which BER/SSBR is modulated by 2-HG dependent suppression of Polβ that is synthetically lethal in combination with DNA alkylating agents or PARG inhibition in IDH1 mutant cells.

PARP1 is an essential enzyme involved in the base excision repair pathway; BER is responsible for removing damaged DNA bases caused by oxidation, deamination, or alkylation [1]. Therefore, deficits in BER confer sensitivity to alkylating agents [98]. Given that PARP1 activity is regulated by NAD^+ bioavailability [58], we considered that the low basal NAD^+ levels in IDH1 mutant glioma could impair the activation potential of PARP1. However, despite having significantly low NAD^+ levels, PARP1 activation was not suppressed in U-87MG/IDH1(R132H) cells in response to treatment with the DNA alkylating agent MNNG.

Since PAR accumulation at the DNA lesion site is required, for the recruitment of BER proteins XRCC1 and Polβ [62], we investigated the recruitment assembly/disassembly dynamics of PAR in LivePAR expressing cells following 355-nm laser microirradiation. However, consistent with our PAR immunoblot data, we found no measurable difference in PAR foci intensity or foci recruitment kinetics, following 355-nm laser microirradiation, between the U-87MG/IDH1(R132H) and U-87MG cell lines. This data suggests that PARP1 activation potential was not altered in U-87MG/IDH1(R132H) cells despite low basal levels of NAD^+.

Just as crucial as PARP1 activation at the DNA lesion site is the recruitment and complex assembly of vital BER proteins such as XRCC1 and Polβ [134, 142]. XRCC1 binds to PAR and serves as a scaffolding protein for other BER factors, including Polβ and LIGIII [135]. The dual functionality of Polβ to serve as both a DNA polymerase and a 5' dRP lyase for removing toxic intermediates is highly important to protect against the damage caused by alkylating agents [8, 146, 163]. Central to this is the role of XRCC1 to stabilize Polβ recruitment and complex assembly [135]. Therefore, we investigated the recruitment dynamics of cells expressing XRCC1 fused with EGFP but found no significant difference in XRCC1 foci recruitment intensity or recruitment kinetics in U-87MG/IDH1(R132H) cells compared to the parental cell line. Similarly, we found that the recruitment dynamics of EGFP-Polβ were not altered in the U-87MG/IDH1(R132H) cells compared to the parental cell line.

Our lab and others have reported that defects in BER/SSBR proteins, especially XRCC1 and Polβ, confer chemosensitivity to damage caused by alkylating agents and

other chemotherapeutics such as PARG inhibitors [56, 98, 135]. We analyzed the protein expression of PARP1, PARP2, XRCC1, Polβ, and PCNA. We found a 50% decrease in Polβ protein expression in U-87MG/IDH1(R132H) cells compared to the parental cell line but no significant change in the expression of other BER proteins. Gene expression analysis of mRNA revealed that only PARP1 was significantly elevated in U-87MG/IDH1(R132H) cells, but the expression of other BER proteins was not altered, demonstrating that protein expression and gene expression are not always represented in a 1:1 ratio [196].

The overproduction of 2-HG alters enzyme activity by inhibiting methyltransferase activity, causing widespread epigenetic changes resulting in gene suppression and genome instability[157]. However, 2-HG has been reported to regulate protein expression and activity outside of epigenetic control via unknown mechanisms [199]. Therefore, we demonstrated that supplementing cells with exogenous D-2-HG is sufficient to suppress Polβ protein expression in IDH1 wildtype cells, however, inhibition of IDH1 (R132H) alone was not able to restore Polβ expression in IDH1 mutant cells, indicating that protein stability and expression is regulated by oncometabolite 2-HG.

However, the mechanism by which Polβ is regulated by 2-HG is currently unknown. Since we found Polβ gene expression was not significantly different from the wildtype U-87MG cell line, it is unlikely that the regulation of Polβ protein expression is occurring at the transcriptional level. Recently, it was reported that IDH1 mutant glioma cells inhibit the oxidation of RNA 5mC to 5hmC by TET leading to dysregulation of RNA processing [218]. Alternatively, NAD^+ was recently reported to play a role in modulating RNA processing and is added during transcription as the initiating nucleotide [16].

Therefore, it is possible low cellular NAD^+ levels or inhibition of TET by 2-HG in IDH1 mutant cells could disrupt RNA processing in IDH1 mutant cells leading to decreased Polβ protein expression [16]. However, further research will be required to determine the exact mechanism by which Polβ protein expression is suppressed in IDH1 mutant glioma cells.

Cell lines with deficiencies in Polβ have been reported to confer sensitivity to alkylating agents that can be rescued by overexpression of WT Polβ [165]. We demonstrated that U-87MG/IDH1(R132H) cells deficient in Polβ were hypersensitive to alkylating agents MNNG and MMS, as compared to the U-87MG. However, overexpression of Polβ was able to fully rescue the U-87MG/IDH1(R132H) cell line from sensitivity to MMS and MNNG, suggesting that chemosensitivity to alkylating agents is conferred by deficiencies in BER/SSBR capacity, as originally suggested by Sobol, et al [197].

Recently, it was reported that PARG inhibition could enhance chemosensitivity of U-87MG/IDH1(R132H) cells to alkylating agents [130]. More recently, our lab and others have reported that PARG inhibition induces synthetic lethality in cells deficient in XRCC1 and Polβ, due to increased replication stress and hyperPARylation, leading to replication arrest [56, 165]. Consistent with this, we found U-87MG/IDH1(R132H) cells were selectively sensitive PARG inhibition. We demonstrated that PARGi did not deplete cellular NAD^+ levels in U-87MG or U-87MG/IDH1(R132H) cells after 8 hours but was able to induce hyperPARylation in U-87MG/IDH1(R132H) cells compared to the U-87MG cell line leading to replication arrest. Further, we found that overexpression of Polβ could fully rescue the U-87MG/IDH1(R132H) cells from sensitivity to PARG inhibition

suggesting that Polβ deficiency sensitizes IDH1 mutant cells to PARGi. However, further study will be required to determine if inhibiting Polβ would be an effective strategy to overcome PARGi resistance in HGG IDH1 mutant glioma cells.

Previously, we demonstrated that GSCs and glioma cells, defective in NAD^+ biosynthesis, were insensitive to PARGi unless combined with alkylating agents or radiotherapy [60]. However, we found that NAD^+ precursor NRH was able to enhance cellular NAD^+ levels in GSCs up to 10-fold, increasing the PARP1 activation potential, in response to replication stress, to enhance PARGi efficacy, S-phase checkpoint activation and apoptosis. We found that NRH was able to increase cellular NAD^+ levels in U-87MG/IDH1(R132H) cells (2-3-fold) and U-87MG (3-4-fold), and enhanced PARP1 activation potential, consistent with LN428 and GSCs.

Interestingly, we observed nearly a 30-40-fold increase in cellular NADPH levels in U-87MG/IDH1(R132H) between 1-6 hours after treatment with NRH, compared to a ~15-fold increase of NADPH in the U-87MG that peaked at 4 hours. However, we did not observe a significant change in cellular $NADP^+$ levels in either the U-87MG or U-87MG/IDH1(R132H) cells. We found that NRH did not significantly enhance cellular NADH levels in U-87MG cells suggesting that the NADH synthesized from NRH is quickly converted to NAD^+. However, we observed 30-50-fold increase in NADH between 1-6 hours in the U-87MG cell line.

Considering the significant increase in cellular NADPH levels, this suggests that the IDH1 mutant cell line has adapted mechanisms that 1) enhance the catabolism of NRH to NADH, and 2) drive the conversion of NADH to NADPH. Consistent with this, we observed that protein levels of NADP(H) phosphatases are significantly depleted in U-

87MG/IDH1(R132H) cells compared to U-87MG cells. This supports the hypothesis that IDH1 mutant cells have adapted multiple mechanisms to conserve and restore cytosolic NADPH pools [35, 190]. However, further research will be necessary to determine the exact mechanisms that IDH1 mutant cells have adapted to promote the synthesis of NADPH from NADH.

Consistent with our previous studies, we found that NRH alone is not cytotoxic in the U-87MG or U-87MG/IDH1(R132H) cell lines. However, NRH acts synergistically with PARGi to enhance the hyperaccumulation of PAR in U-87MG/IDH1(R132H) cells, leading to replication stress and apoptosis. Further, we found that overexpression of Polβ could rescue IDH1 mutant cells from sensitivity to PARGi, even in the presence of NRH, demonstrating the importance of BER/SSBR in the DDR to for regulating the response to chemotherapeutics (**Figure 4.3.1**). Consistent with our previous reports that NAD^+ bioavailability and defects in BER/SSBR regulate PARP1 activation potential in response to replication stress [210].

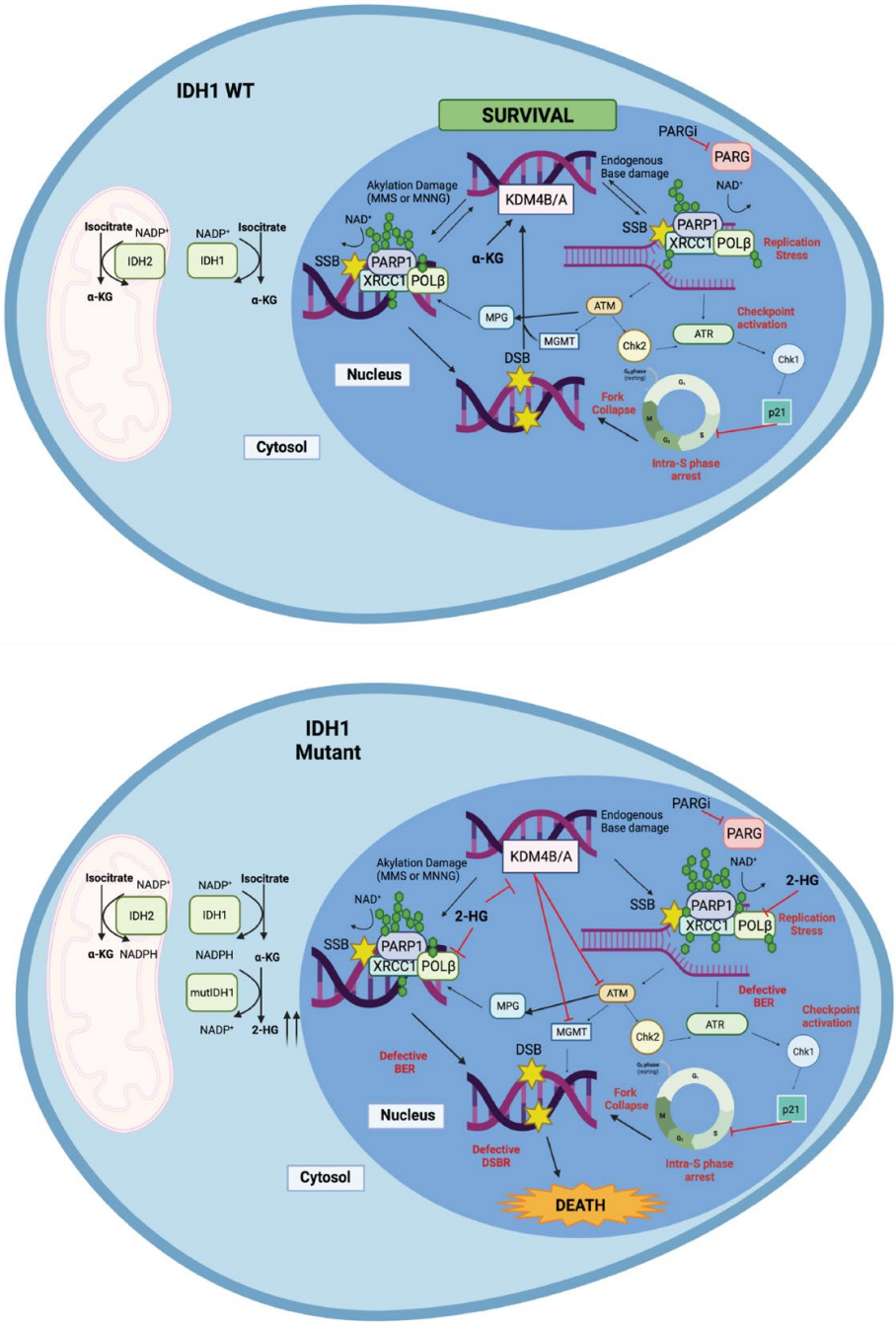

Figure 4.3. Model depicting mechanism of chemosensitivity to alkylating agents and PARGi in IDH1 mutant glioma cells.

Enhanced sensitivity is induced in IDH1 mutant by combined 2-HG suppression of BER protein Polβ, and epigenetic inactivation of HR, treatment with alkylating agents or PARGi enhance replication stress caused by an accumulation of SSBs, leading to replication catastrophe and cell death because of unresolved DNA damage. Created with BioRender.

CHAPTER V: SUMMARY AND CONCLUSIONS

Here, I have demonstrated that NAD^+ bioavailability is an important regulator for PARP1 activation potential and the subsequent recruitment of BER/SSBR proteins Polβ and XRCC1 to the DNA lesion site in response to DNA damage. However, consistent with previous reports by our lab and others, I demonstrated that cellular NAD^+ levels could be significantly reduced by treating cells with NAMPT inhibitor FK866 in LN428, A549, and U2OS cells [57]. FK866 significantly suppressed the accumulation of PAR, and subsequently reduced the recruitment intensity of BER/SSBR proteins XRCC1 and Polβ at the site of DNA damage but did not alter protein recruitment kinetics.

I found that supplementation with NRH enhanced NAD^+ bioavailability in LN428 and U2OS cells, but was unable to enhance NAD^+ in A549 cells, this could be because A549 cells have decreased protein levels of ADK or as a result of NADH to NRH conversion by NUDIX5 [33, 209]. Supplementation with NRH enhanced PAR accumulation following DNA damage and increased the recruitment intensity of Polβ and XRCC1 to the DNA lesion site but did not alter protein recruitment kinetics.

PAR accumulation and assembly of the Polβ/XRCC1 complex was not altered in A549 cells following supplementation of NRH, demonstrating the enhanced PAR accumulation and assembly with Polβ/XRCC1 is dependent on the ability of NRH to enhance cellular NAD^+ levels. Enhanced cellular NAD^+ levels also enhanced PAR accumulation in response to treatment with H_2O_2. Together, these findings support my

conclusion that NAD^+ is an essential regulator of PARP1 and BER/SSBR activity and support the use of NRH as a supplement to enhance cellular DNA repair capacity.

In addition to enhancing PARP1 activation potential in response to DNA damage, I found that NRH enhanced cellular NAD^+ levels to promote PAR accumulation in LN428 glioma cells and glioma stem cells (GSCs) and suppressed replication fork progression. Consistent with previous reports by others, we found GSCs and LN428 cells have elevated protein levels of PARP1 and PARG but are insensitive to PARGi unless combined with irradiation or alkylating agents [5, 75]. However, I found NRH could enhance PARG induced hyperPARylation in LN428 cells, leading to S-phase arrest and cell death in and LN428 cells. We found normal human astrocytes were insensitive to co-treatment with NRH and PARGi, despite observed elevated levels of NAD^+ following supplementation with NRH, demonstrating co-treatment with NRH and PARGi may have therapeutic potential for patients with HGGs.

Further, I demonstrated that co-treatment of NRH and PARGi enhanced activation of PARP1, further elevated and stabilized PAR levels, and increased PARP1 interaction with BER proteins XRCC1 and Polβ and replication associated proteins PCNA and ORC2, demonstrating that PARP1 and BER/SSBR could play a role in recognition of pre-replication complexes, initiation of replication stress and the intra-S phase checkpoint. Further, I found that loss of ORC2 and XRCC1 enhanced PARP1 activation in response to replication stress, and loss of XRCC1 sensitized LN428 cells to PARG inhibition alone. These studies are significant because they demonstrate that NAD^+ bioavailability, PARP1 and BER/SSBR protein expression may be important biomarkers for predicting

To further elucidate the role of NAD^+ mediated regulation of PARP1 and BER/SSBR in the DDR and the response to replication stress, I applied my model to an NAD^+ deficient, IDH1 mutant glioma cancer cell model. I completed these studies in the U-87MG cell line expressing wildtype IDH1, and an isogenic cell line derived from the parental U-87MG cell line, expressing mutant IDH1(R132H). These studies have revealed a unique mechanism by which overproduction of the oncometabolite 2-hydroxyglutarate in IDH1 mutant glioma cells, suppresses BER/SSBR by significantly reducing Polβ protein expression, thereby inducing selective sensitivity to alkylating agents and PARGi.

Contrary to other reports, I found that chemosensitivity of IDH1 mutant glioma cells is independent of low basal NAD^+ levels since PARP1 activation potential was not altered in the IDH1 mutant cells compared to the IDH1 WT cell line in response to treatment with the alkylating agent MNNG. I demonstrated that IDH1 mutant cells were selectively sensitive to the alkylating agents MNNG and MMS as compared to the IDH1 wildtype cell line. However, Polβ overexpression was able to rescue the IDH1 mutant glioma hypersensitive phenotype to MMS, MNNG, demonstrating that Polβ deficiency drives chemosensitivity of IDH1 mutant cells to alkylating agents.

Additionally, I demonstrated that Polβ deficiency enhances the selective sensitivity of IDH1 mutant cells to replication stress induced by PARGi, and overexpression of Polβ rescued the PARGi sensitive phenotype in these IDH1 mutant cells. However, supplementation with NRH significantly enhanced NAD^+ and PARGi induced hyperPARylation, and cell death, suggesting NAD^+ is a limiting factor for PARP1 activation potential in response to replication stress. Similarly, I found that overexpression

of Polβ rescued the NRH + PARGi sensitive phenotype in IDH1 mutant cells, demonstrating that NAD^+ bioavailability and protein expression of Polβ are regulating factors for predicting sensitivity of IDH1 mutant cells to chemotherapeutics. This finding is significant because it highlights the importance of BER for maintaining genome integrity and defines a novel mechanism by which IDH1 mutant cells confer sensitivity to alkylating agents and PARG inhibition.

Additionally, I demonstrated that IDH1 mutant cells regulate metabolism in reverse to synthesize NADPH from NADH, and likely to conserve NADPH pools by downregulating protein levels of NADP(H) phosphatases MESH1 and NOCT. Together, these findings are significant because they support the need for ongoing studies to understand how cancer cells regulate metabolism for predicting patient response to chemotherapeutics. Further, these findings define the significance of NAD^+ bioavailability for regulating PARP1 activation potential and the subsequent recruitment of BER/SSBR proteins to the site of DNA damage. These studies highlight the importance of both canonical and replication associated BER/SSBR in the DDR and support ongoing studies to target BER/SSBR enzyme activity as a strategy to sensitize or re-sensitize drug resistant GSCs and GBM to chemotherapeutic.

APPENDICES

Appendix A: Supplemental Figures

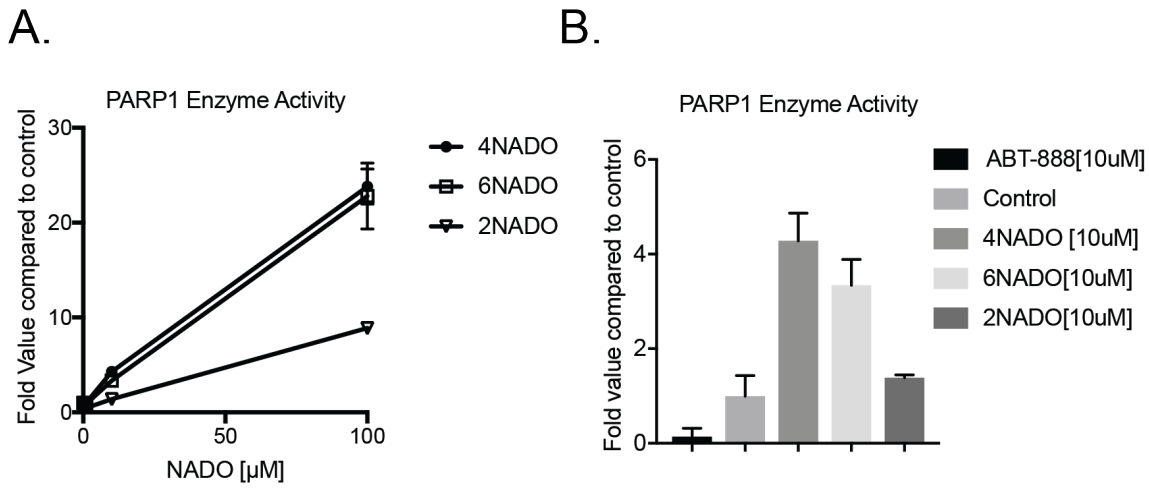

Figure A1. PARP1 enzyme activity.

PARP1 enzyme activity is increased following supplementation with 4NADO and 6 NADO but not 2NADO.

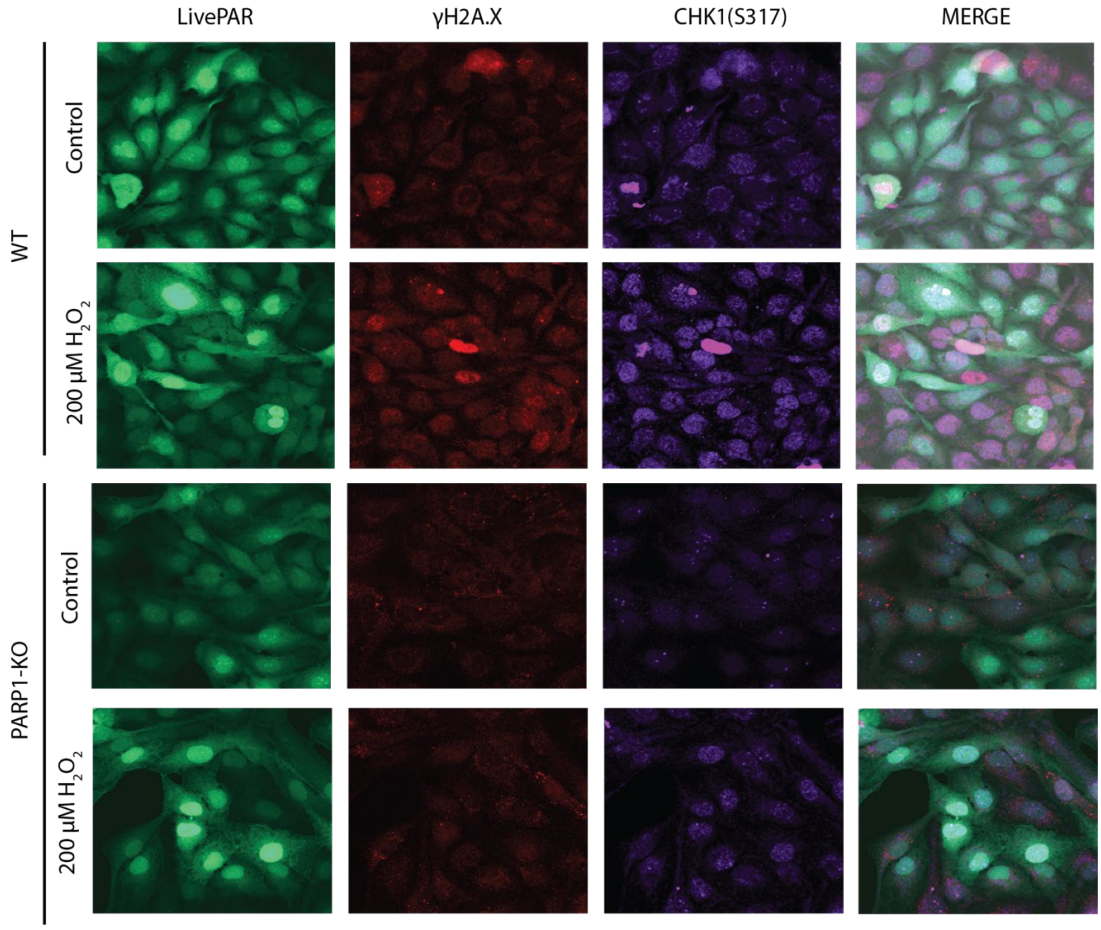

Figure A.2. LivePAR co-localized with Chk1 (S317) and γH2A.X following DNA damage.

Fluorescent confocal images of nuclear enrichment of PAR, as detected with the EGFP-WWE domain of the LivePAR probe LivePAR) with Chk1 (S317) and γH2A.X, following treatment with H_2O_2 (200μM) 15 minutes in LN428/WT and LN428/PARP1-KO cells.

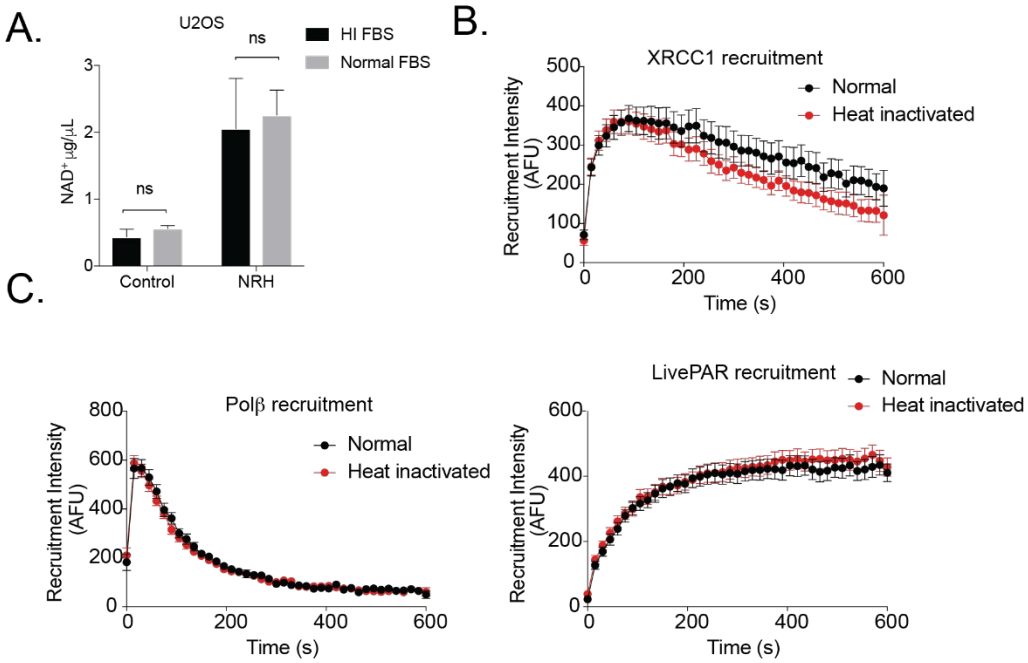

Figure A.3. NAD$^+$/NADH assay and recruitment kinetics of cells grown in normal FBS compared to heat inactivated FBS.

A.NAD$^+$ analysis of U2OS cells following treatment with NRH (100µM, 4hrs) in growth media supplemented with heat inactivated (HI) FBS compared or normal FBS; B.Recruitment of Pol following supplementation with NRH (100 µM) for 4 hours in growth media supplemented with normal FBS or heat inactivated FBS; C. Recruitment of XRCC1 following supplementation with NRH (100 µM) for 4 hours in normal media compared to heat inactivated media; D. Recruitment of LivePAR following supplementation with NRH (100 µM) for 4 hours in growth media supplemented with normal media or heat inactivated media.

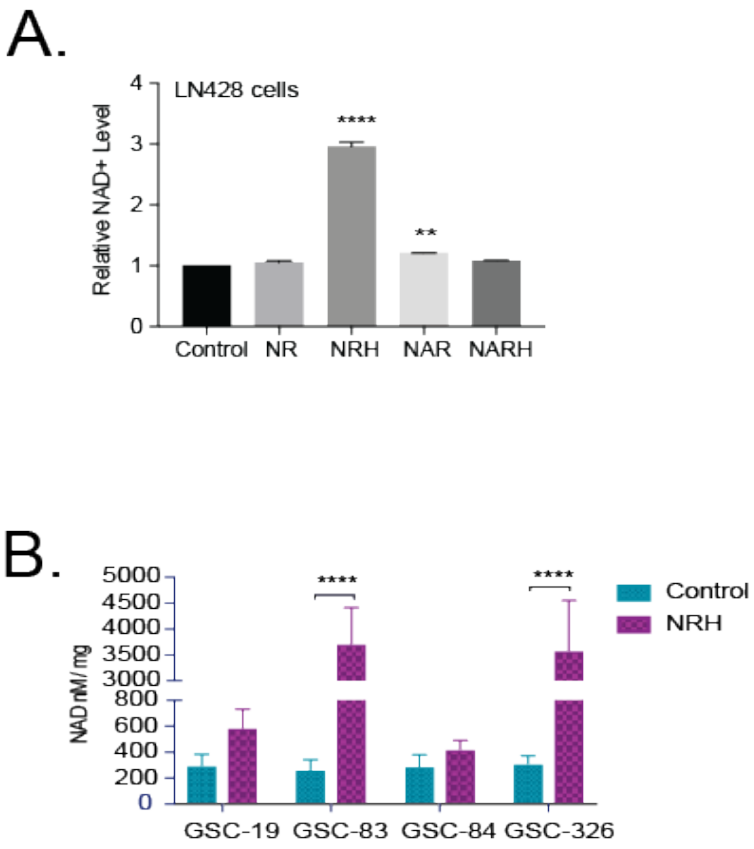

Figure A.4.NAD$^+$/NADH measurement

A. NAD$^+$ analysis of supplementation with NR (100 µM), NRH (100 µM), NAR (100 µM), NARH (100 µM) for 4 hours in normal media compared to heat inactivated media; B. NAD analysis of GSC-19, GSC-83, GSC-84, GSC-326 after supplementation with NRH (100 µM) for 6 hours.

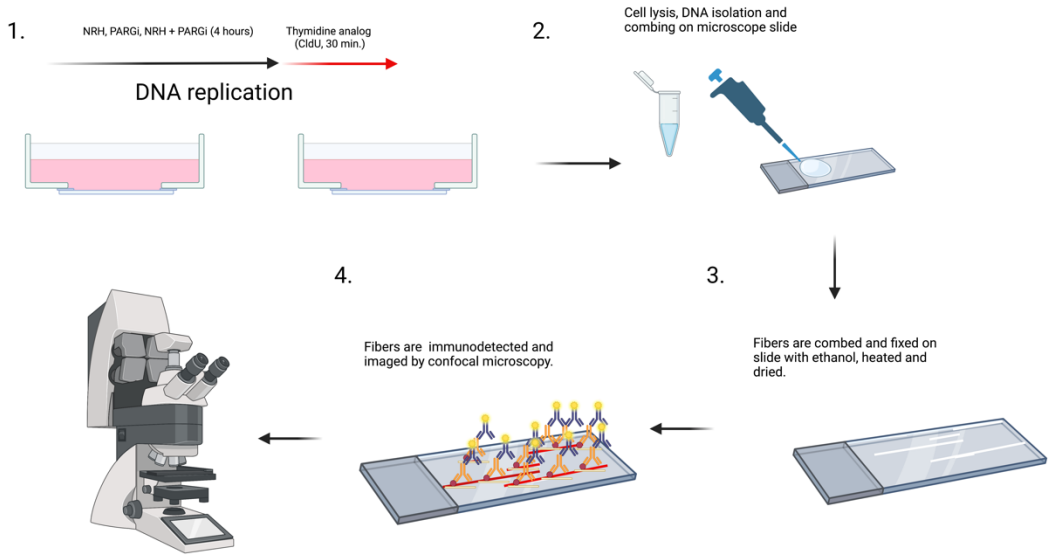

Figure A.5.Graphic depicting DNA fiber assay.

Graphic depicting the DNA fiber assay. Cells are co-treated with NRH (100μM) and PARGi (10μM) for 4 hours. Media is then removed and replenished with media supplemented with CldU analog (30 min.). Cells are lysed and DNA is isolated. Fibers are combed, fixed with ethanol, heated, and dried. Fibers are stained with anti-CldU antibody and a secondary fluorescent antibody. Immunofluorescence is detected by confocal microscopy. Made with BioRender.

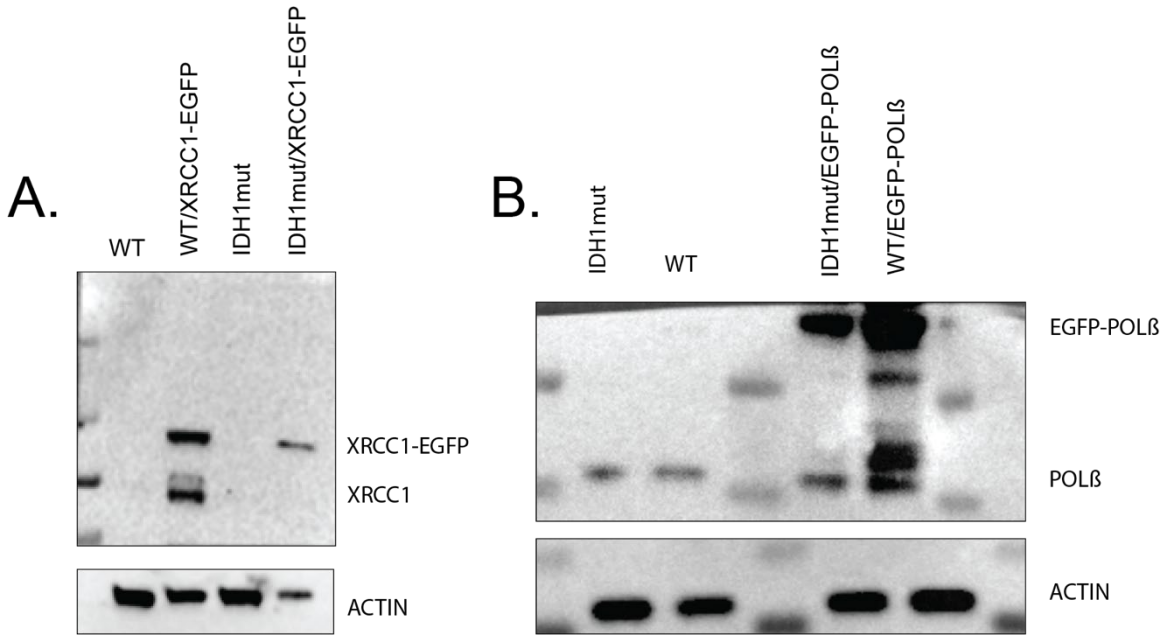

Figure A.6. Immunoblot of XRCC1-EGFP and EGFP-Polβ expression in U-87MG cells.

A. Immunoblot of XRCC1 and EGFP in U-87 IDH1 WT and U-87 U-87MG/EGFP-XRCC1compared to U-87 IDH1-R1332H and U-87IDH1-R132H/EGFP-XRCC1; B. Immunoblot of Polβ and EGFP expression in U-87 WT and U-87 U-87MG/Polβ- EGFP compared to U-87 IDH1-R1332H and U-87IDH1-R132H/ Polβ-EGFP.

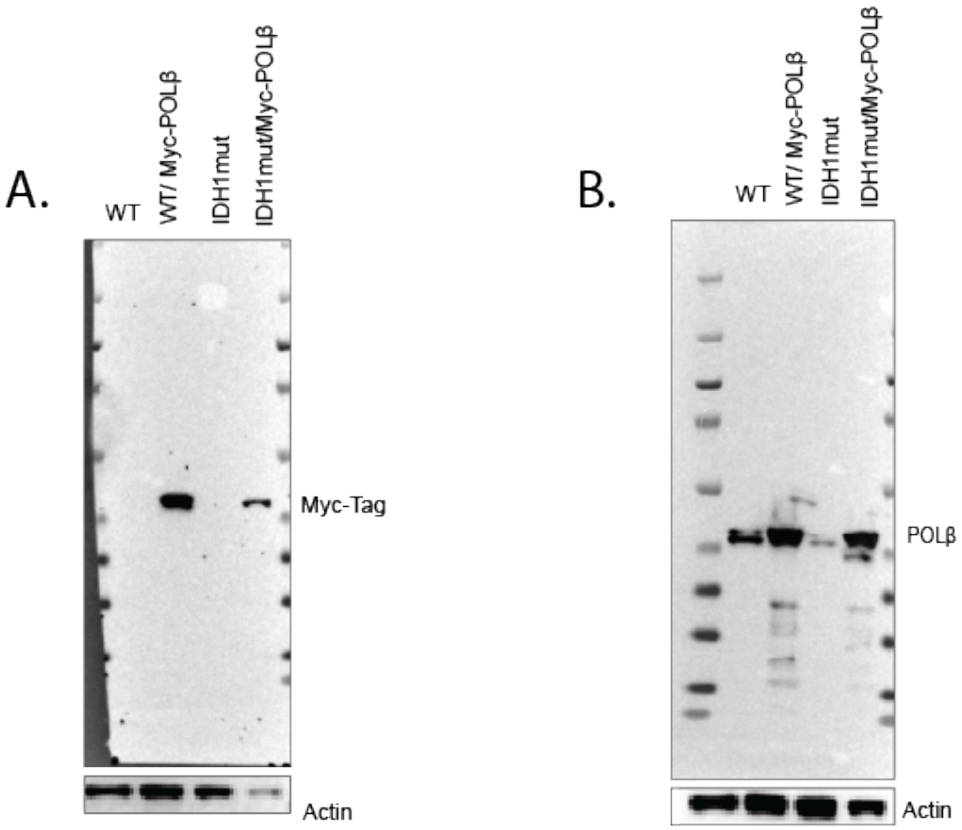

Figure A.7. Immunoblot of myc-Polβ expression in U-87MG cells.

A. Immunoblot Myc-tag expressed in U-87MG, U-87MG/myc-Polβ, U-87/IDH1-R132H, U-87/IDH-R132H/ myc-Polβ; B. Immunoblot of Polβ expressed in U-87/U-87MG, U-87 WT/myc-Polβ, U-87/(IDH1-R132H), U-87/IDH-R132H myc-Polβ.

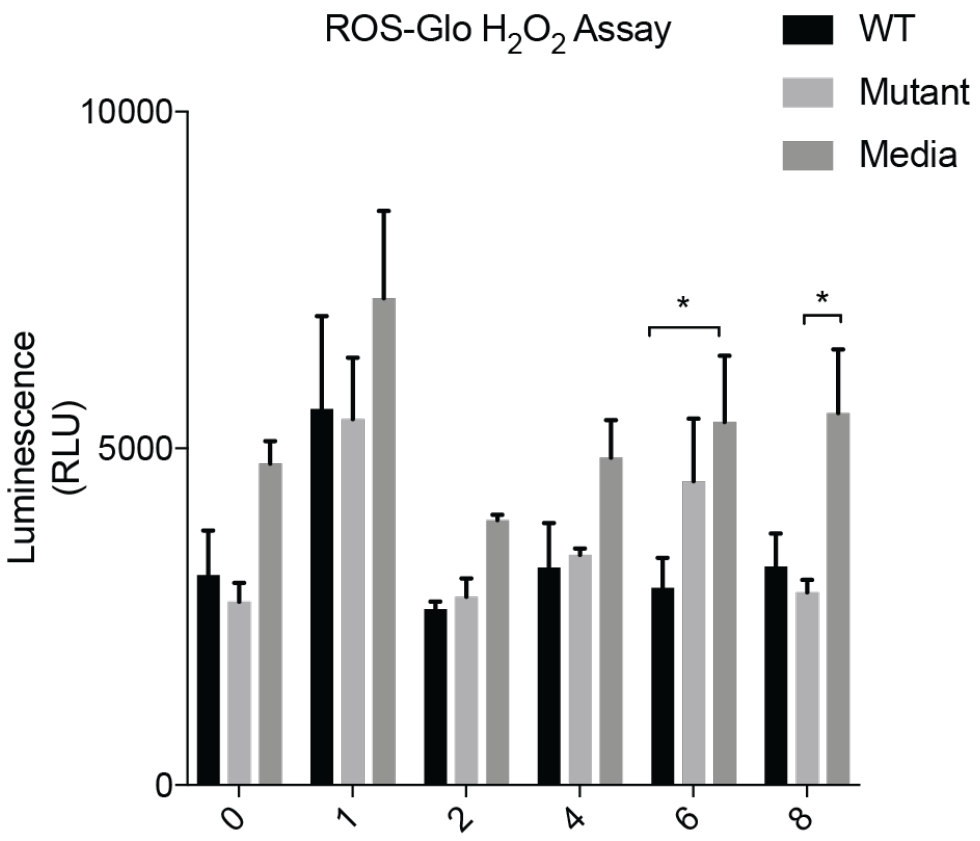

Figure A.8. ROS-Glo H_2O_2 assayX

ROS H_2O_2 assay of U-87MG cells and IDH1-R132H, and media only supplemented with NRH (100 μM) for 0,1,2,4,6,8 hours. B. Relative cell number of U-87MG and IDH1 mutant cells after treatment with NRH (100 μM) for 120 hours.

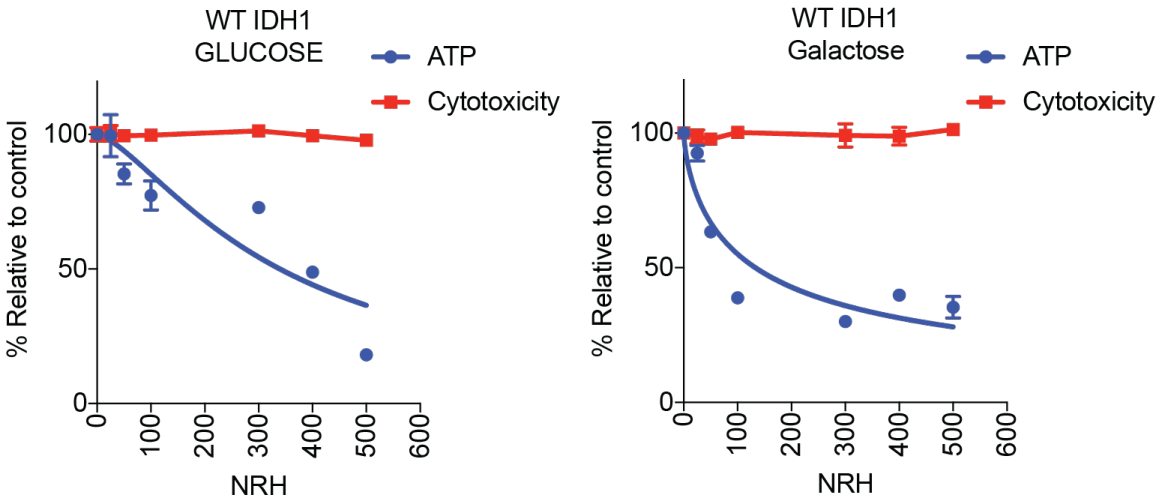

Figure A.9. Mitochondrial dysfunction measured in U-87MG cells.

A. U-87MG cells were seeded in serum free media supplemented with 5% glucose 24 hours prior to treatment with NRH (μM) at the doses indicated for 6 hours; B. U-87MG cells were seeded in serum free media supplemented with 1% galactose 24 hours prior to treatment with NRH (μM) at the doses indicated for 6 hours.

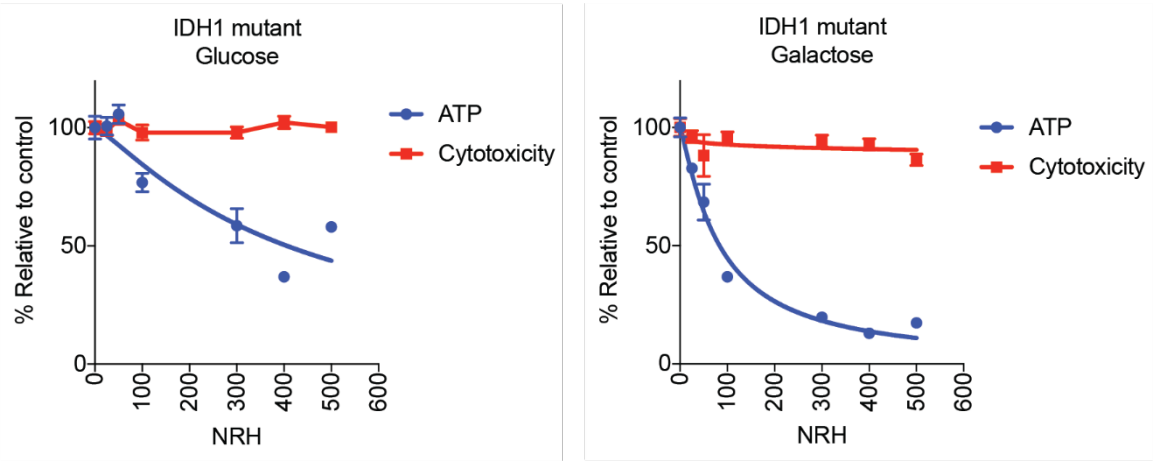

Figure A.10. Mitochondrial dysfunction measured in U-87 MG (IDH1-R132H) cells.

A. IDH1 mutant cells were seeded in serum free media supplemented with 5% glucose 24 hours prior to treatment with NRH (μM) at the doses indicated for 6 hours; B. IDH1 mutant cells were seeded in serum free media supplemented with 1% galactose 24 hours prior to treatment with NRH (μM) at the doses indicated for 6 hours.

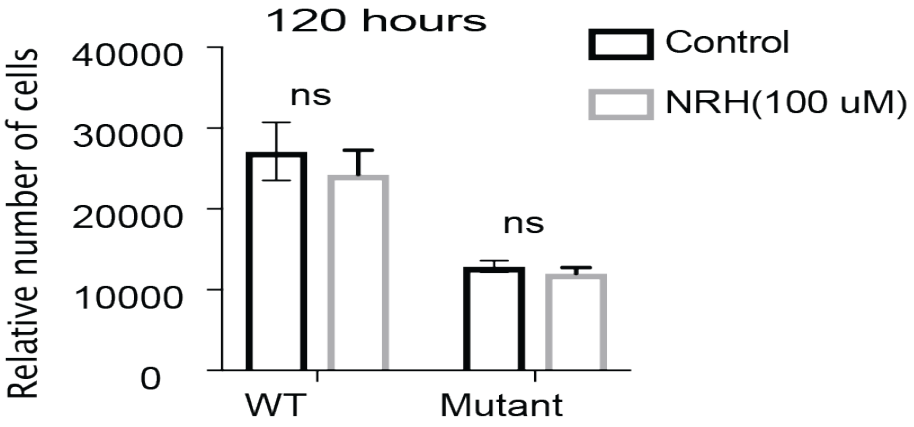

Figure A.11. Relative cell number in U-87MG and U-87MG (IDH1-R132H) following treatment with NRH.

Relative cell number of U-87MG and IDH1 mutant cells after treatment with NRH (100 μM) for 120 hours.

Appendix B: Key Resource Table

Table A1. Antibodies

REAGENT or RESOURCE	SOURCE	IDENTIFIER
Rabbit anti-XRCC1 (Immunoblot- 1:2500)	Bethyl Laboratories	Cat# A300-065A
Mouse anti-Polʖ (Clone 61) (Immunoblot- 1:1000)	Thermo Fisher Scientific	Cat# MA5-12066
Rabbit anti-Polʖ (Immunoblot- 1:1000)	Abcam	Cat# ab175197
Mouse anti-PARP1 (Immunoblot- 1:1000)	Santa Cruz	Cat# sc-8007
Mouse anti-PARP2 (Immunoblot- 1:50)	Enzo Life Sciences	Cat# ALX-804-639-L001
Mouse anti-PCNA (Immunoblot- 1:2500)	Santa Cruz Biotechnology	Cat# sc-56
Mouse anti-PAR (10H) (Immunoblot- 1:1000; Immunofluorescence- 1:200)	Generous gift from Mathias Ziegler (University of Bergen, Norway)	N/A

TABLE A1, continued.

Mouse anti-beta actin (Immunoblot- 1:2500)	Sigma	Cat# A5441
Rabbit anti-beta actin (Immunoblot- 1:1000)	Cell Signalling Technology	Cat# 4970
Rabbit anti-Myc-Tag (Immunoblot- 1:1000)	Cell Signalling Technology	Cat# 2278S
Rabbit anti-γH2AX (Immunoblot- 1:1000)	Cell Signalling Technology	Cat# 97148
Immun-Star Goat anti-mouse-HRP conjugate (Immunoblot- 1:2500)	Bio-Rad	Cat# 170-5047
Immun-Star Goat anti-rabbit-HRP conjugate (Immunoblot- 1:2500)	Bio-Rad	Cat# 170-5046
Rabbit anti-γH2AX (Immunoblot- 1:1000) (Immunofluorescence-1:500)	Cell Signalling Technology	Cat# 97148
Goat anti-mouse secondary antibody, Alexa Fluor 568 (Immunofluorescence-1:500)	Thermo Fisher Scientific	Cat# A11031
Goat anti-rabbit secondary antibody, Alex Fluor Plus 647 (Immunofluorescence-1:500)	Thermo Fisher Scientific	Cat# A32733

Table A2. Chemicals, peptides, and recombinant proteins.

Fetal bovine serum	Bio-Techne	Cat# S11150
Heat-inactivated Fetal bovine serum	Bio-Techne	Cat# S11150H
Penicillin/streptomycin	Thermo Fisher Scientific	Cat# 15140-122
DMEM	Corning	Cat# 15-017-CV
L-glutamine	Thermo Fisher Scientific	Cat# 25030-081
Dimethyl Sulfoxide	Thermo Fisher Scientific	Cat# BP231-1
Puromycin	Sigma-Aldrich	Cat# P9620-10ml
Hygromycin	Thermo Fisher Scientific	Cat# 10687010
Trypsin-EDTA	Thermo Fisher Scientific	Cat# 25200-056
0.2µM PVDF	Bio-Rad	Cat# 162-0174
0.45µM nitrocellulose	Bio-Rad	Cat# 162-0115
0.45µM Durapore Steriflip Filters	Sigma-Aldrich	Cat# SE1M003M00

Table A2, continued.

QIAprep Spin Miniprep Kit	Qiagen	Cat# 27106
QIAGEN DNeasy Blood and Tissue Kit	Qiagen	Cat# 69504
Hydrogen Peroxide (9.8M)	Sigma-Aldrich	Cat# H1009
Hoechst 33342	Thermo Fisher Scientific	Cat# 62249
Formaldehyde solution (37%)	Thermo Fisher Scientific	Cat# BP531-500
Normal Goat Serum (lyophilized)	Thermo Fisher Scientific	Cat# NC9660079
NucBlue Fixed Cell Stain Ready Probes	Thermo Fisher Scientific	Cat# R37606
Alexa Fluor 647 Phalloidin	Thermo Fisher Scientific	Cat# A22287
Alt-R CRISPR S.p. Cas9 Nuclease 3NLS	IDT	Cat# 1074182
Alt-R CRISPR-Cas9 tracrRNA	IDT	Cat# 1072533
Opti-MEM™ I Reduced Serum Medium	Thermo Fisher Scientific	Cat# 31985062
Lipofectamine™ RNAiMAX Transfection Reagent	Thermo Fisher Scientific	Cat# 13778075

Table A2, continued.

Protease inhibitor cocktail tablets	Thermo Fisher Scientific	Cat# 88666
Blotting grade non-fat dry milk	Bio-Rad	Cat# 170-6404
Nupage 4-12% Bis-Tris gel	Invitrogen	Cat# NP0323BOX
Clarity Western ECL Substrate	Bio-Rad	Cat# 1705060
SuperSignal West Femto Maximum Sensitivity Substrate	Thermo Fisher Scientific	Cat# 34095
DC protein assay kit	Bio-Rad	Cat# 5000112
ABT-888 (Veliparib)	Selleckchem	Cat# S1004
PDD00017273	Sigma-Aldrich	Cat# SML1781
QuikChange II XL Site-directed Mutagenesis Kit	Agilent	Cat# 200521
TransIT-X2 Transfection Reagent	Mirus Bio	Cat# MIR 6005
FK866	NIMH chemical drug supply company, (Bethesda, MD).	N/A

Table A2, continued.

EnzyChrom™ NAD^+/NADH assay kit	BioAssay Systems	Cat# EZND-100
FastDigest MluI	Thermo Fisher Scientific	Cat# FD0564
FastDigest BamHI	Thermo Fisher Scientific	Cat# FD0054
T7 DNA Ligase	New England Biolabs	Cat# M0318
RNAse	Thermo Fisher Scientific	Cat# EN0531
Propidium Iodide	Sigma-Aldrich	Cat# P4170
Bromodeoxyuridine (BrdU)	Sigma-Aldrich	Cat# B5002
Polybrene	Sigma-Aldrich	Cat# 107689
1-[(2R,3R,4S,5R)-3,4-Dihydroxy-5-(hydroxymethyl)tetrahydrofuran-2-yl]-4H-pyridine-3-carboxamide (NRH)	Marie Migaud	

Table A3. **Cell lines**

U2OS (Human osteosarcoma tumor cell line)	ATCC	Cat# HTB-96
A549 (Human adenocarcinoma tumor cell line)	ATCC	Cat# CCL-185
U-87 MG	ATCC	Cat# HTB-14
U-87 MG/IDH1(R132H)	ATCC	Cat# HTB-14IG
LN428		

Table A4. **Recombinant DNA**

pLentiCRISPRv2 (Cas9 plus cloning site for gRNA; contains a puromycin resistance cassette)	[219]	Addgene (#52961)
pLENTI-CRISPR-V2-XRCC1-KO-g1 (Cas9 plus XRCC1 gRNA #1; contains a puromycin resistance cassette)	Generous gift from Wim Vermeulen (Erasmus MC, NL)	[220]
pLENTI-CRISPR-V2-XRCC1-KO-g2 (Cas9 plus XRCC1 gRNA #2; contains a puromycin resistance cassette)	Generous gift from Wim Vermeulen (Erasmus MC, NL)	[220]
pLENTI-CRISPR-V2-PARP1-KO-g1 (Cas9 plus PARP1 gRNA #1; contains a puromycin resistance cassette)	Generous gift from Wim Vermeulen (Erasmus MC, NL)	[220]

Table A4, Continued.

pLV-CMV-EGFP-PolB-Hygro (EGFP fused to the N-terminus of Polβ & a hygromycin resistance cassette)	(Koczor et al, 2021)	Addgene (#176056)
pLV-CMV-XRCC1-EGFP-Hygro (EGFP fused to the C-terminus of XRCC1 & a hygromycin resistance cassette)	(Koczor et al, 2021)	Addgene (#176062)
pLV-EF1A-LivePAR-Hygro (PAR binding domain with EGFP tag & a hygromycin resistance cassette)	(Koczor et al, 2021)	Addgene (#176063)
pLV-CMV-Myc-PolB-PAMmut-Hygro (EGFP fused to the N-terminus of PolB containing a mutation in the PAM site used by PolBKOg1 & a hygromycin resistance cassette)	(Koczor et al, 2021)	Addgene (#176086)

Table A5. Software and algorithms

Image J	Image J	https://imagej.nih.gov/ij/ Versions 1.48v-1.53j
Adobe Illustrator (for preparation of figures)	Adobe Systems	https://www.adobe.com/products/illustrator.html Version 2021
GraphPad Prism	GraphPad	https://www.graphpad.com/ Version 8 (Mac OS X)
MIDAS	(Koczor et al, 2021)	https://doi.org/10.5281/zenodo.5534950
NIS-Elements	Nikon Instruments	NIS-Elements Versions 4.51 and 5.11

Appendix C: BioRender Figure Citation

Figure 1.2, Figure 1.3, and Figure 4.3.1, Appendix Figure A.5 were created using Biorender.com

Appendix D: Authorship Rights

The Chapter 3.1 figures from "Temporal dynamics of base excision/single-strand break repair protein complex assembly/disassembly are modulated by the PARP/NAD(+)/SIRT6 axis" published in Cell Reports were used in accordance with the open access article distributed under the Creative Commons Attribution License (CY BY 4.0).

The Chapter 3.2 figures from "NAD(+) bioavailability mediates PARG inhibition-induced replication arrest, intra S-phase checkpoint and apoptosis in glioma stem cells" published in NAR Cancer were used in accordance with the open access article distributed under the Creative Commons Attribution License (CY BY 4.0).

REFERENCES

1. Saville, K.M., J. Clark, A. Wilk, G.D. Rogers, J.F. Andrews, C.A. , and R.W. Sobol, *NAD(+)-mediated regulation of mammalian base excision repair.* DNA Repair (Amst), 2020. **93**: p. 102930.
2. Fouquerel, E., E.M. Goellner, Z. Yu, J.P. Gagne, M. Barbi de Moura, T. Feinstein, D. Wheeler, P. Redpath, J. Li, G. Romero, M. Migaud, B. Van Houten, G.G. Poirier, and R.W. Sobol, *ARTD1/PARP1 negatively regulates glycolysis by inhibiting hexokinase 1 independent of NAD+ depletion.* Cell Rep, 2014. **8**(6): p. 1819-1831.
3. Morales, J., L. Li, F.J. Fattah, Y. Dong, E.A. Bey, M. Patel, J. Gao, and D.A. Boothman, *Review of poly (ADP-ribose) polymerase (PARP) mechanisms of action and rationale for targeting in cancer and other diseases.* Crit Rev Eukaryot Gene Expr, 2014. **24**(1): p. 15-28.
4. Gupta, S.K., E.J. Smith, A.C. Mladek, S. Tian, P.A. Decker, S.H. Kizilbash, G.J. Kitange, and J.N. Sarkaria, *PARP Inhibitors for Sensitization of Alkylation Chemotherapy in Glioblastoma: Impact of Blood-Brain Barrier and Molecular Heterogeneity.* Front Oncol, 2018. **8**: p. 670.
5. Pautier, P., N. Penel, I. Ray-Coquard, A. Italiano, E. Bompas, C. Delcambre, J.O. Bay, F. Bertucci, J. Delaye, C. Chevreau, D. Cupissol, L. Bozec, J.C. Eymard, E. Saada, N. Isambert, C. Guillemet, M. Rios, S. Piperno-Neumann, G. Chenuc, and F. Duffaud, *A phase II of gemcitabine combined with pazopanib followed by pazopanib maintenance, as second-line treatment in patients with advanced*

leiomyosarcomas: A unicancer French Sarcoma Group study (LMS03 study). Eur J Cancer, 2020. **125**: p. 31-37.

6. Kaelin, W.G., *The Concept of Synthetic Lethality in the Context of Anticancer Therapy.* Nature Reviews Cancer, 2005. **5**(9): p. 689-698.
7. Fang, Q., B. Inanc, S. Schamus, X.H. Wang, L. Wei, A.R. Brown, D. Svilar, K.F. Sugrue, E.M. Goellner, X. Zeng, N.A. Yates, L. Lan, C. Vens, and R.W. Sobol, *HSP90 regulates DNA repair via the interaction between XRCC1 and DNA polymerase beta.* Nat Commun, 2014. **5**: p. 5513.
8. Cabelof, D.C., Z. Guo, J.J. Raffoul, R.W. Sobol, S.H. Wilson, A. Richardson, and A.R. Heydari, *Base excision repair deficiency caused by polymerase beta haploinsufficiency: accelerated DNA damage and increased mutational response to carcinogens.* Cancer Res, 2003. **63**(18): p. 5799-807.
9. Tang, J.B., E.M. Goellner, X.H. Wang, R.N. Trivedi, C.M. St Croix, E. Jelezcova, D. Svilar, A.R. Brown, and R.W. Sobol, *Bioenergetic metabolites regulate base excision repair-dependent cell death in response to DNA damage.* Mol Cancer Res, 2010. **8**(1): p. 67-79.
10. Jelezcova, E., R.N. Trivedi, X.H. Wang, J.B. Tang, A.R. Brown, E.M. Goellner, S. Schamus, J.L. Fornsaglio, and R.W. Sobol, *Parp1 activation in mouse embryonic fibroblasts promotes Pol beta-dependent cellular hypersensitivity to alkylation damage.* Mutat Res, 2010. **686**(1-2): p. 57-67.
11. Wilson, S.H. and T.A. Kunkel, *Passing the baton in base excision repair.* Nat Struct Biol, 2000. **7**(3): p. 176-8.

12. Fouquerel, E. and R.W. Sobol, *ARTD1 (PARP1) activation and NAD(+) in DNA repair and cell death.* DNA Repair (Amst), 2014. **23**: p. 27-32.

13. Tang, J.B., D. Svilar, R.N. Trivedi, X.H. Wang, E.M. Goellner, B. Moore, R.L. Hamilton, L.A. Banze, A.R. Brown, and R.W. Sobol, *N-methylpurine DNA glycosylase and DNA polymerase beta modulate BER inhibitor potentiation of glioma cells to temozolomide.* Neuro Oncol, 2011. **13**(5): p. 471-86.

14. Virtuoso, A., R. Giovannoni, C. De Luca, F. Gargano, M. Cerasuolo, N. Maggio, M. Lavitrano, and M. Papa, *The Glioblastoma Microenvironment: Morphology, Metabolism, and Molecular Signature of Glial Dynamics to Discover Metabolic Rewiring Sequence.* Int J Mol Sci, 2021. **22**(7).

15. Garcia, J.H., S. Jain, and M.K. Aghi, *Metabolic Drivers of Invasion in Glioblastoma.* Frontiers in Cell and Developmental Biology, 2021. **9**.

16. Xie, N., L. Zhang, W. Gao, C. Huang, P.E. Huber, X. Zhou, C. Li, G. Shen, and B. Zou, *NAD+ metabolism: pathophysiologic mechanisms and therapeutic potential.* Signal Transduction and Targeted Therapy, 2020. **5**(1): p. 227.

17. Fang, E.F., S. Lautrup, Y. Hou, T.G. Demarest, D.L. Croteau, M.P. Mattson, and V.A. Bohr, *NAD(+) in Aging: Molecular Mechanisms and Translational Implications.* Trends Mol Med, 2017. **23**(10): p. 899-916.

18. Radenkovic, D., Reason, and E. Verdin, *Clinical Evidence for Targeting NAD Therapeutically.* Pharmaceuticals (Basel), 2020. **13**(9).

19. Wang, X., H.-J. He, X. Xiong, S. Zhou, W.-W. Wang, L. Feng, R. Han, and C.-L. Xie, *NAD+ in Alzheimer's Disease: Molecular Mechanisms and Systematic*

Therapeutic Evidence Obtained in vivo. Frontiers in Cell and Developmental Biology, 2021. **9**.

20. Brakedal, B., C. Dölle, F. Riemer, Y. Ma, G.S. Nido, G.O. Skeie, A.R. Craven, T. Schwarzlmüller, N. Brekke, J. Diab, L. Sverkeli, V. Skjeie, K. Varhaug, O.-B. Tysnes, S. Peng, K. Haugarvoll, M. Ziegler, R. Grüner, D. Eidelberg, and C. Tzoulis, *The NADPARK study: A randomized phase I trial of nicotinamide riboside supplementation in Parkinson's disease.* Cell Metabolism, 2022. **34**(3): p. 396-407.e6.
21. Amjad, S., S. Nisar, A.A. Bhat, A.R. Shah, M.P. Frenneaux, K. Fakhro, M. Haris, R. Reddy, Z. Patay, J. Baur, and P. Bagga, *Role of NAD+ in regulating cellular and metabolic signaling pathways.* Molecular Metabolism, 2021. **49**: p. 101195.
22. Giroud-Gerbetant, J., M. Joffraud, M.P. Giner, A. Cercillieux, S. Bartova, M.V. Makarov, R. Zapata-Pérez, J.L. Sánchez-García, R.H. Houtkooper, M.E. Migaud, S. Moco, and C. Canto, *A reduced form of nicotinamide riboside defines a new path for NAD(+) biosynthesis and acts as an orally bioavailable NAD(+) precursor.* Mol Metab, 2019. **30**: p. 192-202.
23. Audrito, V., V.G. Messana, and S. Deaglio, *NAMPT and NAPRT: Two Metabolic Enzymes With Key Roles in Inflammation.* Frontiers in Oncology, 2020. **10**.
24. Liu, L., X. Su, W.J. Quinn, 3rd, S. Hui, K. Krukenberg, D.W. Frederick, P. Redpath, L. Zhan, K. Chellappa, E. White, M. Migaud, T.J. Mitchison, J.A. Baur, and J.D. Rabinowitz, *Quantitative Analysis of NAD Synthesis-Breakdown Fluxes.* Cell Metab, 2018. **27**(5): p. 1067-1080 e5.

25. Cohen, M.S., *Interplay between compartmentalized NAD(+) synthesis and consumption: a focus on the PARP family.* Genes Dev, 2020. **34**(5-6): p. 254-262.

26. Garrido, A. and N. Djouder, *NAD(+) Deficits in Age-Related Diseases and Cancer.* Trends Cancer, 2017. **3**(8): p. 593-610.

27. Yang, Y., N. Zhang, G. Zhang, and A.A. Sauve, *NRH salvage and conversion to NAD+ requires NRH kinase activity by adenosine kinase.* Nature Metabolism, 2020. **2**(4): p. 364-379.

28. Yang, Y., F.S. Mohammed, N. Zhang, and A.A. Sauve, *Dihydronicotinamide riboside is a potent NAD(+) concentration enhancer in vitro and in vivo.* J Biol Chem, 2019. **294**(23): p. 9295-9307.

29. Alabarse, P., H. Qin, F. Hayat, M. Migaud, and R. Liu-Bryan, *DIHYDRONICOTINAMIDE RIBOSIDE (NRH), AN ORALLY BIOAVAILABLE NICOTINAMIDE ADENINE DINUCLEOTIDE (NAD) PRECURSOR, SIGNIFICANTLY INHIBITS POST-TRAUMATIC OSTEOARTHRITIS (OA) DEVELOPMENT AND ASSOCIATED PAIN IN MICE.* Osteoarthritis and Cartilage, 2022. **30**: p. S328.

30. Wu, K., J. Li, X. Zhou, F. Zhou, S. Tang, l. Yi, Y. Wu, and S. Tian, *NADH and NRH as potential dietary supplements or pharmacological agents for early liver injury caused by acute alcohol exposure.* Journal of Functional Foods, 2021. **87**: p. 104852.

31. Zapata-Pérez, R., A. Tammaro, B.V. Schomakers, A.M.L. Scantlebery, S. Denis, H.L. Elfrink, J. Giroud-Gerbetant, C. Cantó, C. López-Leonardo, R.L. McIntyre, M. van Weeghel, Á. Sánchez-Ferrer, and R.H. Houtkooper, *Reduced nicotinamide*

mononucleotide is a new and potent NAD+ precursor in mammalian cells and mice. The FASEB Journal, 2021. **35**(4): p. e21456.

32. Chini, C.C.S., T.R. Peclat, L.S. Gomez, J.D. Zeidler, G.M. Warner, S. Kashyap, D.Z. Mazdeh, F. Hayat, M.E. Migaud, A. Paulus, A.A. Chanan-Khan, and E.N. Chini, *Dihydronicotinamide Riboside Is a Potent NAD+ Precursor Promoting a Pro-Inflammatory Phenotype in Macrophages.* Frontiers in Immunology, 2022. **13**.

33. Sonavane, M., F. Hayat, M. Makarov, M.E. Migaud, and N.R. Gassman, *Dihydronicotinamide riboside promotes cell-specific cytotoxicity by tipping the balance between metabolic regulation and oxidative stress.* PLoS One, 2020. **15**(11): p. e0242174.

34. Makarov, M.V., F. Hayat, B. Graves, M. Sonavane, E.A. Salter, A. Wierzbicki, N.R. Gassman, and M.E. Migaud, *Chemical and Biochemical Reactivity of the Reduced Forms of Nicotinamide Riboside.* ACS Chemical Biology, 2021. **16**(4): p. 604-614.

35. Biedermann, J., M. Preussler, M. Conde, M. Peitzsch, S. Richter, R. Wiedemuth, K. Abou-El-Ardat, A. Krüger, M. Meinhardt, G. Schackert, W.P. Leenders, C. Herold-Mende, S.P. Niclou, R. Bjerkvig, G. Eisenhofer, A. Temme, M. Seifert, L.A. Kunz-Schughart, E. Schröck, and B. Klink, *Mutant IDH1 Differently Affects Redox State and Metabolism in Glial Cells of Normal and Tumor Origin.* Cancers (Basel), 2019. **11**(12).

36. Lucena-Cacace, A., D. Otero-Albiol, M.P. Jiménez-García, J. Peinado-Serrano, and A. Carnero, *NAMPT overexpression induces cancer stemness and defines a novel tumor signature for glioma prognosis.* Oncotarget, 2017. **8**(59): p. 99514-99530.

37. Galli, U., G. Colombo, C. Travelli, G.C. Tron, A.A. Genazzani, and A.A. Grolla, *Recent Advances in NAMPT Inhibitors: A Novel Immunotherapic Strategy.* Front Pharmacol, 2020. **11**: p. 656.

38. Fons, N.R., R.K. Sundaram, G.A. Breuer, S. Peng, R.L. McLean, A.N. Kalathil, M.S. Schmidt, D.M. Carvalho, A. Mackay, C. Jones, Á.M. Carcaboso, J. Nazarian, M.E. Berens, C. Brenner, and R.S. Bindra, *PPM1D mutations silence NAPRT gene expression and confer NAMPT inhibitor sensitivity in glioma.* Nature Communications, 2019. **10**(1): p. 3790.

39. Yaku, K., K. Okabe, K. Hikosaka, and T. Nakagawa, *NAD Metabolism in Cancer Therapeutics.* Front Oncol, 2018. **8**: p. 622.

40. Cohen, A.L., S.L. Holmen, and H. Colman, *IDH1 and IDH2 mutations in gliomas.* Curr Neurol Neurosci Rep, 2013. **13**(5): p. 345.

41. Guo, C., C.J. Pirozzi, G.Y. Lopez, and H. Yan, *Isocitrate dehydrogenase mutations in gliomas: mechanisms, biomarkers and therapeutic target.* Curr Opin Neurol, 2011. **24**(6): p. 648-52.

42. Ju, H.-Q., J.-F. Lin, T. Tian, D. Xie, and R.-H. Xu, *NADPH homeostasis in cancer: functions, mechanisms and therapeutic implications.* Signal Transduction and Targeted Therapy, 2020. **5**(1): p. 231.

43. Kaminska, B., B. Czapski, R. Guzik, S.K. Król, and B. Gielniewski, *Consequences of IDH1/2 Mutations in Gliomas and an Assessment of Inhibitors Targeting Mutated IDH Proteins.* Molecules, 2019. **24**(5).

44. Sociali, G., A. Grozio, I. Caffa, S. Schuster, P. Becherini, P. Damonte, L. Sturla, C. Fresia, M. Passalacqua, F. Mazzola, N. Raffaelli, A. Garten, W. Kiess, M. Cea, A.

Nencioni, and S. Bruzzone, *SIRT6 deacetylase activity regulates NAMPT activity and NAD(P)(H) pools in cancer cells.* Faseb j, 2019. **33**(3): p. 3704-3717.

45. Srinivas, U.S., B.W.Q. Tan, B.A. Vellayappan, and A.D. Jeyasekharan, *ROS and the DNA damage response in cancer.* Redox Biology, 2019. **25**: p. 101084.

46. Valverde, M., J. Lozano-Salgado, P. Fortini, M.A. Rodriguez-Sastre, E. Rojas, and E. Dogliotti, *Hydrogen Peroxide-Induced DNA Damage and Repair through the Differentiation of Human Adipose-Derived Mesenchymal Stem Cells.* Stem Cells Int, 2018. **2018**: p. 1615497.

47. Tateishi, K., H. Wakimoto, A.J. Iafrate, S. Tanaka, F. Loebel, N. Lelic, D. Wiederschain, O. Bedel, G. Deng, B. Zhang, T. He, X. Shi, R.E. Gerszten, Y. Zhang, J.J. Yeh, W.T. Curry, D. Zhao, S. Sundaram, F. Nigim, M.V.A. Koerner, Q. Ho, D.E. Fisher, E.M. Roider, L.V. Kemeny, Y. Samuels, K.T. Flaherty, T.T. Batchelor, A.S. Chi, and D.P. Cahill, *Extreme Vulnerability of IDH1 Mutant Cancers to NAD+ Depletion.* Cancer Cell, 2015. **28**(6): p. 773-784.

48. Ding, C.-K.C., J. Rose, T. Sun, J. Wu, P.-H. Chen, C.-C. Lin, W.-H. Yang, K.-Y. Chen, H. Lee, E. Xu, S. Tian, J. Akinwuntan, J. Zhao, Z. Guan, P. Zhou, and J.-T. Chi, *MESH1 is a cytosolic NADPH phosphatase that regulates ferroptosis.* Nature Metabolism, 2020. **2**(3): p. 270-277.

49. Abshire, E.T., K.L. Hughes, R. Diao, S. Pearce, S. Gopalakrishna, R.C. Trievel, J. Rorbach, P.L. Freddolino, and A.C. Goldstrohm, *Differential processing and localization of human Nocturnin controls metabolism of mRNA and nicotinamide adenine dinucleotide cofactors.* J Biol Chem, 2020. **295**(44): p. 15112-15133.

50. Estrella, M.A., J. Du, L. Chen, S. Rath, E. Prangley, A. Chitrakar, T. Aoki, P. Schedl, J. Rabinowitz, and A. Korennykh, *The metabolites NADP+ and NADPH are the targets of the circadian protein Nocturnin (Curled).* Nature Communications, 2019. **10**(1): p. 2367.

51. Hottiger, M.O., P.O. Hassa, B. Luscher, H. Schuler, and F. Koch-Nolte, *Toward a unified nomenclature for mammalian ADP-ribosyltransferases.* Trends Biochem Sci, 2010. **35**(4): p. 208-19.

52. Rajamohan, S.B., V.B. Pillai, M. Gupta, N.R. Sundaresan, K.G. Birukov, S. Samant, M.O. Hottiger, and M.P. Gupta, *SIRT1 promotes cell survival under stress by deacetylation-dependent deactivation of poly(ADP-ribose) polymerase 1.* Mol Cell Biol, 2009. **29**(15): p. 4116-29.

53. Hassa, P.O., S.S. Haenni, C. Buerki, N.I. Meier, W.S. Lane, H. Owen, M. Gersbach, R. Imhof, and M.O. Hottiger, *Acetylation of PARP-1 by p300/CBP regulates coactivation of NF-kappa B-dependent transcription.* J Biol Chem, 2005.

54. Luo, X. and W.L. Kraus, *On PAR with PARP: cellular stress signaling through poly(ADP-ribose) and PARP-1.* Genes Dev, 2012. **26**(5): p. 417-32.

55. Piao, L., K. Fujioka, M. Nakakido, and R. Hamamoto, *Regulation of poly(ADP-Ribose) polymerase 1 functions by post-translational modifications.* Front Biosci (Landmark Ed), 2018. **23**: p. 13-26.

56. Li, J., K. M. Saville, M. Ibrahim, X. Zeng, S. McClellan, A. Angajala, A. Beiser, J.F. Andrews, M. Sun, C.A. , J. Clark, F. Hayat, M.V. Makarov, A. Wilk, N.A. Yates, M.E. Migaud, and R.W. Sobol, *NAD+ bioavailability mediates PARG*

inhibition-induced replication arrest, intra S-phase checkpoint and apoptosis in glioma stem cells. NAR Cancer, 2021. **3**(4): p. zcab044.

57. Wilk, A., F. Hayat, R. Cunningham, J. Li, S. Garavaglia, L. Zamani, D.M. Ferraris, P. Sykora, J. Andrews, J. Clark, A. Davis, L. Chaloin, M. Rizzi, M. Migaud, and R.W. Sobol, *Extracellular NAD(+) enhances PARP-dependent DNA repair capacity independently of CD73 activity.* Sci Rep, 2020. **10**(1): p. 651.

58. Koczor, C.A., K.M. Saville, J.F. Andrews, J. Clark, Q. Fang, J. Li, R.Q. Al-Rahahleh, M. Ibrahim, S. McClellan, M.V. Makarov, M.E. Migaud, and R.W. Sobol, *Temporal dynamics of base excision/single-strand break repair protein complex assembly/disassembly are modulated by the PARP/NAD(+)/SIRT6 axis.* Cell Rep, 2021. **37**(5): p. 109917.

59. Wilk, A., F. Hayat, R. Cunningham, J. Li, S. Garavaglia, L. Zamani, D.M. Ferraris, P. Sykora, J. Andrews, J. Clark, A. Davis, L. Chaloin, M. Rizzi, M. Migaud, and R.W. Sobol, *Extracellular NAD+ enhances PARP-dependent DNA repair capacity independently of CD73 activity.* Scientific Reports, 2020. **10**(1): p. 651.

60. Goellner, E.M., B. Grimme, A.R. Brown, Y.C. Lin, X.H. Wang, K.F. Sugrue, L. Mitchell, R.N. Trivedi, J.B. Tang, and R.W. Sobol, *Overcoming temozolomide resistance in glioblastoma via dual inhibition of NAD+ biosynthesis and base excision repair.* Cancer Res, 2011. **71**(6): p. 2308-17.

61. Bian, C., C. Zhang, T. Luo, A. Vyas, S.-H. Chen, C. Liu, M.A. Kassab, Y. Yang, M. Kong, and X. Yu, *NADP+ is an endogenous PARP inhibitor in DNA damage response and tumor suppression.* Nature Communications, 2019. **10**(1): p. 693.

62. , C.A., K.M. Saville, J.F. Andrews, J. Clark, Q. Fang, J. Li, R.Q. Al-Rahahleh, M. Ibrahim, S. McClellan, M.V. Makarov, M.E. Migaud, and R.W. Sobol, *Temporal dynamics of base excision/single-strand break repair protein complex assembly/disassembly are modulated by the PARP/NAD(+)/SIRT6 axis.* Cell Rep, 2021. **37**(5): p. 109917.

63. Bonm, A. and S. Kesari, *DNA Damage Response in Glioblastoma: Mechanism for Treatment Resistance and Emerging Therapeutic Strategies.* Cancer J, 2021. **27**(5): p. 379-385.

64. Gralewska, P., A. Gajek, A. Marczak, M. Mikuła, J. Ostrowski, A. Śliwińska, and A. Rogalska, *PARP Inhibition Increases the Reliance on ATR/CHK1 Checkpoint Signaling Leading to Synthetic Lethality-An Alternative Treatment Strategy for Epithelial Ovarian Cancer Cells Independent from HR Effectiveness.* Int J Mol Sci, 2020. **21**(24).

65. Lloyd, R.L., P.W.G. Wijnhoven, A. Ramos-Montoya, Z. Wilson, G. Illuzzi, K. Falenta, G.N. Jones, N. James, C.D. Chabbert, J. Stott, E. Dean, A. Lau, and L.A. Young, *Combined PARP and ATR inhibition potentiates genome instability and cell death in ATM-deficient cancer cells.* Oncogene, 2020. **39**(25): p. 4869-4883.

66. Carruthers, R.D., S.U. Ahmed, S. Ramachandran, K. Strathdee, K.M. Kurian, A. Hedley, N. Gomez-Roman, G. Kalna, M. Neilson, L. Gilmour, K.H. Stevenson, E.M. Hammond, and A.J. Chalmers, *Replication Stress Drives Constitutive Activation of the DNA Damage Response and Radioresistance in Glioblastoma Stem-like Cells.* Cancer Res, 2018. **78**(17): p. 5060-5071.

67. Gaillard, H., T. García-Muse, and A. Aguilera, *Replication stress and cancer.* Nat Rev Cancer, 2015. **15**(5): p. 276-89.

68. Morgan, M.A. and C.E. Canman, *Replication Stress: An Achilles' Heel of Glioma Cancer Stem-like Cells.* Cancer Res, 2018. **78**(24): p. 6713-6716.

69. Salmon, T.B., B.A. Evert, B. Song, and P.W. Doetsch, *Biological consequences of oxidative stress-induced DNA damage in Saccharomyces cerevisiae.* Nucleic Acids Res, 2004. **32**(12): p. 3712-23.

70. Struve, N., K. Hoffer, A.-S. Weik, B. Riepen, L. Krug, M.H. Cetin, J. Burmester, L. Ott, J. Liebing, F. Gatzemeier, J. Müller-Goebel, M. Gerbach, L. Bußmann, A.C. Parplys, K. Unger, W.Y. Mansour, U. Schüller, T. Rieckmann, C. Petersen, K. Rothkamm, S.C. Short, and M. Kriegs, *Increased replication stress and R-loop accumulation in EGFRvIII-expressing glioblastoma present new therapeutic opportunities.* Neuro-Oncology Advances, 2022. **4**(1): p. vdab180.

71. Lupey-Green, L.N., L.B. Caruso, J. Madzo, K.A. Martin, Y. Tan, M. Hulse, and I. Tempera, *PARP1 Stabilizes CTCF Binding and Chromatin Structure To Maintain Epstein-Barr Virus Latency Type.* J Virol, 2018. **92**(18).

72. Sule, A., J. Van Doorn, R.K. Sundaram, S. Ganesa, J.C. Vasquez, and R.S. Bindra, *Targeting IDH1/2 mutant cancers with combinations of ATR and PARP inhibitors.* NAR Cancer, 2021. **3**(2): p. zcab018.

73. Alemasova, E.E. and O.I. Lavrik, *Poly(ADP-ribosyl)ation by PARP1: reaction mechanism and regulatory proteins.* Nucleic Acids Research, 2019. **47**(8): p. 3811-3827.

74. Altmeyer, M., S. Messner, P.O. Hassa, M. Fey, and M.O. Hottiger, *Molecular mechanism of poly(ADP-ribosyl)ation by PARP1 and identification of lysine residues as ADP-ribose acceptor sites.* Nucleic Acids Res, 2009. **37**(11): p. 3723-38.

75. Li, J., M.S. K, M. Ibrahim, X. Zeng, S. McClellan, A. Angajala, A. Beiser, J.F. Andrews, M. Sun, C.A. Koczor, J. Clark, F. Hayat, M.V. Makarov, A. Wilk, N.A. Yates, M.E. Migaud, and R.W. Sobol, *NAD(+) bioavailability mediates PARG inhibition-induced replication arrest, intra S-phase checkpoint and apoptosis in glioma stem cells.* NAR Cancer, 2021. **3**(4): p. zcab044.

76. Kotsantis, P., E. Petermann, and S.J. Boulton, *Mechanisms of Oncogene-Induced Replication Stress: Jigsaw Falling into Place.* Cancer Discovery, 2018. **8**(5): p. 537-555.

77. Berti, M., A. Ray Chaudhuri, S. Thangavel, S. Gomathinayagam, S. Kenig, M. Vujanovic, F. Odreman, T. Glatter, S. Graziano, R. Mendoza-Maldonado, F. Marino, B. Lucic, V. Biasin, M. Gstaiger, R. Aebersold, J.M. Sidorova, R.J. Monnat, Jr., M. Lopes, and A. Vindigni, *Human RECQ1 promotes restart of replication forks reversed by DNA topoisomerase I inhibition.* Nat Struct Mol Biol, 2013. **20**(3): p. 347-54.

78. Ishizuka, S., K. Martin, C. Booth, C.S. Potten, G. de Murcia, A. Burkle, and T.B. Kirkwood, *Poly(ADP-ribose) polymerase-1 is a survival factor for radiation-exposed intestinal epithelial stem cells in vivo.* Nucleic Acids Res, 2003. **31**(21): p. 6198-205.

79. Benedict, B., T. van Harn, M. Dekker, S. Hermsen, A. Kucukosmanoglu, W. Pieters, E. Delzenne-Goette, J.C. Dorsman, E. Petermann, F. Foijer, and H. te Riele, *Loss of p53 suppresses replication-stress-induced DNA breakage in G1/S checkpoint deficient cells.* eLife, 2018. **7**: p. e37868.

80. Giansanti, C., V. Manzini, A. Dickmanns, A. Dickmanns, M.D. Palumbieri, A. Sanchi, S.M. Kienle, S. Rieth, M. Scheffner, M. Lopes, and M. Dobbelstein, *MDM2 binds and ubiquitinates PARP1 to enhance DNA replication fork progression.* Cell Rep, 2022. **39**(9): p. 110879.

81. Hanzlikova, H., I. Kalasova, A.A. Demin, L.E. Pennicott, Z. Cihlarova, and K.W. Caldecott, *The Importance of Poly(ADP-Ribose) Polymerase as a Sensor of Unligated Okazaki Fragments during DNA Replication.* Mol Cell, 2018. **71**(2): p. 319-331 e3.

82. Ying, S., Z. Chen, A.L. Medhurst, J.A. Neal, Z. Bao, O. Mortusewicz, J. McGouran, X. Song, H. Shen, F.C. Hamdy, B.M. Kessler, K. Meek, and T. Helleday, *DNA-PKcs and PARP1 Bind to Unresected Stalled DNA Replication Forks Where They Recruit XRCC1 to Mediate Repair.* Cancer Res, 2016. **76**(5): p. 1078-88.

83. Paes Dias, M., V. Tripathi, I. van der Heijden, K. Cong, E.-M. Manolika, J. Bhin, E. Gogola, P. Galanos, S. Annunziato, C. Lieftink, M. Andújar-Sánchez, S. Chakrabarty, G.C.M. Smith, M. van de Ven, R.L. Beijersbergen, J. Bartkova, S. Rottenberg, S. Cantor, J. Bartek, A. Ray Chaudhuri, and J. Jonkers, *Loss of nuclear DNA ligase III reverts PARP inhibitor resistance in BRCA1/53BP1 double-*

deficient cells by exposing ssDNA gaps. Molecular Cell, 2021. **81**(22): p. 4692-4708.e9.

84. Ying, S., F.C. Hamdy, and T. Helleday, *Mre11-dependent degradation of stalled DNA replication forks is prevented by BRCA2 and PARP1.* Cancer Res, 2012. **72**(11): p. 2814-21.

85. Bryant, H.E., E. Petermann, N. Schultz, A.S. Jemth, O. Loseva, N. Issaeva, F. Johansson, S. Fernandez, P. McGlynn, and T. Helleday, *PARP is activated at stalled forks to mediate Mre11-dependent replication restart and recombination.* EMBO J, 2009. **28**(17): p. 2601-15.

86. Peng, B., R. Shi, J. Bian, Y. Li, P. Wang, H. Wang, J. Liao, W.-G. Zhu, and X. Xu, *PARP1 and CHK1 coordinate PLK1 enzymatic activity during the DNA damage response to promote homologous recombination-mediated repair.* Nucleic Acids Research, 2021. **49**(13): p. 7554-7570.

87. Zhao, Y., C.X. Wang, T.M. Yang, C.S. Li, L.H. Zhang, D.N. Du, R.X. Wang, J. Wang, M. Wei, and X.Q. Ba, *Linking oxidative DNA lesion 8-OxoG to tumor development and progression.* Yi Chuan, 2022. **44**(6): p. 466-477.

88. Visnes, T., C. Benítez-Buelga, A. Cázares-Körner, K. Sanjiv, B.M.F. Hanna, O. Mortusewicz, V. Rajagopal, J.J. Albers, D.W. Hagey, T. Bekkhus, S. Eshtad, J.M. Baquero, G. Masuyer, O. Wallner, S. Müller, T. Pham, C. Göktürk, A. Rasti, S. Suman, R. Torres-Ruiz, A. Sarno, E. Wiita, E.J. Homan, S. Karsten, K. Marimuthu, M. Michel, T. Koolmeister, M. Scobie, O. Loseva, I. Almlöf, J.E. Unterlass, A. Pettke, J. Boström, M. Pandey, H. Gad, P. Herr, A.S. Jemth, S. El Andaloussi, C. Kalderén, S. Rodriguez-Perales, J. Benítez, H.E. Krokan, M. Altun, P. Stenmark,

U.W. Berglund, and T. Helleday, *Targeting OGG1 arrests cancer cell proliferation by inducing replication stress.* Nucleic Acids Res, 2020. **48**(21): p. 12234-12251.

89. Lucena-Cacace, A., M. Umeda, L.E. Navas, and A. Carnero, *NAMPT as a Dedifferentiation-Inducer Gene: NAD+ as Core Axis for Glioma Cancer Stem-Like Cells Maintenance.* Frontiers in Oncology, 2019. **9**.

90. Tateishi, K., F. Higuchi, J.J. Miller, M.V.A. Koerner, N. Lelic, G.M. Shankar, S. Tanaka, D.E. Fisher, T.T. Batchelor, A.J. Iafrate, H. Wakimoto, A.S. Chi, and D.P. Cahill, *The Alkylating Chemotherapeutic Temozolomide Induces Metabolic Stress in IDH1-Mutant Cancers and Potentiates NAD(+) Depletion-Mediated Cytotoxicity.* Cancer Res, 2017. **77**(15): p. 4102-4115.

91. Soll, J.M., R.W. Sobol, and N. Mosammaparast, *Regulation of DNA Alkylation Damage Repair: Lessons and Therapeutic Opportunities.* Trends Biochem Sci, 2017. **42**(3): p. 206-218.

92. Goellner, E.M., B. Grimme, A.R. Brown, Y.-C. Lin, X.-H. Wang, K.F. Sugrue, L. Mitchell, R.N. Trivedi, J.-b. Tang, and R.W. Sobol, *Overcoming Temozolomide Resistance in Glioblastoma via Dual Inhibition of NAD⁺ Biosynthesis and Base Excision Repair.* Cancer Research, 2011. **71**(6): p. 2308-2317.

93. Agnihotri, S., K. Burrell, P. Buczkowicz, M. Remke, B. Golbourn, Y. Chornenkyy, A. Gajadhar, N.A. Fernandez, I.D. Clarke, M.S. Barszczyk, S. Pajovic, C. Ternamian, R. Head, N. Sabha, R.W. Sobol, M.D. Taylor, J.T. Rutka, C. Jones, P.B. Dirks, G. Zadeh, and C. Hawkins, *ATM regulates 3-methylpurine-DNA*

glycosylase and promotes therapeutic resistance to alkylating agents. Cancer Discov, 2014. **4**(10): p. 1198-213.

94. Fujii, S., R.W. Sobol, and R.P. Fuchs, *Double-strand breaks: When DNA repair events accidentally meet.* DNA Repair, 2022. **112**: p. 103303.

95. Galia, A., A.E. Calogero, R. Condorelli, F. Fraggetta, A. La Corte, F. Ridolfo, P. Bosco, R. Castiglione, and M. Salemi, *PARP-1 protein expression in glioblastoma multiforme.* Eur J Histochem, 2012. **56**(1): p. e9.

96. Bj Ras, K.O., M.M.L. Sousa, A. Sharma, D.M. Fonseca, S.G. CK, M. Bj Ras, and M. Otterlei, *Monitoring of the spatial and temporal dynamics of BER/SSBR pathway proteins, including MYH, UNG2, MPG, NTH1 and NEIL1-3, during DNA replication.* Nucleic Acids Res, 2017. **45**(14): p. 8291-8301.

97. Choi, S., Y. Yu, M.R. Grimmer, M. Wahl, S.M. Chang, and J.F. Costello, *Temozolomide-associated hypermutation in gliomas.* Neuro Oncol, 2018. **20**(10): p. 1300-1309.

98. Fu, D., J.A. Calvo, and L.D. Samson, *Balancing repair and tolerance of DNA damage caused by alkylating agents.* Nat Rev Cancer, 2012. **12**(2): p. 104-20.

99. Gupta, D., B. Lin, A. Cowan, and C.D. Heinen, *ATR-Chk1 activation mitigates replication stress caused by mismatch repair-dependent processing of DNA damage.* Proc Natl Acad Sci U S A, 2018. **115**(7): p. 1523-1528.

100. Bonm, A. and S. Kesari, *DNA Damage Response in Glioblastoma: Mechanism for Treatment Resistance and Emerging Therapeutic Strategies.* The Cancer Journal, 2021. **27**(5): p. 379-385.

101. Yan, S., M. Sorrell, and Z. Berman, *Functional interplay between ATM/ATR-mediated DNA damage response and DNA repair pathways in oxidative stress.* Cell Mol Life Sci, 2014. **71**(20): p. 3951-67.

102. Menolfi, D. and S. Zha, *ATM, ATR and DNA-PKcs kinases—the lessons from the mouse models: inhibition ≠ deletion.* Cell & Bioscience, 2020. **10**(1): p. 8.

103. Suwala, A.K., D. Stichel, D. Schrimpf, M. Kloor, A.K. Wefers, A. Reinhardt, S.L.N. Maas, C.P. Kratz, L. Schweizer, M. Hasselblatt, M. Snuderl, M.S.J. Abedalthagafi, Z. Abdullaev, C.M. Monoranu, M. Bergmann, A. Pekrun, C. Freyschlag, E. Aronica, C.M. Kramm, F. Hinz, P. Sievers, A. Korshunov, M. Kool, S.M. Pfister, D. Sturm, D.T.W. Jones, W. Wick, A. Unterberg, C. Hartmann, A. Dodgshun, U. Tabori, P. Wesseling, F. Sahm, A. von Deimling, and D.E. Reuss, *Primary mismatch repair deficient IDH-mutant astrocytoma (PMMRDIA) is a distinct type with a poor prognosis.* Acta Neuropathol, 2021. **141**(1): p. 85-100.

104. McCord, M., A. Steffens, R. Javier, K.-L. Kam, K. McCortney, and C. Horbinski, *The efficacy of DNA mismatch repair enzyme immunohistochemistry as a screening test for hypermutated gliomas.* Acta Neuropathologica Communications, 2020. **8**(1): p. 15.

105. Fuchs, R.P., A. Isogawa, J.A. Paulo, K. Onizuka, T. Takahashi, R. Amunugama, J.P. Duxin, and S. Fujii, *Crosstalk between repair pathways elicits double-strand breaks in alkylated DNA and implications for the action of temozolomide.* eLife, 2021. **10**: p. e69544.

106. Zhang, J., M. Chen, Y. Pang, M. Cheng, B. Huang, S. Xu, M. Liu, H. Lian, and C. Zhong, *Flap endonuclease 1 and DNA-PKcs synergistically participate in*

stabilizing replication fork to encounter replication stress in glioma cells. Journal of Experimental & Clinical Cancer Research, 2022. **41**(1): p. 140.

107. Ray, S., G. Breuer, M. DeVeaux, D. Zelterman, R. Bindra, and J.B. Sweasy, *DNA polymerase beta participates in DNA End-joining.* Nucleic Acids Res, 2018. **46**(1): p. 242-255.

108. Xia, W., S. Ci, M. Li, M. Wang, G.L. Dianov, Z. Ma, L. Li, K. Hua, K.K. Alagamuthu, L. Qing, L. Luo, A.M. Edick, L. Liu, Z. Hu, L. He, F. Pan, and Z. Guo, *Two-way crosstalk between BER and c-NHEJ repair pathway is mediated by Pol-β and Ku70.* Faseb j, 2019. **33**(11): p. 11668-11681.

109. Rose, M., J.T. Burgess, K. O'Byrne, D.J. Richard, and E. Bolderson, *PARP Inhibitors: Clinical Relevance, Mechanisms of Action and Tumor Resistance.* Frontiers in Cell and Developmental Biology, 2020. **8**.

110. Almeida, K.H. and R.W. Sobol, *A unified view of base excision repair: lesion-dependent protein complexes regulated by post-translational modification.* DNA Repair (Amst), 2007. **6**(6): p. 695-711.

111. Huambachano, O., F. Herrera, A. Rancourt, and M.S. Satoh, *Double-stranded DNA binding domain of poly(ADP-ribose) polymerase-1 and molecular insight into the regulation of its activity.* J Biol Chem, 2011. **286**(9): p. 7149-60.

112. Eustermann, S., W.F. Wu, M.F. Langelier, J.C. Yang, L.E. Easton, A.A. Riccio, J.M. Pascal, and D. Neuhaus, *Structural Basis of Detection and Signaling of DNA Single-Strand Breaks by Human PARP-1.* Mol Cell, 2015. **60**(5): p. 742-754.

113. Loeffler, P.A., M.J. Cuneo, G.A. Mueller, E.F. DeRose, S.A. Gabel, and R.E. London, *Structural studies of the PARP-1 BRCT domain.* BMC Struct Biol, 2011. **11**: p. 37.

114. Zhang, Y., X.H. Liao, H.Y. Xie, Z.M. Shao, and D.Q. Li, *RBR-type E3 ubiquitin ligase RNF144A targets PARP1 for ubiquitin-dependent degradation and regulates PARP inhibitor sensitivity in breast cancer cells.* Oncotarget, 2017. **8**(55): p. 94505-94518.

115. Langelier, M.F. and J.M. Pascal, *PARP-1 mechanism for coupling DNA damage detection to poly(ADP-ribose) synthesis.* Curr Opin Struct Biol, 2013. **23**(1): p. 134-43.

116. Dawicki-McKenna, J.M., M.F. Langelier, J.E. DeNizio, A.A. Riccio, C.D. Cao, K.R. Karch, M. McCauley, J.D. Steffen, B.E. Black, and J.M. Pascal, *PARP-1 Activation Requires Local Unfolding of an Autoinhibitory Domain.* Mol Cell, 2015. **60**(5): p. 755-768.

117. Polo, L.M., Y. Xu, P. Hornyak, F. Garces, Z. Zeng, R. Hailstone, S.J. Matthews, K.W. Caldecott, A.W. Oliver, and L.H. Pearl, *Efficient Single-Strand Break Repair Requires Binding to Both Poly(ADP-Ribose) and DNA by the Central BRCT Domain of XRCC1.* Cell Rep, 2019. **26**(3): p. 573-581 e5.

118. O'Neil, N.J., D.M. van Pel, and P. Hieter, *Synthetic lethality and cancer: cohesin and PARP at the replication fork.* Trends Genet, 2013. **29**(5): p. 290-7.

119. Chow, J.P., W.Y. Man, M. Mao, H. Chen, F. Cheung, J. Nicholls, S.W. Tsao, M. Li Lung, and R.Y. Poon, *PARP1 is overexpressed in nasopharyngeal carcinoma*

and its inhibition enhances radiotherapy. Mol Cancer Ther, 2013. **12**(11): p. 2517-28.

120. Bertucci, F., P. Finetti, A. Monneur, D. Perrot, C. Chevreau, A. Le Cesne, J.Y. Blay, O. Mir, and D. Birnbaum, *PARP1 expression in soft tissue sarcomas is a poor-prognosis factor and a new potential therapeutic target.* Mol Oncol, 2019. **13**(7): p. 1577-1588.

121. Green, A.R., D. Caracappa, A.A. Benhasouna, A. Alshareeda, C.C. Nolan, R.D. Macmillan, S. Madhusudan, I.O. Ellis, and E.A. Rakha, *Biological and clinical significance of PARP1 protein expression in breast cancer.* Breast Cancer Res Treat, 2015. **149**(2): p. 353-62.

122. Chornenkyy, Y., S. Agnihotri, M. Yu, P. Buczkowicz, P. Rakopoulos, B. Golbourn, L. Garzia, R. Siddaway, S. Leung, J.T. Rutka, M.D. Taylor, P.B. Dirks, and C. Hawkins, *Poly-ADP-Ribose Polymerase as a Therapeutic Target in Pediatric Diffuse Intrinsic Pontine Glioma and Pediatric High-Grade Astrocytoma.* Mol Cancer Ther, 2015. **14**(11): p. 2560-8.

123. Eder, J.P., D.B. Doroshow, K.T. Do, V.L. Keedy, J.S. Sklar, P. Glazer, R. Bindra, and G.I. Shapiro, *Clinical Efficacy of Olaparib in IDH1/IDH2-Mutant Mesenchymal Sarcomas.* JCO Precision Oncology, 2021(5): p. 466-472.

124. Johnson, N., S.F. Johnson, W. Yao, Y.C. Li, Y.E. Choi, A.J. Bernhardy, Y. Wang, M. Capelletti, K.A. Sarosiek, L.A. Moreau, D. Chowdhury, A. Wickramanayake, M.I. Harrell, J.F. Liu, A.D. D'Andrea, A. Miron, E.M. Swisher, and G.I. Shapiro, *Stabilization of mutant BRCA1 protein confers PARP inhibitor and platinum resistance.* Proc Natl Acad Sci U S A, 2013. **110**(42): p. 17041-6.

125. Sim, H.W., E. Galanis, and M. Khasraw, *PARP Inhibitors in Glioma: A Review of Therapeutic Opportunities.* Cancers (Basel), 2022. **14**(4).

126. Chen, Q., M.A. Kassab, F. Dantzer, and X. Yu, *PARP2 mediates branched poly ADP-ribosylation in response to DNA damage.* Nature Communications, 2018. **9**(1): p. 3233.

127. Houl, J.H., Z. Ye, C.A. Brosey, L.P.F. Balapiti-Modarage, S. Namjoshi, A. Bacolla, D. Laverty, B.L. Walker, Y. Pourfarjam, L.S. Warden, N. Babu Chinnam, D. Moiani, R.A. Stegeman, M.K. Chen, M.C. Hung, Z.D. Nagel, T. Ellenberger, I.K. Kim, D.E. Jones, Z. Ahmed, and J.A. Tainer, *Selective small molecule PARG inhibitor causes replication fork stalling and cancer cell death.* Nat Commun, 2019. **10**(1): p. 5654.

128. Kassab, M.A., L.L. Yu, and X. Yu, *Targeting dePARylation for cancer therapy.* Cell & Bioscience, 2020. **10**(1): p. 7.

129. Mortusewicz, O., E. Fouquerel, J.C. Ame, H. Leonhardt, and V. Schreiber, *PARG is recruited to DNA damage sites through poly(ADP-ribose)- and PCNA-dependent mechanisms.* Nucleic Acids Res, 2011. **39**(12): p. 5045-56.

130. Nagashima, H., C.K. Lee, K. Tateishi, F. Higuchi, M. Subramanian, S. Rafferty, L. Melamed, J.J. Miller, H. Wakimoto, and D.P. Cahill, *Poly(ADP-ribose) Glycohydrolase Inhibition Sequesters NAD(+) to Potentiate the Metabolic Lethality of Alkylating Chemotherapy in IDH-Mutant Tumor Cells.* Cancer Discov, 2020. **10**(11): p. 1672-1689.

131. Ali, R., A. Alblihy, I.M. Miligy, M.L. Alabdullah, M. Alsaleem, M.S. Toss, M. Algethami, T. Abdel-Fatah, P. Moseley, S. Chan, N.P. Mongan, S. Narayan, E.A.

Rakha, and S. Madhusudan, *Molecular disruption of DNA polymerase β for platinum sensitisation and synthetic lethality in epithelial ovarian cancers.* Oncogene, 2021. **40**(14): p. 2496-2508.

132. Chen, S.H. and X. Yu, *Targeting dePARylation selectively suppresses DNA repair-defective and PARP inhibitor-resistant malignancies.* Sci Adv, 2019. **5**(4): p. eaav4340.

133. Gravells, P., J. Neale, E. Grant, A. Nathubhai, K.M. Smith, D.I. James, and H.E. Bryant, *Radiosensitization with an inhibitor of poly(ADP-ribose) glycohydrolase: A comparison with the PARP1/2/3 inhibitor olaparib.* DNA Repair (Amst), 2018. **61**: p. 25-36.

134. Horton, J.K., D.F. Stefanick, R. Prasad, N.R. Gassman, P.S. Kedar, and S.H. Wilson, *Base excision repair defects invoke hypersensitivity to PARP inhibition.* Mol Cancer Res, 2014. **12**(8): p. 1128-39.

135. Dianova, I.I., K.M. Sleeth, S.L. Allinson, J.L. Parsons, C. Breslin, K.W. Caldecott, and G.L. Dianov, *XRCC1–DNA polymerase β interaction is required for efficient base excision repair.* Nucleic Acids Research, 2004. **32**(8): p. 2550-2555.

136. Sawant, A., A.M. Floyd, M. Dangeti, W. Lei, R.W. Sobol, and S.M. Patrick, *Differential role of base excision repair proteins in mediating cisplatin cytotoxicity.* DNA Repair (Amst), 2017. **51**: p. 46-59.

137. Lee, K.J., C.G. Piett, J.F. Andrews, E. Mann, Z.D. Nagel, and N.R. Gassman, *Defective base excision repair in the response to DNA damaging agents in triple negative breast cancer.* PLoS One, 2019. **14**(10): p. e0223725.

138. Hirota, K., M. Ooka, N. Shimizu, K. Yamada, M. Tsuda, M.A. Ibrahim, S. Yamada, H. Sasanuma, M. Masutani, and S. Takeda, *XRCC1 counteracts poly(ADP ribose)polymerase (PARP) poisons, olaparib and talazoparib, and a clinical alkylating agent, temozolomide, by promoting the removal of trapped PARP1 from broken DNA.* Genes Cells, 2022. **27**(5): p. 331-344.

139. Wu, Z., X. Miao, Y. Zhang, D. Li, Q. Zou, Y. Yuan, R. Liu, and Z. Yang, *XRCC1 Is a Promising Predictive Biomarker and Facilitates Chemo-Resistance in Gallbladder Cancer.* Frontiers in Molecular Biosciences, 2020. **7**.

140. Gong, L., M. Luo, R. Sun, L. Qiu, C. Chen, and Z. Luo, *Significant Association Between XRCC1 Expression and Its rs25487 Polymorphism and Radiotherapy-Related Cancer Prognosis.* Frontiers in Oncology, 2021. **11**.

141. Adamowicz, M., R. Hailstone, A.A. Demin, E. Komulainen, H. Hanzlikova, J. Brazina, A. Gautam, S.E. Wells, and K.W. Caldecott, *XRCC1 protects transcription from toxic PARP1 activity during DNA base excision repair.* Nature Cell Biology, 2021. **23**(12): p. 1287-1298.

142. Breslin, C., P. Hornyak, A. Ridley, S.L. Rulten, H. Hanzlikova, A.W. Oliver, and K.W. Caldecott, *The XRCC1 phosphate-binding pocket binds poly (ADP-ribose) and is required for XRCC1 function.* Nucleic Acids Res, 2015. **43**(14): p. 6934-44.

143. Demin, A.A., K. Hirota, M. Tsuda, M. Adamowicz, R. Hailstone, J. Brazina, W. Gittens, I. Kalasova, Z. Shao, S. Zha, H. Sasanuma, H. Hanzlikova, S. Takeda, and K.W. Caldecott, *XRCC1 prevents toxic PARP1 trapping during DNA base excision repair.* Mol Cell, 2021. **81**(14): p. 3018-3030.e5.

144. Tebbs, R.S., L.H. Thompson, and J.E. Cleaver, *Rescue of Xrcc1 knockout mouse embryo lethality by transgene-complementation.* DNA Repair (Amst), 2003. **2**(12): p. 1405-1417.

145. Zhang, G., J. Zhang, Y. Gao, Y. Li, and Y. Li, *Strategies for targeting undruggable targets.* Expert Opin Drug Discov, 2022. **17**(1): p. 55-69.

146. Howard, M.J., Y. Rodriguez, and S.H. Wilson, *DNA polymerase β uses its lyase domain in a processive search for DNA damage.* Nucleic Acids Research, 2017. **45**(7): p. 3822-3832.

147. Sobol, R.W., R. Prasad, A. Evenski, A. Baker, X.P. Yang, J.K. Horton, and S.H. Wilson, *The lyase activity of the DNA repair protein beta-polymerase protects from DNA-damage-induced cytotoxicity.* Nature, 2000. **405**(6788): p. 807-10.

148. Bridge, G., S. Rashid, and S.A. Martin, *DNA mismatch repair and oxidative DNA damage: implications for cancer biology and treatment.* Cancers (Basel), 2014. **6**(3): p. 1597-614.

149. Martin, S.A., N. McCabe, M. Mullarkey, R. Cummins, D.J. Burgess, Y. Nakabeppu, S. Oka, E. Kay, C.J. Lord, and A. Ashworth, *DNA polymerases as potential therapeutic targets for cancers deficient in the DNA mismatch repair proteins MSH2 or MLH1.* Cancer Cell, 2010. **17**(3): p. 235-48.

150. Yuhas, S.C., D.J. Laverty, H. Lee, A. Majumdar, and M.M. Greenberg, *Selective Inhibition of DNA Polymerase β by a Covalent Inhibitor.* Journal of the American Chemical Society, 2021. **143**(21): p. 8099-8107.

151. Sun, X. and S. Turcan, *From Laboratory Studies to Clinical Trials: Temozolomide Use in IDH-Mutant Gliomas.* Cells, 2021. **10**(5).

152. Wang, P., J. Wu, S. Ma, L. Zhang, J. Yao, Katherine A. Hoadley, Matthew D. Wilkerson, Charles M. Perou, K.-L. Guan, D. Ye, and Y. Xiong, *Oncometabolite D-2-Hydroxyglutarate Inhibits ALKBH DNA Repair Enzymes and Sensitizes IDH Mutant Cells to Alkylating Agents.* Cell Reports, 2015. **13**(11): p. 2353-2361.

153. Kamaletdinova, T., Z. Fanaei-Kahrani, and Z.Q. Wang, *The Enigmatic Function of PARP1: From PARylation Activity to PAR Readers.* Cells, 2019. **8**(12).

154. Han, S., Y. Liu, S.J. Cai, M. Qian, J. Ding, M. Larion, M.R. Gilbert, and C. Yang, *IDH mutation in glioma: molecular mechanisms and potential therapeutic targets.* British Journal of Cancer, 2020. **122**(11): p. 1580-1589.

155. Yan, H., D.W. Parsons, G. Jin, R. McLendon, B.A. Rasheed, W. Yuan, I. Kos, I. Batinic-Haberle, S. Jones, G.J. Riggins, H. Friedman, A. Friedman, D. Reardon, J. Herndon, K.W. Kinzler, V.E. Velculescu, B. Vogelstein, and D.D. Bigner, *IDH1 and IDH2 mutations in gliomas.* N Engl J Med, 2009. **360**(8): p. 765-73.

156. Sulkowski, P.L., C.D. Corso, N.D. Robinson, S.E. Scanlon, K.R. Purshouse, H. Bai, Y. Liu, R.K. Sundaram, D.C. Hegan, N.R. Fons, G.A. Breuer, Y. Song, K. Mishra-Gorur, H.M. De Feyter, R.A. de Graaf, Y.V. Surovtseva, M. Kachman, S. Halene, M. Günel, P.M. Glazer, and R.S. Bindra, *2-Hydroxyglutarate produced by neomorphic IDH mutations suppresses homologous recombination and induces PARP inhibitor sensitivity.* Sci Transl Med, 2017. **9**(375).

157. Sulkowski, P.L., S. Oeck, J. Dow, N.G. Economos, L. Mirfakhraie, Y. Liu, K. Noronha, X. Bao, J. Li, B.M. Shuch, M.C. King, R.S. Bindra, and P.M. Glazer, *Oncometabolites suppress DNA repair by disrupting local chromatin signalling.* Nature, 2020. **582**(7813): p. 586-591.

158. Wang, Y.Q., P.Y. Wang, Y.T. Wang, G.F. Yang, A. Zhang, and Z.H. Miao, *An Update on Poly(ADP-ribose)polymerase-1 (PARP-1) Inhibitors: Opportunities and Challenges in Cancer Therapy.* J Med Chem, 2016. **59**(21): p. 9575-9598.

159. Wang, L., C. Liang, F. Li, D. Guan, X. Wu, X. Fu, A. Lu, and G. Zhang, *PARP1 in Carcinomas and PARP1 Inhibitors as Antineoplastic Drugs.* Int J Mol Sci, 2017. **18**(10).

160. O'Sullivan Coyne, G., A.P. Chen, R. Meehan, and J.H. Doroshow, *PARP Inhibitors in Reproductive System Cancers: Current Use and Developments.* Drugs, 2017. **77**(2): p. 113-130.

161. Sunada, S., A. Nakanishi, and Y. Miki, *Crosstalk of DNA double-strand break repair pathways in poly(ADP-ribose) polymerase inhibitor treatment of breast cancer susceptibility gene 1/2-mutated cancer.* Cancer Sci, 2018. **109**(4): p. 893-899.

162. Izumi, T. and I. Mellon, *Chapter 17 - Base Excision Repair and Nucleotide Excision Repair*, in *Genome Stability*, I. Kovalchuk and O. Kovalchuk, Editors. 2016, Academic Press: Boston. p. 275-302.

163. Sobol, R.W., *Genome instability caused by a germline mutation in the human DNA repair gene POLB.* PLoS Genet, 2012. **8**(11): p. e1003086.

164. Lee, P.R., D.R. Lee, P. Lee, and M. Arch, *2010: U.S. drug and alcohol policy, looking back and moving forward.* J Psychoactive Drugs, 2010. **42**(2): p. 99-114.

165. Donigan, K.A., K.-w. Sun, A.A. Nemec, D.L. Murphy, X. Cong, V. Northrup, D. Zelterman, and J.B. Sweasy, *Human POLB Gene Is Mutated in High Percentage*

*of Colorectal Tumors**. Journal of Biological Chemistry, 2012. **287**(28): p. 23830-23839.

166. Qin, J., Y. Zhu, Y. Ding, T. Niu, Y. Zhang, H. Wu, L. Zhu, B. Yuan, Y. Qiao, J. Lu, K. Liu, Z. Dong, G. Jin, X. Chen, and J. Zhao, *DNA polymerase β deficiency promotes the occurrence of esophageal precancerous lesions in mice.* Neoplasia, 2021. **23**(7): p. 663-675.

167. Mao, P., K. Joshi, J. Li, S.H. Kim, P. Li, L. Santana-Santos, S. Luthra, U.R. Chandran, P.V. Benos, L. Smith, M. Wang, B. Hu, S.Y. Cheng, R.W. Sobol, and I. Nakano, *Mesenchymal glioma stem cells are maintained by activated glycolytic metabolism involving aldehyde dehydrogenase 1A3.* Proc Natl Acad Sci U S A, 2013. **110**(21): p. 8644-9.

168. Hsu, P.D., D.A. Scott, J.A. Weinstein, F.A. Ran, S. Konermann, V. Agarwala, Y. Li, E.J. Fine, X. Wu, O. Shalem, T.J. Cradick, L.A. Marraffini, G. Bao, and F. Zhang, *DNA targeting specificity of RNA-guided Cas9 nucleases.* Nat Biotechnol, 2013. **31**(9): p. 827-32.

169. Liang, X., J. Potter, S. Kumar, Y. Zou, R. Quintanilla, M. Sridharan, J. Carte, W. Chen, N. Roark, S. Ranganathan, N. Ravinder, and J.D. Chesnut, *Rapid and highly efficient mammalian cell engineering via Cas9 protein transfection.* J Biotechnol, 2015. **208**: p. 44-53.

170. Kiss, A., A.P. Ráduly, Z. Regdon, Z. Polgár, S. Tarapcsák, I. Sturniolo, T. El-Hamoly, L. Virág, and C. Hegedűs, *Targeting Nuclear NAD(+) Synthesis Inhibits DNA Repair, Impairs Metabolic Adaptation and Increases Chemosensitivity of U-2OS Osteosarcoma Cells.* Cancers (Basel), 2020. **12**(5).

171. Robaszkiewicz, A., K. Erdelyi, K. Kovacs, I. Kovacs, P. Bai, E. Rajnavolgyi, and L. Virag, *Hydrogen peroxide-induced poly(ADP-ribosyl)ation regulates osteogenic differentiation-associated cell death.* Free Radic Biol Med, 2012. **53**(8): p. 1552-64.

172. Dutta, A., C. Yang, S. Sengupta, S. Mitra, and M.L. Hegde, *New paradigms in the repair of oxidative damage in human genome: mechanisms ensuring repair of mutagenic base lesions during replication and involvement of accessory proteins.* Cell Mol Life Sci, 2015. **72**(9): p. 1679-98.

173. Sykora, P., K.L. Witt, P. Revanna, S.L. Smith-Roe, J. Dismukes, D.G. Lloyd, B.P. Engelward, and R.W. Sobol, *Next generation high throughput DNA damage detection platform for genotoxic compound screening.* Scientific Reports, 2018. **8**(1): p. 2771.

174. Fang, Q., B. Inanc, S. Schamus, X.-h. Wang, L. Wei, A.R. Brown, D. Svilar, K.F. Sugrue, E.M. Goellner, X. Zeng, N.A. Yates, L. Lan, C. Vens, and R.W. Sobol, *HSP90 regulates DNA repair via the interaction between XRCC1 and DNA polymerase β.* Nature Communications, 2014. **5**(1): p. 5513.

175. Holton, N.W., J.F. Andrews, and N.R. Gassman, *Application of Laser Micro-irradiation for Examination of Single and Double Strand Break Repair in Mammalian Cells.* J Vis Exp, 2017(127).

176. Gassman, N.R. and S.H. Wilson, *Micro-irradiation tools to visualize base excision repair and single-strand break repair.* DNA Repair (Amst), 2015. **31**: p. 52-63.

177. Levone, B.R., S. Lombardi, and S.M.L. Barabino, *Laser microirradiation as a tool to investigate the role of liquid-liquid phase separation in DNA damage repair.* STAR Protocols, 2022. **3**(1): p. 101146.

178. Martinez-Pastor, B., G.G. Silveira, T.L. Clarke, D. Chung, Y. Gu, C. Cosentino, L.S. Davidow, G. Mata, S. Hassanieh, J. Salsman, A. Ciccia, N. Bae, M.T. Bedford, D. Megias, L.L. Rubin, A. Efeyan, G. Dellaire, and R. Mostoslavsky, *Assessing kinetics and recruitment of DNA repair factors using high content screens.* Cell Reports, 2021. **37**(13): p. 110176.

179. Chen, Q., C. Bian, X. Wang, X. Liu, M. Ahmad Kassab, Y. Yu, and X. Yu, *ADP-ribosylation of histone variant H2AX promotes base excision repair.* The EMBO Journal, 2021. **40**(2): p. e104542.

180. Ronson, G.E., A.L. Piberger, M.R. Higgs, A.L. Olsen, G.S. Stewart, P.J. McHugh, E. Petermann, and N.D. Lakin, *PARP1 and PARP2 stabilise replication forks at base excision repair intermediates through Fbh1-dependent Rad51 regulation.* Nature Communications, 2018. **9**(1): p. 746.

181. Kulikova, V., K. Shabalin, K. Nerinovski, A. Yakimov, M. Svetlova, L. Solovjeva, A. Kropotov, M. Khodorkovskiy, M.E. Migaud, M. Ziegler, and A. Nikiforov, *Degradation of Extracellular NAD(+) Intermediates in Cultures of Human HEK293 Cells.* Metabolites, 2019. **9**(12).

182. Hanzlikova, H. and K.W. Caldecott, *Perspectives on PARPs in S Phase.* Trends Genet, 2019. **35**(6): p. 412-422.

183. Genois, M.-M., J.-P. Gagné, T. Yasuhara, J. Jackson, S. Saxena, M.-F. Langelier, I. Ahel, M.T. Bedford, J.M. Pascal, A. Vindigni, G.G. Poirier, and L. Zou, *CARM1*

regulates replication fork speed and stress response by stimulating PARP1. Molecular Cell, 2021. **81**(4): p. 784-800.e8.

184. Nakatani, T., J. Lin, F. Ji, A. Ettinger, J. Pontabry, M. Tokoro, L. Altamirano-Pacheco, J. Fiorentino, E. Mahammadov, Y. Hatano, C. Van Rechem, D. Chakraborty, E.R. Ruiz-Morales, P.Y. Arguello Pascualli, A. Scialdone, K. Yamagata, J.R. Whetstine, R.I. Sadreyev, and M.-E. Torres-Padilla, *DNA replication fork speed underlies cell fate changes and promotes reprogramming.* Nature Genetics, 2022. **54**(3): p. 318-327.

185. Chen, G. and X. Deng, *Cell Synchronization by Double Thymidine Block.* Bio Protoc, 2018. **8**(17).

186. Sears, R.M., D.G. May, and K.J. Roux, *BioID as a Tool for Protein-Proximity Labeling in Living Cells.* Methods Mol Biol, 2019. **2012**: p. 299-313.

187. Roux, K.J., D.I. Kim, B. Burke, and D.G. May, *BioID: A Screen for Protein-Protein Interactions.* Curr Protoc Protein Sci, 2018. **91**: p. 19.23.1-19.23.15.

188. Song, B., X.S. Liu, K. Davis, and X. Liu, *Plk1 phosphorylation of Orc2 promotes DNA replication under conditions of stress.* Mol Cell Biol, 2011. **31**(23): p. 4844-56.

189. Higa, M., Y. Matsuda, J. Fujii, N. Sugimoto, K. Yoshida, and M. Fujita, *TRF2-mediated ORC recruitment underlies telomere stability upon DNA replication stress.* Nucleic Acids Research, 2021. **49**(21): p. 12234-12251.

190. Bassal, M.A., S.E. Samaraweera, K. Lim, B.A. Benard, S. Bailey, S. Kaur, P. Leo, J. Toubia, C. Thompson-Peach, T. Nguyen, K.Z.Y. Maung, D.A. Casolari, D.G. Iarossi, I.S. Pagani, J. Powell, S. Pitson, S. Natera, U. Roessner, I.D. Lewis, A.L.

Brown, D.G. Tenen, N. Robinson, D.M. Ross, R. Majeti, T.J. Gonda, D. Thomas, and R.J. D'Andrea, *Germline mutations in mitochondrial complex I reveal genetic and targetable vulnerability in IDH1-mutant acute myeloid leukaemia.* Nature Communications, 2022. **13**(1): p. 2614.

191. Smolková, K. and P. Ježek, *The Role of Mitochondrial NADPH-Dependent Isocitrate Dehydrogenase in Cancer Cells.* International Journal of Cell Biology, 2012. **2012**: p. 273947.

192. Yang, H., D. Ye, K.L. Guan, and Y. Xiong, *IDH1 and IDH2 mutations in tumorigenesis: mechanistic insights and clinical perspectives.* Clin Cancer Res, 2012. **18**(20): p. 5562-71.

193. Lin, L., J. Cai, Z. Tan, X. Meng, R. Li, Y. Li, and C. Jiang, *Mutant IDH1 Enhances Temozolomide Sensitivity via Regulation of the ATM/CHK2 Pathway in Glioma.* Cancer Res Treat, 2021. **53**(2): p. 367-377.

194. Hu, C., K. Wang, C. Damon, Y. Fu, T. Ma, L. Kratz, B. Lal, M. Ying, S. Xia, D.P. Cahill, C.M. Jackson, M. Lim, J. Laterra, and Y. Li, *ATRX loss promotes immunosuppressive mechanisms in IDH1 mutant glioma.* Neuro-Oncology, 2021: p. noab292.

195. Caccese, M., T. Ius, M. Simonelli, M. Fassan, D. Cesselli, A. Dipasquale, F. Cavallin, M. Padovan, A. Salvalaggio, M.P. Gardiman, M. Skrap, V. Zagonel, and G. Lombardi, *Mismatch-Repair Protein Expression in High-Grade Gliomas: A Large Retrospective Multicenter Study.* Int J Mol Sci, 2020. **21**(18).

196. Koussounadis, A., S.P. Langdon, I.H. Um, D.J. Harrison, and V.A. Smith, *Relationship between differentially expressed mRNA and mRNA-protein correlations in a xenograft model system.* Scientific Reports, 2015. **5**(1): p. 10775.

197. Sobol, R.W., J.K. Horton, R. Kühn, H. Gu, R.K. Singhal, R. Prasad, K. Rajewsky, and S.H. Wilson, *Requirement of mammalian DNA polymerase-beta in base-excision repair.* Nature, 1996. **379**(6561): p. 183-6.

198. Inoue, S., W.Y. Li, A. Tseng, I. Beerman, A.J. Elia, S.C. Bendall, F. Lemonnier, K.J. Kron, D.W. Cescon, Z. Hao, E.F. Lind, N. Takayama, A.C. Planello, S.Y. Shen, A.H. Shih, D.M. Larsen, Q. Li, B.E. Snow, A. Wakeham, J. Haight, C. Gorrini, C. Bassi, K.L. Thu, K. Murakami, A.R. Elford, T. Ueda, K. Straley, K.E. Yen, G. Melino, L. Cimmino, I. Aifantis, R.L. Levine, D.D. De Carvalho, M. Lupien, D.J. Rossi, G.P. Nolan, R.A. Cairns, and T.W. Mak, *Mutant IDH1 Downregulates ATM and Alters DNA Repair and Sensitivity to DNA Damage Independent of TET2.* Cancer Cell, 2016. **30**(2): p. 337-348.

199. Du, X. and H. Hu, *The Roles of 2-Hydroxyglutarate.* Front Cell Dev Biol, 2021. **9**: p. 651317.

200. Jin, G., Z.J. Reitman, C.G. Duncan, I. Spasojevic, D.M. Gooden, B.A. Rasheed, R. Yang, G.Y. Lopez, Y. He, R.E. McLendon, D.D. Bigner, and H. Yan, *Disruption of wild-type IDH1 suppresses D-2-hydroxyglutarate production in IDH1-mutated gliomas.* Cancer Res, 2013. **73**(2): p. 496-501.

201. Maynard, S., S.H. Schurman, C. Harboe, N.C. de Souza-Pinto, and V.A. Bohr, *Base excision repair of oxidative DNA damage and association with cancer and aging.* Carcinogenesis, 2009. **30**(1): p. 2-10.

202. Chang, D.K., A. Goel, L. Ricciardiello, D.H. Lee, C.L. Chang, J.M. Carethers, and C.R. Boland, *Effect of H(2)O(2) on cell cycle and survival in DNA mismatch repair-deficient and -proficient cell lines.* Cancer Letters, 2003. **195**(2): p. 243-51.

203. Chandel, N.S., D.S. McClintock, C.E. Feliciano, T.M. Wood, J.A. Melendez, A.M. Rodriguez, and P.T. Schumacker, *Reactive oxygen species generated at mitochondrial complex III stabilize hypoxia-inducible factor-1alpha during hypoxia: a mechanism of O2 sensing.* Journal of Biological Chemistry, 2000. **275**(33): p. 25130-8.

204. Long, L.H., A. Hoi, and B. Halliwell, *Instability of, and generation of hydrogen peroxide by, phenolic compounds in cell culture media.* Arch Biochem Biophys, 2010. **501**(1): p. 162-9.

205. Shi, J., B. Sun, W. Shi, H. Zuo, D. Cui, L. Ni, and J. Chen, *Decreasing GSH and increasing ROS in chemosensitivity gliomas with IDH1 mutation.* Tumor Biology, 2015. **36**(2): p. 655-662.

206. Liu, Y., Y. Lu, O. Celiku, A. Li, Q. Wu, Y. Zhou, and C. Yang, *Targeting IDH1-Mutated Malignancies with NRF2 Blockade.* J Natl Cancer Inst, 2019. **111**(10): p. 1033-1041.

207. Fan, Z., P.J. Beresford, D. Zhang, Z. Xu, C.D. Novina, A. Yoshida, Y. Pommier, and J. Lieberman, *Cleaving the oxidative repair protein Ape1 enhances cell death mediated by granzyme A.* Nature Immunology, 2003. **4**(2): p. 145-153.

208. Frouin, I., G. Maga, M. Denegri, F. Riva, M. Savio, S. Spadari, E. Prosperi, and A.I. Scovassi, *Human proliferating cell nuclear antigen, poly(ADP-ribose)*

polymerase-1, and p21waf1/cip1. A dynamic exchange of partners. J Biol Chem, 2003. **278**(41): p. 39265-8.

209. Koczor, C.A., K.M. Saville, J.F. Andrews, J. Clark, Q. Fang, J. Li, R.Q. Al-Rahahleh, M. Ibrahim, M.V. Makarov, M. Migaud, and R.W. Sobol, *Temporal dynamics of base excision / single-strand break repair protein complex assembly and disassembly are modulated by the PARP/NAD+/SIRT6 axis.* Cell Reports, 2021. **In Press**.

210. Li, J., K. M. Saville, M. Ibrahim, X. Zeng, S. McClellan, A. Angajala, A. Beiser, J.F. Andrews, M. Sun, C.A. Koczor, J. Clark, F. Hayat, M.V. Makarov, A. Wilk, N.A. Yates, M.E. Migaud, and R.W. Sobol, *NAD+ bioavailability mediates PARG inhibition-induced replication arrest, intra S-phase checkpoint and apoptosis in glioma stem cells.* NAR Cancer, 2021. **3**(4): p. zcab044.

211. JimÈnez-GarcÌa, M.P., E.M. Verdugo-Sivianes, and A. Lucena-Cacace, *Nicotinamide adenine dinucleotide+ metabolism biomarkers in malignant gliomas.* Cancer Translational Medicine, 2016. **2**: p. 189 - 196.

212. Ohsaki, E., K. Ueda, S. Sakakibara, E. Do, K. Yada, and K. Yamanishi, *Poly(ADP-ribose) polymerase 1 binds to Kaposi's sarcoma-associated herpesvirus (KSHV) terminal repeat sequence and modulates KSHV replication in latency.* J Virol, 2004. **78**(18): p. 9936-46.

213. Simbulan-Rosenthal, C.M., D.S. Rosenthal, A.H. Boulares, R.J. Hickey, L.H. Malkas, J.M. Coll, and M.E. Smulson, *Regulation of the expression or recruitment of components of the DNA synthesome by poly(ADP-ribose) polymerase.* Biochemistry, 1998. **37**(26): p. 9363-70.

214. Yang, Z., M.I. Nejad, J.G. Varela, N.E. Price, Y. Wang, and K.S. Gates, *A role for the base excision repair enzyme NEIL3 in replication-dependent repair of interstrand DNA cross-links derived from psoralen and abasic sites.* DNA Repair (Amst), 2017. **52**: p. 1-11.

215. Albelazi, M.S., P.R. Martin, S. Mohammed, L. Mutti, J.L. Parsons, and R.H. Elder, *The Biochemical Role of the Human NEIL1 and NEIL3 DNA Glycosylases on Model DNA Replication Forks.* Genes (Basel), 2019. **10**(4).

216. Ooka, M., T. Abe, K. Cho, K. Koike, S. Takeda, and K. Hirota, *Chromatin remodeler ALC1 prevents replication-fork collapse by slowing fork progression.* PLoS One, 2018. **13**(2): p. e0192421.

217. Rangaswamy, S., A. Pandey, S. Mitra, and M.L. Hegde, *Pre-Replicative Repair of Oxidized Bases Maintains Fidelity in Mammalian Genomes: The Cowcatcher Role of NEIL1 DNA Glycosylase.* Genes (Basel), 2017. **8**(7).

218. Xu, Q., K. Wang, L. Wang, Y. Zhu, G. Zhou, D. Xie, and Q. Yang, *IDH1/2 Mutants Inhibit TET-Promoted Oxidation of RNA 5mC to 5hmC.* PLOS ONE, 2016. **11**(8): p. e0161261.

219. Sanjana, N.E., O. Shalem, and F. Zhang, *Improved vectors and genome-wide libraries for CRISPR screening.* Nat Methods, 2014. **11**(8): p. 783-784.

220. Slyskova, J., M. Sabatella, C. Ribeiro-Silva, C. Stok, A.F. Theil, W. Vermeulen, and H. Lans, *Base and nucleotide excision repair facilitate resolution of platinum drugs-induced transcription blockage.* Nucleic Acids Res, 2018. **46**(18): p. 9537-9549.

BIOGRAPHICAL SKETCH

Name of Author: Kate M. Saville

Undergraduate Schools Attended:

Virginia Western Community College, Roanoke, Virginia

The University of Alabama, Tuscaloosa, Alabama

The University of South Alabama College of Medicine, Mobile Alabama

Degrees Awarded:

Associate of Science in Health Sciences, 2008, Roanoke, Virginia

Bachelor of Science in Biology, 2014, Tuscaloosa, Alabama

Doctor of Philosophy in Basic Medical Sciences, 2022, Mobile, Alabama